Novel Single-Site Titanosilicates with Targeted Connectivity and Nuclearity of Titanium(IV): Synthesis, Characterization and Catalytic Properties in Alkylphenol Oxidation

A Dissertation Presented for the
Doctor of Philosophy
Degree
The University of Tennessee, Knoxville

Nan Chen
August 2012

Copyright © 2012 by Nan Chen.

All rights reserved.

Dedication

I dedicate this dissertation to my grandma Ye, Guilan.

May her soul rest in peace in heaven.

Acknowledgement

This dissertation could not have come to its finish without the supports from my mentors, friends and family. Professor Craig Barnes, my research advisor, has not only taught me so much knowledge and many skills in organometallic chemistry, but also influenced me with his passion in research. During the most difficult times, he understood and encouraged me so that I could grow not only as a chemist but also an individual.

I am so glad to get to know Dr. Richard Mayes, Dr. Michael Peretich, Dr. Joshua Abbott, and all the members of Barnes' research group. They have helped me from the very beginning of my graduate study, and always provided their insights and helps in need. My sincere thanks go to Dr. Ming-Yun Lee, a former Barnes' group member, who offered a large amount of time and effort in collecting XAS data.

The time in graduate school has been the most memorable five years in my life. I am blessed with great friends who witnessed the changes on me during this time. I owe my deepest gratitude to these dearest friends. Especially, I would like to thank Terry and Rosann Douglass who have been always loving and caring ever since we met in 2008. It is them who convinced me of the existence of unconditional love beyond any worldly differences between people.

Last but not least, I would like to thank my parents, Guiqin Wang and Daoyuan Chen. No words can describe my love for them. They have been providing me everything in every possible way, and encouraged their only child to pursue what she believed important. I am forever grateful for the unsurpassable love.

Abstract

Titanosilicates are a family of porous materials that have shown excellent catalytic activity in olefin epoxidation and many other selective oxidation reactions. These materials have been extensively studied in the past few decades. One of the central questions in these investigations has been to define the catalytically active centers. The traditional synthesis of wet impregnation followed by calcination often produces more than one type of catalytic center within the same matrix, i.e. different coordination, connectivity and nuclearity. Each type potentially possesses unique catalytic activity. Co-existence of multiple catalytic centers makes it impossible to establish the relationship between the structure of titanium center and catalytic activity.

The goal of this research was to establish a structure-function relationship in titanosilicate materials through targeted synthesis of single-site nanostructured catalysts, in which titanium centers are isolated from one another while possessing the uniform structure. A building block synthetic methodology was utilized to prepare a series of catalysts, namely 2-connected (2C), 3-connected (3C), 4-connected (4C) and tetranuclear (Ti_4 [subscript 4]) titanium catalysts. These materials were characterized in detail via gravimetric analysis, solid state NMR, diffuse reflectance UV spectroscopy, infrared spectroscopy, BET surface area and X-ray absorption spectroscopy (XANES and EXAFS). Catalytic activity of each catalyst was examined in the oxidation of 2, 3, 6-trimethylphenol with aqueous hydrogen peroxide to give the corresponding benzoquinone. Under identical conditions, high to mediocre catalytic activity has been observed in a sequence of Ti_4 [subscript 4] > 2C > 3C ≈ 4C, in terms of both conversion and selectivity. All synthesized catalysts showed excellent stability and recyclability with aqueous hydrogen peroxide at elevated temperature. A structure-function relationship was therefore developed through targeted synthesis of novel single-site titanosilicate catalysts.

Table of Contents

Chapter I: Background of Single-Site Heterogeneous Catalysts 1
1.1 Introduction of Catalysts 1
1.1.1 What is a catalyst? 1
1.1.2 Evaluation of catalysts 3
1.1.3 Homogeneous catalysts 4
1.1.4 Heterogeneous catalysts 7
1.1.5 Preparation of heterogeneous catalysts 9
1.2 Single-Site Heterogeneous Catalysts (SSHCs) 16
1.2.1 Introduction 16
1.2.2 Four principle categories and synthesis 16
1.3 Titanosilicate Catalysts 22
1.3.1 Development of titanosilicates 22
1.3.2 Titanium silicalite-1 (TS-1) 24
1.3.3 Mesoporous titanosilicate materials 32
1.4 Overview of Dissertation 36
1.4.1 Motivation and goals 36
1.4.2 Atomically dispersed and clustered Ti centers 38
1.4.3 Catalytic properties in phenol oxidation 39
Chapter II. General Synthesis & Characterization 40
2.1 Building Block Methodology 40
2.1.1 General methodology 40
2.1.2 Building block 43
2.1.3 Linkers 45
2.1.4 Method of sequential additions 45
2.1.5 Gravimetric analysis 51
2.2 Diffuse Reflectance UV-Visible Spectroscopy 52
2.2.1 Introduction 52
2.2.2 DRUV spectra and interpretation 54
2.2.3 Sample preparation & data collection 54
2.3 X-ray Absorption Spectroscopy (XAS) 56
2.3.1 Introduction 56
2.3.2 Sample preparation & data collection 61
2.3.3 General interpretation of XAS spectra 62

2.4 Other Characterization Techniques 70
2.4.1 ICP elemental analysis 70
2.4.2 Nitrogen adsorption/desorption (BET) 72
2.4.3 Vibrational spectroscopy 72
Chapter III. Synthesis and Primary Characterization of Atomically Dispersed Titanosilicate Catalysts 75
3.1 Synthesis and Preliminary Characterization 75
3.1.1 Titanium precursors 75
3.1.2 Synthesis & connectivity 76
3.1.3 Elemental analysis (ICP) 76
3.2 Infrared Spectra 81
3.2.1 Sample preparation 81
3.2.2 Result and conclusion 81
3.3 Diffuse Reflectance UV Spectra 85
3.3.1 Sample preparation 85
3.3.2 Result and discussion 90
3.4 XANES & EXAFS 93
3.4.1 Sample preparation 93
3.4.2 XANES results 93
3.4.3 EXAFS results of 2C-, 3C-, and 4C-1 dose 99
3.4.4 EXAFS results of 2C-, 3C-, and 4C-MeOH 110
3.5 Characterization of Ti-peroxide System 114
3.5.1 TS-1/peroxide system 114
3.5.2 DRUV spectra of peroxide samples 115
3.5.3 XAS results of peroxide samples 116
3.6 Conclusion of Atomically Dispersed Titanium Centers 119
Chapter IV. Synthesis and Primary Characterization of Isolated Tetranuclear Titanosilicate Catalyst 120
4.1 Synthesis and Gravimetric Analysis 120
4.1.1 Tetranuclear titanium precursor 120
4.1.2 Synthesis of tetranuclear titanium catalyst 121
4.1.3 Synthesis of tetranuclear titanium-POSS analogue 122
4.1.4 Summary of synthesis 124
4.2 Characterization of Embedded Tetranuclear Titanium Center 126

4.2.1 Vibrational spectra 126
4.2.2 DRUV 129
4.2.3 XANES 129
4.3 Conclusion of Tetranuclear Titanium Sites 133
Chapter V. Secondary Characterization: Catalytic Properties in Alkylphenol Oxidation with Aqueous Hydrogen Peroxide 134
5.1 Background and Experimental 134
5.1.1 Heterogeneous activation of aqueous hydrogen peroxide 134
5.1.2 Titanosilicates in alkylphenol oxidation reactions 135
5.1.3 Experimental 137
5.1.4 Characterization of products 137
5.2 Evaluation of Catalytic Activity 140
5.2.1 Results and discussion 140
5.2.2 Stability and recyclability 151
5.3 Summary 153
Chapter VI. Conclusion and Future Research 153
6.1 Conclusion 153
6.1.1 Single-site catalysts with targeted titanium centers 153
6.1.2 Catalytic properties and mechanistic study 154
6.1.3 Structure-function relationship 156
6.2 Direction of Future Research 156
6.2.1 Incorporation of various titanium clusters 156
6.2.2 Epoxidation catalyzed by mesoporous single-site titanosilicates 156
References 158
Vita 169

List of Figures

Figure 1. An alternative reaction pathway with lower activation barrier created by the catalyst .. 2
Scheme 1. Regio- or enantio-selectivity in epoxidation of allyl alcohol with Ti catalysts 3
Figure 2. Homogeneous catalysts in forms of discrete metal complexes..... 4
Figure 3. Catalytic cycle of alkene hydrogenation (M= metal; L_n= coordinating ligands)..... 6
Figure 4. Hypothesized structures of isolated metal centers on a supporting matrix..... 8
Figure 5. Metal sites deposited on zeolite (ZSM-5) surface by different mechanisms.....11
Figure 6. Sol-gel processing in the preparation of solid materials.....14
Figure 7. Grafting titanium(IV) centers on silica MCM-41. 18
Figure 8. Localization of Ni(II)-O-Ni(II) and Ni(I) sites within the channel of zeolite. [Ni (dark blue), Al (light blue), O (red), Si (yellow)] (Reprinted from reference 37).....18
Figure 9. Chiral Rh(I)-based cation tethered on silica surface through triflate counter ion 20
Figure 10. Rh(I)-based cation tethered on sulfonate-modified silica 20
Figure 11. Supercage structure in faujasite zeolites. 21
Figure 12. Structures of dinuclear Ti sites proposed by previous studies 23
Figure 13. The structure of orthorhombic form of silicalite-1 (MFI type) showing the 12 crystallographically distinct T sites (The oxygen atoms are omitted for clarity).....26
Figure 14. Hydrolysis of [$Ti(OSi)_4$] in aqueous H_2O_2 (up) and conversion between 3-connected Ti-hydroxide and Ti-hydroperoxide (bottom) 26
Figure 15. TS-1 catalyzed reactions (Reprinted from reference 54) 30
Figure 16. Higher coordination Ti centers in the system of TS-1/H_2O_2/H_2O (Reproduced from reference 62).....30
Figure 17. Influence of structure of reactants on reaction rate with TS-1.....31
Figure 18. Examples of Ti-silsesquioxane (Reprinted from reference 70).....35
Figure 19. Titanium centers with different connectivity on silica matrices 38
Figure 20. Oxidation of 2, 3, 6-trimethylphenol (TMP) into 2, 3, 5-trimethyl-p-benzoquinone.....39
Figure 21. Sequential additions in building block methodology.....41
Figure 22. Three different mononuclear compounds and one tetranuclear cluster used as titanium precursors.....42
Figure 23. Illustration of the [Si_8O_{12}] core structure of the [Si_8O_{12}]($OSnMe_3$)$_8$ building block 44
Figure 24. First step reactions between $Ti(OiPr)_{4-x}Cl_x$ (x = 2, 3 or 4, top to bottom) and bb 48
Figure 25. Second crosslinking (step #2) and passivation (step #3) of 2C-, 3C- and 4C-Ti (from top to bottom) 49

Figure 26. Multiple reactions in the step of methanol passivation 50
Figure 27. DRUV spectrum of TS-1, Ti-MCM-41 and amorphous TiO_2-SiO_2 (Reprinted from reference 80) 55
Figure 28. Diffuse reflection on the surface of sample powder 55
Figure 29. A core electron is excited by a X-ray photon of the proper energy 58
Figure 30. (A) Picture and schematic drawing of an EXAFS experimental setup. (B) Fluorescence sample geometry and detector. (Reprinted from reference 86) 59
Figure 31. An example of X-ray absorption spectrum of NiO (Reprinted from reference 86) 60
Figure 32. The copper plate loaded with samples and sealed with polypropylene windows 61
Figure 33. Illustration of typical absorption edges (XANES) for T_d (4-coordinated) and O_h (6-coordinated) titanium centers, and absorption shoulder from the presence of Ti-Cl. (Inset: ΔFWHM and the main edge energy) 64
Figure 34. (Top) Normalized XANES regions of 4-, 5- and 6-coordinated of Ti(IV) center in a series of metal oxide compounds; (Bottom) correlation between pre-edge feature and coordination of Ti center (Reprinted from reference 88) 66
Figure 35. (A) First (N_1) and second (N_2) shells around the absorber (N_0); (B) Single scattering paths labeled 1 (N_0-N_1-N_0) and 2 (N_0-N_2-N_0) and a triangular multiple scattering path labeled 3 (N_0-N_2-N_1-N_0) (Reprinted from reference 86) 67
Figure 36. Best fit between experimental results and computed EXAFS employing the full multiple scattering method. (Reprinted from reference 66) 71
Figure 37. (a) IR spectra of outgassed thin pellets of Ti-free silicalite (curve 1) and TS-1 with increasing Ti-content x (curve 2-5). The horizontal line represents the fwhm of the 960 cm^{-1} band for sample 2-5. (b) Intensity W of the 960 cm^{-1} IR band (normalized) as a function of TiO_2 wt% (full squares), and corresponding Raman counts (open squares) (Reprinted from reference 96) 74
Figure 38. Raman incidence and three types of excitation of photons (Rayleigh, Stokes and Anti-Stokes scattering). 74
Figure 39. Overlaid ^1H NMR spectra of (blue) $Ti(OiPr)_4$, (red) $Ti(OiPr)_2Cl_2$, (green) $Ti(OiPr)Cl_3$ 77
Figure 40. NMR spectrum of the volatiles collected after each step of synthesis 78
Figure 41. Illustration of 2C-Ti center embedded in a bb matrix 82
Figure 42. Infrared spectra of 2C-Ti, 3C-Ti and 4C-Ti in comparison with Ti-free silicon platform 83
Figure 43. Full infrared spectra of 2C, 3C, 4C-Ti and Ti-free platform 84

Figure 44. Synthesis of 2C-Ti samples and proposed structures of Ti sites (sample 1, 2 and 3) 87
Figure 45. Synthesis of 3C-Ti samples and proposed structures of Ti sites (sample 4, 5 and 6) 88
Figure 46. Synthesis of 4C-Ti samples and proposed structures of Ti sites (sample 7, 8 and 9) 89
Figure 47. DRUV spectra of 2C, 3C and 4C-1 dose (samples 1, 4, 7, at stage 1) before (top) and after (bottom) correction for tin.....91
Figure 48. DRUV spectra of 2C-, 3C- and 4C-Ti catalysts after passivation (samples 2,4,6 at stage 2) 92
Figure 49. (left) Stacked XANES region of sample 1-3 of 2C-1 dose, 2C-MeOH and 2C-H_2O_2); (right) zoomed in pre-edge peaks 95
Figure 50. Illustration of the titanium centers in 2C-Ti change from 4- to 5-coordinated 97
Figure 51. (left) Stacked XANES region of sample 4-6 of 3C-1 dose, 3C-MeOH and 3C-H_2O_2); (right) zoomed in pre-edge peaks 98
Figure 52. (left) Stacked XANES region of sample 7-9 of 4C-1 dose, 4C-MeOH and 4C-H_2O_2); (right) zoomed in pre-edge peaks 100
Figure 53. EXAFS molecular models for 2C-Ti (2 models), 3C-Ti (2 models), 4C-Ti (1 model)101
Figure 54. 2C-1 dose in χ(k) and k3-weighted R space functions with two structural models ..104
Figure 55. 3C-1 dose in χ(k) and k3-weighted R space functions with two structural models ..106
Figure 57. R space of 2C-MeOH overlaid with 2C-1 dose 111
Figure 58. R space of 3C-MeOH overlaid with 3C-1 dose 112
Figure 59. R space of 4C-MeOH, 4C-H_2O_2 overlaid with 4C-1 dose.....113
Figure 60. Titanium center in TS-1 after exposed to aqueous hydrogen peroxide 114
Figure 61. 2C- 3C- and 4C-Ti after contact with aqueous H_2O_2 (sample 3,6,9) 115
Figure 62. EXASF fitting of 4C-H_2O_2 data in k and R spaces 117
Figure 63. (a) X-ray crystal structure of [$Ti_4(\mu_3\text{-}O)_2Cl_6(\mu_2\text{-}O_2CPh)_6$] (Reprinted from reference [73]); (b) Simplified cluster structure with carbon and hydrogen atoms omitted.....121
Figure 64. Gravimetric results and hypothesized titanium centers in Ti_4O_2-bb and Ti_4O_2-POSS (blue stars symbolize -O-SnMe3 active corners on bb or POSS).....123
Figure 65. (Top) Possible tetranuclear titanium centers in Ti_4O_2-bb catalyst (all μ_2-oxygen atoms are connected to silicon atoms); (bottom) possible tetranuclear titanium centers in Ti_4O_2-POSS analogue (μ_2-oxygen atoms are connected to either carbon or silicon atoms) 125

Figure 66. IR spectra of embedded tetranuclear titanium center (absorption band of Ti-O-Si vibration) 127
Figure 67. Raman spectra of tetranuclear titanium center before and after the reaction with bb 128
Figure 68. DRUV spectra of tetranuclear titanium center before and after the reaction with bb 130
Figure 69. (Left) XANES and early EXAFS regions of Ti_4O_2, Ti_4O_2-bb and Ti_4O_2-POSS; (right) (gray pre-edge data from reference 88) coordination numbers of titanium in each material according to the position and height of pre-edge peaks 131
Figure 70. Titanium center in TS-1 interacts with H_2O_2 during catalytic oxidation 135
Figure 71. Four types of titanium centers synthesized and used for TMP oxidation 136
Figure 72. Linear relation of FID signal as a function of the concentration, biphenyl (red) and TMP (blue) 139
Figure 73. A plot of percentage of unreacted TMP vs. time 141
Figure 74. Activation of 4-connected titanium center with aqueous hydrogen peroxide 143
Figure 75. ^{1}H NMR spectrum of hydrogen peroxide with chloroform as internal standard 145
Figure 76. ^{1}H NMR peak area of H_2O_2 decreases due to decomposition t = 0, 1, 2 hour (bottom to top) 147
Figure 77. ln(Rate) vs. ln[H_2O_2] in peroxide decomposition catalyzed by 2C-, 3C-, 4C-Ti (bottom) and TS-1(top) 149
Figure 78. Free radical mechanism on titanium center with hydrogen peroxide (Reproduced from reference 72) 150
Figure 79. Recyclability of 2C-Ti catalyst in terms of conversion and selectivity 152
Figure 80. Four types of titanium centers in building block matrices: 2C-Ti, 3C-Ti, 4C-Ti and Ti_4 (surrounding -OSi bonds are omitted) 154

List of Tables

Table 1. TS-1 synthetic methodologies and parameters vs. Final Si/Ti and morphology 28
Table 2. An example of the calculation of the connectivity 52
Table 3. Elements in the expression of scattering path 69
Table 4. Synthesis and connectivity of atomically dispersed titanium catalysts 79
Table 5. Preferable [Ti : bb] ratio, molecular formula, and Ti content following insertion of titanium, second crosslinking and passivation with methanol.....80
Table 6. Elemental Analysis of 4C-Ti, 3C-Ti, and 2C-Ti passivated materials 80
Table 7. Elemental composition (Ti and Sn) before and after methanol passivation.....80
Table 8. DRUV and XAS sample list 86
Table 9. Ti K-edge parameters.....94
Table 10. Structural parameters obtained from fits to 2C-1 dose.....105
Table 11. Structural parameters obtained from fits to 3C-1 dose.....107
Table 12. Structural parameters obtained from fits to 4C-1 dose.....109
Table 13. EXAFS modeling parameters of 2C-MeOH 111
Table 14. EXAFS modeling parameters of 3C-MeOH 112
Table 15. EXAFS modeling parameters of 4C-MeOH 113
Table 16. EXAFS fitting parameter of 4C-H_2O_2 data.....118
Table 17. Ti K-edge parameters for tetranuclear titanium samples.....130
Table 18. Results of catalytic properties in oxidation of TMP to TMBQ 141
Table.19 Reaction orders obtained from ln(Rate)-ln[H_2O_2] relationship 150
Table 20. Stability of titanosilicate catalysts 152

Chapter I: Background of Single-Site Heterogeneous Catalysts

1.1 Introduction of Catalysts

1.1.1 What is a catalyst?

Chemical transformations are essential to living organisms and manufacture of most fuels, plastics and pharmaceuticals. A chemical reaction must not only be thermodynamically favorable, but also occur at a sufficient rate, to be practically useful. Reaction rate relates closely with activation barrier, i.e. the higher activation barrier, the slower reaction rate.

One way to accelerate the rates is by elevating the temperature, which enhances the kinetic energy of the reactant molecules. But high temperatures can also bring many other problems that limit the feasibility of this approach. For example, side reactions and low selectivity, decomposition of reactants, reactions that are hard to control, uneconomic and finally the cost of energy.

Alternatively, catalysts provide a more economic and effective approach to increasing rates of reaction. Interaction between catalyst and reactant essentially alters the reaction pathway, leading to lower activation barriers (Figure 1) thereby increasing the reaction rate at lower temperature. Enzymes, the best catalysts evolved from nature, work effectively at ambient temperature. For example, nitrogenase is a family of enzymes that convert inert nitrogen (N_2) in atmosphere into ammonia (NH_3), avoiding a very high uncatalyzed activation barrier (E_A = 420 kJ·mol^{-1}).[1] The subtle structures and superior functions of enzymes have inspired many innovative studies in fields such as biocatalysis and organometallic chemistry.[2] Today, over 90% of the commercially produced chemical products worldwide depend on catalysts, equivalent to nearly one trillion USD in products annually. The demand for catalysts, covering almost every aspect of modern society, was valued at approximately 29.5 billion USD in 2010. These numbers are expected to grow rapidly and continuously.[2]

The growing chemical and materials markets demand not only larger scale production but, more importantly, catalysts with superior performance. Compared to biological catalysts, current synthetic analogues are quite primitive in terms of both structure and function, indicating the tremendous potential for the development of new and better catalysts. Take the same example of nitrogen fixation. Instead of the mild conditions needed for nitrogenase, severe conditions (720-820 K and 30-70 MPa) are required for the industrial equivalent. The catalyst

used represents metallic iron with small additions of potassium oxide and alumina, which has undergone no fundamental changes since its invention in 1918.

It is clear that any improvements on catalytic performance can lead directly to lower cost of energy, raw materials and even reduced environmental impact. Strategic design, preparation and implementation of catalysts is the way to accomplish these goals. Fundamentally, designing new and improved catalysts requires deep knowledge of the structure and working mechanism of catalysts.

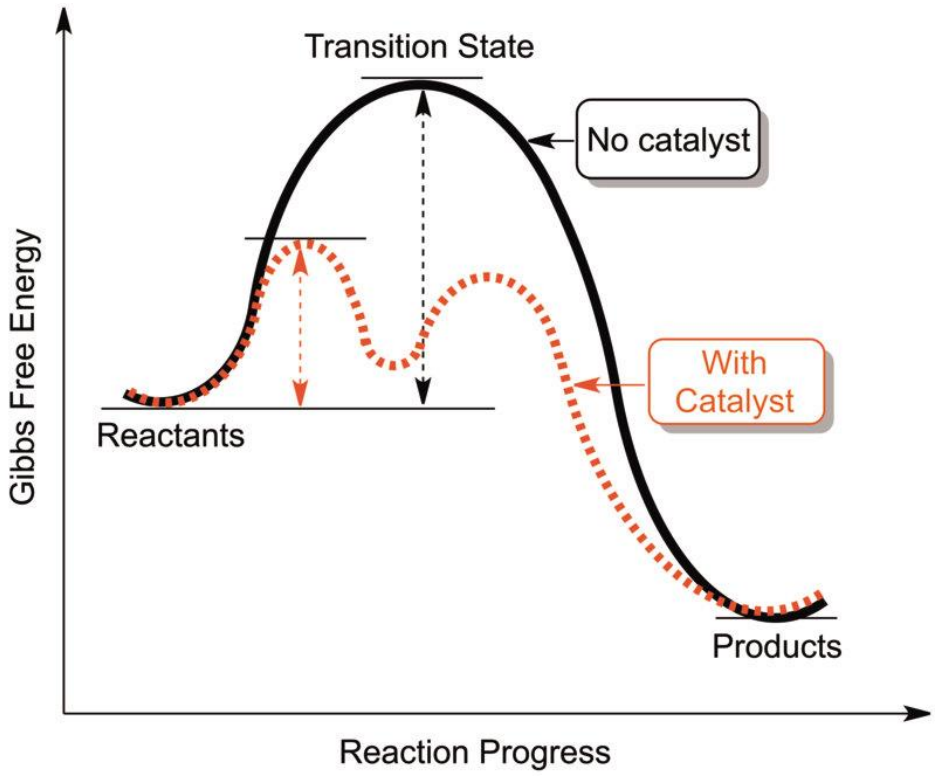


Figure 1. An alternative reaction pathway with lower activation barrier created by the catalyst

1.1.2 Evaluation of catalysts

Improving high catalytic performance is a major driving force in developing catalysts. Catalytic activity and selectivity are perhaps the most important properties of a catalyst. Catalytic activity may be quantitatively expressed as turnover number (TON) and turnover frequency (TOF). TON is defined as number of reactant molecules reacted per catalytic site. TOF is TON per unit time. Initial TOF and average TOF are commonly used to characterize the speed of catalytic reaction.

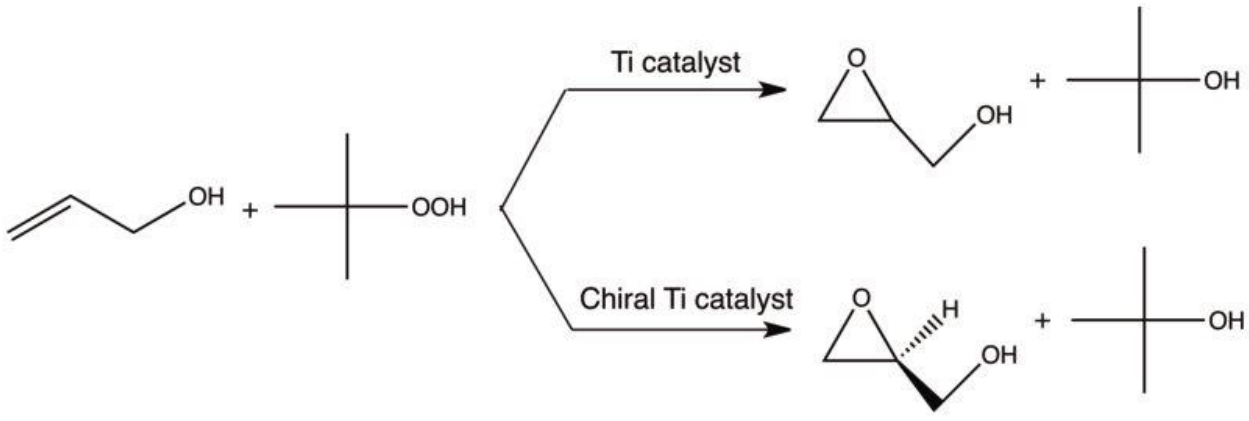
$$TON = \frac{\text{reacted reactant (mol)}}{\text{catalyst (mol)}}$$

Equation 1-1

$$TOF = \frac{TON}{\text{time (min)}}$$

Equation 1-2

The selectivity exhibited by a catalyst can also be of several different types, chemoselectivity, regioselectivity, enantioselectivity, etc. When more than one product is possible, design of optimal catalyst promotes the reaction with a strong preference toward a single desired product, enhancing the selectivity. Scheme 1 shows the epoxidation reaction between allyl alcohol and tert-butyl hydroperoxide (TBHP). The top reaction is an example of regioselectivity. Ti(IV) tetraisopropoxide and several titanosilicates [3-5] catalyze epoxidation of alkene rather than oxidation of the alcohol present. The product of glycidol contains two enantiomers. The bottom reaction of Scheme 1 illustrates the Sharpless asymmetric epoxidation catalysis. Enantioselective epoxidation can be achieved in high yield by using the Ti-tartrate system, i.e. $Ti(OiPr)_4$ with (+) or (-) dialkyl tartrate (DAT).



Scheme 1. Regio- or enantio-selectivity in epoxidation of allyl alcohol with Ti catalysts

Recyclability of catalysts is another important aspect of a catalytic process. The first step in recycling a catalyst is to separate the catalyst from the reaction solution. Separation is usually much easier with heterogeneous than homogeneous catalysts, as will be discussed in section 1.1.3. Following separation, good stability and reusability are desired so that the catalyst may be recycled as many times as possible. Poor recyclability increases the cost particularly when expensive metals such as platinum and rhodium are involved.

Depending on the individual catalytic system, other factors such as macroscopic diffusion, susceptibility toward poisoning and catalyst life must also be taken into consideration. In heterogeneous catalysis, for example, the macrosopic size and shape of the catalyst particles is relevant for properties such as pressure drop, mechanical strength and attrition resistance. Mesoscopic properties such as specific surface area and porosity affect the intraparticle mass transfer of the catalysts. In summary, catalytic activity, selectivity, recyclability as well as other properties need to be carefully evaluated. These parameters are crucial in optimizing the catalyst and catalysis conditions, and in understanding the catalytic mechanism.

1.1.3 Homogeneous catalysts

A catalytic system is defined as homogeneous or heterogeneous catalysis based on the number of phases present. Homogeneous catalysis is a mono-phase process in which all reactants and catalysts are in the same phase, typically a liquid or gas. These catalysts are soluble in the solution, and often take the forms of discrete metal complexes such as metallocene complexes, Cp_2MCl_2 (M = Ti, Zr, Hf). (left in Figure 2)

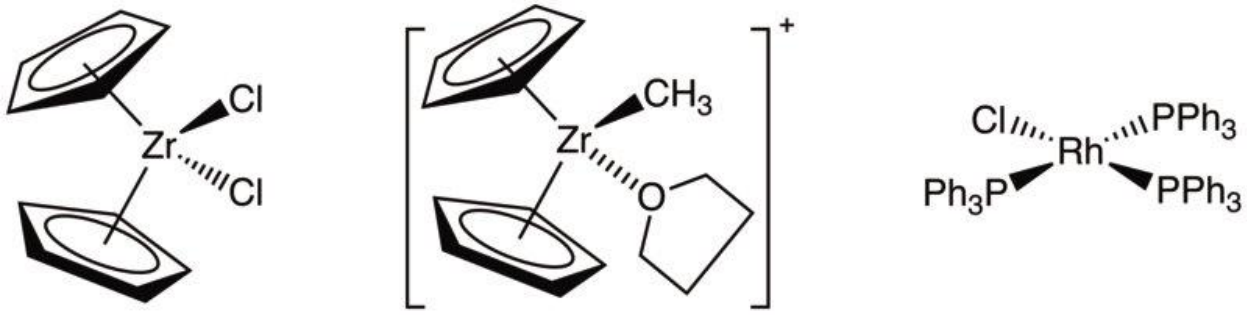


Figure 2. Homogeneous catalysts in forms of discrete metal complexes

Homogeneous catalysts are generally molecular complexes composed of a metallic core (mono- or poly-nuclear) and coordinating ligands. The metallic core is frequently the site where the catalytic transformation takes place. As illustrated in Figure 3, a typical catalytic cycle involves a series of reactions, such as oxidative addition, reductive elimination, insertion, -elimination. The choice of ligands in a catalyst ensemble is also crucial in many ways, such as: (1) modulation of the electron density on the frontier atomic orbitals centered on the active atom(s) with LUMO and HOMO character; (2) control or preservation of the geometry of the site (in terms of structure, number, and location of the metal atoms and of coordinative vacancies) during the catalytic cycle; (3) cooperative activity in the diffusion of the reactants from and to the active center. The ease of synthesis and characterization makes it convenient to adjust the molecular structures and, what is more important, to understand the catalytic performance at a molecular level, i.e. kinetics and mechanisms of catalytic cycle, key intermediates, etc. for homogeneous catalysts.

Homogeneous catalysts dominate the production of many industrially valuable chemicals, such as acetic acid, alcohols, plastics, high-performance polymers, fine chemicals, etc.. The production processes cover a variety of chemical reactions, such as carbonylation, hydrocarboxylation, hydroformylation and polymerization. The commercial success of homogeneous catalyst is associated with high selectivity that is available through optimized catalyst structure and catalysis process.

On the other hand, some disadvantages prevent homogeneous catalysts from broader application. The upper temperature limit for homogeneous catalysis is approximately 250 °C and is limited either by the boiling point of solvent or the thermal stability of catalyst. Therefore, homogeneous catalysts are rarely applied to high-temperature processes such as those involved in refining crude oil. Difficult recovery of catalysts and short catalyst life also add up the cost in practical applications for homogeneous catalysts.

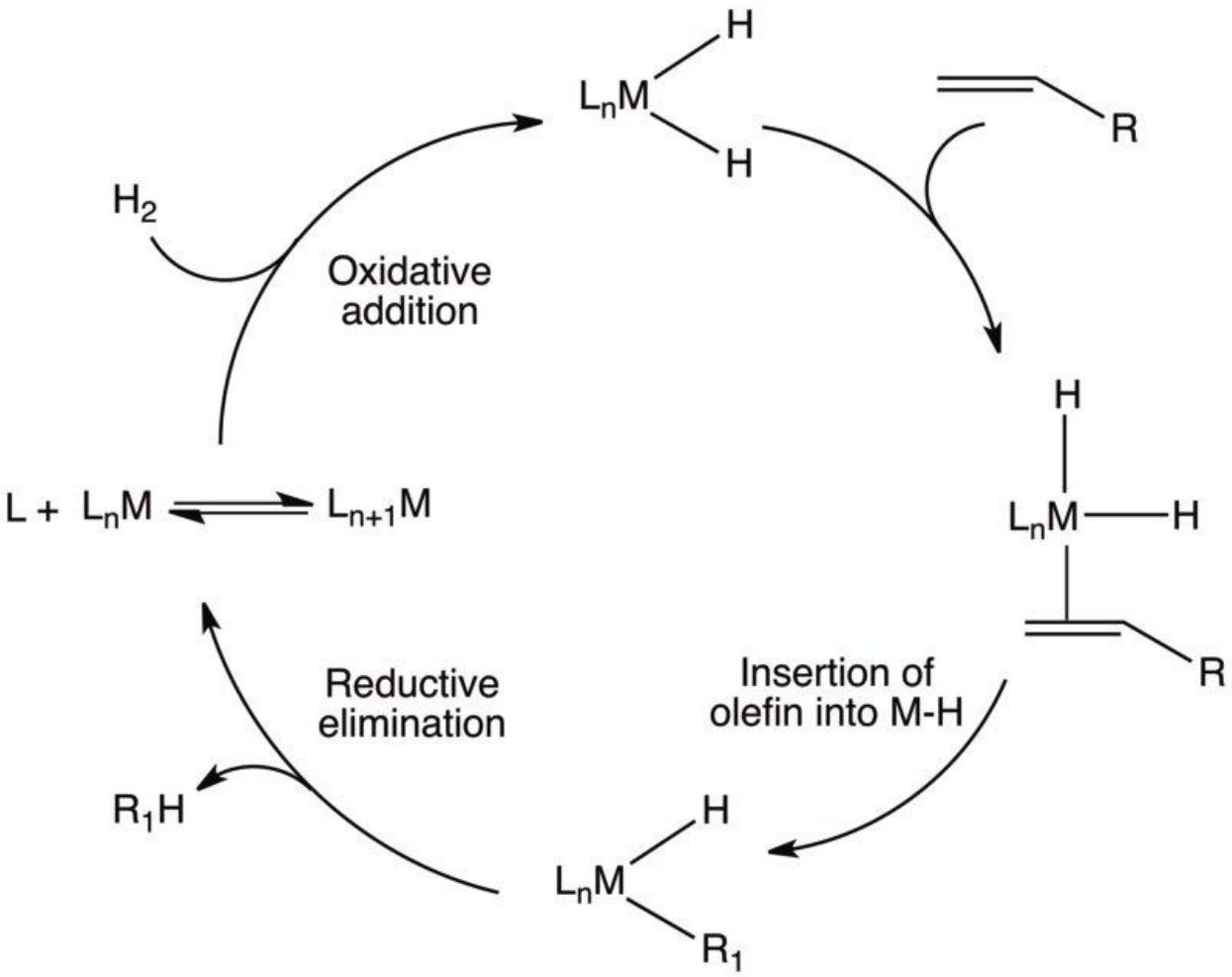


Figure 3. Catalytic cycle of alkene hydrogenation (M= metal; L_n= coordinating ligands)

1.1.4 Heterogeneous catalysts

In heterogeneous catalysis, reactant and catalyst exists in different phases. Common combinations are: (1) solid catalysts + gas reactants; (2) solid catalysts + solution reactants; and (3) catalysts and reactants dissolved in immiscible solvents. A common form for heterogeneous catalysts is an insoluble solid support that has a large array of ions or atoms on the surfaces onto which catalytic active species such as metal-containing precursors are incorporated through various synthetic methods.

For heterogeneous catalysts, the microscopic length scale involves the composition of the supported particle, the surface structure of the supporting matrix and interaction between the two phases. All these factors determine the intrinsic activity and selectivity of the catalysts. As a matter of fact, most heterogeneous catalysts are characterized by a spectrum of supported catalyst species, the size of which can vary over a wide length range. Typically these sites include small crystallites of the precursor and nanoparticles which interact extensively with surface functionality. In a few cases large particles (>50 nm) are designed for better activity. For example, ethylene epoxidation calls for supported silver particle larger than 100 nm.[6] A number of nano-scale (1 - 50 nm) supported particles have exhibited enhanced catalytic activity.[7, 8] Titania supported gold particles with diameter between 2 - 3 nm exhibit superior catalytic activity in oxidation of CO to CO_2.[7] Varying particle size of supported nickel changes the adsorption/dissociation energy for CO, and thereby affects the activity in Fischer-Tropsch synthesis of hydrocarbon from synthesis gas.[8] These phenomena can be partially explained by changes in surface structure, electronic properties and interaction between supported phases and supports.[9] Finally precursor molecules can adsorb individually, exchanging ligands with surface groups to form atomically dispersed active metal sites. Although many factors should be taken into account, theoretically, these atomically dispersed active centers share similar catalytic properties with their homogeneous analogue, which is drastically different from the bulk materials. In practice, the superior properties of atomically dispersed catalysts have been confirmed in some cases. The best example may be the isolated titanium(IV) centers in crystalline titanium silicalite-1 (TS-1) are responsible for a number of selective oxidation and solid-acid reactions.[10] Even if only one surface species were to be present, heterogenous surface functionalities can lead to a distribution of active sites (Figure 4).

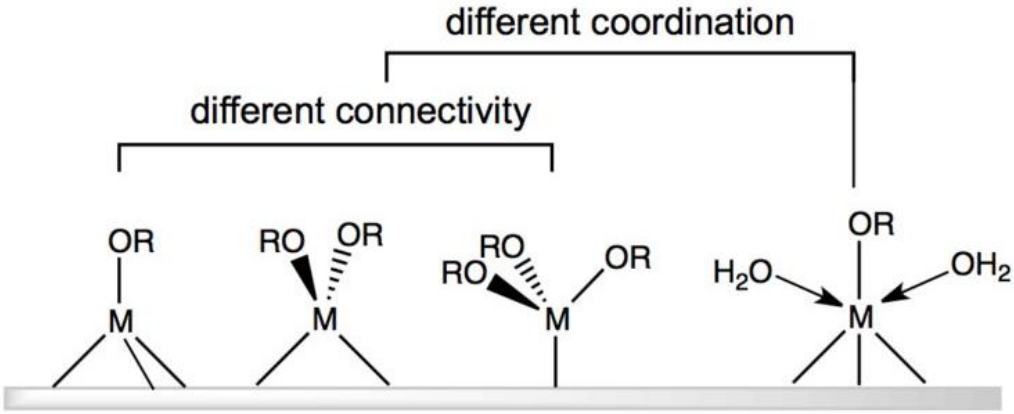


Figure 4. Hypothesized structures of isolated metal centers on a supporting matrix

Heterogeneous catalysts exhibit a number of properties that are crucial in terms of large scale industrial production. The most important amongst others are the excellent thermal stability and easy recovery that requires no more than filtration or decantation, significantly lowering the cost in application. For these reasons heterogeneous catalysts have been widely employed in the petrochemical industry, creating tremendous dollar value annually. Fundamental refining of crude oil almost entirely depends on heterogeneous catalysts. To convert heavier fractions in crude oil into high-octane gasoline, initial hydrodesulfurization employs alumina-supported cobalt molybdenum sulfide as the catalyst, followed by reformation process that involves acidified alumina-supported platinum and rhenium. Catalytic processes like these coverts 90% of the crude oil into various kinds of fuels. The final 10% provides raw materials for many downstream chemicals, in which heterogeneous catalysts also play an important role. Mixed metal oxides and rare earth exchanged aluminosilicates catalysts are commonly used in steam reforming and cracking reactions, producing synthesis gas ($CO + H_2$) and other small fragments of hydrocarbons.[2, 9]

The catalytic activity and selectivity of heterogeneous catalysts relate closely to their intrinsic microscopic structure. The number of catalytic species on the supported phase, relative to total area of the supporting phase, needs to be small enough to ensure site isolation and avoid aggregation but at the same time high enough to exhibit high activity. However, even when starting with single type of catalytic precursor, most heterogeneous catalysts end up having multiple types of sites by the end of synthesis. Traditional synthetic methods for the preparation of heterogeneous catalysts often generate a number of inaccessible and/or inactive

supported centers. It is generally believed that only a small percentage of the supported centers remain active after incorporation onto the surfaces of many supports. The density of active centers is thereby greatly diminished, in other words, lower catalytic activity per unit mass catalyst. Further, different types of centers, i.e. connectivity, coordination and nuclearity, may be present, each exhibits different energetics, activity and selectivity. The multisite nature of traditional catalysts has resulted in disadvantageous characteristics and catalytic properties. As a result, the catalytic activity and selectivity of heterogeneous catalysts is generally lower than that of its molecular homogeneous analogue.

The characterization of structures of heterogeneous catalysts is also challenging, which essentially limits the understanding and development of these materials. Standard techniques frequently fail to selectively characterize the catalytic centers within the broad matrix of sites present. Instead structural information, primarily about the catalytic centers, is usually collected through a combination of advanced spectroscopies and techniques. The lack of knowledge specific to the catalytic active centers makes it rather difficult to control and tailor their corresponding catalytic performances.

In terms of improving performance of heterogeneous catalysts, one of the central topics is to investigate the microscopic structure that is related to their catalytic behavior. Advances in characterization methods such as X-ray adsorption spectroscopy (XAS) and electronic microscopies (SEM, TEM) have contributed to an understanding of the structure-activity relationship at a molecular-level. On the other hand, new synthetic strategies are needed to target a specific structure and develop a clear correlation between that structure and desired catalytic performance.

1.1.5 Preparation of heterogeneous catalysts

Current progress in the development of heterogeneous catalysts depends, to a high degree, on the evolution of synthetic methods. The first solid catalysts were comprised of active metal catalyst phase and supports available from nature, for example, Bauxite (a type of aluminum ore) and “kieselguhr” (a natural silica support material).[2] Since then, various supported catalysts have been synthesized with increasingly better control of the structure, including particle size, dispersion, porosity, local coordination sphere around catalytic center and etc..[9] In the catalyst manufacturing, the supporting phase is synthesized, shaped and subsequently loaded with active species. For the last couple decades, nanostructured carbon and silica materials have served as common supporting phases in a wide variety of new

catalysts, such as carbon nanotubes, and mesoporous silicas MCM-41 and SBA-15.[11, 12] Various methods of binding active metal to supports have been employed to control surface structures at certain stages of the synthesis, as is described in the following sections.

1. Electrostatic adsorption and Ion exchange

The two methods, electrostatic adsorption (EA) and ion exchange (IE), share similar reactants and comparable reaction conditions. In both methods, water-soluble metal salts are used as the precursors. Metal cations replace charge-compensating ions on the surface of supports, and afterwards counter ion byproducts and excess solution are washed away. These two methods are best demonstrated in the preparation of cation-exchanged zeolitic materials. Zeolites represent a family of three-dimensional microporous aluminosilicates with superior cation-exchange capacity. Distinct mechanisms are followed by IE and EA in the uptake of cations into silica supports. Ion exchange is a pH independent process, in which incorporated metal ions replace framework Al(III) in a stoichiometric fashion.[13] In contrast, electrostatic adsorption is strongly pH dependent. The metal cations interact with the surface silanols (≡Si-OH) instead of the Lewis acidic sites, and the exchange capacity does not always match the stoichiometric ratio between proton and metal cation.[13, 14] When both mechanisms occur simultaneously, zeolites are “over-exchanged” and two types of adsorbed metal species are formed (Figure 5).[15] To obtain the uniformity of catalytic sites, the use of high Al content zeolite and acidic reaction conditions can inhibit the EA pathway to where it becomes negligible. However, it is worth mentioning that multiple types of catalytic sites are still likely to form, because of the varying local environments around framework Al(III) atoms where IE occurs.

2. Deposition-precipitation

Ever since being patented in 1943, deposition-precipitation (DP) has been applied as a generic method to obtain metals, metal oxides, metal sulfides or metal hydroxides as small particles onto a solid support. Soluble metal precursors are introduced into a suspension of a supporting material like silica, at the surface of which metal-containing precipitates forms exclusively.[16] The presence of the support stabilizes the precipitate thermodynamically. Moreover, the interaction of precipitate with support lowers the surface free energy of small particles, which otherwise inhibits the precipitation.

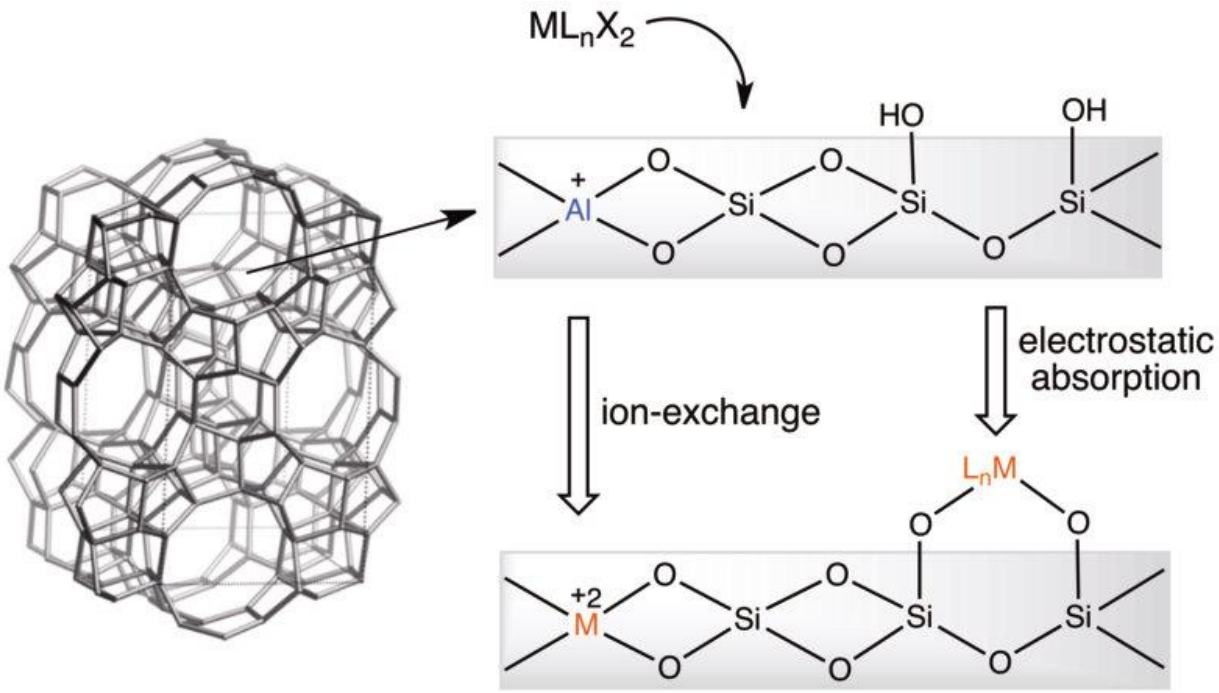


Figure 5. Metal sites deposited on zeolite (ZSM-5) surface by different mechanisms.

The choice of method to bring about precipitation depends on the particular metal species and the type of support. One method involves increasing pH through the addition of an alkaline solution or the hydrolysis of urea. Hydroxyl ions then react with metal cations, forming metal hydroxide precipitates. (Equation 1-3 and 1-4) A second general method involves reduction of solvated metal ions to metal, metal oxide or hydroxide. A reducing agent such as formaldehyde is added to the suspension of silica supports and metal cations, causing deposition of small metal particles on the silica support. (Equation 1-5) With metals of multiple oxidation states, some studies reduced high valent metal with hydrazine and brought about deposition of metal oxide or hydroxide. (Equation 1-6) Lastly, catalytically active metals may be adsorbed onto the surface by removing stabilizing ligands through evaporation or oxidation. Ligands such as ammonia and ethylenediamine tetraacetic acid (EDTA) can stabilize metal cations through coordination and avoid aggregation. Removal of these ligands effectively initiates the deposition process.

$$CO(NH_2)_2(aq) + 3H_2O \longrightarrow CO_2(g) + 2NH_4^+(aq) + 2OH^-(aq)$$ Equation 1-3

$$Ni^{2+}(aq) + 2\ OH^-(aq) \longrightarrow Ni(OH)_2(s)$$ Equation 1-4

$$2\ Ag(NH_3)_2^+(aq) + HCHO(aq) + 3OH^-(aq) \longrightarrow 2\ Ag(s) + 4\ NH_3(aq) + HCOO^-(aq) + 2\ H_2O$$ Equation 1-5

$$4\ MoO_4^{2-}(aq) + 3\ N_2H_4(aq) + 4\ H_2O \longrightarrow 4\ Mo(OH)_3(s) + 3\ N_2(g) + 8OH^-(aq)$$ Equation 1-6

Generally, DP generates thermally stable catalysts that have high metal loadings and relatively narrow particle-size distributions. The highly reproducible procedure makes it one of the high-throughput methods in industry. On the other hand, it is difficult to control the rates of nucleation and precipitation that determine the deposited crystal size.

3. Impregnation and drying

As the name indicates, two primary steps are involved in this approach to catalyst synthesis. The initial step is called impregnation, during which the precursor solution is introduced into the voids of the support where adsorption occurs. Afterward, a drying step is taken to eliminate the solvent. This synthetic method has been the favorite of the industry as

well as at a laboratory scale, because of its convenient operation and complete deposition of the precursors.

Depending on the different procedures, some common types of impregnation are: (1) Dry or incipient wetness impregnation involving either a dried or water-vapor-treated support. The key is to control the volume of precursor solution to equal the pore volume of the support. (2) Wet impregnation: The support is filled with water, sometimes prior to which water-soluble gas like ammonia is used to replace the air inside the pores. The actual impregnation is carried out under diffusional conditions, when the water-filled support is immersed in an excess amount of precursor solution. (3) Two-solvent system: Based on dry impregnation, this method also benefits from using small amounts of precursor solution, but moreover, the reaction can be stirred in a liquid phase. The difference is made by suspending the hydrophilic support in an organic solvent before adding the aqueous precursor solution.

The main drawback of impregnation approaches to catalyst synthesis is the lack of control in the final distribution of the active phase which largely depends on the morphology and surface structures of the pre-made support. It is very difficult to achieve a homogeneous distribution especially when the industry prefers the supports in the form of extrudates or pellets rather than powders. Moreover, the drying step can change the deposited active sites in many ways. The temperature required for drying is up to the boiling point of the solvent, and in some cases lower for gentle drying. High temperature can cause thermal elimination of active species other than the solvent, or other detrimental chemical reactions to happen. Meanwhile, the speed of drying also plays a role in the final composition. It is known that instead of uniform composition, egg-yolk or egg-shell types of structures result from various conditions of impregnation and drying. [17]

4. Sol-gel processing

All three methods above deal with the incorporation of catalytic active species onto the pre-made supporting materials. One unmentioned issue is to control the structure/texture of these supports critical to the catalytic properties. The sol-gel method has been successfully adapted to the preparation of xero- and aerogel materials. Porous materials such as silica and alumina are perfect candidates in terms of incorporating catalytic active species. Furthermore, sol-gel processing has also been used in synthesis of various catalysts, for example, mono- or multi-metallic monophasic oxides, and catalysts with adsorbed or entrapped active species. Figure 6 illustrates the general process of sol-gel method in preparing solid materials.

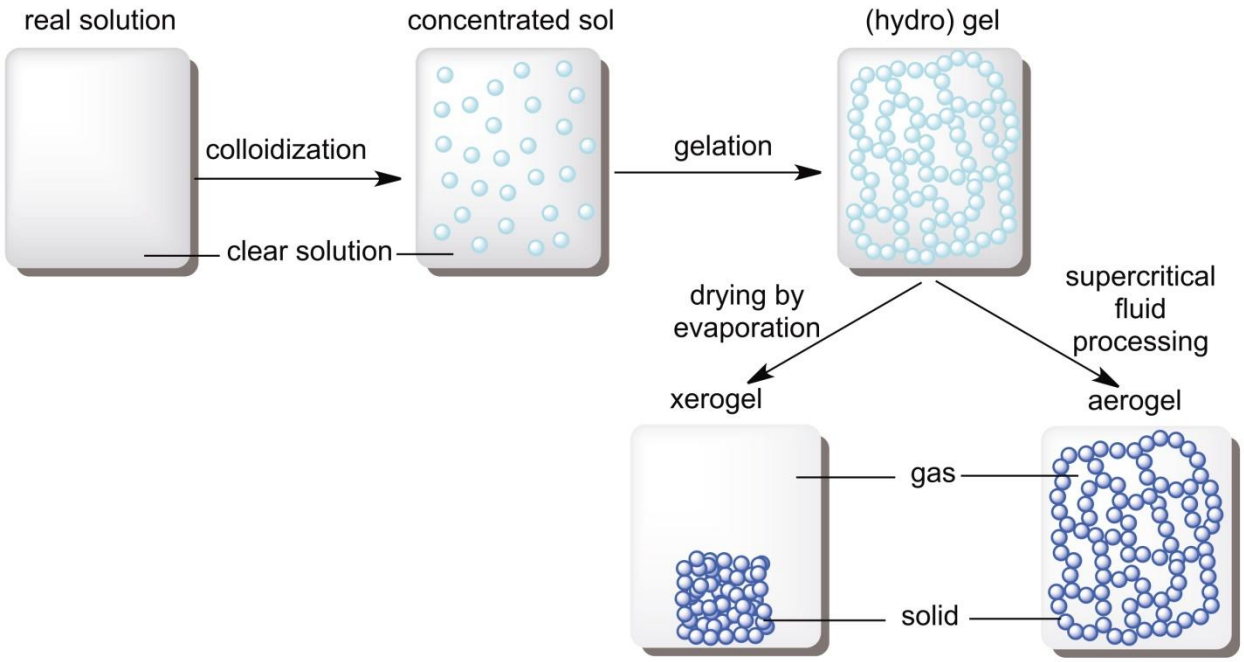


Figure 6. Sol-gel processing in the preparation of solid materials

It is featured by the formation of stable colloidal solution (sol), followed by anisotropic condensation of colloidal particles (micelles). During the step of gelation, polymeric chains in the form of (hydro) gels are formed by chemical bonding between functional groups at the surface. Finally, xerogels or aerogels with high porosity and surface area is produced depending on the drying method of choice. The condensation part of chemistry is traditionally accomplished by hydrolytic reactions, i.e. hydrolysis of hydrated metal ions or metal alkoxides.[18] More recently, nonhydrolytic sol-gel processing has begun to develop, which is based on reactions such as esterification of metal chelate complexes[19], and direct condensation between metal alkoxides and metal chlorides or acetates.[20, 21]

5. Hydrothermal synthesis

Hydrothermal synthesis is often combined with sol-gel, templating or other synthetic techniques to prepare crystalline materials like zeolites and some mixed-metal oxides. The method is characterized by the use of water and high temperature above 100 °C that enhances crystallization. The most well-known product by this method is the family of synthetic zeolite materials, each of which has distinct pore size, architecture and chemical composition. It is reported that over thirty elements can be incorporated with zeolites, potentially leading to a large number of catalysts.[22] Initially a supersaturated solution is made with silica source (e.g. tetraethyl orthosilicate, TEOS) and alumina source (e.g. aluminum alkoxide) in the presence of structure directing agent (SDA) such as tetraalkylamines. Once the mixture forms a hydrogel or precipitate, the mineralizing agent (alkali salts, OH^-, F^-, etc.) is added as a catalyst to convert the gel/precipitate into what is referred to as the precursor species. Based on the classical crystallization theory, the precursors assemble into nuclei in the basic solution and subsequently grow into crystals over hours/days.[23] Preparation of some other crystalline oxide-based materials also involves hydrothermal treatment, for example, the titanium silicate (TiO_2-SiO_2) catalysts prepared by Corma *et al.*.[24]

1.2 Single-Site Heterogeneous Catalysts (SSHCs)

1.2.1 Introduction

During the last two decades, strategically designed single-site heterogeneous catalysts (SSHCs) have attracted much attention in both academic and industrial research. It has been discovered that decreasing particle size can lead to significant enhancement in catalytic activity. [7, 25, 26] This discovery directed researchers naturally to the design of molecular and atomic level catalytic centers. As mentioned previously, the inhomogeneity of catalytic centers is considered the main reason for low selectivity of heterogeneous catalysts. Therefore, a current goal in catalysis science is to have structurally identical catalytic centers on the supporting matrix, so that selectivity and recyclability can be achieved simultaneously. From the fundamental point of view, there are also further benefits associated with SSHCs. One major benefit would be the possible in-depth kinetic and mechanistic study of catalytic turnover, which is very difficult with traditional solid catalysts that contain a variety of sites. Further, the catalytic activity can be evaluated on a per site basis and compared with corresponding molecular analogues, which is essential in order to establish structure-function relationships and to direct the design and synthesis of new catalysts with enhanced performances.

J. M. Thomas *et al.*[27] suggests that "single site" in the context of heterogeneous catalysts should satisfy the following criteria, mainly focusing on the catalytic active centers: (1) Each active center is spatially isolated and does not cross-talk with one another in any forms; (2) Each has the same energy of interaction between it and a reactant; (3) Each may have one or more atoms, but all sites must be identical and have well-characterized structure.

According to most definition of single-site catalysts, enzymes are the true single-site catalysts. In this context, enzymes may be pictured as discrete nanoscale entities in a fluid phase like water. Their active center frequently consists of a metallic core surrounded by ligands that completely define the coordination sphere, which as a whole interacts with the small molecules in a single particular manner. In terms of synthetic heterogeneous catalysts, isolation of the sites remains a central concern, as most traditional synthetic methods do not address the problem of thermodynamically favorable aggregation of nanoscale particles.

1.2.2 Four principle categories and synthesis

Strategies have been developed over the years to synthesize numerous SSHCs, of which many have played an important role in academic research as well as in industrial

chemical processes. Four categories of SSHCs based on final forms of deposited catalytic species have been explicitly summarized by J. M. Thomas *et al.*[27] Despite many distinct types of catalytic species, the majority of SSHCs rely on the high-surface-area supports that are generally porous silica or metal oxides. Dozens of kinds of silicate materials have been synthesized since the early 1990s. Those are characterized by high surface area (up to 2500 m^2/g), ordered mesoporous structures with tunable pore sizes (diameter of 2 - 50 nm) with uniform distributions. In addition, silanol (Si-OH) groups on their surfaces are reactive toward the metal precursors, as well as can be functionalized prior to deposition for various purposes.[28]

The following section is a brief outline of some common synthetic methods in use for preparing single-site heterogeneous catalysts and representative examples.

1. Isolated ions, atoms, molecular complexes anchored on high-area supports

Ions: Metallocene and metal alkoxysiloxy species, $M[(OSi(OR)_3]_n$, are perhaps the most common precursors in grafting transition-metal ions onto the silica surfaces. Covalent bonds form between the metallic center and residual pendent silanol groups, followed by calcination for removal of the organic groups on the metal precursor. Numerous supported metal centers, including Ti(IV) (Figure 7) [29, 30], Mo(VI) [31-33], Fe(III)[34], Cu(I)[35], Cr(VI) and VO(IV)[36], have been reported. While dispersed mononuclear sites are often desirable, polynuclear ones are likely to form in most syntheses. Generally, the amount of metal precursor needs to be small enough to ensure site isolation and avoid the formation of M-O-M bridges, which limits the loading of active components. Nickel-exchanged zeolite (ZSM-5) has been recently studied and proposed with two types of sites, Ni(II)-O-Ni(II) and Ni(I) (Figure 8). [37] In this case, an initial step of reduction reaction is required to obtain uniformly Ni(I) sites.

Atoms: Single Pd atoms on the surface of thin film MgO has been synthesized by quadrupole mass-spectroscopy assisted chemical vapor deposition (CVD) and found to exhibit unique catalytic activity in cyclotrimerization of acetylene.[38]

Molecular complexes: Supported molecular species instead of ions or atoms are desired when the metal precursor, usually catalytically active in the molecular form, has non-symmetric local environment that plays a role in the catalytic process. The molecular species can be grafted or tethered onto the surface of the supports. Some examples are microcrystalline α-$TiCl_3$ Ziegler-Natta catalysts (chloride ion vacancy), and sulfated alumina supported $M(C_5Me_5)_2(CH_3)_2$ (M = Zr or Th) and $TiCp_2(CH_3)_2$.[39]

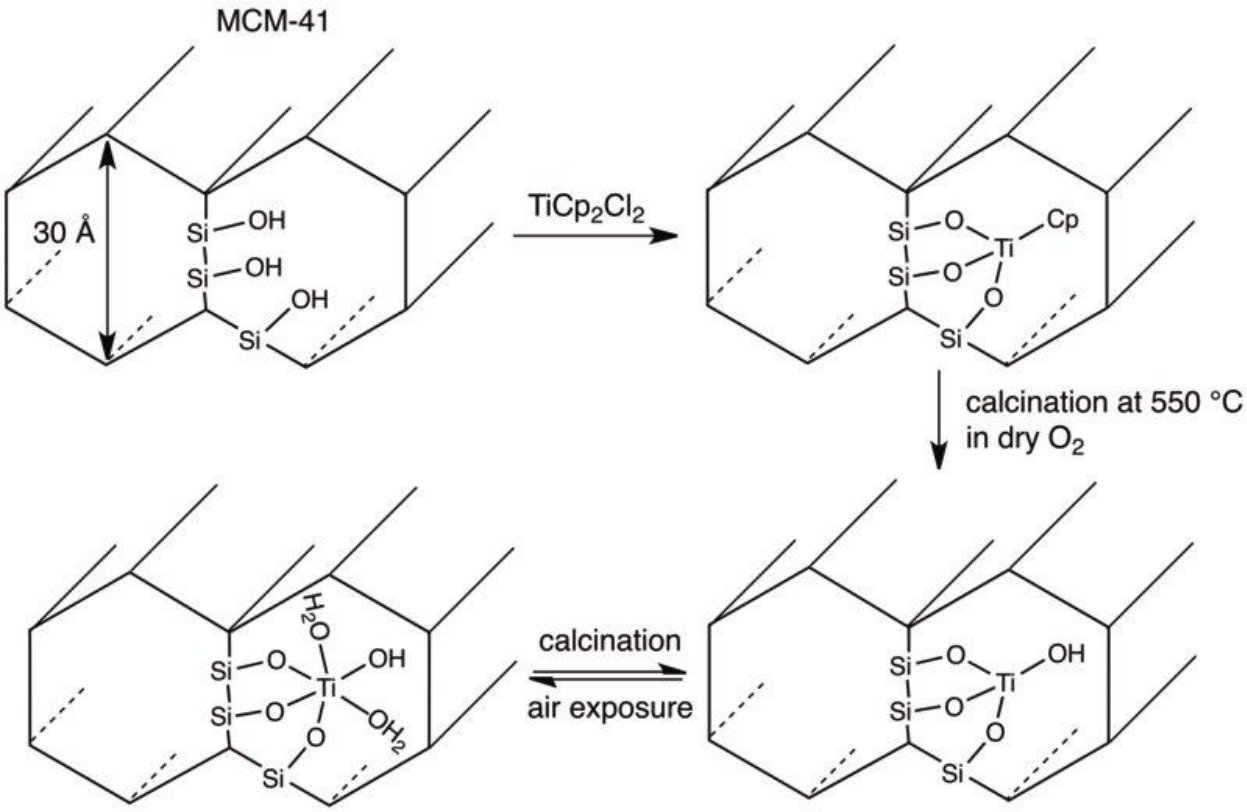


Figure 7. Grafting titanium(IV) centers on silica MCM-41.

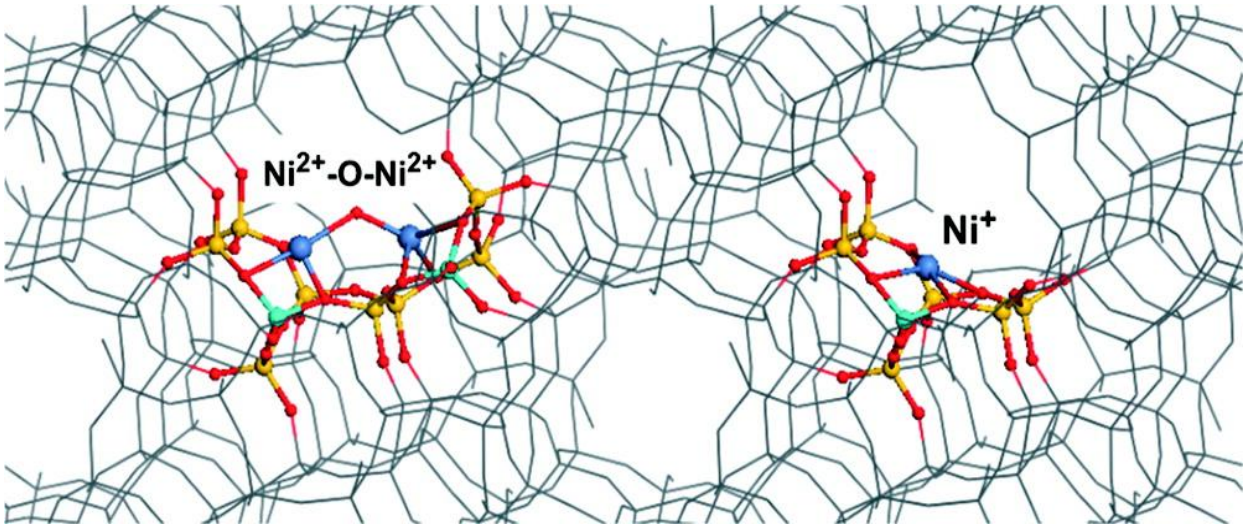


Figure 8. Localization of Ni(II)-O-Ni(II) and Ni(I) sites within the channel of zeolite. [Ni (dark blue), Al (light blue), O (red), Si (yellow)] (Reprinted from reference 37)

In any case, compared to the molecular precursors, similar or even better catalytic activity has been observed in the supported catalyst because of the effective site isolation and unchanged local environment around each metal center.

2. Organometallic chiral catalysts

Organometallic chiral catalysts refer to those with constrained geometry, specifically the chiral or enantiomeric organic species tethered on concave silica supports (Figure 9).[40] Enhanced catalytic performance compared to the molecular species has been observed and explained by the confinement effect on the orientation of the reactant relative to the catalytic center.[41] "Spacer" molecules such as tri-alkoxysilane, sulfonate and triflate (Figure 9 and 10) [40, 42] are also used to modify the silica surface. The surface silanols are passivated prior to the grafting of metal precursor. In this manner, the metal precursors are tethered only to the modified anchoring sites and kept from interactions with the silica surface or one another.

3. Ship-in-bottle catalysts

As the name indicated, ship-in-bottle catalysts are encapsulated species inside the interconnected micropores of zeolites, without necessarily any interaction with the support surface.[43] The absence of covalent bonds between catalyst and support causes the least disruption to the catalytic center compared to grafting or tethering, which is crucial especially in the preparation of enantioselective catalysts.[43] More importantly, the metallic centers are effectively isolated within the pores, inhibiting deactivation due to dimerization or other side reactions.[44] Ship-in-bottle synthesis is also utilized to prepare immobilized enzymes, which exhibits excellent recyclability (>1000 cycles).[45]

The internal voids within tridirectional zeolites such as faujasite X and Y are interconnected via smaller cavities (apertures) with a diameter of 3, 5, or 7 Å. (Figure 11). [46] To encapsulate the active catalyst, the building blocks of the catalyst are dissolved in a proper solvent and diffuse into the zeolite pores by impregnation. The catalyst is then assembled within the pore, typically in the form of a metal complex that consists of a metal center and stabilizing ligands such as porphyrin or bipyridine. The size and bulk of the complex makes it impossible to diffuse out of the apertures. In catalytic reactions, these zeolite supercages exhibit shape-selectivity, i.e. only small enough reactants can diffuse through the apertures and approach the catalytic center.[47]

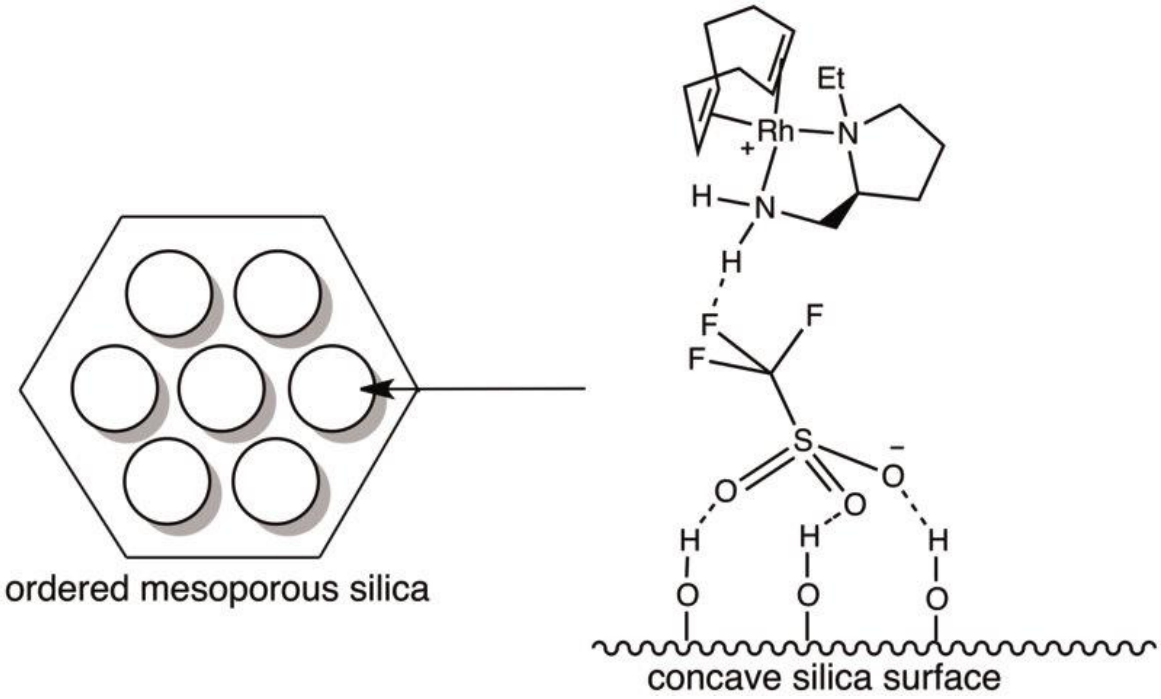


Figure 9. Chiral Rh(I)-based cation tethered on silica surface through triflate counter ion

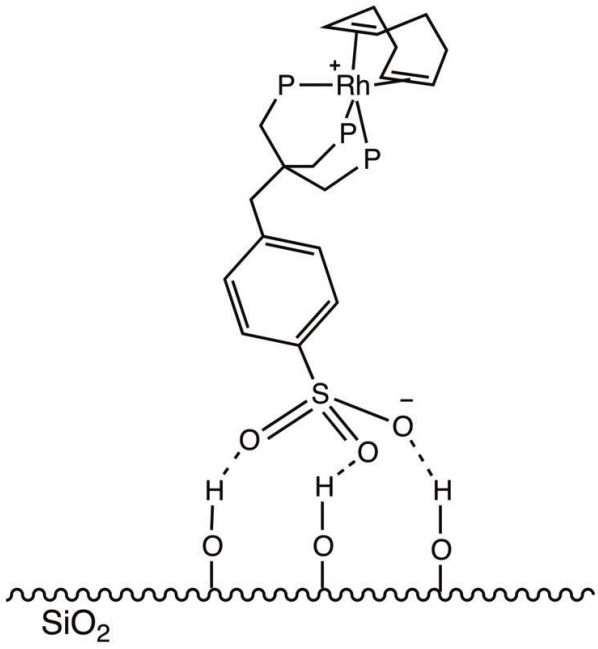


Figure 10. Rh(I)-based cation tethered on sulfonate-modified silica

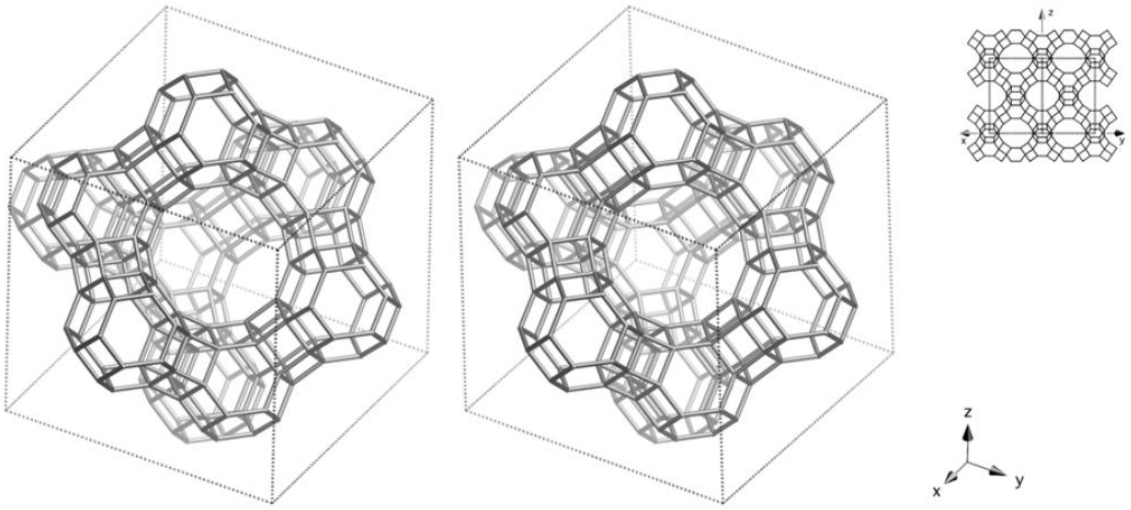


Figure 11. Supercage structure in faujasite zeolites.

The major drawback of encapsulation is the difficulty in removing any unreacted species or byproducts during the formation of metal complexes, which could generate inactive catalytic sites.

4. Open-structure solid catalysts

Open-structure aluminosilicates, aluminophosphates (AlPOs), framework-substituted silicates and MAlPOs (M = Mg, Co, Mn, Zn, etc.) are also representatives of uniform heterogeneous catalysts. A number of metal-substituted porous crystalline materials have been prepared mostly with ion exchange and impregnation syntheses. Highly dispersed atomic metal sites have exhibited unique catalytic activity and selectivity, compared to metal oligomers or bulk materials. After framework substitution, calcination is often involved to stabilize the crystalline structure, and the final products often show exceptional hydrothermal stability in catalysis. For example, the widely used selective oxidation catalyst titanium silicalite-1 (TS-1) is based on ZSM-5 silica framework, in which some tetrahedral Si are isomorphously replaced by Ti(IV) up to a limited percentage (~2.5 wt% Ti). More details concerning this catalyst are presented in section 1.3.2.

1.3 Titanosilicate Catalysts

1.3.1 Development of titanosilicates

Before titanosilicate catalysts, aluminosilicate zeolites exhibited shape-selectivity depending on the variety of available zeolitic lattices, and catalytic activity from the isolated Lewis acidic centers. The success of aluminosilicate brought some major breakthroughs in industrial chemical processing, and further inspired numerous investigations of transition metal cation (Ti^{4+}, Fe^{3+}, or V^{3+}, etc.) substituted silicates. Atomically dispersed titanium(IV) centers in homogeneous catalysts like titanium tetra-isopropoxide show important catalytic activity distinct from that of bulk titania, for example, in polymerization and epoxidation of olefins.[2] But it has been found that aggregation of titanium molecular species causes fast deactivation of non-supported catalysts and limits their industrial application. Titanosilicates catalysts are intended to address the issue by immobilizing the [Ti(IV)O_4] units in an array of [SiO_4] silicates. Meanwhile, the ordered porous structure in titanosilicates functions as micro-channels that perform size-selectivity toward reactants and products.

The content of active sites (Ti wt% or titanium mol%) is an important parameter for titanosilicates. TS-1 contains up to ~2 wt% titanium but with a high cost of manufacture (over $100/kg)[48], which can only be justified by high-valued chemical products and good recyclability of the catalyst. A number of titanosilicates were prepared later through various ways and reportedly the titanium content reaches up to 30 wt%.[49] The benefit from increasing titanium content is obvious as this increases the density of active centers which potentially translates into high catalytic rates for the catalyst. But high titanium content bring up other issues. Multiple types of titanium centers have been observed, when titanium centers aggregate and form catalytically inactive oligomer or crystalline titania. In some cases, these centers may also leach out of the matrix and into the solution. In such cases, it is critical to ensure true heterogeneous catalysis. In other words, the recyclability of such catalysts depends on the hydrothermal stability of titanium toward leaching especially with aqueous H_2O_2 in use so that active homogeneous species are not formed.

Porosity and surface area are also important properties of heterogeneous catalysts. In contrast to the significant progress made in scientific investigations, TS-1 has not been extensively used in industrial plants, notwithstanding its enormous potential as selective oxidation catalyst. As far as is currently known, the ammoximation of cyclohexanone, propylene epoxidation and phenol hydroxylation are the only industrial examples that utilize TS-1 as

catalyst. One of the main reasons is the small pore size (5 - 6 Å) of the MFI lattice in TS-1. A large number of complex reactants, potentially oxidized into high-valued chemicals, are too large to enter the micropores of TS-1.

Later a variety of meso- and macroporous titanosilicates were synthesized, such as Ti-β, Ti-MCM and Ti-SBA, so that a much broader spectrum of reactants are covered.[50] The titanium centers of these catalysts are not as well understood as of TS-1, and generally lower chemoselectivity is observed. With the advances made with *in situ* characterization techniques, significantly more information about the titanium centers has been obtained but still far from enough to unambiguously identify the active sites involved. It has not been possible to establish a well-defined structure-property relationship for titanosilicates catalysts. Tetrahedral Ti(IV) centers in Ti-MCM-41 suggested by spectroscopic evidence, however, shows distinctly different catalytic properties from supposedly the same catalytic centers in TS-1. Observations like this indicate that the catalytic activity depends on not only the state and total coordination number (CN) of Ti, but probably other factors that include: (1) the connectivity of the titanium ion to silicate matrix; (2) the influence of extra-framework Ti; (3) the influence of impurities; (4) the types of surface acidic sites; (5) the influence of surface hydrophobicity/hydrophilicity.

Not only atomic titanium centers, silica supported polynuclear Titanium centers with the substructure of Ti-O-Ti bridge(s) were also found to be active catalysts in a variety of reactions. Silica supported dinuclear titanium species (Figure 12, left) is an active catalyst in cyclohexene epoxidation with tert-butylhydroperoxide (TBHP) as the oxidant.[51] Dinuclear (Figure 12, middle and right) and tetranuclear titanium clusters grafted on mesoporous silica have been prepared and exhibited high selectivity in catalyzing phenol oxidation with aqueous H_2O_2.[52]

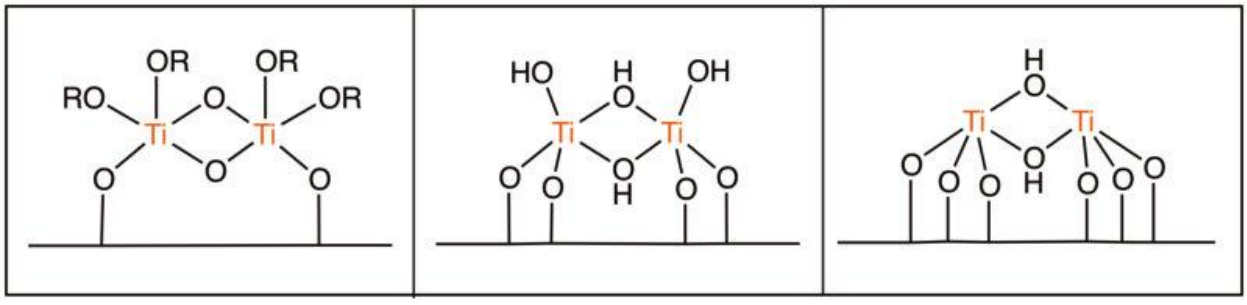


Figure 12. Structures of dinuclear Ti sites proposed by previous studies

The structures of dinuclear titanium centers were hypothesized based on the surface density of hydroxy groups (OH/nm^2) that is quantified before and after grafting with titanium precursors.[51, 52] Nevertheless, it presents major difficulties in predicting the structure of active centers, partially because of the calcination at 500-1500 °C under oxygen flow prior to use.[21] After all, the role of Ti-O-Ti bridge in titanosilicates has not yet been completely understood.

The knowledge about the active centers at the molecular level is far from adequate. The various titanosilicates as active catalysts, however, provide a basic picture, based on empirical knowledge, about the desirable physical and chemical properties of materials. Multiple factors need to be taken into consideration, for example, the uniform distribution of titanium centers in the matrix. Single-site heterogeneous catalysts combine the major advantages of homogeneous and heterogeneous catalysts, so that high activity and selectivity can be obtained with stable and recyclable solid catalysts. The choice of reactants to make these materials is related to the pore size of silicate framework that plays a role in catalytic selectivity of some titanosilicates. A wide range of titanium content is also desirable that maximizes the density of active centers, and potentially lower the cost especially in large scale production. To develop new catalysts that possess these qualities requires novel synthetic methodology in conjunction with advanced characteristic techniques, and fundamentally a good understanding of the catalysts and the working mechanisms.

1.3.2 Titanium silicalite-1 (TS-1)

In 1983, titanium silicalite-1 (TS-1) was discovered by Taramasso *et al.*[53] and has shown remarkable catalytic properties in a number of selective oxidation reactions. The isomorphous substitution of Ti(IV) in TS-1 is confirmed by a series of spectroscopies and other techniques, and possesses unique catalytic activity that is absent in bulk titania with 6-coordinated [$Ti(IV)O_6$] and bridging titanium centers [Ti-O-Ti].[54] Further, TS-1 exhibits good stability and catalytic efficiency when exposed to aqueous hydrogen peroxide (H_2O_2).

1. Structures: active sites of Ti(IV) and hydrophobicity

As one of the milestones in the history of titanosilicate catalysts, the structure and catalytic property of TS-1 have been extensively studied. Isolated 4-coordinated Ti(IV) exist in TS-1 and are responsible for the catalytic activity in a variety of selective oxidation reactions.[55, 56] The composition of TS-1 can be expressed in the formula of $(TiO_2)_x(SiO_2)_{1-x}$ with the $Ti/(Ti + Si) \leq 2.5$ atom%.[48, 55]

X-ray diffraction (XRD) and neutron diffraction are powerful tools for determining the crystalline structures like TS-1. XRD is especially useful in defining the unit cell and lattice parameters. Below the upper limit for incorporation of titanium in TS-1, a linear dependence of lattice parameters and unit cell volume on the titanium content has been discovered, which clearly defines the upper limit of Ti(IV) insertion in the zeolite framework. XRD has also been used to define the crystalline structure to be the MFI type of zeolite. It is also crucial that MFI framework exhibits the flexibility, for example, for the reversible transformation between lattices of orthorhombic and monoclinic symmetry. This flexibility allows the framework to host much larger Ti(IV) ions (0.42 Å) than Si(IV) (0.26 Å), and is thought to allow Ti(IV) to change coordination numbers (4 → 6) and geometries (Td → Oh) while remaining associated with the silicate lattice. Because of the significant difference in the ionic radii of Ti(IV) and Si(IV), distorted pseudo-tetrahedral Ti(IV) centers are embedded in the framework of TS-1.[57] Further, neutron diffraction reveals that the Ti(IV) ions populate 3 - 5 different types of the 12 T sites within the MFI zeolite lattice (Figure 13).[58] However, the low concentration of titanium makes it challenging to determine the substitution sites, and different conclusions can be found from past studies.[59, 60]

One of the key features of TS-1 is the superior stability against titanium leaching in aqueous H_2O_2, which is the main reason causing metal-silica catalysts to deactivate.[61] The hydrolysis of Ti-O-Si bridge occurs inevitably in the presence of water and H_2O_2 at elevated temperature. In fact, mechanistic studies indicate that the breakage of Ti-O-Si is an essential step for initiating the catalytic cycle involving fully embedded [$Ti(OSi)_4$] units.[54] By the end of hydrolysis, 4-connected [$Ti(OSi)_4$] centers open up three coordination spheres and transform to 3-connected (tripodal) titanium units with several possible structures (Figure 14).[54] The open structure of 3-connected titanium center allows it to coordinate with small molecules (reactants) more readily. As the catalytic reaction goes on, titanium species are liable to be leached out due to the increasing degree of hydrolysis. Without the mechanism being completely understood, it is generally believed that the decrease in connectivity of titanium with silicate framework leads to elimination of Ti(IV) centers in the form of hydroxide, oxide or other molecular species.

The stability of TS-1 within aqueous environment is associated with the local structure around titanium center as well as the hydrophobic surface of catalyst. The titanium centers in TS-1 are incorporated through framework substitution and thereby possess the highest connectivity, whereas the surface-grafted titanium centers (connectivity < 4) found in many

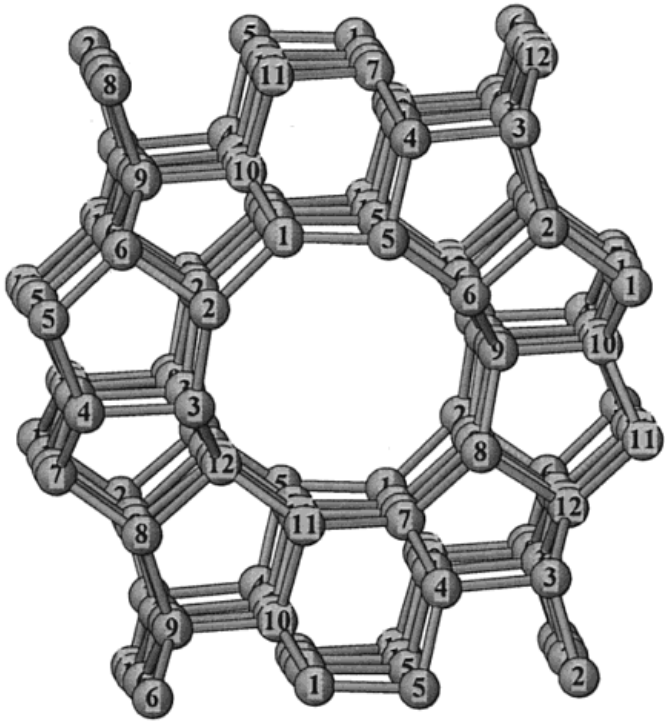


Figure 13. The structure of orthorhombic form of silicalite-1 (MFI type) showing the 12 crystallographically distinct T sites (The oxygen atoms are omitted for clarity)

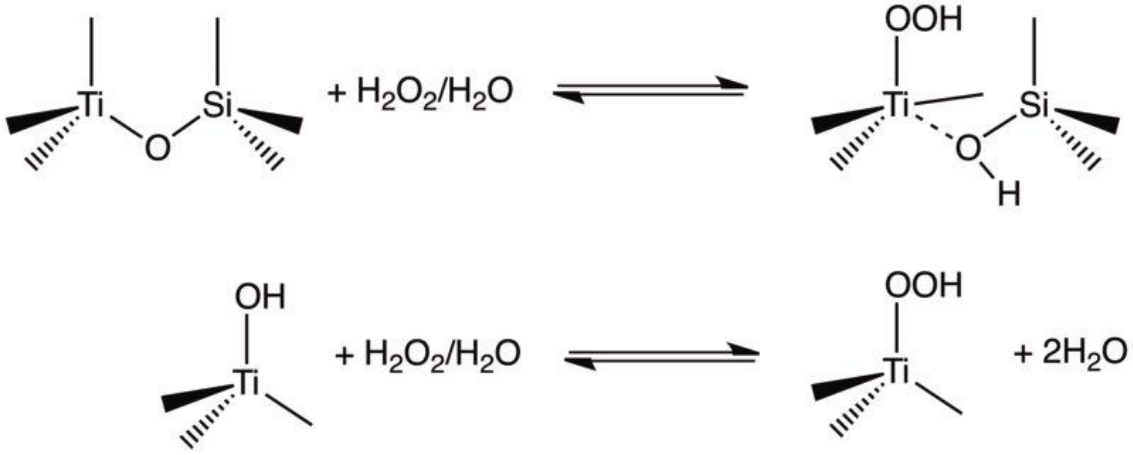


Figure 14. Hydrolysis of $[Ti(OSi)_4]$ in aqueous H_2O_2 (up) and conversion between 3-connected Ti-hydroxide and Ti-hydroperoxide (bottom)

other titanosilicates are more likely to be leached out. The hydrophobic surface also plays a role in stabilizing Ti. Due to the fact that both Ti(IV) and Si(IV) are tetravalent, Brønsted acidity is not anticipated from the substitution. This hypothesis is confirmed by the inactivity of well-synthesized TS-1 in Brønsted acid-catalyzed reaction in the absence of H_2O_2. As a result, the surface of TS-1 is highly hydrophobic and hinders water molecules from entering the pores where titanium centers locate. Further, hydrophobic reactants such as alkenes are preferentially adsorbed by TS-1. Therefore, hydrolysis of Ti-O-Si (Figure 14) that is essential to titanium leaching is much more oppressed in the case of TS-1 than the hydrophilic amorphous Ti-SiO_2.

2. Synthesis

TS-1 has been synthesized mainly by wet impregnation method, however, over a dozen different versions have been reported that employ different titanium or Si precursors, structure-directing agents, gel compositions, sequence of additions, reaction temperatures and times, crystallization and calcination conditions, etc.. Table 1 summarizes some typical synthesis methodologies, which illustrates the impact from synthesis parameters on the final structure and composition of TS-1.

3. Catalytic properties

Compared to most other titanosilicates, TS-1 has shown extraordinary hydrophobicity, and thus purely Brønsted acid-catalyzed reactions by TS-1 have not been observed. The superior catalytic activities originate mainly from the coordinatively unsaturated titanium ions (Lewis acidity of Ti). The hydrophobicity has been proven crucial to its excellent stability against aqueous environment, and more importantly its capability of activating H_2O_2 as the oxidant. Most metal-silicates, for example W(VI), V(V), Cr(III), and most Ti(IV)-silicates, deactivate quickly in the presence of water due to severe leaching of metal ions. Due to this fact, even though using H_2O_2 presents many benefits, for example, environmental friendly byproduct (water) and easy purification of the products, the application of H_2O_2 has been limited to oxide-based catalysts. More frequently, metal-silicate catalysts are used in conjunction with organic hydroperoxides such as tert-butyl hydroperoxide (TBHP). But higher cost is expected from (1) more expensive oxidants (ROOH vs. H_2O); and (2) more complex separation between desired products and byproducts (ROH vs. H_2O).

Table 1. TS-1 synthetic methodologies and parameters vs. Final Si/Ti and morphology

Synthesis methodology	Composition [a, b]	Temp Time	Si/Ti	Crystalline size & morphology	Ref.
Hydrothermal synthesis (mixed alkoxide)	TEOS TEOT TPAOH base, distilled water	448 K 6-30 d	90-30	parallelepipeds with round edges	53
Hydrothermal synthesis (dissolved Ti)	(1) Tetrapropylammonium peroxytitanate: TEOT in distilled water, aqueous H_2O_2 and aqueous TPAOH (2) add colloidal silica and TPAOH	278K	90-30	parallelepipeds with round edges	53
Wetness impregnation (prehydrolysis)	(1)TEOS in dry iPrOH is hydrolyzed in aqueous TPAOH (2) $Ti(OBu)_4$ as titanium source	433 K 1-5 d	≥10	cuboid (< 1 μm)	110
Growth from TS-1 seeds	TS-1 seeds TPABr (structure-directing agent) ammonia, water, amines	nr	nr	(100% crystallinity)	109
Sol-gel (Template-impregnation)	(1)Obtain dried SiO2-TiO2 cogel (2)Dry impregnation by adding aqueous TPAOH and heated in microwave (3)Dry and then calcine the crystalline product	823 K 5h (calcine)	50	round shaped particles (~0.5 μm)	106

[a] Common components in wetness impregnation or hydrothermal synthesis include Si and titanium sources and structure-directing agent;

[b] Tetraethylorthosilicate (TEOS), tetraethyltitanate (TEOT), tetrapropylammonium hydroxide (TPAOH)

TS-1 is one of the few examples that utilize H_2O_2 efficiently without undergoing significant leaching. In fact, a variety of epoxidation and oxidation reactions using aqueous H_2O_2 can be selectively catalyzed by TS-1 (Figure 15).[54] Taking advantage of its single-site nature, some researchers have started investigating the reaction mechanisms and intermediates during the catalytic cycle. The initial step of activation of titanium center is illustrated in Figure 16. After TS-1 is exposed to aqueous H_2O_2, spectroscopic evidence agrees with higher-coordinated titanium centers, suggesting the formation of Ti-peroxo and Ti-hydroperoxo intermediates (Figure 16). [62] The coordination of titanium and peroxide reduces the electron density at the peroxide O-O bond and makes it more susceptible to attack by nucleophiles such as alkenes.

The activity in a specific reaction is closely associated with the pore size of MFI framework that favors smaller molecules and thereby has a major impact on the choice of reactants. Epoxidation of alkenes is one of the most studied TS-1-catalyzed reactions. With the small size of propene, the direct conversion to its epoxide with aqueous H_2O_2 can be obtained in near quantitative yields. The rate decreases with an increase in the chain length of the alkene molecule (1-hexene > 1-octene > 1-dodecene), which is mainly attributed to diffusion constraints. Generally, a large steric hindrance from the reactant or reactive functional group results in much slower reactions or inactivity. Therefore, for example, the reaction rate of epoxidation decreases in the sequence of 1-hexene > 2-hexene > 3-hexene. When multiple oxidizable functional groups coexist, such as diene or unsaturated alcohol, steric factor influence the selectivity by favoring the terminal double bond (non-substituted) that is sterically less hindered (Figure 17).

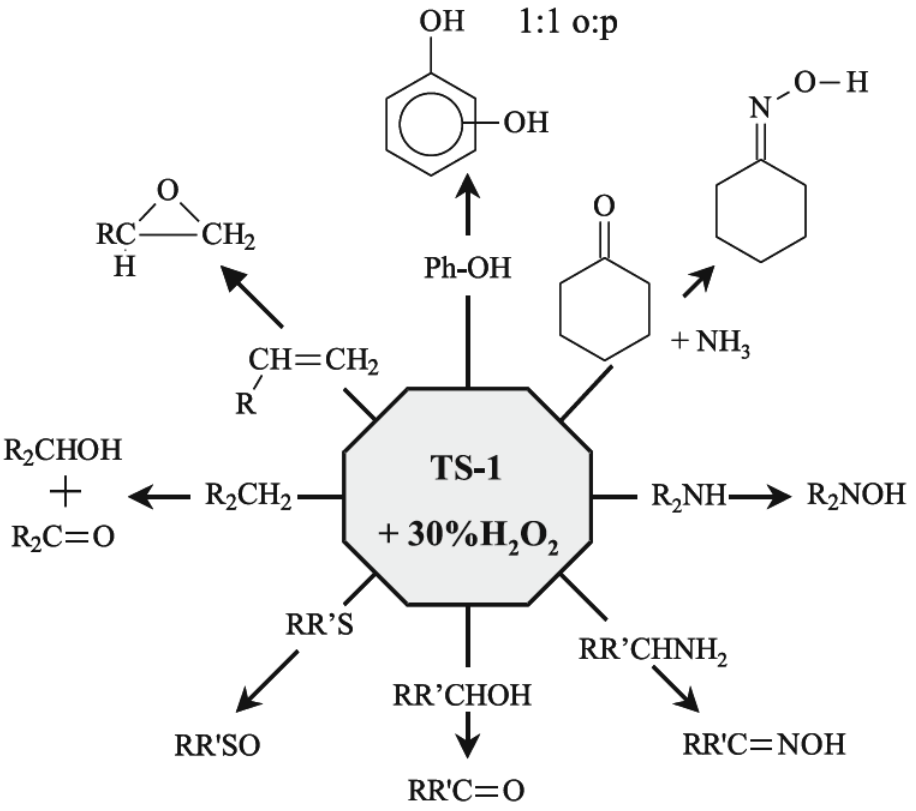


Figure 15. TS-1 catalyzed reactions (Reprinted from reference 54)

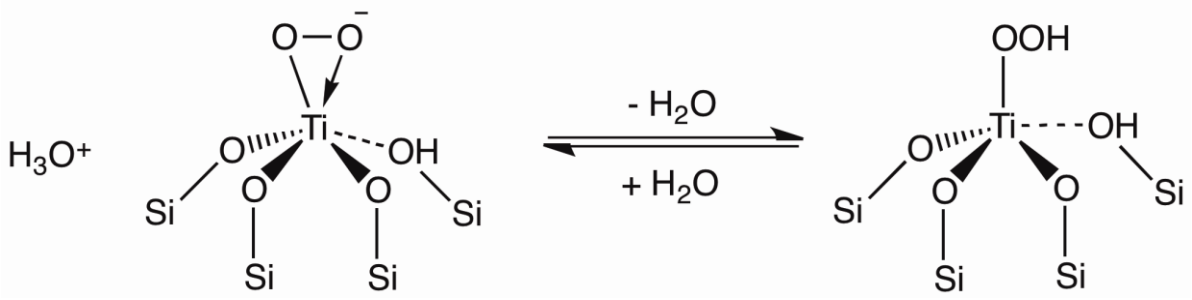


Figure 16. Higher coordination Ti centers in the system of TS-1/H_2O_2/H_2O (Reproduced from reference 62)

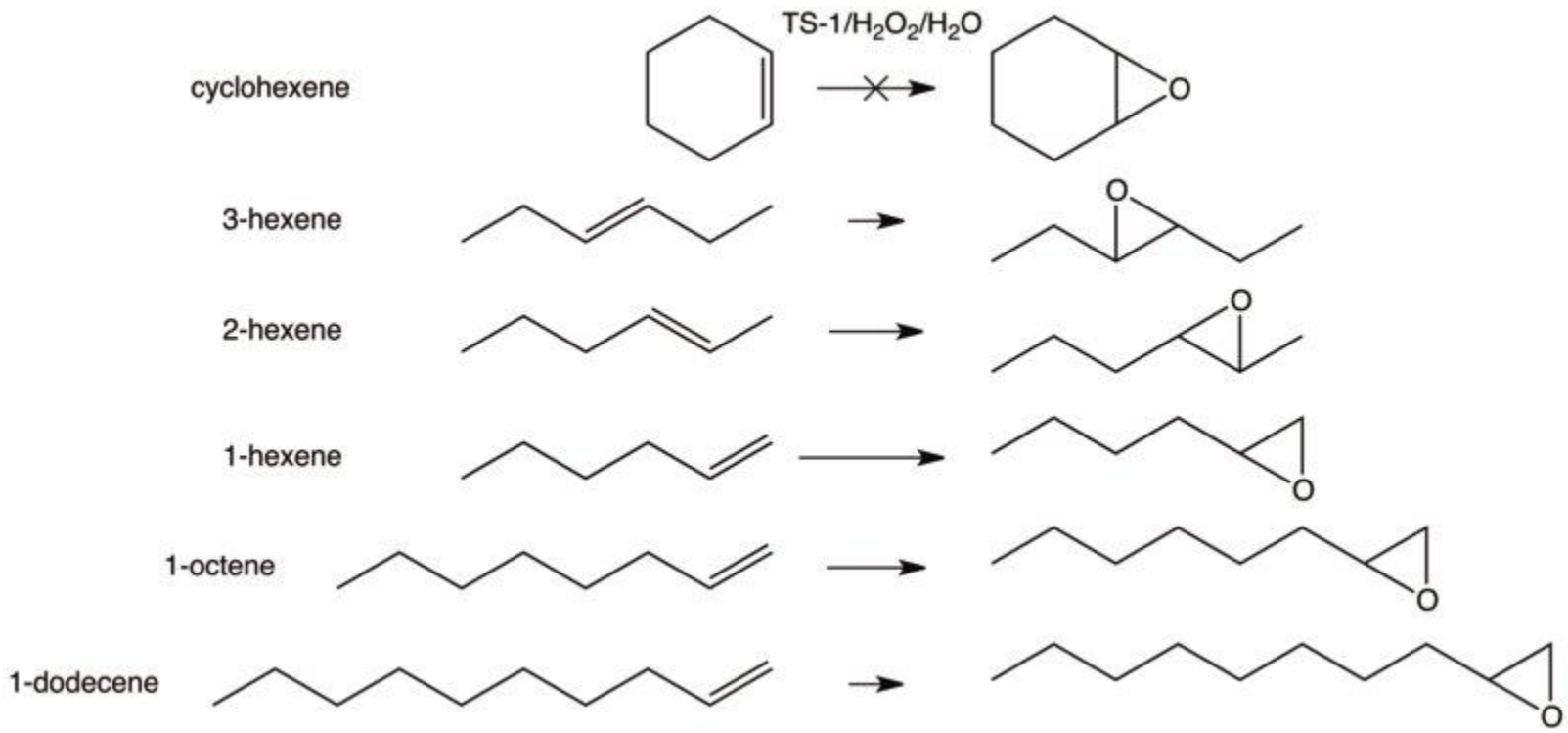


Figure 17. Influence of structure of reactants on reaction rate with TS-1

One of the major disadvantages of TS-1 is related with the small pores of MFI framework that excludes a number of potential reactants. For example, no significant conversion of cyclohexene is observed due to the large size of six-member ring, while the conversion of 1-hexene with a chain structure reaches nearly 100%. The requirements to the size of reactants significantly limit the use of TS-1 in industrial plants, because majority of high-valued chemical compounds are prepared with reactants of complex structures.

Moreover, the capacity of framework substituted titanium (active site) in TS-1 has an upper limit of approximately 2.5 wt%. Above the upper limit, the existence of non-framework titanium centers is confirmed by spectroscopies and the non-linear relation between unit cell parameters and titanium content. The non-framework titanium species such as crystalline titania or titanium oligomers with Ti-O-Ti bridge and/or high-coordinated titanium usually possess undesirable catalytic activity/inactivity, and therefore lower overall selectivity of the catalyst is observed as expected.

1.3.3 Mesoporous titanosilicate materials

There have been many attempts to synthesize titanosilicate molecular sieves with larger pore sizes to eliminate the steric constraints so that more complex molecules can be utilized to produce high-valued chemicals. Several tens of mesoporous silicates containing titanium ions in various structural and geometric locations have been synthesized and their chemical, physical and catalytic properties investigated. These molecular sieves are characteristic of uniform pore sizes (1.5-40 nm), large surface areas (up to 2500 m^2/g) and tunable structures.[63]

The construction of ordered porous materials depends on self-assembly in which (parts of) molecules spontaneously organize into structurally welk-defined aggregates. Noncovalent or weak interactions including van der Waals, electrostatic, and hydrophobic interactions, hydrogen and coordination bonds, and π-π stacking are involved in the self-assembling process. A number of different kinds of disorder on the atomic or molecular scale exist, but periodical mesoscopic morphology is displayed and most mesostructures belong to hexagonal and cubic phases. Two common pathways are utilized in the self-assembling synthesis: (1) the cooperative interaction between surfactants and silica sources to form mesostructures; (2) semiliquid-crystal template pathway. At the final stage of either pathway, organic surfactants or templates are to be removed by calcination, extraction, microwave digenstion or oxidative decomposition. Amongst the family of mesoporous titanosilicates, Ti-MCM-41, Ti-MCM-48 and Ti-SBA-15 have been extensively studied and therefore are taken as examples.

1. Ti-MCM-41

Ti-MCM-41 is synthesized by hydrothermal and postsynthetic grafting techniques. Quaternary cationic surfactants $C_nH_{2n+1}N(CH_3)_3X$ (n = 8-10, 12, 14, and 16; X = Cl and Br) were used as templates in the synthesis of MCM-41 mesoporous silica.[64] The average diameter of MCM-41 is ~4.0 nm that is characterized by XRD and TEM.[64] The pore channels are approximated as cylinders with the pore-wall thickness is estimated to be ~1 nm, and the surface area is generally higher than 1000 m^2/g.[64, 65]

Mainly two type of Ti-MCM-41 have been prepared through different synthetic methodologies, generating titanium centers of various locations and structures. The framework Ti-MCM-41 refers to the MCM-41 framework containing embedded titanium centers, during the synthesis of which the source of titanium such as $Ti(OiPr)_4$ is introduced simultaneously with Si source, typically $Si(OEt)_4$ or $Si(OMe)_4$. Usually only part of the titanium sites substitute in the Si framework and reside in the Si walls. In order to prepare titanium grafted onto the surface of MCM-41 (Ti↑MCM-41), MCM-41 silica is pre-made and subsequently titanium precursor such as titanocene is grafted on the silica surface.[66] Based on the characteristic evidence, it is proposed that after calcination most of titanium sites possess tripodal (3-connected) tetrahedral structure in comparison to the fully embedded sites (4-connected) in framework Ti-MCM-41.

2.Ti-MCM-48

The pore diameter of MCM-48 is 2.4-2.7 nm, surface area 1000-1450 m^2/g, pore volume 0.8-1.1 cm^3/g.[67] Specific type of mesostructures including 2D (p6mm) or 3D ($P6_3/mmc$) hexagonal and cubic ($Ia\bar{3}d$) can be attained by varying the packing parameters of surfactants, for example, g value that is defined by the total volume, hydrophilic headgroup area and kinetic tail length of surfactant molecules. The dry surface of pre-made MCM-48 framework is then grafted with titanium in the form of $Ti(OiPr)_4$. In direct synthesis of Ti-MCM-48, TEOS and $Ti(OiPr)_4$ are used as the sources of Si and Ti, respectively, and Gemini-type surfactants $C_{18\text{-}12\text{-}18}$ or cetyl-benzyl dimethylammonium chloride (CBDAC) are used as templates.[67]

3.Ti-SBA-15

SBA-15 belongs to 2D hexagonally mesostructured silica. It shares the same space group (p6mm) as the 2D hexagonal MCM-41, but larger pore size (~6.5 - 10 nm) and thicker pore-wall (3.1-4.8 nm) by hydrothermal synthesis. The uniform tubular channels of Ti-SBA-15

(surface area 600-900 m^2/g, pore volume 0.6-1.3 cm^3/g) can be prepared by direct and grafting methods by using triblock copolymers, poly(ethylene oxide)-poly(propylene oxide)-poly(ethylene oxide) in acidic medium. Synthesis of Ti-SBA-15 by incipient-wetness impregnation with $Ti(OiPr)_4$ has also been reported followed by calcination.[68] Titanosilicates prepared by varying synthetic methods and with choices of components differ to some extent in structural parameters and catalytic properties.

One of the reasons for limited application of heterogeneous catalysts is the heterogeneity of active sites. In fact, it was confirmed with XAS that calcination can cause significant changes to grafted metal centers in coordination, connectivity to silica matrices and sometimes nuclearity.[21, 33] For the purpose of this research, the majority of titanosilicates that are prepared by hydrothermal or grafting methods with calcination, fail as the objects of investigation due to the presence of multiple titanium sites of two categories, framework incorporated and extra-framework.

Single-site heterogeneous catalysts (SSHCs) of many structural and catalytic merits are the target candidates for the purposes of this research. As introduced above a few methodologies for preparation of SSHCs have been developed, but very few are successful in terms of targeting the local environment within and around the metal active centers. Currently, control of connectivity around a titanium center in a silicate matrix has only been achieved with homogeneous molecular species, i.e. Ti-silsesquioxane complexes. [69] These silsesquioxane complexes serve as excellent molecular models for the active sites on the atomic level. Much useful information about the catalytic processes has been acquired through the studies particularly involving 1-, 2- or 3-connected atomic titanium center, titanium dimer and tetramer silsesquioxane species (Figure 18).[70] Under the catalytic conditions, these soluble complexes participate as homogeneous catalysts rather than heterogeneous ones. Recently it was reported that 3-connected Ti-silsesquioxane was deposited on polydimethylsiloxane (PDMS) membranes and characterized by DRUV, forming active catalysts for alkene epoxidation.[71]

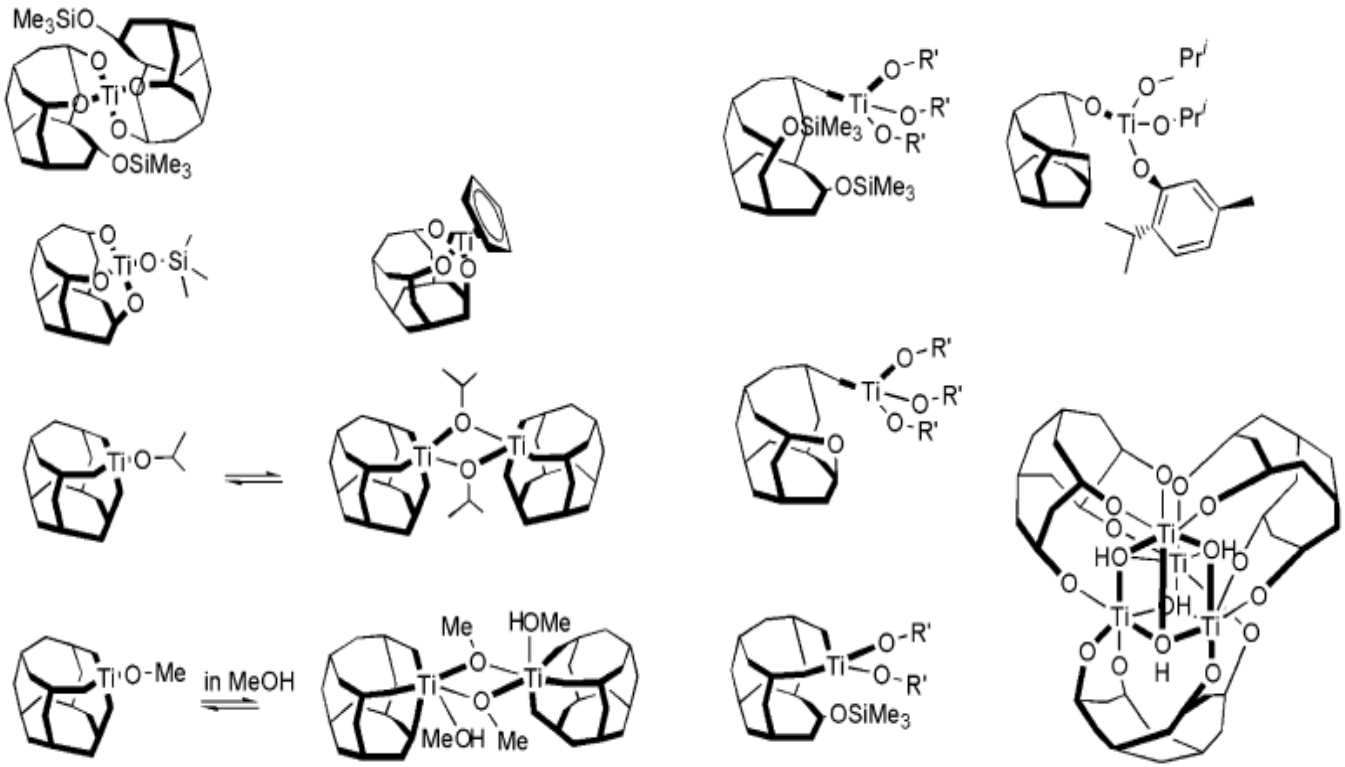


Figure 18. Examples of Ti-silsesquioxane (Reprinted from reference 70)

1.4 Overview of Dissertation

1.4.1 Motivation and goals

Titanosilicate catalysts have been studied intensively for over three decades and significant success has been attained in the synthesis of various kinds of titanosilicate. TS-1 was one of the first titanosilicates discovered with excellent catalytic properties, leading to extensive study on a family of titanosilicates. During the past couple decades, a number of mesoporous titanosilicates were synthesized by hydrothermal and wet impregnation. Many of these have been demonstrated to be active catalysts that are able to accommodate a number of complex reactants normally too bulky to enter the micropores such as those in TS-1. However, mesoporous titanosilicates such as Ti-MCM-41 and Ti-MCM-48, when compared with TS-1, show lower chemoselectivity and H_2O_2 efficiency in olefin epoxidation reactions.

The catalytic property of zeolite-based titanosilicate depends on the following factors: (1) the state, connectivity and nuclearity of titanium ions; (2) the presence and nature of extra-framework Ti; (3) the influence of impurities; (4) the types of surface acidic sites; (5) the surface hydrophobicity/hydrophilicity; (6) the crystal size.

TS-1 and Ti-MCM-41 have been intensively investigated and characterized amongst the family of titanosilicates. Theoretically and empirically the selectivity of catalyst depends to a high degree on the nature of the active sites. It is thus difficult to explain the drastically different selectivity between the two titanosilicate analogues, since in both frameworks Ti(IV) ions are isolated and in near tetrahedral locations. With limited knowledge about the catalyst structure, the major differences that exist are in the pore sizes and in the surface hydrophilicity/hydrophobicity. It has been proven that the surface hydrophilicity contributes to the instability of catalyst and quick decomposition of H_2O_2 relevant to inefficient utilization of H_2O_2 as the oxidant.[72] With the help of modern techniques especially X-ray absorption spectroscopy the coordination and connectivity (framework coordination) of the active sites in titanosilicates can be characterized on the atomic level. It has been discovered that TS-1 contains mostly $[Ti(OSi)_4]$ type centers, whereas most of titanium centers in Ti-MCM-41 are thought to be tripodally $[Ti(OSi)_3(OH)]$ connected to the silicate support in near tetrahedral geometries. This suggests that the connectivity between titanium center and the silica support should play a key role in the catalytic property.

The goal of the research described here was to develop and apply a general methodology for targeted synthesis of single-site titanosilicate catalysts. Specifically we wished to develop a methodology that would lead to preparation of atomically dispersed, single-site catalysts in which the connectivity of the titanium atoms to the surrounding silicate support could be targeted and changed as desired.

Furthermore, each of the titanium atom sites in the matrix must also be kept isolated from all others as an inherent feature of the strategy and not utilize the compromise of low loading strategies to obtain isolated sites. The resulting materials must also be porous and exhibit high surface area and therefore high site density per unit volume or weight.

Finally, we also wanted to be able to incorporate single-site, site isolated, polynuclear titanium oxo catalyst sites, e.g. tetranuclear Ti4Ox sites, into these matrices analogous to atomically dispersed systems. With such single-site materials in hand we then sought to develop a well-defined structure-function relationship between titanium atoms with specific connectivities to the surrounding porous silicate matrix and their catalytic activity in the oxidation of phenols to benzoquinones with peroxide. The structure-function relationship should contribute to the fundamental understanding of catalytic processes in specific reactions. In order to observe the effects of varying structures of catalysts, but excluding the influence from other factors like hydrophilicity/hydrophobicity, the experimentation should be conducted on a family of catalysts that share the common mesostructure with the only variables being the local structure of active sites.

The strategy in this research is to design targeted single-site titanosilicate catalysts that exhibit (1) well-defined structure around every titanium center supported by multiple independent lines of characterization; (2) all titanium centers are isolated from one another; and (3) exhibit consistent mesostructures (porosity, hydrophilicity/hydrophobicity, etc.) within a family of catalysts. Practically, a building block (bb)-based synthetic approach is presented in conjunction with the structural characterization using advanced spectroscopies and techniques. Most importantly, the catalytic performances of these materials are evaluated in the selective oxidation of alkyl-substituted phenol to the corresponding benzoquinone. The catalytic properties of titanium active sites are demonstrated to be highly sensitive to the local structure (connectivity and nuclearity). XAS plays a crucial role in the investigation of both structure and catalytic intermediates. The relationship between structure and catalytic activity of the catalytic

sites is helpful to direct future design of titanosilicates. The approach of structural control is applicable with other metal-silicate catalysts on a number of catalytic reactions.

1.4.2 Atomically dispersed and clustered Ti centers

A family of catalysts are prepared, each of which contains a specific type of titanium center, namely 2-connected (2C-Ti), 3-connected (3C-Ti) and 4-connected (4C-Ti) (Figure 19). The building block synthetic methodology generates the homogeneity of titanium centers (single-site) that is later confirmed by a number of independent lines of characterization.

In order to investigate the catalytic property of polynuclear titanium center, polynuclear complex, $[Ti_4Cl_6(\mu_2\text{-}O_2CPh)_6(\mu_3\text{-}O)_2]$ [73], that contains Ti-O-Ti substructure and chloride groups was taken as the titanium precursor and the similar bb synthetic methodology makes it possible to incorporate isolated the tetranuclear titanium clusters into a silicate bb matrix. Therefore, the catalytic properties of polynuclear species can be evaluated and compared with that of atomically dispersed titanium catalysts. The actual structure of polynuclear center will be proposed in Chapter 4 based on a variety of characterization data.

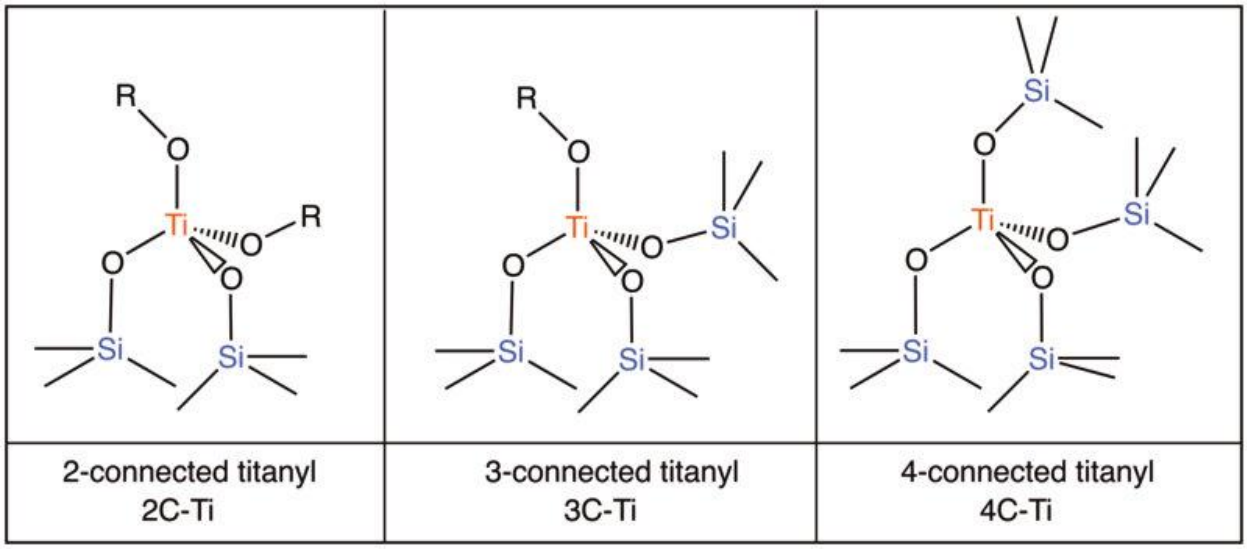


Figure 19. Titanium centers with different connectivity on silica matrices

1.4.3 Catalytic properties in phenol oxidation

Finally, the catalytic properties are of great interest, and are evaluated as secondary characterization of these single-site catalysts. The as-synthesized catalysts are applied to the alkyl-substituted phenol oxidation with aqueous H_2O_2, as shown in Figure 20. The desired product, 2, 3, 5-trimethyl-p-benzoquinone, is a high-value chemical and key intermediate for synthesizing Vitamin E. Although possessing large commercial potential, the knowledge about the catalytic mechanism of this reaction is very limited. Based on previous researches, some preliminary results have shown the difference in catalytic selectivity between mononuclear and polynuclear titanium centers.[52] In this research, the structure-function relationship is established according to the catalytic performance of single-site catalysts. More importantly, to our knowledge, this is the first study reported on how connectivity around titanium center may influence the catalytic property of titanosilicate in phenol oxidation reaction, possibly following a free radical mechanism.

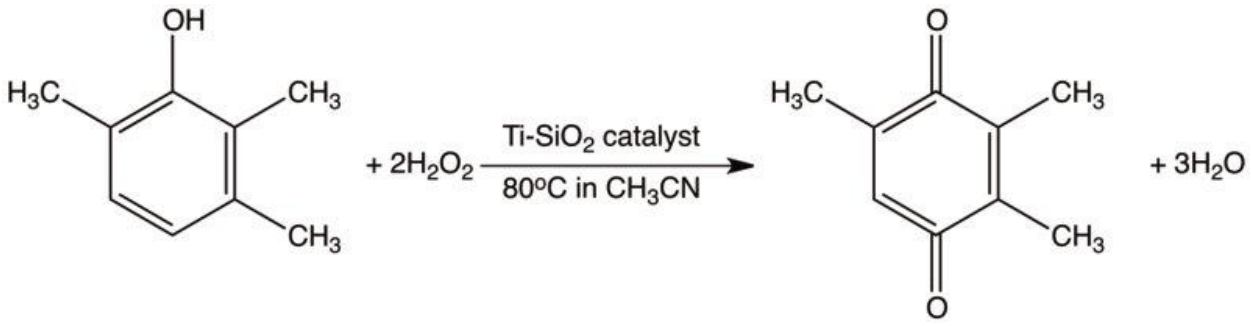


Figure 20. Oxidation of 2, 3, 6-trimethylphenol (TMP) into 2, 3, 5-trimethyl-p-benzoquinone

Chapter II. General Synthesis & Characterization

2.1 Building Block Methodology

2.1.1 General methodology

Barnes et al. has developed the synthetic methodology for the preparation of a uniform distribution of isolated, identical metal sites within a silicate matrix.[74] Trimethyltin-functionalized silsesquioxane building block (bb) is employed as the silicon source, and the active metal precursors are high valent metal complexes containing reactive chloride groups. The crosslinking process is driven by the exothermic reaction between M-Cl (M = Ti or Si) and Si-O-$SnMe_3$ functionalities. The irreversible metathesis reaction forms Ti-O-Si or Si-O-Si linkages through which titanium centers are incorporated growing building block matrix. The amount of byproduct, trimethyltin chloride ($ClSnMe_3$), is directly related to the connectivity around titanium (Ti-O-Si) (section 2.1.5). Previously, this methodology has been successfully applied in preparing silicate bb supported single-site vanadium catalysts.[75] Targeted vanadium active centers were uniformly dispersed throughout the matrix as confirmed by characterization including X-ray absorption spectroscopy (XAS) and ^{17}O SSNMR.[75]

As illustrated in Figure 21, two pathways are available that produce different locations of active sites by simply altering the sequence of reactions, referred to as the method of sequential additions (MSA). The first pathway (upper path in Figure 21) is used to synthesize “embedded” catalyst sites by introducing metal precursors in a limiting amount in the first step of the synthesis. As a result, the metal center resides within the bb matrix, in other words, none of the chloride groups on the metal precursors should remain after reaction with bb. In the second step, the M-bb oligomers undergo further cross linking with an inert linker, typically silicon tetrachloride ($SiCl_4$). To obtain metal centers on the surface of the silicate support, the metal centers must be introduced after the formation of silica matrix, so that they can only interact with the unreacted -$SnMe_3$ groups on the surface of material.

Within the context of the research described here, the first pathway producing “embedded” catalysts sites is applied to preparing all materials. Because it is known that surface titanium species are vulnerable to leaching in an aqueous environment and thus less ideal for catalysis applications. In order to target the structure of active centers, a family of titanium precursors are chosen, including mononuclear alkoxylated chlorotitanates $TiCl_x(OR)_{4-x}$ (x = 2, 3 or 4), and a tetranuclear titanium cluster. (Figure 22)

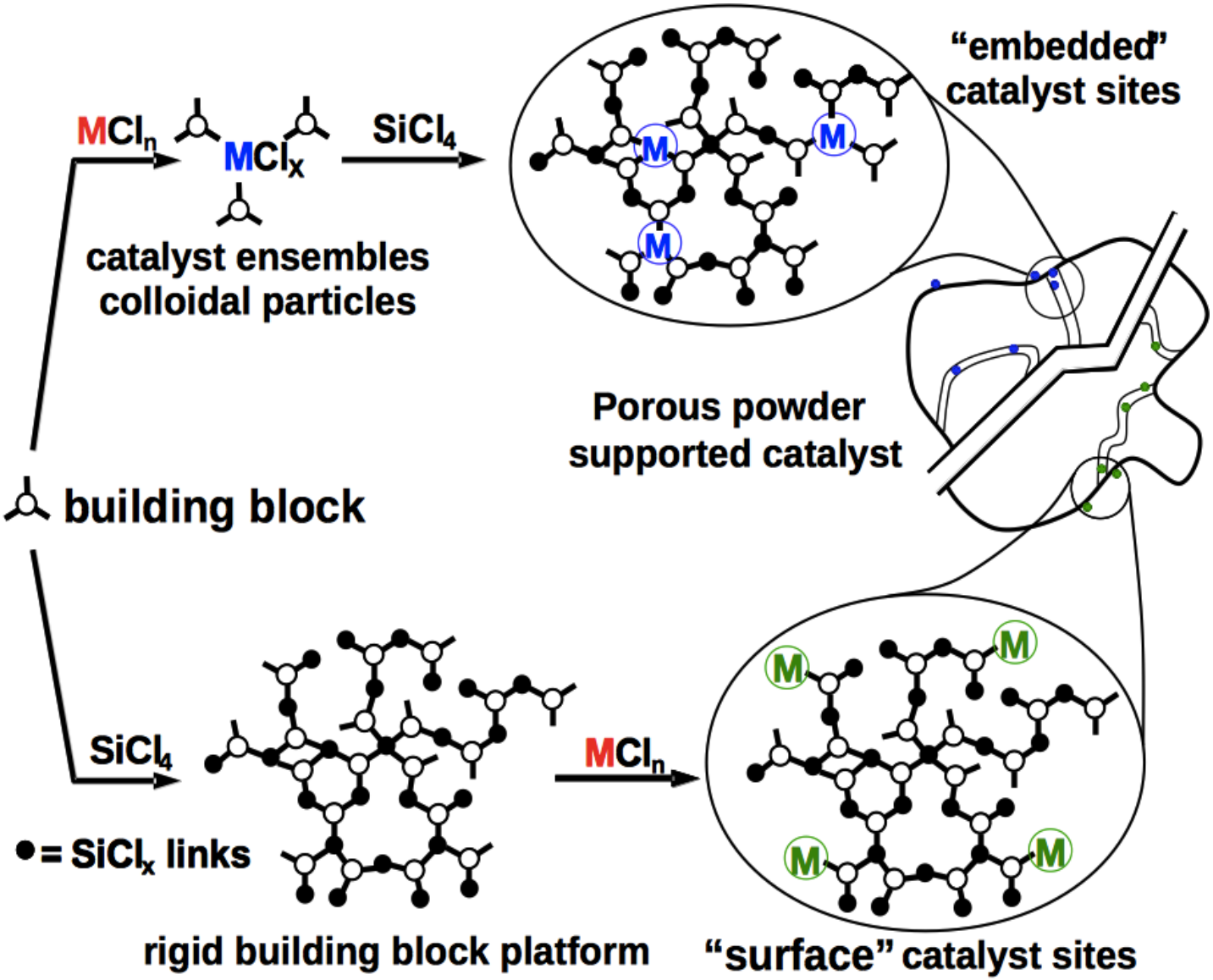


Figure 21. Sequential additions in building block methodology

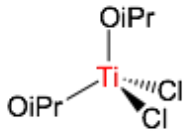
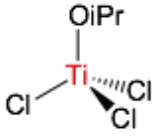
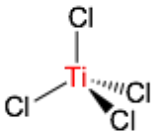
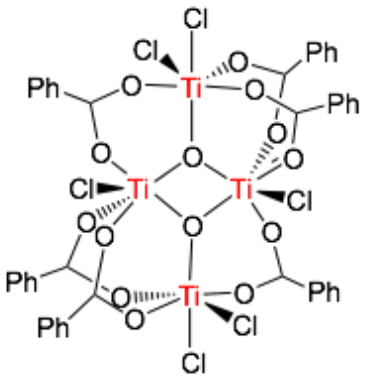
			
$TiCl_2(OiPr)_2$	$TiCl_3(OiPr)$	$TiCl_4$	$Ti_4Cl_6(\mu_3\text{-}O)_2(\mu_2\text{-}O_2CC_6H_5)_6$

Figure 22. Three different mononuclear compounds and one tetranuclear cluster used as titanium precursors

Following the two steps of crosslinking shown in Figure 21, the material is passivated with methanol, dried, and ready for use as the catalyst. The mesostructures of the final materials are closely related to the stoichiometric ratios used in each step of synthesis as well as the passivation conditions. Typically, high surface area (200 - 500 m^2/g) and meso-size pores (diameter ≥20 Å) are obtained according to nitrogen adsorption/desorption analysis.

The entire preparation takes 4 - 5 days compared to 5 - 14 days required for the conventional syntheses that include crystallization and calcination prior to use. Due to the fact that no organic template is involved in this methodology, calcination is unnecessary, which benefits in many ways. It is ideal to avoid calcination that could easily alter the nature of titanium sites in the matrix. From a practical point of view, a more cost- and energy-efficient approach of preparing titanosilicate catalysts is presented.

2.1.2 Building block

The choice of building block (bb) is critical for the isolation and homogeneity of active metal centers. Mononuclear silicon compounds such as TEOS that are used as silicon precursors in traditional impregnation syntheses, generally produce a variety of sites such as $[=Si(OTi)_2]$, $[-Si(OTi)_3]$ and $[Si(OTi)_4]$ groups. These units may also react intra- or inter-molecularly and form Ti-O-Ti linkages. When TEOS or other small Si molecules are employed, higher titanium content often leads to the formation of cluster and titania domains.[49, 76] Thus, it is necessary to isolate titanium centers atomically, so as to prevent the formation of undesired polynuclear centers.

Building block plays a key role in this methodology. Octa(trimethyltin) silsesquioxane $[Si_8O_{20}](SnMe_3)_8$ has a cubic structure, of which the Si corners (indicated as blue atoms in Figure 23) are equivalent and provide one type of linking sites. Figure 23 illustrates the core of bb $[Si_8O_{20}]$, and each corner of bb is functionalized with a trimethyltin group $(-SnMe_3)$ (not shown in the figure). The bb complex was prepared following the original synthesis by Feher.[77] Only one open site in the coordination sphere around silicon is available for reaction and all 8 silicon atoms of bb are equivalent. Trimethyltin group $(-SnMe_3)$ bonded to the silicon corner reacts with high valent metals or silicon chlorides (Ti-Cl or Si-Cl), forming trimethyltin chloride $(ClSnMe_3)$ and $[\equiv Si_{bb}\text{-}O\text{-}M]$ linkage (in which Si_{bb} represents the corner silicon from building block, and M stands for Ti or Si).

The size (diameter ≥ 1nm) of the $[Si_8O_{20}](OSnMe_3)_8$ bb and its structural rigidity makes it impossible for titanium centers on different corners of bb to interact with one another. By choosing a nanometer-sized bb, titanium centers are effectively isolated from one another and polynuclear titanium center (Ti-O-Ti bridge) is highly unlikely when mononuclear titanium precursors are employed. In addition, bb shows good thermal stability when heated under vacuum at 400 ºC. No obvious change was observed in NMR, UV-Vis and Infrared spectroscopies.

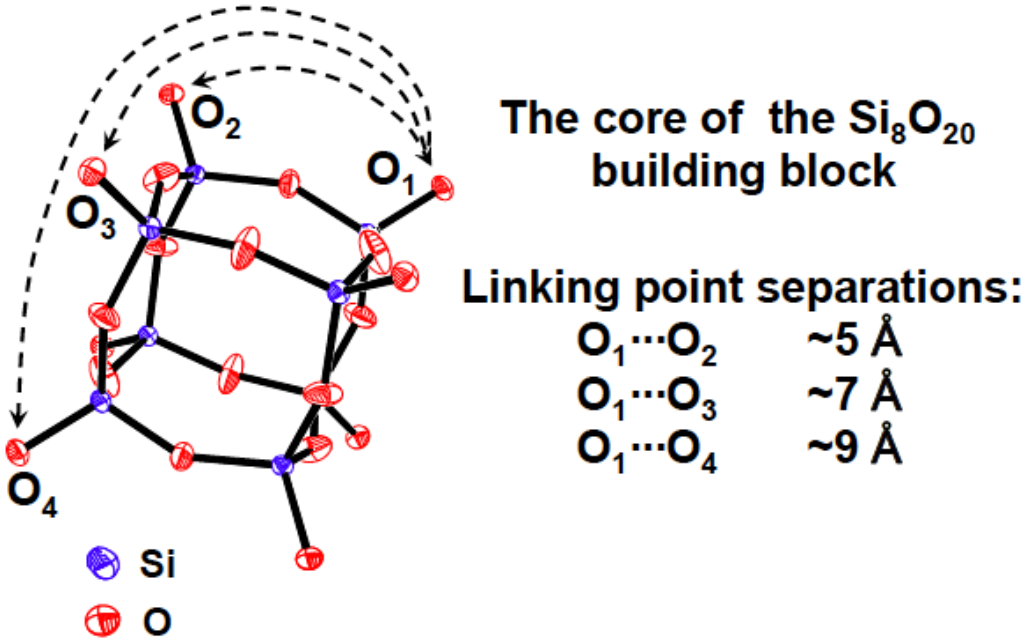


Figure 23. Illustration of the $[Si_8O_{12}]$ core structure of the $[Si_8O_{12}](OSnMe_3)_8$ building block

2.1.3 Linkers

Two categories of linkers are involved:

1. Metal precursors (active linkers): titanium tetrachloride ($TiCl_4$), isopropoxy-trichloro-titanium [$TiCl_3(OiPr)$], d2sopropoxy-dichloro-titanium [$TiCl_2(OiPr)_2$] and polynuclear [$Ti_4Cl_6(\mu_2\text{-}O_2CPh)_6(\mu_3\text{-}O)_2$]. (Figure 22, section 2.1.1) These nomonuclear titanium-containing linkers and tetranuclear core (Ti_4O_2) are incorporated into the matrix and become the sites for catalysis.

2. Inert linker: silicon tetrachloride ($SiCl_4$): Once a titanium site surrounded by Si8-bb's is created in the step above, long-range structures are formed from these oligomers with inert silicon linkers. The second crosslinking step serves to improve the stability of these heterogeneous matrices. Moreover, the second crosslinking creates the crucial meso-sized pores that serve as the diffusional channels and provide surface area on which adsorption/desorption of small molecules occur.

Titanium tetrachloride ($TiCl_4$, Aldrich, 99.9%), titanium tetraisopropoxide ($Ti(OiPr)_4$, Fischer Scientific, 98+%) and tetrachlorosilane ($SiCl_4$, Fischer Scientific, 99.5+%) were distilled and stored in Teflon sealed glass vessels under vacuum prior to use. Alkoxylated chlorotitanates, [$TiCl_3(OiPr]$ and [$TiCl_2(OiPr)_2$], and [$Ti_4Cl_6(\mu_2\text{-}O_2CPh)_6(\mu_3\text{-}O)_2$] complex were prepared following the previously established procedures.[73, 78] Details will be discussed in Chapter 3 and 4. All the linkers and the silsesquioxane building block were characterized with NMR and IR, and the spectra collected were consistent with the original literature.

2.1.4 Method of sequential additions

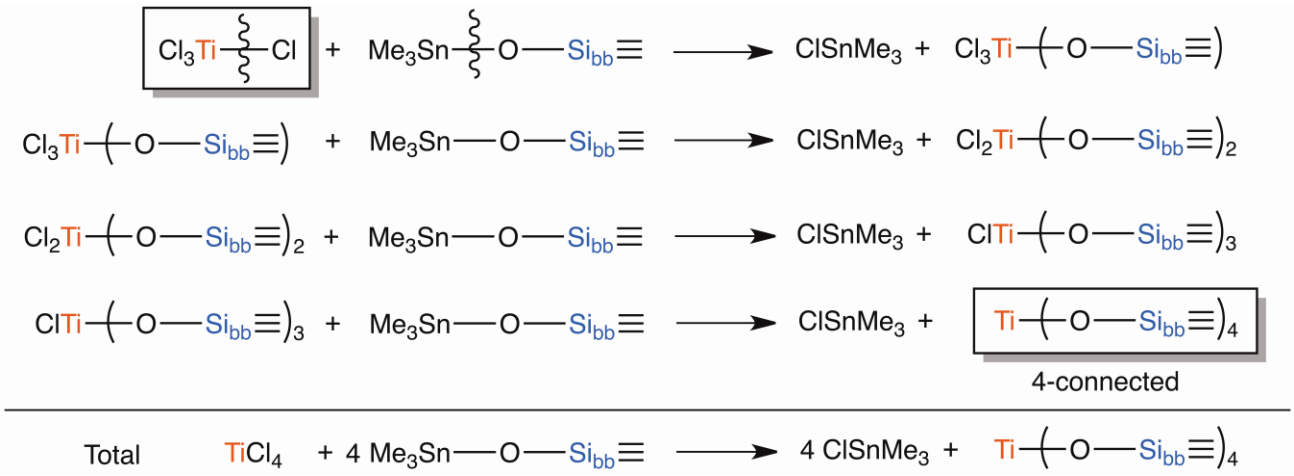
1. Experimental:

Toluene and hexanes were distilled, dried over Na/K alloy, and stored in sealed glass vessels under vacuum. Volatile liquid reactants and organic solvents were vapor transferred into reaction flasks for most syntheses. Experiments with air-sensitive materials were performed using Schlenk techniques under high vacuum or in the nitrogen atmosphere glove box. Glassware was pre-treated with trimethylchlorosilane/triethylamine to remove any silanol groups on their surfaces, and then rinsed with de-ionized water and dried in the oven. The volatile components, such as $TiCl_4$ and the solvent of toluene, are added into Schlenk vessel through vapor transfer at -78 °C (dry ice). Solid reactants such as alkoxylated chlorotitanates $Ti(OR)_{4-x}Cl_x$ and the silicate bb are added to reactions in the glove box. The reaction Schlenk

vessel is heated at 80 °C while stirring at 400 rpm for 24 hours. Under these conditions, a pale precipitate forms typically in 30 minutes out of a clear solution. After 24 hours of heating/stirring, the mixture of precipitates and clear solution is dried at 80 °C under vacuum for 18 hours to remove any volatiles components, including byproduct Me_3SnCl and toluene. After the first step of crosslinking, the residue appears as an off-white solid.

2. Three major steps of sequential additions are involved in the synthesis of atomically dispersed titanium catalysts:

Step #1: To make the mononuclear titanium catalyst, the proper titanium precursor must be used to react with dehydrated bb in the solvent of toluene at 80 °C for 24 h. The stoichiometric ratio between titanium to bb is critical to achieving fully embedded titanium centers. For example, to make 4-connected (4C) titanium catalyst, titanium tetrachloride ($TiCl_4$) is used as the precursor. When limiting amounts of $TiCl_4$ is used, all chloride groups (Ti-Cl) are reacted and replaced with Ti-O-Si linkages, so that homogeneous [TiO_4] sites are embedded in the matrices. As illustrated in Equation 2-1, a series of consecutive irreversible metathesis reactions occur involving the functional groups of chloride (-Cl) and trimethyltin (-$SnMe_3$) on the corner of bb, form Ti-O-Si linkages and the byproduct of trimethyltin chloride (Me_3SnCl). It is important to note that 1:1 stoichiometric ratio between the moles of Me_3SnCl and [Ti-O-Si] linkages formed. Taking advantage of this, connectivity that is defined to be the number of Ti-O-Si linkage per titanium site can be quantified by the gravimetric measurement of the mass of $ClSnMe_3$ produced in a crosslinking reaction (section 2.1.5).



Equation 2-1. Step by step metathesis reactions between $TiCl_4$ and bb

Following the same methodology, 2C- and 3C-Ti catalysts start with alkoxylated chlorotitanates, $Ti(OiPr)_{4-x}Cl_x$ (x = 2 or 3), as the precursors. When these titanium precursors are the limiting reactant, the reaction involving three types of mononuclear titanium compounds and trimethyltin functional groups on bb are illustrated in Figure 24.

Step #2: As shown in Figure 25, the second step in building the final solid involves silicon tetrachloride ($SiCl_4$, 99.8+%, Acros Organics) as the inert linker to grow matrices with long-range structure. Two equivalents of $SiCl_4$ to bb are vapor transferred into the original Schlenk vessel after the first crosslinking is finished. Based on the gravimetric measurement, 2.0-2.5 out of 4 chlorides on each silicon generally react and are replaced by $Si\text{-}O\text{-}Si_{bb}$ linkages (1.5-2.0 silyl chlorides are left per silicon). The reaction takes place in toluene at 80 °C with vigorous stirring over 48 h. A colorless gel forms near the surface of the solution during this time. Toluene and byproduct Me_3SnCl are then removed under vacuum at 80 °C (12 hours). The residue appears to be an off-white loose powder.

At this point in the synthesis, matrix building is finished. What remains to be done is to remove both residual trimethyltin groups and reactive silyl chloride groups, so that a “clean” titanosilicate catalyst is produced. This step is referred to as the passivation step.

Step #3: The resulting materials are passivated with excess methanol (2 methanol : 1 silyl chloride) in toluene as the solvent. The process, as illustrated in Figure 26, replaces Si-Cl with Si-OMe, and generates hydrochloric acid (HCl) that can then react with trimethyltin groups. The byproduct Me_3SnCl can then be removed by heating under vacuum. By the end of passivation, Si-Cl and Si-O-Sn groups in the matrices should be replaced by $Si\text{-}OCH_3$ and Si-OH, and therefore the final catalyst (as-synthesized catalyst) should be much more air and moisture stable. The only active species in the silica matrices should be the incorporated titanium centers. Virtually all the residual tin can be removed in this step and the actual weight percentage (Sn wt%) is below 1.0% according to ICP elemental analysis.

Finally, these passivated catalysts are ready to be used in the oxidation reaction with aqueous H_2O_2. Illustrations of 4-connected (4C), 3-connected (3C) and 2-connected (2C) titanium centers within the bb matrix are shown in Figure 19. The structure of tetranuclear titanium center will be discussed in Chpater IV based on the results of characterization.

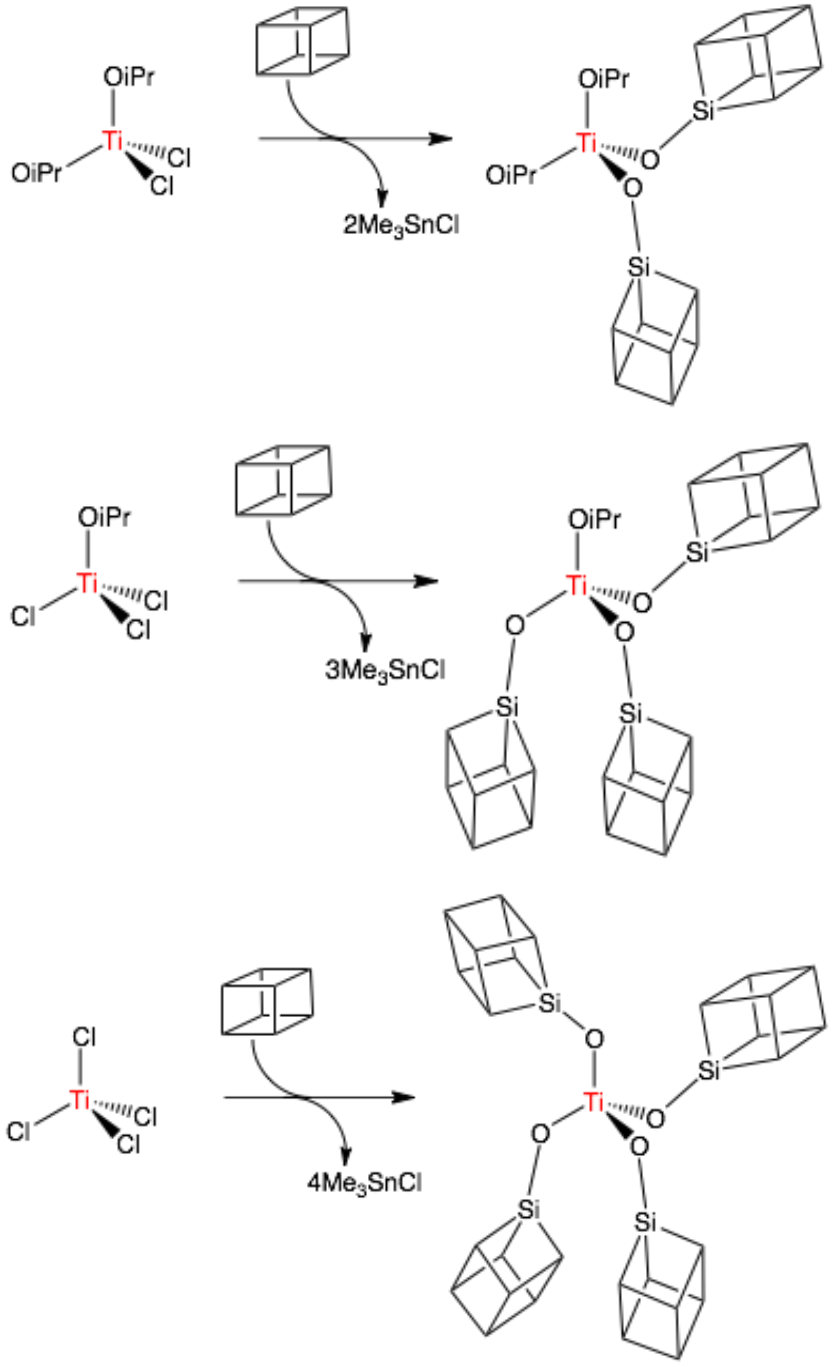


Figure 24. First step reactions between $Ti(OiPr)_{4-x}Cl_x$ (x = 2, 3 or 4, top to bottom) and bb

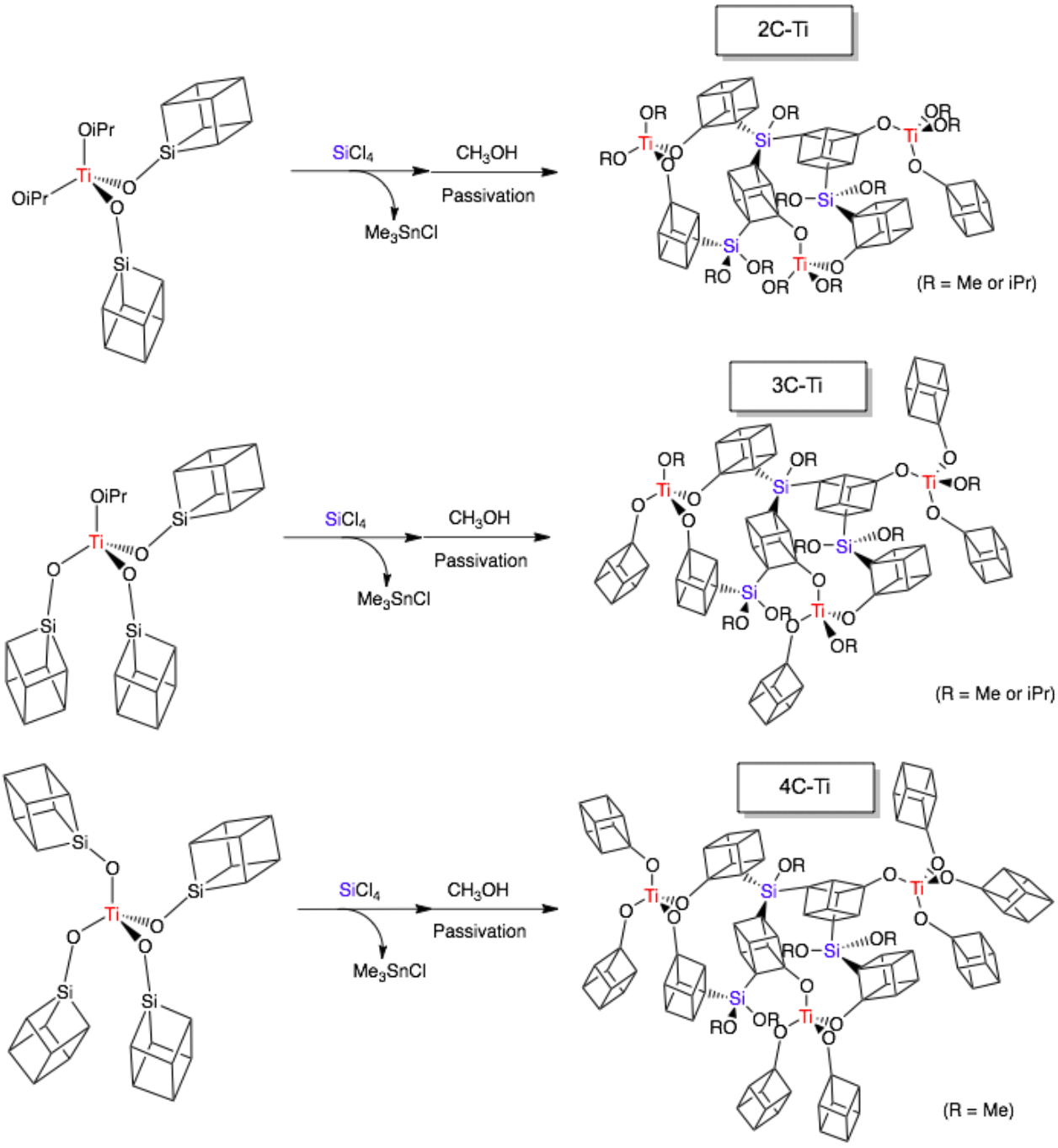


Figure 25. Second crosslinking (step #2) and passivation (step #3) of 2C-, 3C- and 4C-Ti (from top to bottom)

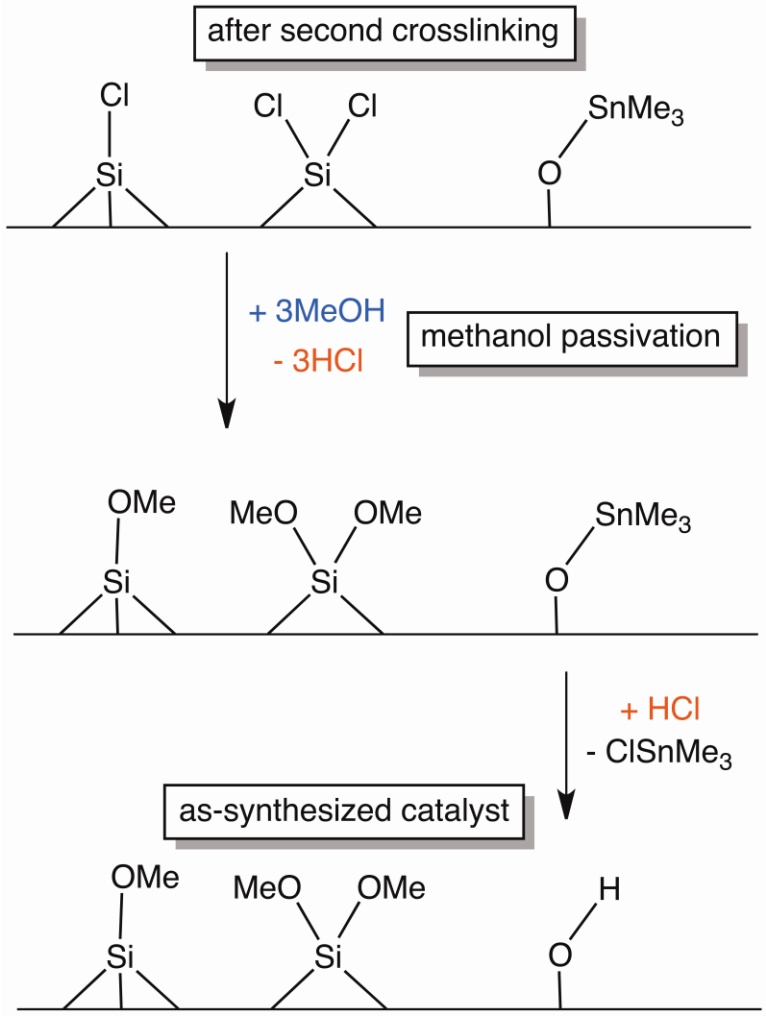


Figure 26. Multiple reactions in the step of methanol passivation

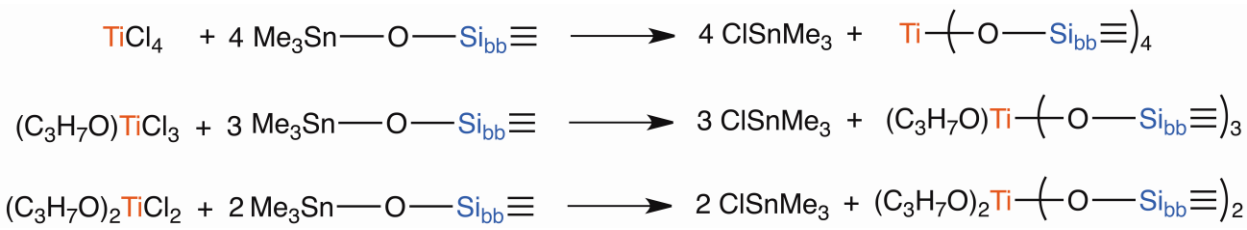
3. Preparation of Ti-free platform:

The building block synthetic methodology is also applied to preparing a Ti-free platform that is characterized for comparison purposes, for example, with IR, DRUV and BET surface area. During step #1 in synthesis, the titanium precursor is replaced with silicon tetrachloride ($SiCl_4$), followed by the normal synthetic procedures (step #2 and step #3 passivation). The final sample of Ti-free platform appears as a white loose powder.

2.1.5 Gravimetric analysis

Connectivity of a titanium center in a silica matrix is defined to be the number of Ti-O-Si linkages around the titanium center. Much effort has been devoted to prepare and characterize the isolated titanium centers that possess specific connectivities. Throughout the history of titanosilicates, it has been challenging to characterize or confirm the local structures around titanium on the atomic level. In previous studies starting with silica, the structures of dimeric titanium centers were hypothesized based on the weight change from the loss of surface hydroxy groups (-OH), according to thermogravimetric analysis (TGA).[51] The varying amount of surface hydroxy is correlated to the process of titanium deposition, and thus used to prove or disprove the hypothesized structures of titanium centers.

Gravimetric analysis is used to characterize the local structure of titanium centers in this research but in a more direct way than previously attempted. Because of the irreversible metathesis reactions and the formation of volatile byproduct ($ClSnMe_3$), the local connectivity around titanium center can be preliminarily characterized with the gravimetric measurements. The weight loss during the first crosslinking reaction is solely caused by the removal of volatile trimethyltin chloride ($ClSnMe_3$). Therefore, by measuring the weight change before and after the reaction, mmol of $ClSnMe_3$ can be solved, and is equivalent to mmol of Ti-O-Si linkage, according to the reaction equation below. (Equation 2-2)



Equation 2-2

In the reactions above, the [Ti-O-Si] formed and [$ClSnMe_3$] lost are equal. Knowing the amount of titanium precursor and $ClSnMe_3$, the connectivity, defined as Ti-O-Si linkages per titanium site, can be obtained with Equation 2-3. An example of the actual calculation is shown in Table 2.

$$\text{Connectivity} = \frac{[\text{Ti-O-Si}]}{[\text{Ti center}]} = \frac{\left[\text{ClSnMe}_3\right](\text{mmol})}{\left[\text{Ti}\right](\text{mmol})}$$

Equation 2-3

Table 2. An example of the calculation of the connectivity

m (apparatus) [a]	empty glassware + stir bar	230.500 g
m(bb)	bb	1.500 g (0.809 mmol)
m(Ti)	$TiCl_4$	0.077g (0.404 mmol)
m_0 [a]	= m(apparatus) + m(bb) + m(Ti precursor)	232.077 g
m_t [b]	the weight after reaction	231.762 g
m($ClSnMe_3$)	= m_0- m_t	0.315 g $ClSnMe_3$ (1.58 mmol)
Connectivity	[$ClSnMe_3$] ÷ [Ti]	3.91

[a] m(apparatus) and m_0 must be determined after the reaction vessel has been evacuated

[b] m_t is measured by weight after the reaction, when all the volatiles have been removed (solvent and any byproduct) and the vessel is evacuated

Gravimetric analysis provides critical information about the connectivity around titanium centers, because the weight change is directly and quantitatively related to the bonding between titanium and silica bb. The results for atomically dispersed titanium centers are presented in Chapter 3. The tetranuclear titanium cluster and bb undergo a more complex reaction. Gravimetric analysis of the embedded cluster is very helpful to understanding the reaction and is discussed in detail in Chapter IV.

2.2 Diffuse Reflectance UV-Visible Spectroscopy

2.2.1 Introduction

Diffuse reflectance UV-Visible (DRUV) spectroscopy has been widely used in characterizing the titanium centers in titanosilicates.[54, 69, 79, 80] Absorption bands arise from

ligand-to-metal charge transfer (LMCT), typically from ligand oxygen to an unoccupied d orbital of the central titanium ion ($Ti^{4+}O^{2-} \rightarrow Ti^{3+}O^{-}$). The position of the absorption band maximum depends on the coordination and ligand environments of titanium center, and thus is often used to interpret the structure. According to the ligand field theory, LMCT between coordinating ligand (X = Si-O$^-$, H-O$^-$, R-O$^-$, etc.) and empty d orbitals of Ti(IV) can be estimated from the optical electronegativities χ of X and Ti(IV) by the following equation[81, 82]:

$$\bar{\nu}(\mathrm{cm}^{-1}) = 30000\left[\chi_{opt}(\mathrm{X}) - \chi_{opt}(\mathrm{Ti})\right] \qquad \text{Equation 2-4}$$

The coordination of titanium center has the major impact on the absorption. $\chi_{opt}(\mathrm{Ti})$ of tetrahedral and octahedral geometry are 1.85 and 2.05 respectively.[81] LMCT of octahedral titanium is expected to absorb at a lower wavenumber compared to tetrahedral titanium center, which is consistent with the trend seen in most titanosilicates. Amorphous TiO_2-SiO_2 that contains primarily 6-coordinated titanium exhibits significant red shift in the maximum of absorption band (~290 nm) compared to 4-coordinated titanium in TS-1 (~210 nm). Along with the coordination geometry, the identity of the ligands around titanium centers also influences the position of the absorption band. According to some literature [82], some arbitrary values of $\chi_{opt}(\mathrm{X})$ are Si-O$^-$ (3.17), H-O$^-$ (2.9), HOO$^-$ (3.45), H_2O (3.5). Usually hydration of titanosilicate results in not only an increase in coordination of titanium (tetrahedral to octahedral) but also lower $\chi_{opt}(\mathrm{X})$ due to the change from Si-O$^-$ to H-O$^-$. The red shift in absorption band after hydration is a combined results of both effects.

The spectral differences among titanium ions in silicate matrices can also be related to the different Ti-O-Si bond angles.[83] When the geometry changes from O_h to T_d, the bond angle of Ti-O-Si increases, causing the hybridization of bridging oxygen around titanium center changes from sp^3 to sp^2 and eventually sp that favors π electron donating. As a result, the non-bonding e orbital splits into bonding e_π and anti-bonding e_π*, and the latter becomes LUMO in T_d geometry with higher energy than that in O_h. Therefore, LMCT increases from O_h to T_d geometry, and the larger band gap is consistent with the blue shifts observed in DRUV absorption.

Quantum size effect also plays a role in DRUV spectra of titanosilicates. Red shifts of absorption edges are observed with high titanium content. In some cases, when small titania particles are present and the wavelength of absorption is related to the particle size. In

summary, a number of factors appear to influence the wavelength of absorption band, including coordination number of Ti, coordinating ligands, size of the titanium particle (quantum size effect), existence of nano-sized separate titania phase, etc.. The complex influences make it impossible to quantitatively calculate LMCT using Equation 2-4. Nevertheless, DRUV spectroscopy is very helpful to qualitatively interpreting the geometry and coordination of titanium centers.

2.2.2 DRUV spectra and interpretation

Heterogeneous catalysts that have multiple types of titanium centers, generally, exhibit overlapping UV/Vis absorption features. Spectral deconvolution is sometimes necessary to clarify the overlapping features. Different interpretations of the absorption features commonly exist due to the complex factors that affect the spectra as discussed above. Empirically, isolated tetrahedral titanium centers [$Ti(OSi)_4$] or [$Ti(OSi)_3(OH)$] are believed to have an absorption feature centering below ~230 nm. Variation between 205-230 nm is observed with different types of matrix and connectivity, for example, ~210 nm for TS-1 and TS-2, ~220 nm for Ti-MCM-41 (Figure 27)[80], and 205-220 nm for Ti-beta prepared in F^- medium (Ti-beta(F)). Structural Distortion from T_d geometry[84] and higher coordination number around titanium result in red shifts, for example, ~260 nm (5-coordinated Ti) or 270-290 nm (6-coordinated Ti).[10] Large anatase particles is characteristic of an absorption maximum at ~330 nm, and rutile absorbs at the wavelength of ~400 nm. The empirical relationship between the structure of titanium center to the wavelength of absorption is very useful in characterizing the titanium species and providing clues in identifying the coordination or ligand environments around titanium.

2.2.3 Sample preparation & data collection

Diffuse reflectance UV spectrometer is an ideal tool for characterizing powdered or crystalline materials. Incident radiation impinges on a flat surface of sample powder, and subsequently reflects in the forms of diffuse reflection and specular reflection.(Figure 28) Only diffuse reflection that is scattered within the sample and returned to the surface is collected and directed to the detector. Strong specular reflection may cause spectral distortion for highly reflecting samples, which can be reduced by sample dilution. DRUV samples are usually diluted with a non-absorbing matrix such as potassium bromide (KBr), which leads to deeper penetration of the incident beam into the sample. The sample to matrix ratio varies with different compositions of the samples, and some studies recommend 1-5 wt%.

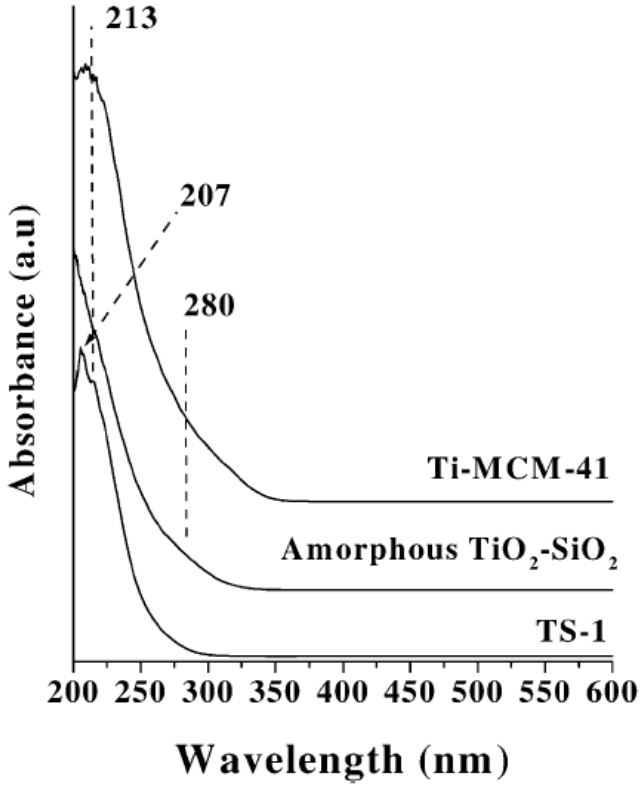


Figure 27. DRUV spectrum of TS-1, Ti-MCM-41 and amorphous TiO_2-SiO_2 (Reprinted from reference 80)

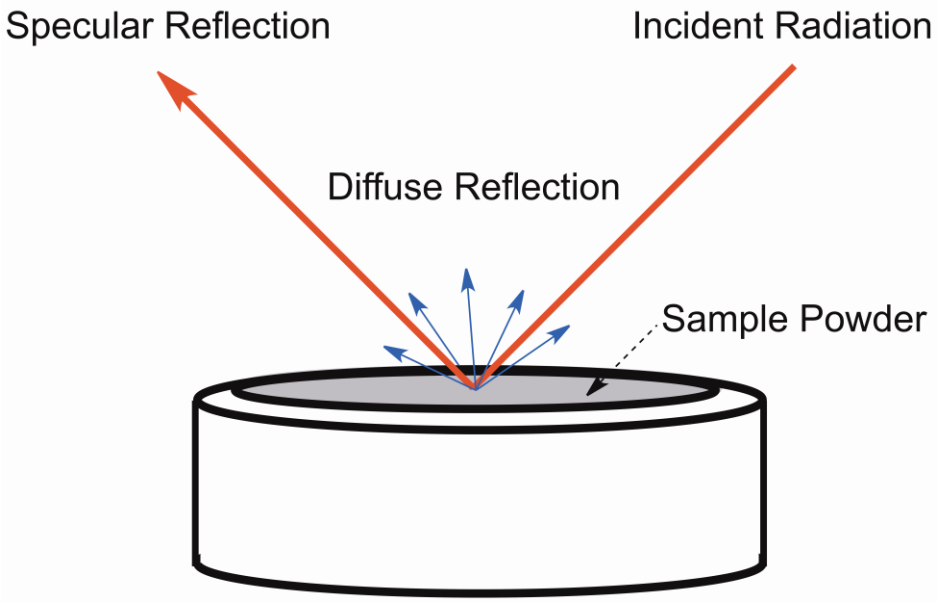


Figure 28. Diffuse reflection on the surface of sample powder

In this research, all samples are titanosilicate materials with titanium content of 2-8 wt%. According to the relative intensity and shape of spectra, the sample to KBr ratio is optimized to be in the range of 50 wt% - 100 wt% (without KBr).

Wig-L-Bug® grinder/mixer is used to mix the sample powders with dry KBr as the matrix. The homogeneity of the mixture ensures the reliability and reproducibility of the spectra. Small particle size contributes to the quality of spectra by reducing specular reflection, and with narrow bandwidths and better relative intensity. Finally, the mixture of powders is then loaded into an air-tight *in situ* cell, of which the main purpose in this research is to keep from air and moisture. The sample cup inside the *in situ* cell should be filled to the top edge with powder, and a smooth and flat top surface is also crucial. All preparations are completed under nitrogen atmosphere in a glove box. Absorption spectra of wavelength 200-600 nm are collected with UV-Vis spectrometer (Evolution 600) under scan mode. The spectrum of pure dry KBr is collected at the beginning of each measurement as the baseline to be subtracted from the sample spectra.

The subject samples in this research are different from traditional titanosilicates in terms of using tin-functionalized bb. When measuring DRUV spectra, the remaining alkyltin groups contribute to the absorption feature at 200-210 nm, close to where the absorption of tetrahedral titanium centers is (210-230 nm). Therefore, Ti-free platform (section 2.1.4, Chapter 2) is used as a second background for DRUV spectra of titanium-containing materials, in order to correct the influence of tin. The spectrum function of platform is timed by an arbitrary coefficient (0.1-1.0), depending on the amount of alkyltin in the material, and subtracted from the sample spectral data.

2.3 X-ray Absorption Spectroscopy (XAS)

2.3.1 Introduction

X-ray absorption spectroscopy (XAS) is a powerful tool to investigate the chemical environment of the absorber atoms in amorphous materials.[85] Kelly *et al.* have provided an detailed introduction about XAS that covers the theoretical background and data processing.[86] X-ray absorption occurs when an atom absorbs the energy of an X-ray, which is used to excite electrons into higher energy electron orbitals that are unoccupied, or into the continuum where the electron is no longer associated with the atom. (Figure 29) The promotion of an electron into a higher energy state by X-ray absorption is short lived. Within approximately a femto-

second (10^{-15} s), the core hole is filled by an electron that transitions from a higher energy orbital.

The number of X-rays transmitted (I_t) through a sample is given by the intensity of X-rays impinging on the sample (I_0) decreased exponentially by the thickness of the sample (x) and the absorption coefficient of the sample (μ).

$$I_t = I_0 e^{-\mu x}$$ Equation 2-5

The X-ray absorption coefficient (μ) is the probability for an X-ray to be absorbed by a sample. X-ray absorption spectroscopy involves measuring μ as a function of X-ray energy. A typical experimental setup for XAS is shown in Figure 30. The X-rays go through an ionization chamber to measure the number of incident X-rays (I_0), then through the sample, and then through another ionization chamber to measure the number of transmitted X-rays (I_t). The X-ray absorption coefficient is determined by rearranging Equation 2-6.

$$\mu x = \ln\left(\frac{I_0}{I_t}\right)$$ Equation 2-6

X-ray fluorescence occurs when an electron from a higher-energy orbital fills the core hole and in doing so releases an X-ray, the energy of which is equivalent to the energy difference between the two orbitals, and unique for a given electronic transition of each element. Therefore, florescence radiation is proportional to the number of core holes generated during excitation process. The absorption coefficient is derived from the number of florescence photons (I_f).

$$\mu x \propto \frac{I_f}{I_0}$$ Equation 2-7

In either type of collection mode, transmission or florescence, the absorption coefficient (μ) is a function of the incident X-ray energy. The probability for absorption increases sharply when the incident X-ray energy equals the energy required to excite an electron to an unoccupied electron orbital or to completely ionize the electron. Figure 31 displays a typical XAS spectrum collected in transmission mode. The step in the absorption coefficient is called the absorption edge. In general, the XAS signal for transmission data decreases as the energy increases while the XAS signal for fluorescence data increases as the energy increases.

The energy of a specific edge increases as the atomic number of the element increases. This is because elements with greater atomic numbers have more positively charged nuclei from a greater number of protons, and therefore, they have a greater binding energy of an electron in a given atomic orbital. For each element, the K-shell electrons are closest to the atom's nucleus, and therefore they have greater binding energy than the L-shell electrons.

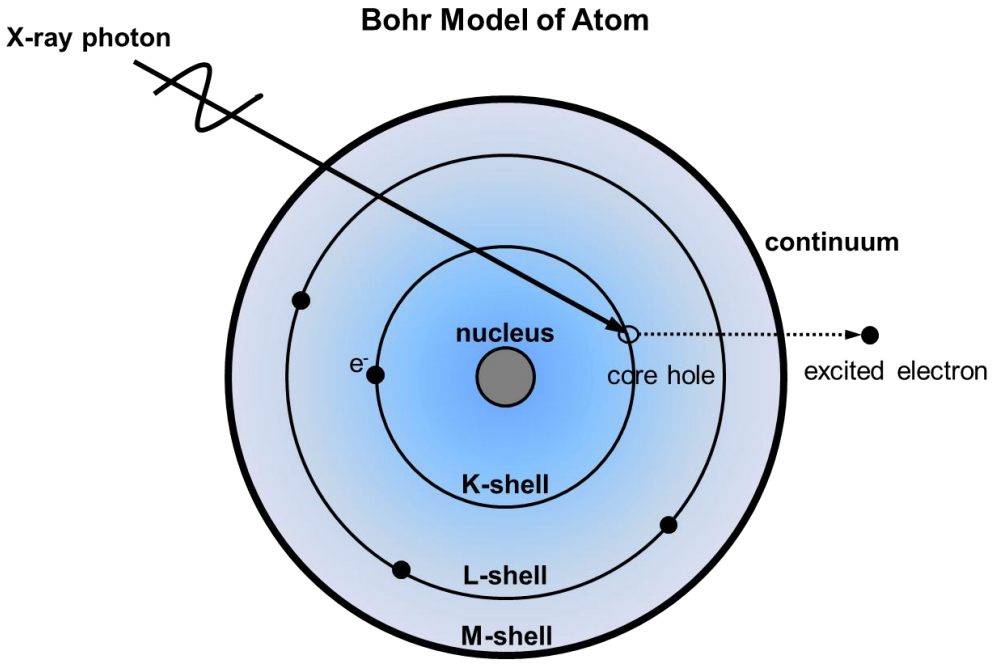


Figure 29. A core electron is excited by a X-ray photon of the proper energy

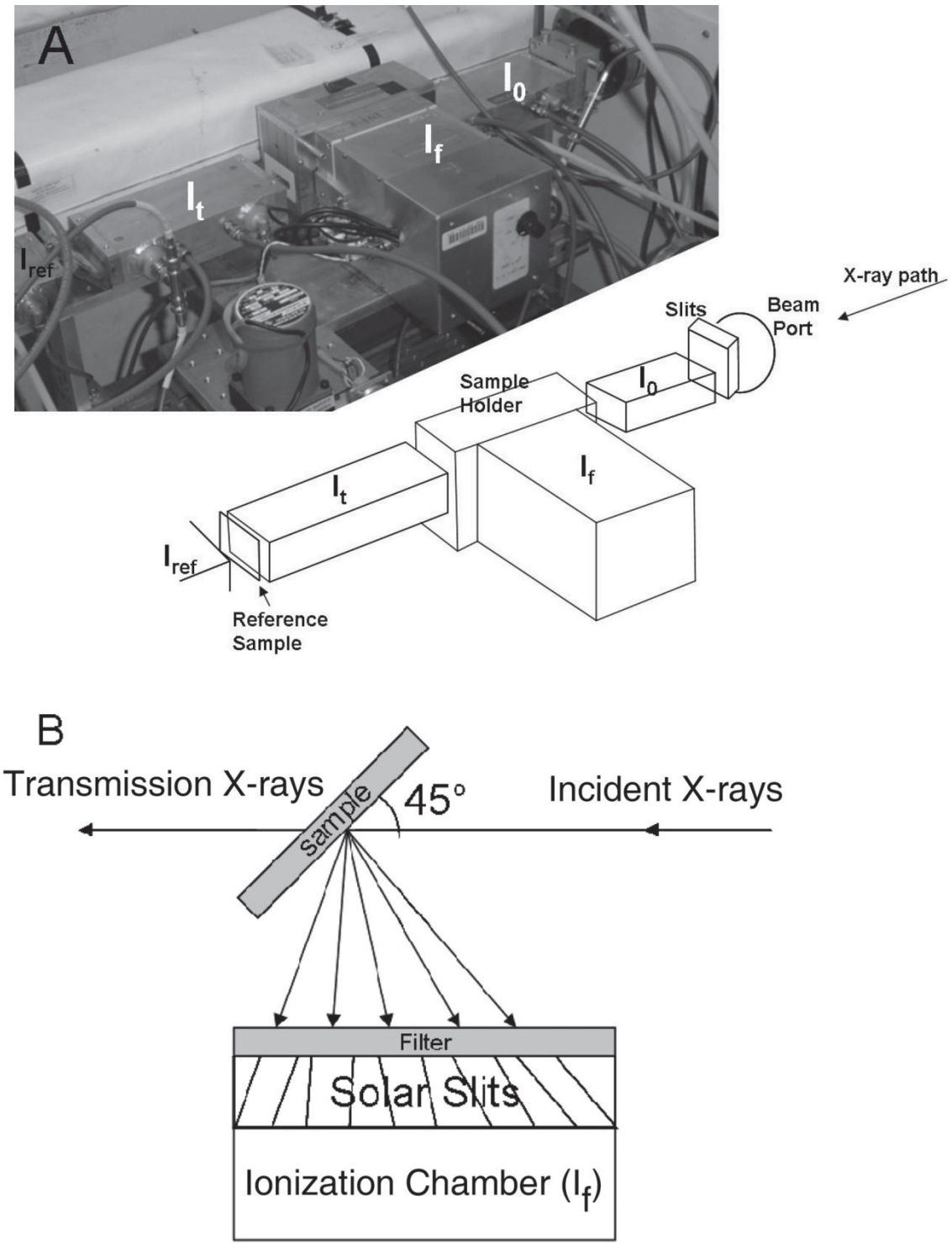


Figure 30. (A) Picture and schematic drawing of an EXAFS experimental setup. (B) Fluorescence sample geometry and detector. (Reprinted from reference 86)

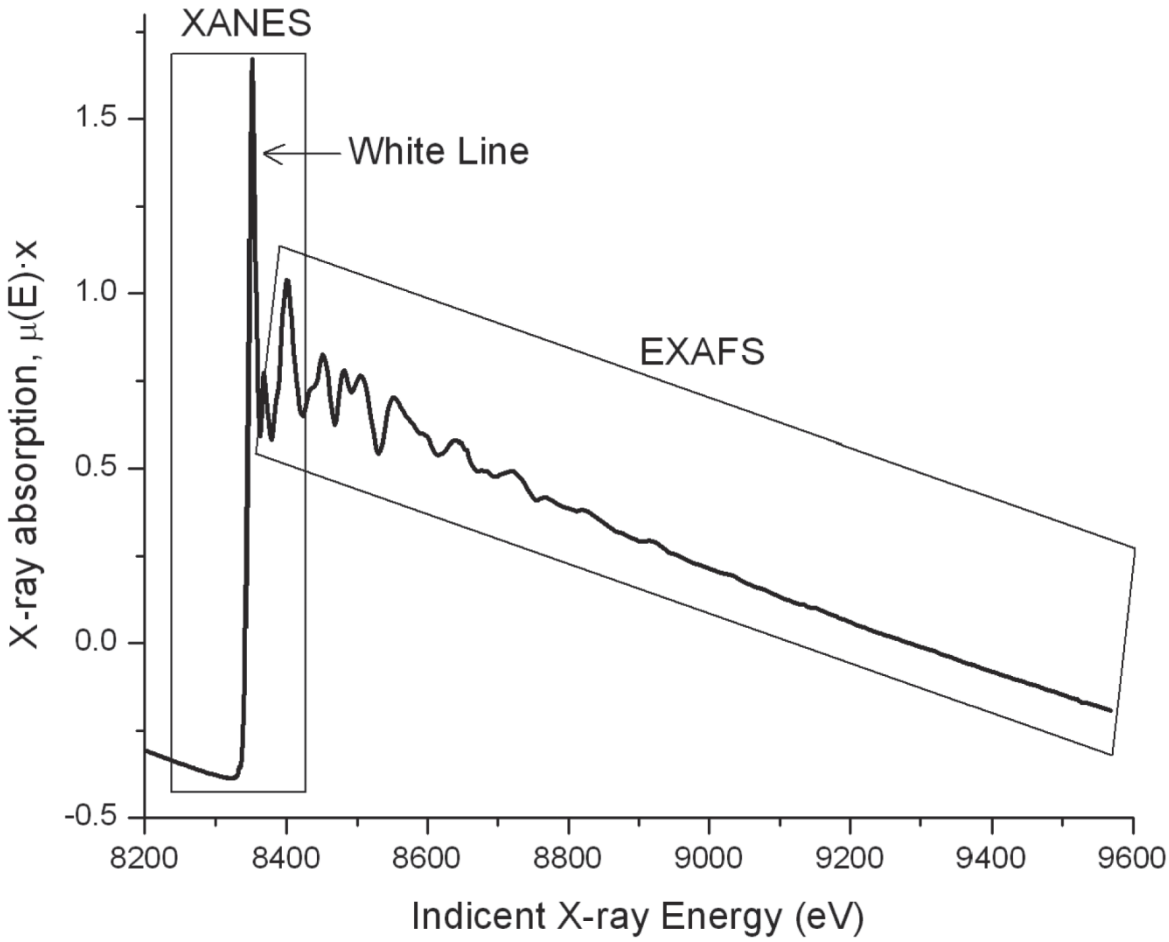


Figure 31. An example of X-ray absorption spectrum of NiO (Reprinted from reference 86)

2.3.2 Sample preparation & data collection

A thin copper plate is used as the sample cell to contain XAS samples. The thickness of the plate is 1 mm and three rectangular holes (15 mm × 7 mm) on each plate function as the sample compartments. (Figure 32) Thin polypropylene windows (7.5 μm) are fixed to the copper plate with two-sided transparent tape to seal the sample cell.

Prior to being loaded into the cell, samples were ground into fine powders with Wig-L-Bug. No noticeable improvement in the spectrum was observed from diluting the sample with boron nitride or graphite. All spectra reported here were collected with the pure sample powder. It was not necessary to dilute samples because of the generally low content of absorber atoms (Ti) in the samples. All the sample preparation was carried out under nitrogen atmosphere in a glove box.

XAS spectra of Ti-containing samples were collected in fluorescence mode at the National Synchrotron Light Source (NSLS) beam lines X19A and X18B with a solid-state passivated implanted planar silicon (PIPS) detector. In this research, Ti(IV) is the absorber atom in all samples. The absorption K edge of titanium is located at the energy of approximately 4975-4985 eV. Titanium foil shows a pre-edge peak at 4966 eV that is used to calibrate the beam energy at the beginning and end of data collection.

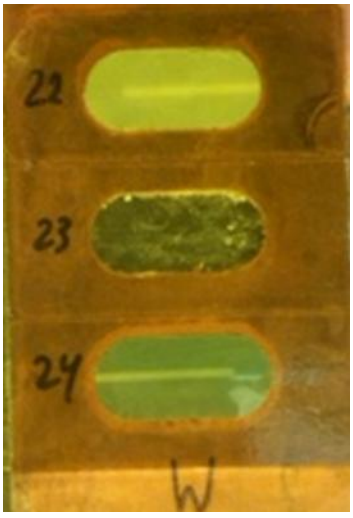


Figure 32. The copper plate loaded with samples and sealed with polypropylene windows

Figure 31 shows a typical XAS spectrum that consists of two regions: X-ray Absorption near edge structure (XANES) and extended X-ray absorption fine structure (EXAFS). XANES refers to the region from -200 eV to +75 eV relative to the main edge, and EXAFS region is 75-1000 eV above the edge. During the collection of spectra, different step sizes and integration time are used in different energy ranges (step size, integration time, energy range): (5 eV, 1s, -200 to -15 eV), (0.5 eV, 2s, -15 to +75 eV), (1.5 eV, 3s, +75 to +550 eV), (5 eV, 4s, +550 to +1000 eV).

Three or four scans were collected for each sample and processed with IFFEFT data analysis software suite (Athena and Artemis programs) developed by Ravel, B. *et. al.* from NSLS. The FEFF 8 modeling program was used to analyze EXAFS spectra. The theoretical phase and amplitude functions were generated from the function of FEFF 8 within Artemis.

2.3.3 General interpretation of XAS spectra

This research followed the standard XAS data processing reported previously.[75] The main steps of the procedure includes:

1. Glitch removal

2. Truncating and aligning the spectrum

3. Averaging multiple scans and merging into one spectrum

4. Defining threshold energy (E_0): Absorption edge energy, or threshold energy, (E_0) is generally defined as the point of inflection of the absorption edge, and can provide information about the oxidation state of the absorbing atom. In this study, the energy at half height of the absorption edge is used to define E_0.

5. Defining pre-edge and post-edge lines: These lines are determined with two data points on the absorption curve, respectively. The difference between pre- and post-edge lines at the energy of E_0 determines the absorption step height.

6. Normalization of the spectrum: this is done by dividing the measured spectra by the absorption step height and subtracting a regressed line determined by the pre-edge region from the entire spectra.

7. Background subtraction and Fourier transform (EXAFS processing): A smooth absorption edge background curve is generated based on the absorption edge energy with Athena, and subtracted during the Fourier transform of EXAFS signal.

These steps of data processing and analysis can be performed using one of several computational programs (e.g. IFEFFIT, WinXAS, GNXAS). Abundant chemical and structural information about the metal sites, including coordination, backscattering shell of atoms and bond lengths, are available in a full EXAFS analysis.

The basic processing of XAS spectra is crucial for accurately fitting the data to the theoretical phase and amplitude factors derived from a structural model. The step height determines the amplitude of the EXAFS oscillations and is therefore correlated to the EXAFS parameters such as the amplitude reduction factor (S_0^2), and the coordination number (N). The pre-edge, post-edge, and resulting step height should always be checked before the $\chi(k)$ spectrum is further processed. Normalized spectra (E) can be used in EXAFS analysis to visually check the alignment of the spectra and to look for spectral changes between successive scans from the same sample.

1. XANES:

The absorption features in near-edge region of the spectrum, from -200 eV (below the main edge) to +75 eV (above the edge), correlate closely to the oxidation state and symmetry around the absorber atom. In the spectra of titanium K edge, the intensity of pre-edge feature arising from the electronic transition from 1s to 3d orbital of titanium is sensitive to the coordination symmetry of titanium center. The position and height of pre-edge peak reveal much structural information about the titanium center. The XANES region of 6-coordinated octahedral titanium (O_h) such as titania anatase exhibits multiple pre-edge peaks of low intensity. Because the excitation of the 1s electron to the empty 3d orbital of Ti(IV) in O_h symmetry is Laporte forbidden, namely the $1s(A_{1g})\rightarrow 3d(T_{2g})$, $1s(A_{1g})\rightarrow 3d(E_g)$ transitions for d^0 configuration. Ti(IV) center in tetrahedral (T_d) geometry is characterized by a sharp and intense pre-edge peak arising from $A_1\rightarrow T_2$ transition, which is allowed in T_d symmetry due to significant hybridization of the 3d and 4p orbitals.[59, 87] Typically O_h titanium center shows multiple weak bands, and shifts to higher energy. The sharpness of pre-edge peak is defined by the width at half height of the peak (ΔFWHM).(Figure 33)

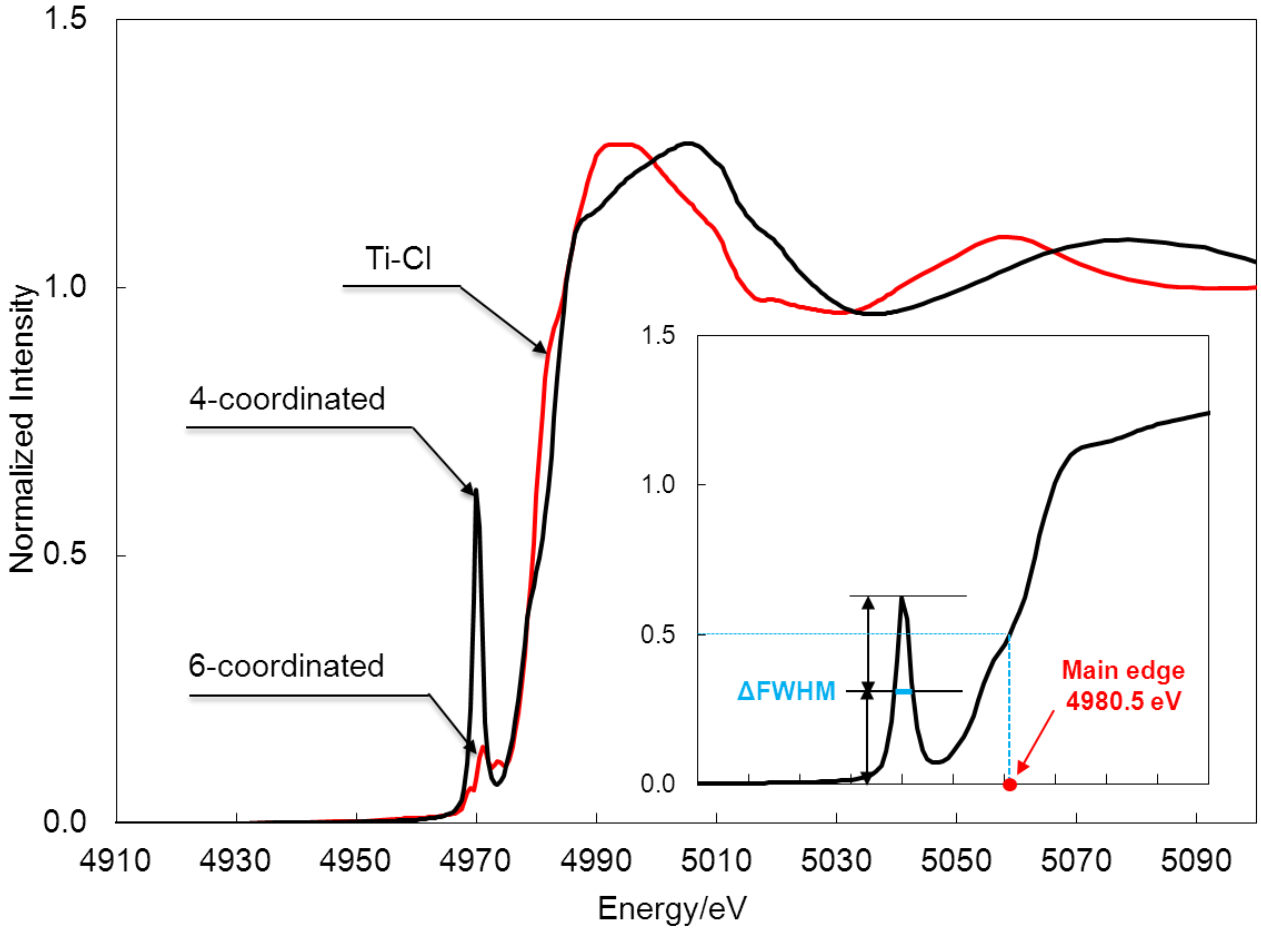


Figure 33. Illustration of typical absorption edges (XANES) for T_d (4-coordinated) and O_h (6-coordinated) titanium centers, and absorption shoulder from the presence of Ti-Cl. (Inset: ΔFWHM and the main edge energy)

Main edge energy is defined as the energy at half height, and shifts with the oxidation state of the absorber atom. Because Ti(IV) is the only absorber in this research, the position of main edge is mainly associated with the ligands in coordination spheres. A smooth edge is usually observed when Ti(IV) coordinates only with oxygen. When chloride is present in the first shell around titanium (Ti-Cl), a pronounced absorption shoulder is observed on the main edge. (Figure 33) The intensity of the shoulder increases with the number of Ti-Cl bonds. The lower shoulder on the main edge has been previously assigned to a Ti-based 1s→4p shakedown transition.[87]

Farges *et al.*[88] investigated the relation between pre-edge features and coordination number (CN) of Ti(IV) center in a number of Ti-containing metal oxides (Figure 34). It is clear that both pre-edge height and position shifts with varying CN's. Specifically, pre-edge peak of 4-coordianted titanium species locates at energy below 4970 eV. The intensity is related to the long-range order of the material. In the cases of mixed oxides with well-defined lattices such as TS-1, intensity of pre-edge peak is above 65% edge jump. Amorphous materials tend to show lower intensity. More discussion is provided in section 3.4 (Chapter 3). 6-coordinated titanium center has multiple pre-edge peaks with intensity below 40% edge jump due to the centrosymmetry. The position of pre-edge peak shifts sensitively with the coordination. 4-coordinated titanium locates below 4970 eV, whereas 6-coordianted above ≥4971 eV. The study suggests that the shift in pre-edge position be associated with a shift in the Fermi energy due to the varying coordinations.[88] XANES and EXAFS have also been applied to investigate the changes in coordination of the titanium centers in TS-1 with ammonia, pyridine and deuteriated acetonitrile (CD_3CN) as molecular probes.[89, 90] The change in CN from 4 to 6 accompanies with progressive reduction in the pre-edge intensity in XANES spectra.

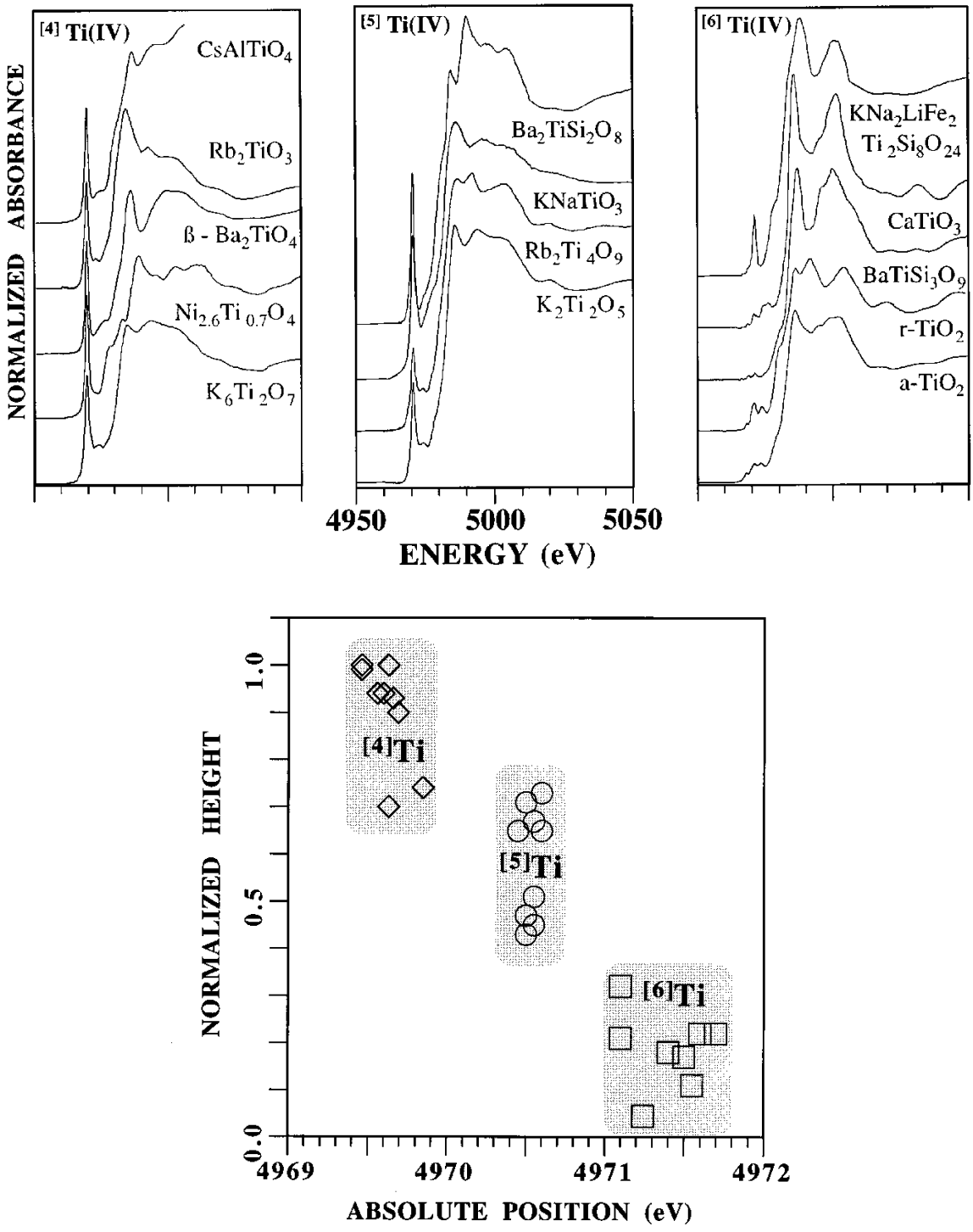


Figure 34. (Top) Normalized XANES regions of 4-, 5- and 6-coordinated of Ti(IV) center in a series of metal oxide compounds; (Bottom) correlation between pre-edge feature and coordination of Ti center (Reprinted from reference 88)

2. EXAFS:

The spectral region referred to as the extended X-ray absorption fine structure (EXAFS) spectral region may be used to determine local molecular bonding environments of elements. EXAFS oscillations superimposed on a smooth background edge (Figure 31) contain information on the types and numbers of atoms in coordination with absorber atoms, their interatomic distances, and the degree of local molecular bonding disorder. Above the absorption edge, the energy of X-ray excites an electron into the continuum. The energy beyond that need for ionization is released in the form of photoelectron with increasing kinetic energy. The photoelectron waves are scattered only from the atoms surrounding the absorber. The oscillatory part of the absorption coefficient is associated with the relative phases of photoelectron waves, which depends on the wavelength (energy) and the interatomic distances between absorber and scattering atoms (bond distances).[86]

Each atom at the same radial distance from the absorber, i.e. a shell, contributes to the same component of the EXASF signal. Single scattering paths are from one shell of atoms, and multiple scattering paths are from multiple shells. (Figure 35) Degeneracy of each scattering path is equivalent to the number of equivalent paths. In the case of single scattering path, the degeneracy equals to the coordination number (CN) in the corresponding shell. For example, in Figure 35 (B) path 1 or 2 has a degeneracy of 4, and path 3 has a degeneracy of 8.

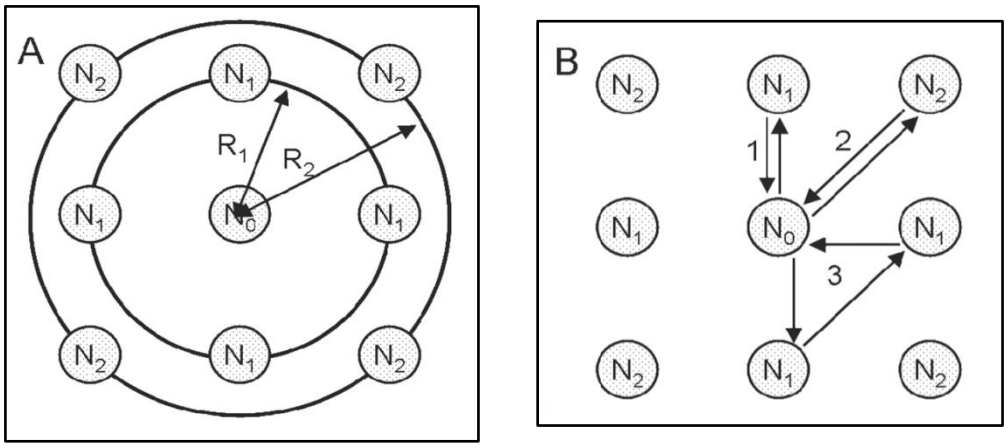


Figure 35. (A) First (N_1) and second (N_2) shells around the absorber (N_0); (B) Single scattering paths labeled 1 (N_0-N_1-N_0) and 2 (N_0-N_2-N_0) and a triangular multiple scattering path labeled 3 (N_0-N_2-N_1-N_0) (Reprinted from reference 86)

XAS spectra are originally collected in E-space (energy-space). (Figure 31) EXAFS is best understood in terms of the wave behavior of the photo-electron created in the absorption process. Because of this, it is common to convert the x-ray energy (E) to k, the wavenumber of the photo-electron, which has dimensions of 1/distance and is defined as Equation 2-8.

$$k = \sqrt{\frac{2m_e(E-E_0)}{\hbar}}$$ Equation 2-8

In the equation, E_0 is the absorption edge energy and m_e is the electron mass. The primary quantity for EXAFS is then $\chi(k)$, the oscillations as a function of photo-electron wavenumber. Backscattering fine structure is extracted from the smooth absorption edge background and is displayed as $\chi(k)$ in reciprocal space (k-space). To emphasize the oscillations, $\chi(k)$ is often multiplied by a power of k typically k^2 or k^3. The k-space data are then converted into R-space plots through Fourier transform. Figure 36 shows a typical k-space and R-space plots (solid lines).

The different frequencies apparent in the oscillations in $\chi(k)$ correspond to different near-neighbor coordination shells. A structural model for the absorber site is constructed using estimates of bond lengths and angles found in literature. In this study, ChemDraw is used to generate and optimize these models based on bond length and angle data found in the literature.[59, 91-94] Scattering paths are generated by FEFF 8 after importing the structural model. In order to fit a model to experimental data, each path can be written in the following form:

$$\chi_i(k) = \frac{(N_i S_0^2) F_{eff_i}(k)}{kR_i^2} \sin[2kR_i + \varphi(k)] e^{-2\sigma_i^2 k^2} e^{\frac{-2R}{\lambda(k)}}$$ Equation 2-9

$$R_i = R_{0i} + \Delta R_i$$ Equation 2-10

$$k = \sqrt{\frac{2m_e(E-E_0+\Delta E_0)}{\hbar}}$$ Equation 2-11

Each of the elements in Equation 2-9 is defined in Table 3.

Table 3. Elements in the expression of scattering path

$N_i S_0^2$	to modify the amplitude of the EXAFS signal and do not have a k-dependence; amplitude reduction factor (S_0^2) usually has a value between 0.7 and 1.0; coordination number N_i
$F_{eff_i}(k)$	provided by the analysis software and does not affect any fit parameters
$\frac{1}{R_i^2}$	the inverse dependency on distance diminishes the EXAFS with increasing distance from the absorber (R_i)
$\sin[2kR_i + \varphi(k)]$	the oscillations in the EXAFS signal with a phase of [$2kR_i + \varphi(k)$]
$e^{-2\sigma_i^2 k^2}$	contains a classic Debye-Waller factor (σ^2), in order to model dynamic (thermal) disorder as well as static disorder (structural heterogeneity)
$e^{\frac{-2R}{\lambda(k)}}$	depends on λ(k), which is provided/calculated by the analysis software and does not affect any fit parameters
ΔR_i	a change in the interatomic distance relative to the initial path length R_i
ΔE_0	a change in the photoelectron energy which is used to align the energy scale of the theoretical spectrum to match the measured spectrum

The experimental data is compared with the function generated from the structural model (Figure 36, dotted lines). Fit parameters (S_0^2, N, ΔR, ΔE_0, σ^2) are defined for each scattering path followed by an iterative refinement of these fit parameters. A fitting procedure by Artemis is fulfilled when the fit parameters converge to stable and acceptable values and the statistical measures of the fit (R-factor, χ^2 , and reduced χ^2) are also acceptable.

2.4 Other Characterization Techniques

2.4.1 ICP elemental analysis

Inductively coupled plasma atomic emission spectroscopy (ICP-AES) is a useful tool for quantifying trace metals in digestible solids or inorganic solutions. 5-6 solutions at different concentration of titanium (5-50 ppm) are first made from a titanium standard solution for ICP purposes (1000 mg/L, Sigma-Aldrich) and de-ionized (DI) water. Once these solutions are measured by ICP, a calibration curve of intensity vs. concentration is plotted automatically on the instrument.

A sample solution is made as follows: 10-30 mg of sample powder (2-8 wt% Ti) was digested with concentrated nitric acid (2.0 mL) and hydrofluoric acid (2.0 mL), and diluted into ~50 g of solution with DI water. Three to four solutions of each sample at different concentrations were analyzed with the average value reported finally.

Titanium content is an important parameter for heterogeneous catalyst. Ideally, titanium from the precursor should be converted at 100% to the active sites in the final catalyst. Therefore, the number of active sites in a catalytic reaction can be obtained based on Tiwt%. More importantly, turn over frequency (TOF) becomes available and enables the catalytic activity to be evaluated on a per site basis.

In principle, the non-hydrolytic synthesis prior to passivation should not cause titanium leaching. As mentioned above, the step of passivation involves the formation of hydrochloric acid, which is effective in removing the alkyltin groups but may possibly break Ti-O-Si linkages. Titanium contents in the catalyst must be compared with the estimated values. More details will be discussed in Chapter 3 and IV.

Titanium leaching is commonly observed when titanosilicates are used in conjunction with aqueous hydrogen peroxide. Stability of titanosilicates is critical to their practical application. Therefore, titanium contents before and after catalysis must also be quantified.

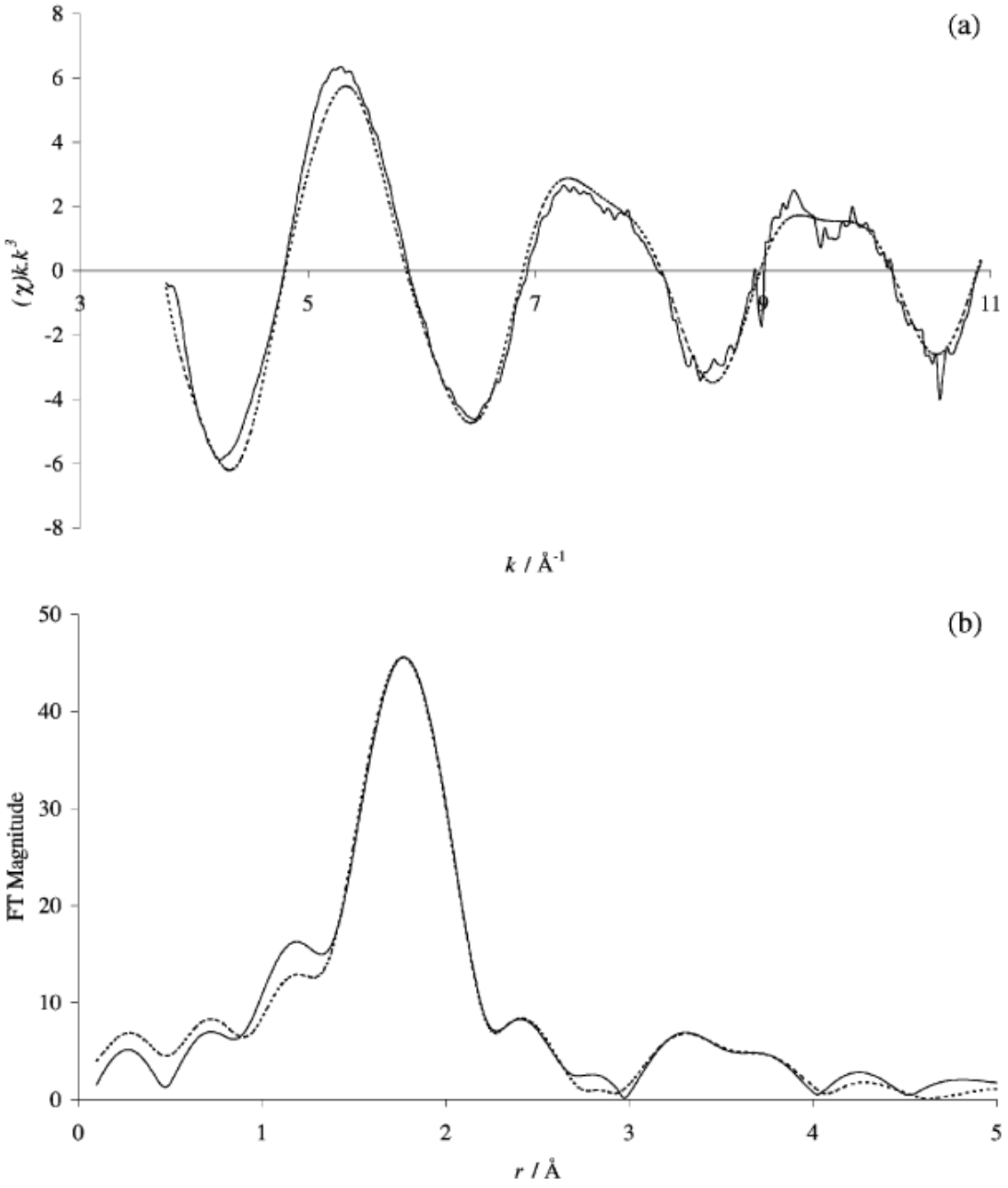


Figure 36. Best fit between experimental results and computed EXAFS employing the full multiple scattering method. (Reprinted from reference 66)

2.4.2 Nitrogen adsorption/desorption (BET)

Brunauer-Emmett-Teller (BET) surface area analysis provides precise specific surface area evaluation of materials by nitrogen multilayer adsorption measured as a function of relative pressure using a fully automated analyzer. The technique encompasses external area and pore area evaluations to determine the total specific surface area in m^2/g.

Approximately 100 mg powder of the sample is used for surface area measurement. The samples include all Ti-containing catalysts after passivation, Ti-MCM-48 and Ti-free platform for comparison. Ti-containing catalysts and Ti-free platform in this study typically have surface areas in the range of 200-500 m^2/g. Ti-MCM-48 prepared following literature procedure [95] has a surface area of 1200 m^2/g that is consistent with literature. Taking advantage of the sequential addition methodology described in this study, Barnes group has discovered that the surface area of these catalysts is adjustable by varying the ratio of linker-bb in each step of synthesis.

2.4.3 Vibrational spectroscopy

1. IR

Infrared spectroscopy is one of the most common techniques used to characterize heterogeneous catalysts. Absorption bands in IR spectra correspond to specific vibrations in a molecule through changes in the dipole moment. The frequency and intensity of these bands are therefore useful for studying the molecules or bonds of the proper symmetry.

In the case of studying TS-1, the atomic substitution of titanium in the silicate framework gives rise to the characteristic vibrational bands. The vibrational band at ~960 cm^{-1} is a fingerprint vibration thought to indicate lattice substitution of titanium centers, which was reported in the original TS-1 patent.[53] Based on many studies on infrared features of titanosilicates, it is generally concluded that the 960 cm^{-1} band arises from the stretching of Si-O bonds in Ti-O-Si bridges.[96-99] Figure 37 displays the 700-1050 cm^{-1} range of typical IR spectra of TS-1 as well as Ti-free silicalite. While the 960 cm^{-1} band is completely absent in Ti-free silicalite, the one in TS-1 increases proportionally with titanium content in both IR and Raman spectra.[96] Later an analogous band in 960-970 cm^{-1} range has been used to characterize other titanosilicates, namely, TS-2, Ti-ZSM-48, Ti-beta, and Ti-MCM-41.[100] It was concluded that the absorption in the range of 960-970 cm^{-1} is associated with the stretching of Si-O bonds in Si-O-Ti linkages.[99] Another very strong band at 1125 cm^{-1} is commonly present in titanosilicates. The

fact that the 1125 cm^{-1} band is enhanced by UV-excited Raman suggests the total symmetry of the vibrations with respect to the absorbing center. Thus, the 1125 cm^{-1} band is unequivocally assigned to the symmetric stretching of the TiO_4 tetrahedron. These vibration bands are useful in identifying the existence of atomically dispersed titanium in silicate. But the attempt to calculate titanium content by integrating the absorption bands has not met with much success.

2. Raman

Raman is a spectroscopic technique used to study the vibrational and rotational modes of a sample and is a complementary technique to IR. Besides of its high resolution and wide spectral range, another important advantage of Raman spectra over infrared lies in the fact that water does not produce a significant Raman signal. Raman spectra are acquired by irradiating a sample with an intense source of monochromatic radiation, typically a visible laser. Figure 38 illustrates that the monochromatic radiation can be scattered either elastically (i.e. Rayleigh scattering) or inelastically (i.e. Raman scattering). Only a small percentage of the light is inelastically scattered, and the amount is inversely proportional to the wavelength of the incident light to the fourth power. Raman scattering can be divided into two types: Stokes and anti-Stokes. The emitted photon of Stokes scattering has less energy than the incident photon, whereas in the case of anti-Stokes scattering, the emitted photon is blue-shifted relative to the incident photon.

In principle, the remaining organic groups such as trimethyltin (-SnMe3) and chloride groups (Ti-Cl, Si-Cl) should observed in Raman spectra. Unfortunately, fluorescence is known to be a common problem when visible excitation sources are used, because the intensity of fluorescence exceeds 10^6 times of that of the Raman signal. Impurity such as aromatic solvents can render the Raman signal undetectable. In this research, fluorescence caused a major problem to the atomically dispersed titanium catalysts, i.e. 2C-, 3C- and 4C-Ti. Nevertheless, reasonable spectra of the tetranuclear titanium cluster and embedded Ti_4 catalyst were obtained with much useful information. Details are discussed in section 4.2.2, Chapter IV.

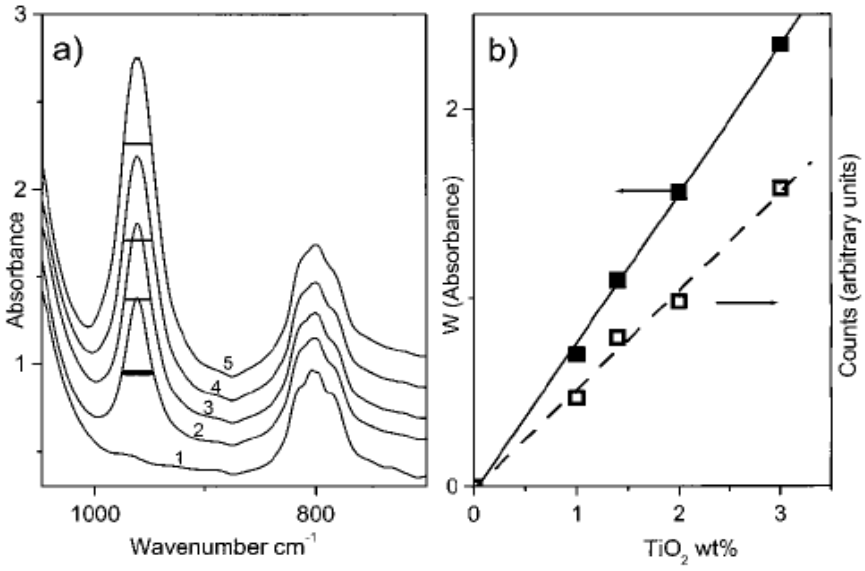


Figure 37. (a) IR spectra of outgassed thin pellets of Ti-free silicalite (curve 1) and TS-1 with increasing Ti-content x (curve 2-5). The horizontal line represents the fwhm of the 960 cm^{-1} band for sample 2-5. (b) Intensity W of the 960 cm^{-1} IR band (normalized) as a function of TiO_2 wt% (full squares), and corresponding Raman counts (open squares) (Reprinted from reference 96)

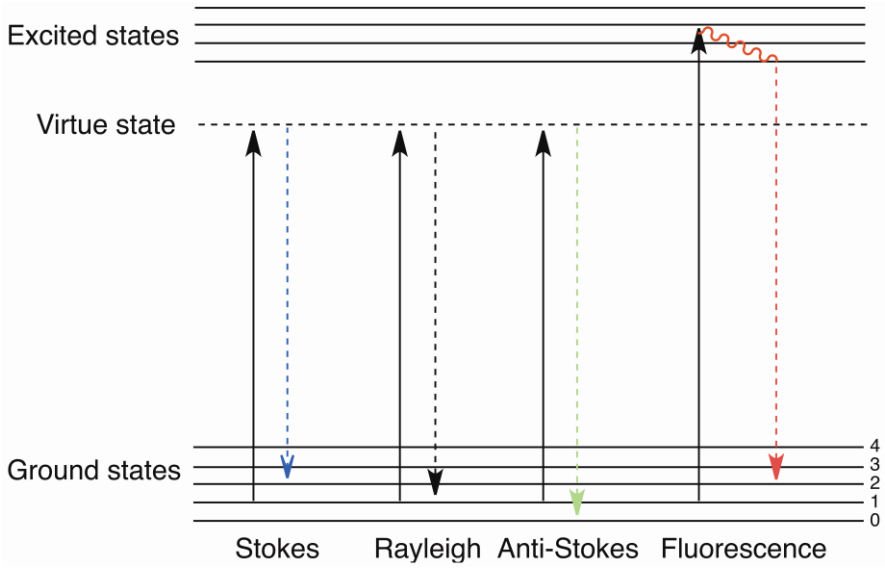


Figure 38. Raman incidence and three types of excitation of photons (Rayleigh, Stokes and Anti-Stokes scattering).

Chapter III. Synthesis and Primary Characterization of Atomically Dispersed Titanosilicate Catalysts

3.1 Synthesis and Preliminary Characterization

3.1.1 Titanium precursors

The synthesis of atomically dispersed titanium catalysts requires mononuclear titanium compounds with chloride functional groups, namely, titanium tetrachloride $TiCl_4$, isopropoxy titanium trichloride $TiCl_3(OiPr)$ and d2sopropoxy titanium dichloride $TiCl_2(OiPr)_2$. The alkoxylated chlorotitanates were prepared by mixing titanium tetrachloride $TiCl_4$ and titanium tetraisopropoxide $Ti(OiPr)_4$, following the procedures developed by Kimigaito *et al.*.[78] The stoichiometric ratios between the two reactions, $TiCl_4$ and $Ti(OiPr)_4$, need to be carefully controlled in order to obtain the desirable product rather than a mixture of two.

$$TiCl_4 + Ti(OiPr)_4 \longrightarrow 2\ TiCl_2(OiPr)_2$$

Equation 3-1

$$3\ TiCl_4 + Ti(OiPr)_4 \longrightarrow 4\ TiCl_2(OiPr)_2$$

Equation 3-2

The starting materials include titanium tetrachloride ($TiCl_4$, 99%, Sigma-Aldrich), Titanium tetraisopropoxide ($Ti(OiPr)_4$, 98+%, Sigma-Aldrich). All chemicals are distilled and stored in vacuumed glass vessels prior to use. The glassware for the reaction is silylated with trimethylsilyl chloride, and then kept in an oven at 80°C prior to use. Initially, $Ti(OiPr)_4$ is added into a silylated Schlenk vessel, followed by ~25 mL of dry n-hexane through vapor transfer at -78.2 °C. $TiCl_4$ is added through vapor transfer at a ratio of either [1 $Ti(OiPr)_4$: 1 $TiCl_4$] or [1$Ti(OiPr)_4$: 3$TiCl_4$], according to equation 3-1 and 3-2. The clear solution is kept stirring and cooled with dry ice when adding $TiCl_4$. Once all reactants are added, the solution is allowed to warm to room temperature and react for 3 hours. In either case (di- or tri-chloride compound), a light yellow precipitate forms almost immediately. The Schlenk vessel is kept in darkness during the reaction in case of any decomposition by the light. Once the reaction is complete, the solvent and volatiles are removed under vacuum at room temperature. The solid product is dried under vacuum over night at room temperature away from the light.

Titanium dichloride and trichloride compounds have been found very reactive. To slow the rate of self-decomposition, storage under nitrogen in a glove box is recommended for these

compounds, which gradually decolorize and turn gray within 1-2 weeks even under nitrogen atmosphere. In this study, alkoxylated chlorotitanates were stored under nitrogen and prepared less than 24 hours before use. NMR spectra of $Ti(OiPr)Cl_3$ and $Ti(OiPr)_2Cl_2$ in deuteriated benzene (C_6D_6) were collected and compared with that of $Ti(OiPr)_4$. As shown in Figure 39, when the ratio of $TiCl_4$ and $Ti(OiPr)_4$ is controlled to be exactly 1:1 or 3:1, the only peaks that are observed are from the desired products. The trend of the chemical shifts is consistent with what is reported in the literature.[78] Peaks indicating mixtures appear when the $TiCl_4$ to $Ti(OiPr)_4$ ratio is inaccurate. The product can then be separated from the impurities through sublimation.

3.1.2 Synthesis & connectivity

The general process of preparing atomically dispersed titanium catalysts is described in Chapter 2. The three types of titanium centers, i.e. 4-connected (4C-Ti), 3-connected (3C-Ti) and 2-connected (2C-Ti), were obtained by using different titanium precursors in the first step of reaction (step #1 in section 2.1.4). Specifically, $TiCl_4$ is used for preparing 4C-Ti, $TiCl_3(OiPr)$ for 3C-Ti, and $TiCl_2(OiPr)_2$ for 2C-Ti. Following each step of synthesis, the volatiles were removed by vacuum and collected in a glass secondary trap kept cold in liquid nitrogen. The NMR spectra (Figure 40) of the volatiles confirm that the only byproduct is trimethyltin chloride ($ClSnMe_3$) as expected. It is critical to use a limiting amount of titanium precursor relative to bb to ensure all chlorides on titanium precursors are reacted. As described in Chapter 2, the connectivity around titanium centers can be obtained from gravimetric analysis. Table 4 summarizes the preferable range of [Ti: bb] ratios in preparing samples containing 4C-, 3C- and 2C-Ti centers, and compare the estimated with the actual connectivity for each type of the catalyst. These results based on gravimetric analysis are reproducible and consistent with the estimated value (± ~10 %). The targeted connectivity verifies that the hypothesized reaction mechanism, i.e. irreversible metathesis reaction between Si-O-$SnMe_3$ and Ti-Cl. Speaking of the synthetic methodology, the gravimetric results as well as other characterization validate the effective control of the connectivity around titanium center by using different precursors.

3.1.3 Elemental analysis (ICP)

The molecular composition of these catalysts can be predicted with the amount of reactants and gravimetric analysis. Titanium content (Ti wt%) can be estimated with [Ti : bb] ratio and the molecular formula. Table 5 summarizes the estimated values for titanium contents in these catalysts that are 2-5 times as much as that in TS-1. These values are based on the assumption that all titanium precursors are successfully embedded without leaching.

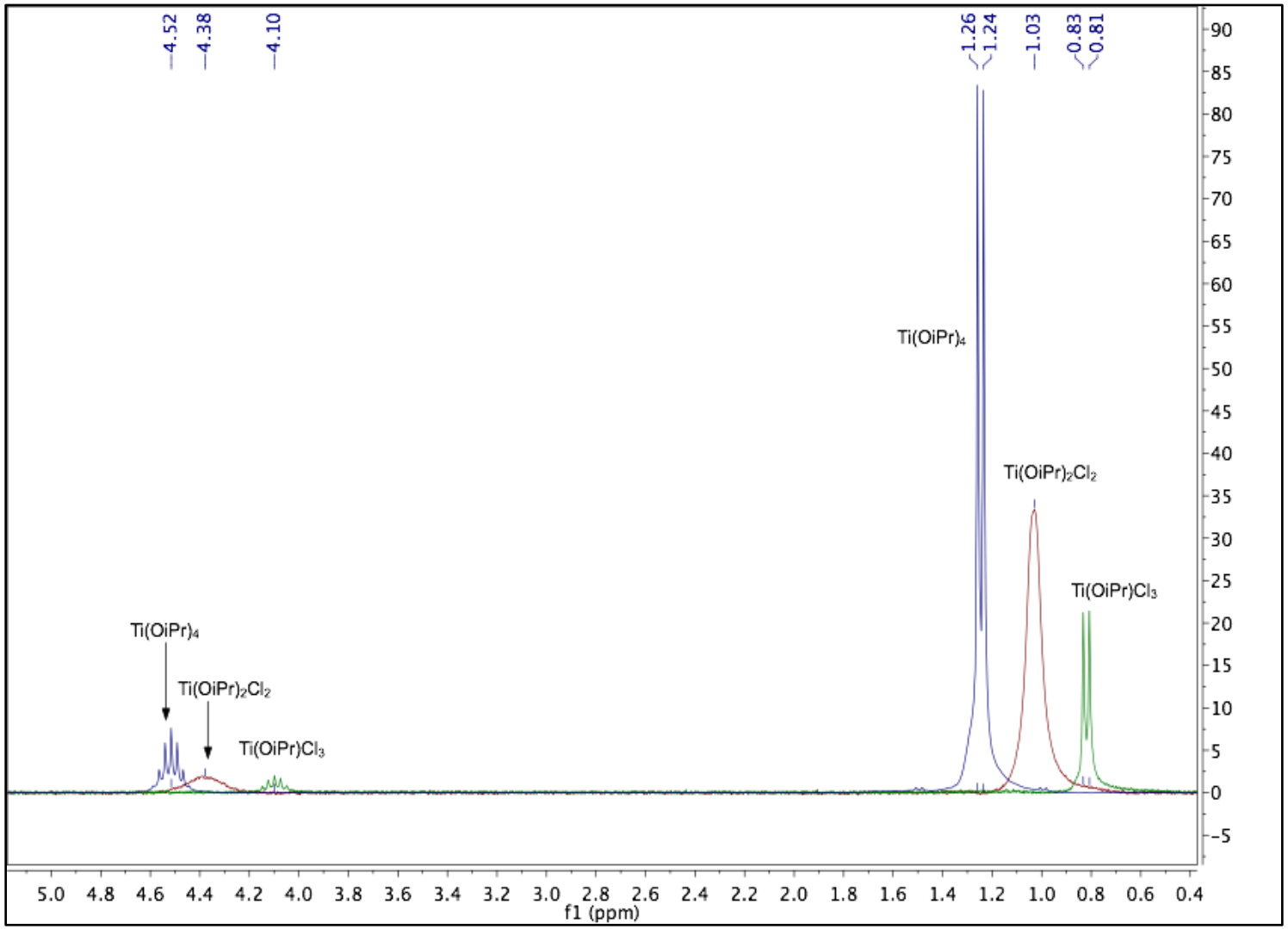


Figure 39. Overlaid ^{1}H NMR spectra of (blue) $Ti(OiPr)_4$, (red) $Ti(OiPr)_2Cl_2$, (green) $Ti(OiPr)Cl_3$

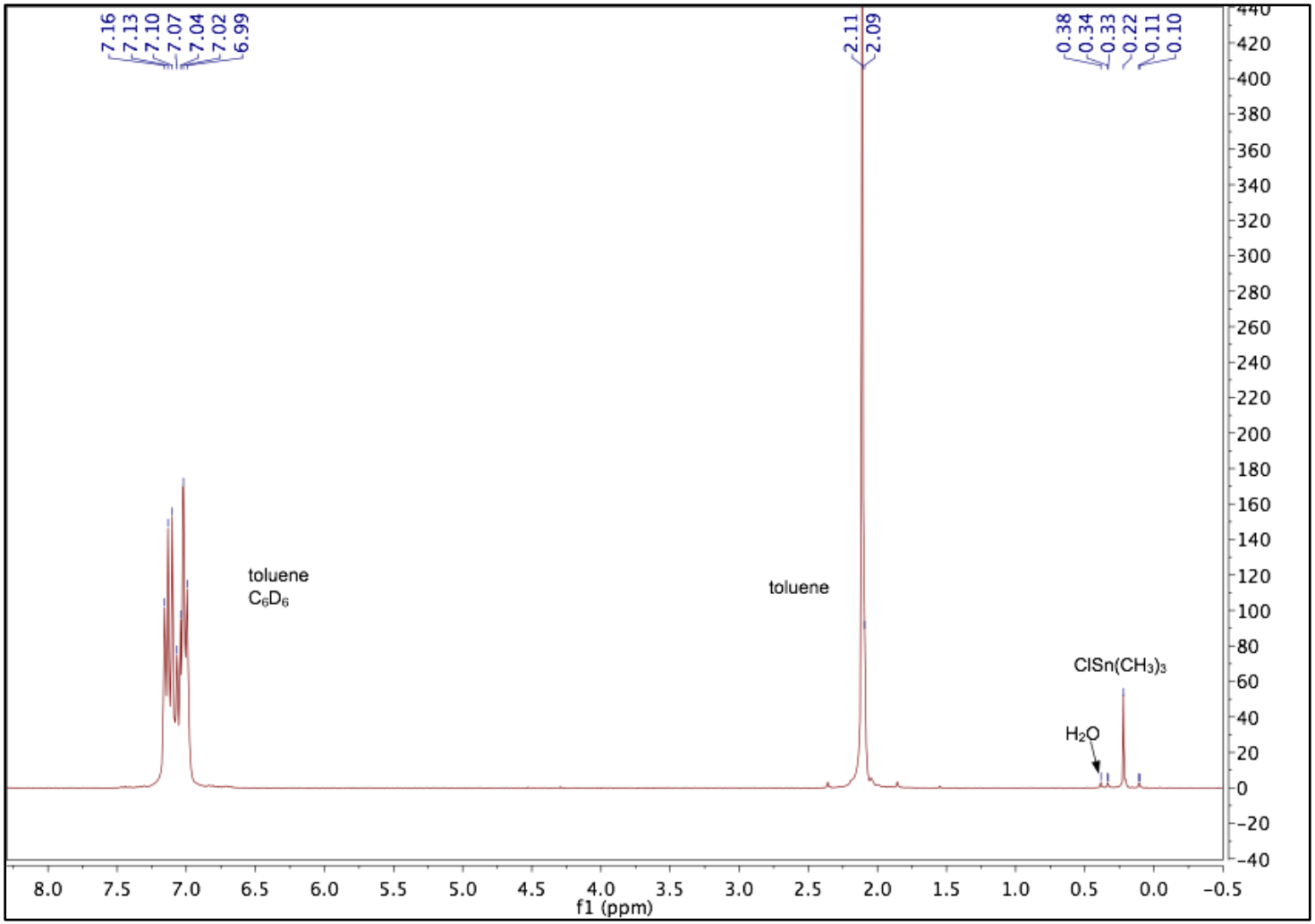


Figure 40. NMR spectrum of the volatiles collected after each step of synthesis

Table 4. Synthesis and connectivity of atomically dispersed titanium catalysts

Ti Sample	Precursor	Ti : bb = x : 1 x value	Estimated Connectivity	Actual Connectivity
4C-Ti	$TiCl_4$	0.5-0.7	4	4.0 ± 0.1
3C-Ti	$Ti(OiPr)Cl_3$	0.7-1.0	3	2.9 ± 0.1
2C-Ti	$Ti(OiPr)_2Cl_2$	1.0-2.0	2	1.8 ± 0.1

During the first two steps of non-hydrolytic reactions titanium leaching is highly unlikely, but the following methanol passivation generates hydrochloric acid (HCl) that possibly breaks Ti-O-Si linkages.

To verify the titanium content in these catalysts, the passivated materials were analyzed with inductively coupled plasma atomic emission spectroscopy (ICP-AES). The results are shown in Table 6. The actual Ti wt% in 2C-, 3C- and 4C-Ti catalysts (column 3) is consistent with the estimate, i.e. no titanium leaching occurred throughout synthesis and all titanium were incorporated and stabilized within the matrices. A very small amount of Sn (< 1 Sn : 100 Si) is detected in the passivated catalysts. While changing the amount of titanium and silicon chloride linkers in synthesis, titanium to tin ratio tends to vary and is generally above [4 Ti : 1 Sn].

Elemental analysis data summarized in Table 7 confirms that the final step of passivation eliminates the majority of the remaining trimethyltin groups in the matrices by showing a drastic decrease in Sn wt% after passivation. Assuming no leaching of titanium, a small increase in titanium wt% (column 2, Table 7) is expected due to the total weight loss during passivation. The actual titanium content by ICP-AES measurement before and after passivation is consistent with the corresponding gravimetric values. Therefore, it is concluded that any titanium initially added has been incorporated with the matrices. Methanol passivation is proven to be an effective method of removing tin, without leaching titanium out of the matrices.

Table 5. Preferable [Ti : bb] ratio, molecular formula, and Ti content following insertion of titanium, second crosslinking and passivation with methanol

Ti Sample	xTi : 1bb [a]	Molecular Formula	Ti wt%$_{(thero.)}$ [b]
4C-Ti	0.5-0.7	$Ti_xSi_{10}O_{20}(OCH_3)_{4x}$	3.5 – 4.6%
3C-Ti	0.7-1.0	$Ti_x(OiPr)_xSi_{10}O_{20}(OCH_3)_{3x}$	4.7 – 6.4%
2C-Ti	1.0-2.0	$Ti_x(OiPr)_{2x}Si_{10}O_{20}(OCH_3)_{2x}$	6.2 – 10.2%
TS-1	0.010-0.025 (xTi : 1Si)	$(TiO_2)_x(SiO_2)$	0.8 – 1.9%

[a] The range of Ti: Si ratio is estimated based on the ratio of [Ti : bb] in the first step of synthesis and subsequently [2$SiCl_4$: bb] is used in the second step of synthesis

[b] The ranges of Ti wt%$_{(thero.)}$ are calculated based on x (column 2) and the formula (column 3)

Table 6. Elemental Analysis of 4C-Ti, 3C-Ti, and 2C-Ti passivated materials

Ti Sample	Ti wt% $_{(theor.)}$ (± 10%)	Ti wt% $_{(ICP-AES)}$ (± 10%)	Sn wt% $_{(ICP-AES)}$ (± 10%)	Ti : Sn (mol)
4C-Ti	3.5	3.2	1.8	4.4 : 1
3C-Ti	6.1	5.5	1.8	7.6 : 1
2C-Ti	8.0	7.6	0.32	59 : 1

Table 7. Elemental composition (Ti and Sn) before and after methanol passivation

2C-Ti [a]	Ti wt% $_{(grav.)}$ [b] (± 10%)	Ti wt% $_{(ICP-AES)}$ (± 10%)	Sn wt% $_{(ICP-AES)}$ (± 10%)	Ti : Sn (mol)
Before passivation	2.5	2.3	5.1	1.1 : 1
After passivation	2.7	2.6	0.47	14 : 1

[a] 2C-Ti sample was synthesized by reacting 0.6 mmol of $TiCl_2(OiPr)_2$ with 1.0 mmol of bb, and then 3.0 mmol $SiCl_4$

[b] Titanium wt% $_{(grav.)}$ is calculated according to the initial amount of titanium added and the mass of the final product

3.2 Infrared Spectra

3.2.1 Sample preparation

The passivated catalysts, 2C-Ti, 3C-Ti and 4C-Ti, were characterized with IR spectroscopy. Besides of the catalysts, Ti-free platform was prepared with the bb methodology described in Chapter 2. The inert linker silicon tetrachloride ($SiCl_4$) was used to cross link the silica bb, followed by methanol passivation. The example of preparing 2C-Ti and its embedded titanium centers in the matrix (stage 2) are illustrated in Figure 41. Ti-free platform was characterized with IR and compared with the catalysts. The platform is different from Ti-containing catalysts in that does not contain titanium-based sites, but at the same time it exhibits a similar bb-based structure with the actual catalysts. Therefore, when comparing the spectra of platform and catalysts, it is reasonable to assign any new spectral features to titanium-based structures within these matrices, particularly Ti-O-Si linkages.

The sample powders of titanium catalysts and Ti-free platform were dried under vacuum at 80 °C before measurements. A small amount of sample powder (~3 mg) was mixed with potassium bromide (KBr, ~500 mg). The mixture was ground into fine powder with Wig-L-Bug, and then pressed into thin pellets. Transmittance spectra were collected in the wavenumber range of 400-4000 cm^{-1} with Thermo Scientific IR100 FT-IR spectrometer in a glove box. All experiments are conducted under nitrogen atmosphere.

3.2.2 Result and conclusion

Figure 42 shows overlaid infrared spectra of three atomically dispersed titanium-silicate materials as well as Ti-free platform. Two absorption bands at ~1080 cm^{-1} and ~1200 cm^{-1} are assigned to internal and external anti-symmetric Si-O stretching vibrations. The feature at ~800 cm^{-1} is attributed to the symmetric stretching of Si-O bonds, the position of which varies for each sample. All samples contain Si-O-Si groups and therefore the four curves share these common bands arising from Si-O stretching. The absorption shoulder at 960-970 cm^{-1} is a fingerprint band that has been assigned to Ti-O-Si bridges, specifically Si-O vibration in Ti-O-Si.[54] Three spectral curves of titanium-containing samples show clearly this Ti-O-Si fingerprint, suggesting successful incorporation of titanium into the silica matrix.[54] As expected, Ti-free platform (green line, Figure 42) does not have this absorption shoulder. The lack of appreciable absorption in the region beyond 3500 cm^{-1} indicates the absence of hydroxy groups (Figure 43), which otherwise may contribute to the absorption at ~960 cm^{-1}

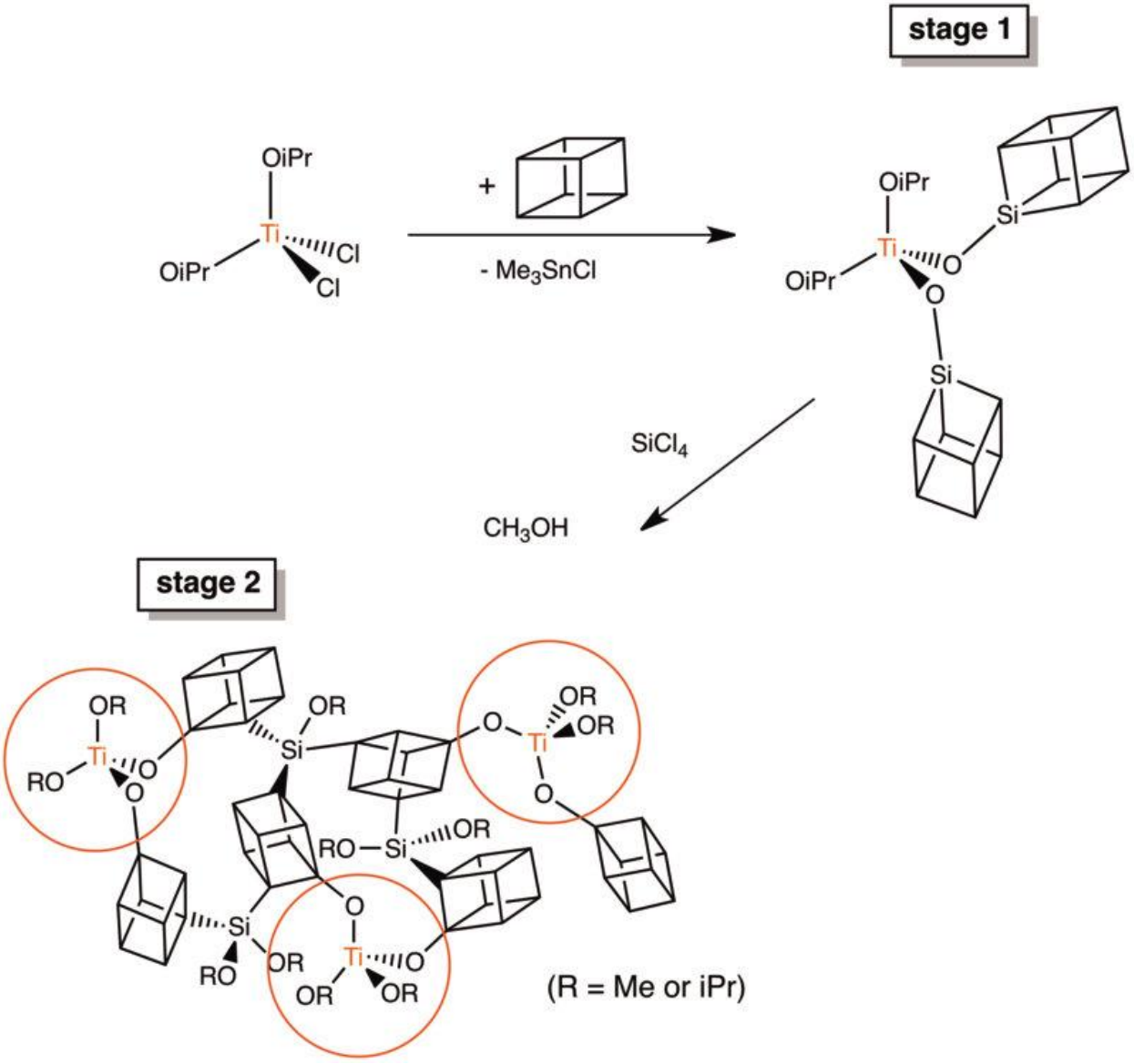


Figure 41. Illustration of 2C-Ti center embedded in a bb matrix

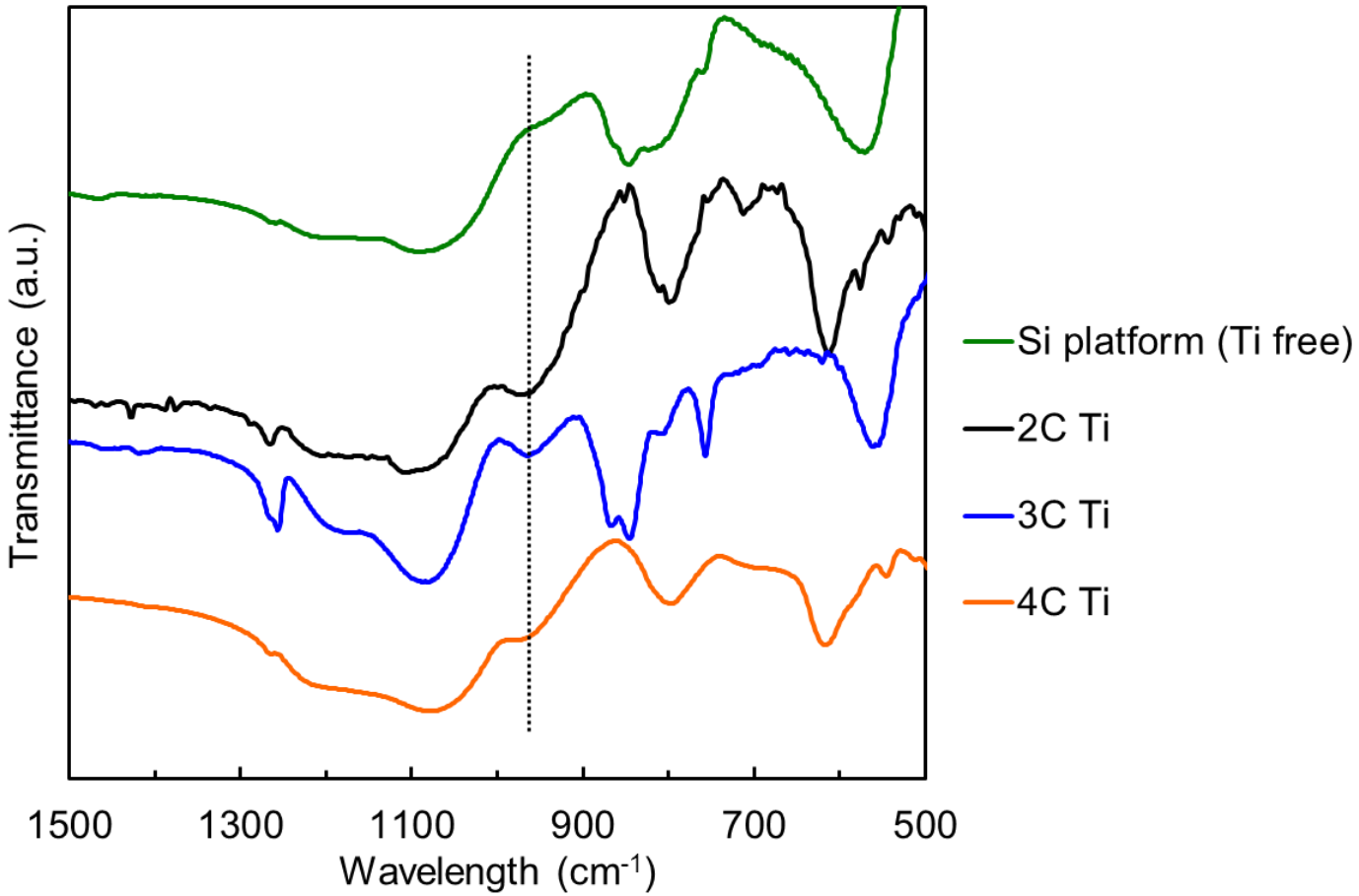


Figure 42. Infrared spectra of 2C-Ti, 3C-Ti and 4C-Ti in comparison with Ti-free silicon platform

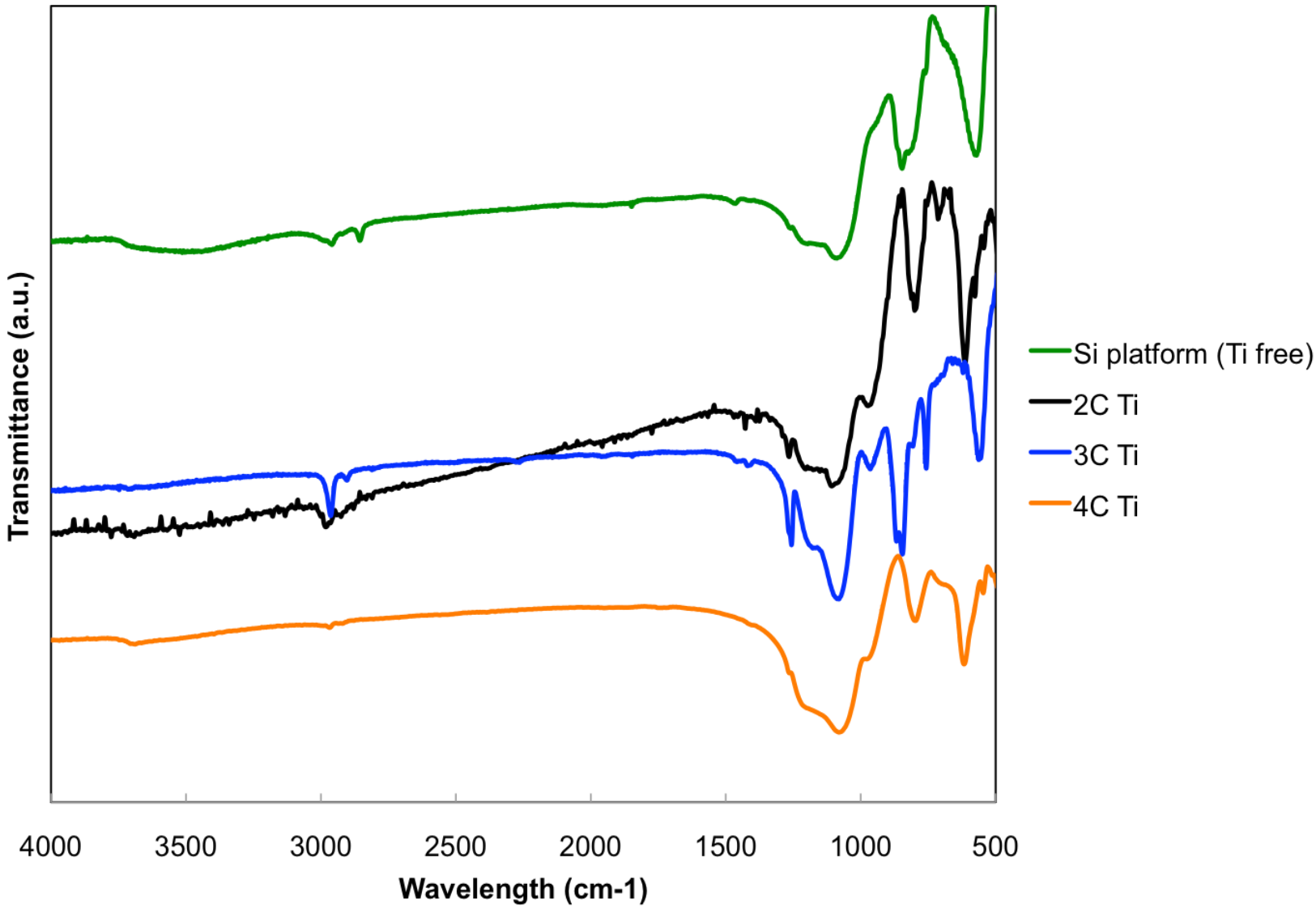


Figure 43. Full infrared spectra of 2C, 3C, 4C-Ti and Ti-free platform

3.3 Diffuse Reflectance UV Spectra

3.3.1 Sample preparation

Table 8 lists the samples that were prepared and characterized with diffuse reflectance UV spectroscopy (DRUV). The preparation process for the different types of 2C-Ti, 3C-Ti and 4C-Ti samples is illustrated in Figure 44-46. For each type of atomically dispersed titanium catalyst DRUV spectra have been collected after first crosslinking (stage 1), after passivation (stage 2), and after exposed to aqueous hydrogen peroxide (H_2O_2/H_2O) (stage 3).

Preparation for 2C-Ti samples are described below as an example.

Stage 1: After the first crosslinking between $TiCl_2(OiPr)_2$ and bb, 2-connected titanium-bb oligomers (sample 1) are formed. Gravimetric analysis suggests the connectivity should be approximately two.

Stage 2: The oligomers are reacted with inert linker $SiCl_4$, forming a porous matrix where titanium centers are embedded. Subsequently, these materials are passivated with methanol. At this stage the passivated catalyst is named as sample 2. Normally, these catalysts are reasonably stable to air and moisture, and ready to be used in a reaction. Infrared spectrum verifies the existence of Ti-O-Si linkages. Elemental analysis confirms that titanium centers are successfully incorporated into the matrix with essentially no leaching.

Stage 3: H_2O_2/H_2O (50% w/w, ~1.0 mL) is added to the catalyst (2C-Ti, 100 mg). The original white color turns to bright yellow instantly, and then slowly decolorizes when left in air over a period of ~5 hours. The sample is dried briefly until most liquid is removed and the sample appears a half dry yellow solid. It is important to collect DRUV spectra before significant decolorization occurs. In Figure 44, the Ti-peroxo species at stage 3 is one of the possible structures that have been proposed in the literature by Bordiga *et al.*.[59, 62] In this research, most of characterization data are in agreement with the hypothesized species that contain Ti-peroxo structure. More details are presented in following sections.

3C-Ti (samples 4-6) and 4C-Ti (samples 7-9) are prepared following similar procedures. Spectra collection parameters and procedures are described in Chapter 2.

Table 8. DRUV and XAS sample list

No.	Sample	Description	Figure	Stage
1	2C-1 dose	$TiCl_2(OiPr)_2$ + bb	42	1
2	2C-MeOH	methanol passivated catalyst		2
3	2C-H_2O_2	Sample 2 + H_2O_2/H_2O		3
4	3C-1 dose	$TiCl_3(OiPr)$ + bb	43	1
5	3C-MeOH	methanol passivated catalyst		2
6	3C-H_2O_2	Sample 5 + H_2O_2/H_2O		3
7	4C-1 dose	$TiCl_4$ + bb	44	1
8	4C-MeOH	methanol passivated catalyst		2
9	4C-H_2O_2	Sample 8+ H_2O_2/H_2O		3

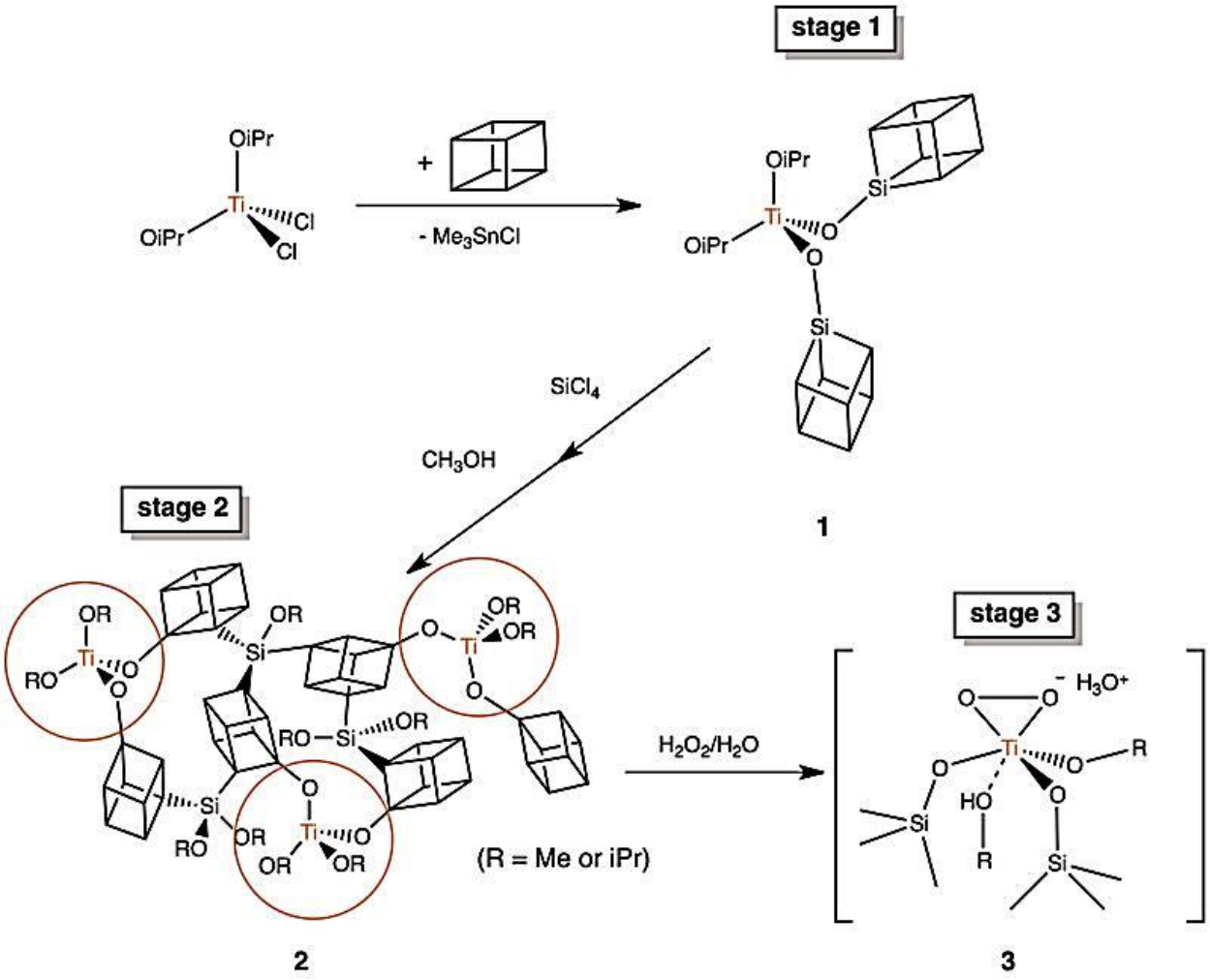


Figure 44. Synthesis of 2C-Ti samples and proposed structures of Ti sites (sample 1, 2 and 3)

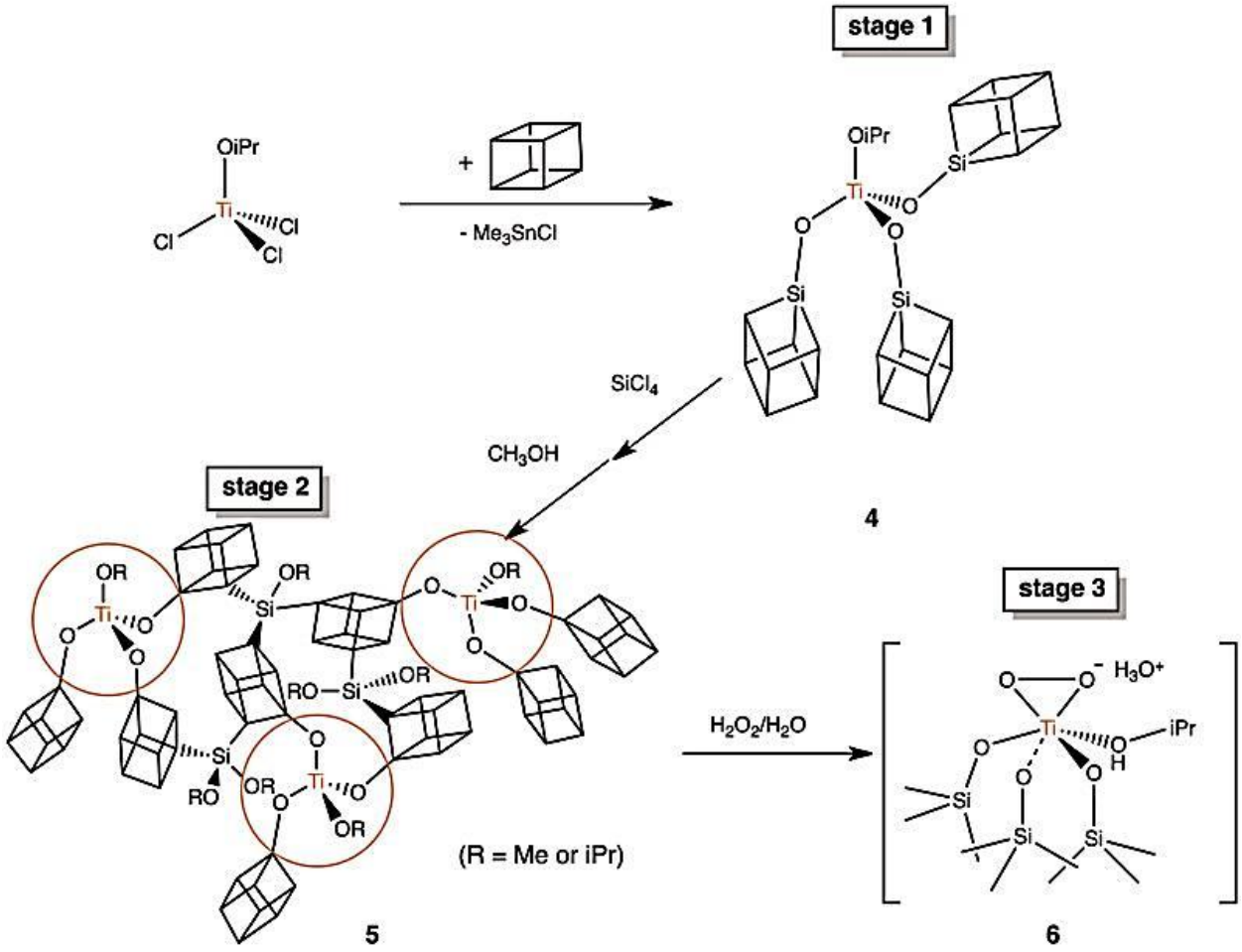


Figure 45. Synthesis of 3C-Ti samples and proposed structures of Ti sites (sample 4, 5 and 6)

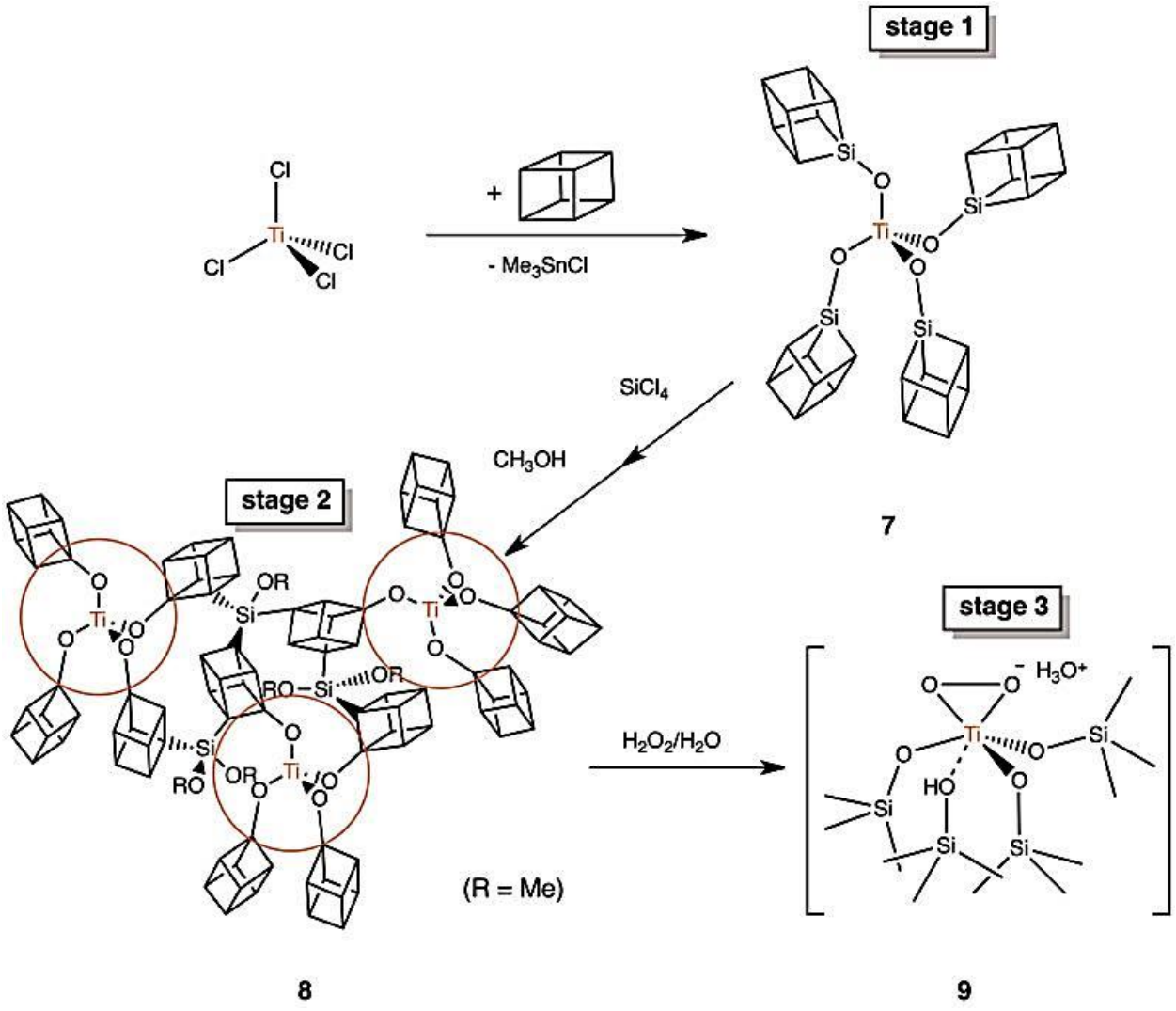


Figure 46. Synthesis of 4C-Ti samples and proposed structures of Ti sites (sample 7, 8 and 9)

3.3.2 Result and discussion

The subject samples in this research are prepared in a different manner compared to traditional titanosilicates in terms of the usage of tin-functionalized bb. Any remaining tin species contribute to the absorption at ~200-210 nm. Therefore, a Ti-free platform (1.6 wt% Sn) is prepared and measured with DRUV as described in section 2.1.4 and 2.2.3 (Chapter 2), in order to correct the spectra for presence of tin. The spectrum function of platform is multiplied by an arbitrary coefficient (0.1-1.0) that depends on the amount of tin in the material, and then subtracted from the sample spectrum. Figure 47 presents the original (top) and corrected (bottom) spectra of 2C-, 3C- and 4C-1 dose (samples 1, 4, 7). The intensity of absorption below 210 nm is reduced after the correction.

The three curves exhibit similar patterns, although each has different connectivity of titanium centers. The absence of absorption beyond 320 nm is consistent with the absence of titania (anatase) domain. Titanium centers in 2C-Ti, 3C-Ti and 4C-Ti are expected to have different connectivities while all being 4-coordinated pseudo-tetrahedral. But comparing with TS-1 that contains exclusively tetrahedral titanium centers, the DRUV absorption bands of these materials are broader. It is important to note that at this stage titanium-containing oligomers are structurally flexible, compared to TS-1 or other rigid silicate matrices.[69] The broadness is consistent with the flexible disordered species, in which a higher number of vibrational levels are superimposed on the electronic transitions. Besides the broadness, the absorption maxima locate at higher wavelength of 230-250 nm than TS-1 (210 nm).[92] Similar broad and red-shifted absorption bands have been observed in UV spectra of 4-coordinated Ti silsesquioxane complexes studied previously.[69] The reason for red shift may be the structural distortion from T_d-geometry, associated with the strong intermolecular interactions at high concentration.[69]

Spectra of 2C-, 3C- and 4C-Ti catalysts after passivation (samples 2, 5, 8) are presented in Figure 48. After passivation the majority of alkyltin groups are removed. Therefore, the skirt of the absorption peak assigned to tin is no longer observed. The three spectral curves share similar patterns to one another. The maximum at 220-225 nm is assigned to tetrahedral titanium center in these silicate bb matrices. Titania anatase phase that is normally observed between 330-350 nm is not observed. In summary, DRUV spectra are highly consistent with the expected 4-coordinated titanium centers in 2C-, 3C- and 4C-Ti.

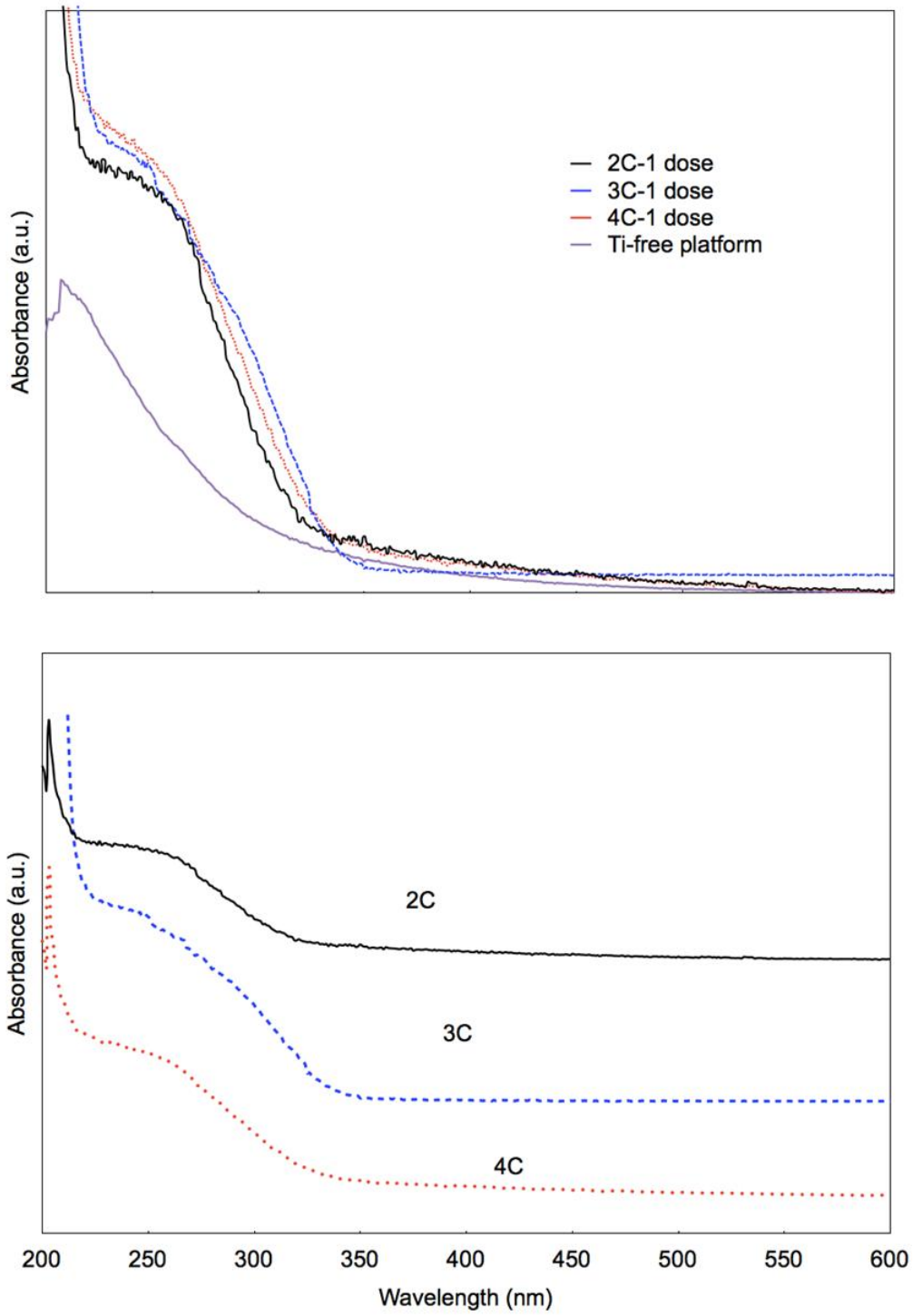


Figure 47. DRUV spectra of 2C, 3C and 4C-1 dose (samples 1, 4, 7, at stage 1) before (top) and after (bottom) correction for tin

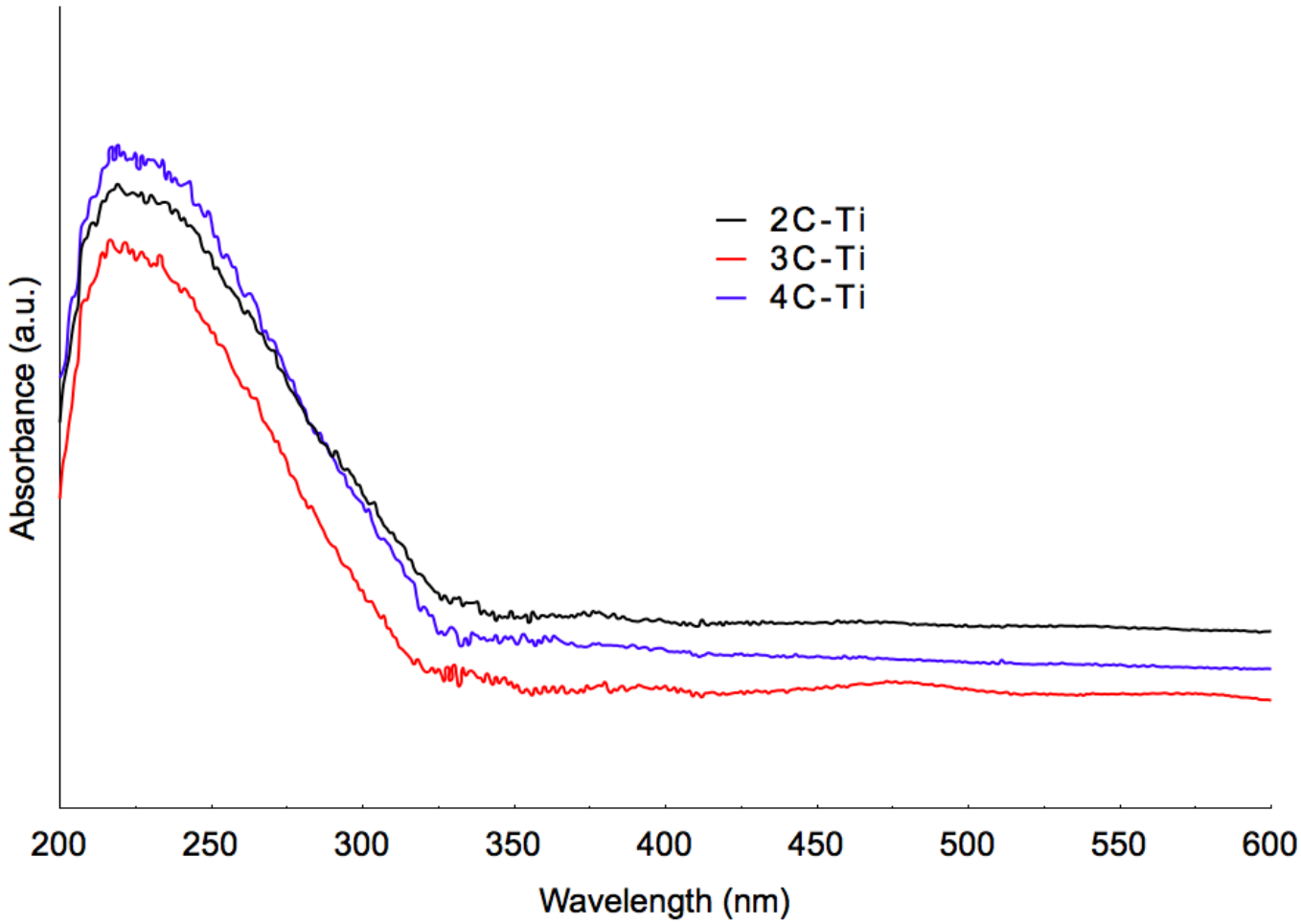


Figure 48. DRUV spectra of 2C-, 3C- and 4C-Ti catalysts after passivation (samples 2,4,6 at stage 2)

3.4 XANES & EXAFS

3.4.1 Sample preparation

The set of 9 samples described above (section 3.3, Figure 44-46 and Table 8) is also characterized with X-ray absorption spectroscopy (XAS). The sample packing is presented in Chapter 2 (section 2.3.2 and 2.3.3).

3.4.2 XANES results

XANES spectra for each type of titanium center are collected and the parameters summarized in Table 9. Exposure to hydrogen peroxide causes significant changes in the XANES spectra for each of the three titanium silicate samples. An analysis of the spectra for the peroxide samples, namely 2C-H_2O_2, 3C-H_2O_2, and 4C-H_2O_2 (samples 3, 6, 9), is presented with other characterization data in section 3.5. The spectra of the samples at stage 1 and 2 are discussed below.

The XANES region, especially the pre-edge peak, is sensitive to the coordination and ligands around the titanium center, as illustrated in Figure 33 (Chapter 2). When chloride groups are present in the first shell around titanium, a shoulder on the main absorption edge is observed due to the ligand to metal shakedown transition.[87] None of atomically dispersed titanium samples (stages 1-3) has shown this absorption shoulder in XANES spectra. The absence of evidence of chloride supports that [Ti-O-Si] bridges form by replacing all of the [Ti-Cl] groups in the chloroalkoxy precursors as they react with the tin-functionalized bb.

1. 2C-1 dose, 2C-MeOH (sample 1, 2)

Figure 49 shows overlay plots of XANES spectra of 2-connected Ti sites, 2C-1 dose (sample 1), 2C-MeOH (2) and 2C-H_2O_2 (3). As discussed in Chapter 2 (section 2.3.1), the symmetry of the local environment around the absorber Ti atoms in these matrices affects both position and intensity of the pre-edge peaks. The samples synthesized in this research are amorphous materials that lack the long-range order found in TS-1. Tetrahedral titanium, for example, in TS-1 shows a sharp pre-edge peak that locates at below 4070 eV and has intensity above 70 % of the main absorption edge (entry 11 in Table 9). In comparison, sample 1 shows a less intense and slightly broader pre-edge peak (entry 1 in Table 9).

Table 9. Ti K-edge parameters

Entry	Samples	Description	Pre-edge Peak Energy/eV	Peak Width ΔFWHM/eV	[a] Peak Intensity/%	[b] Main Edge /eV
1	2C-1 dose	$TiCl_2(OiPr)_2$ + Si_8Sn_8	4969.4	2.1	51	4980.8
2	2C-MeOH	methanol passivated catalyst	4969.4	2.3	34	4980.2
3	2C-H_2O_2	2 + H_2O_2/H_2O	4970.8 (4968.8; 4973.8)	2.3	20	4981.0
4	3C-1 dose	$TiCl_3(OiPr)$ + Si_8Sn_8	4969.4	2.0	54	4980.7
5	3C-MeOH	methanol passivated catalyst	4969.4	2.1	49	4980.3
6	3C-H_2O_2	5 + H_2O_2/H_2O	4970.8 (4969.0, 4973.8) [c]	2.5	17	4980.5
7	4C-1 dose	$TiCl_4$ + Si_8Sn_8	4969.2	2.0	48	4980.8
8	4C-MeOH	methanol passivated catalyst	4969.2	2.2	37	4980.4
9	4C-H_2O_2	8+ H_2O_2/H_2O	4970.8 (4969.0, 4973.8) [c]	2.7	21	4981.1
10	$Ti(OSiPh_3)_4$	4-connected Ti compound	4970	1.4	82	4980.4
11	TS-1	in vacuo [59]	4967	1.4	79	-
12	TS-1/H_2O_2	10 + H_2O_2/H_2O [59]	not reported	3.4	9	-

[a] Peak height relative to the edge jump normalized to 1.0;
[b] Main edge position is determined by the energy at 50% full edge jump;
[c] Multiple pre-edge features are observed in the peroxide samples.

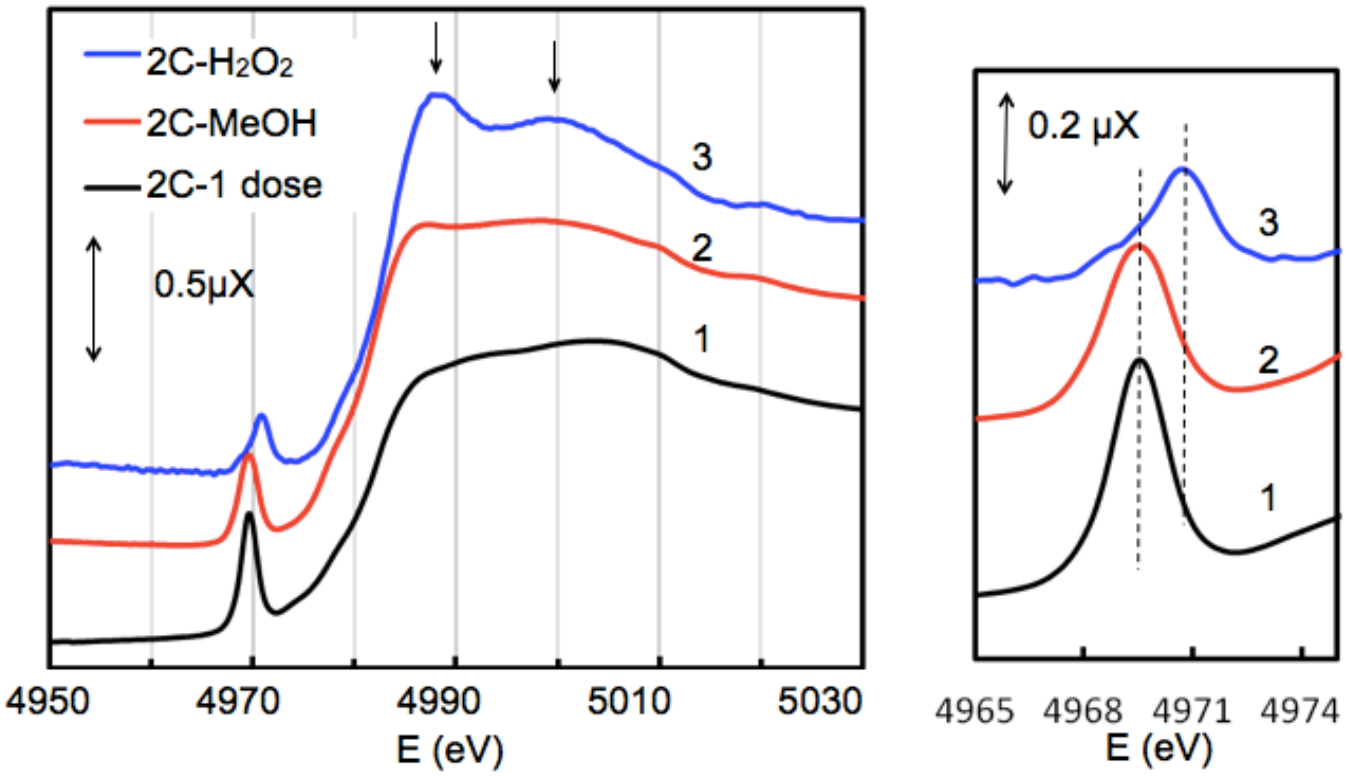


Figure 49. (left) Stacked XANES region of sample 1-3 of 2C-1 dose, 2C-MeOH and 2C-H_2O_2); (right) zoomed in pre-edge peaks

Similar pre-edge peak broadening has been previously observed in materials lacking long-range order and was rationalized as an effect of disorder, with the decrease in intensity explained by the f-sum rule.[101] According to the f-sum rule the overall integrated strength of an absorption band should remain constant even while disorder broadens the pre-edge feature. This should in turn lead to a decrease in the height of the pre-edge feature. The pre-edge position in the range of 4969-4970 eV is consistent with 4-coordinated Ti sites based upon a comprehensive study on a series of Ti-containing oxides and silicates.[93] 5- or 6-coordinated Ti center usually exhibits distinctly different pre-edge peaks located in the range of 4970-4972 eV. In summary, the existence of T_d-geometry Ti centers in 2C-1 dose (sample 1) is supported by the corresponding features in pre-edge region.

2C-MeOH (sample 2) should contain isolated 4-coordinated $[Ti(OSi)_2(OR)_2]$ units within bb matrix. After passivation, the pre-edge peak broadens slightly and become less intense (51%→34%). Several factors may cause the reduction in pre-edge intensity. Coordination of additional methoxy or hydroxy groups, some of the titanium centers may turn into 5- and/or 6-coordinated (Figure 50), which is characterized by a lower pre-edge peak. When the majority of the titanium centers become 5- or 6-coordinated, pre-edge position is expected to shift ~1 - 2 eV to higher energy. In fact, the pre-edge position of sample 2 is perfectly aligned with that of sample 1, which indicates that only a small portion of the Ti sites become higher-coordinated possibly due to the passivation.

2. 3C-1 dose, 3C-MeOH (sample 4, 5)

XANES spectra of 3C-Ti samples should be similar to those observed for 2C-Ti. 3C-Ti samples contain 4-coordinated $[Ti(OSi)_3(OR)]$ units. As expected, the pre-edge feature of 3C-1 dose (sample 4) is sharp and intense, characteristic of T_d-symmetry Ti sites (Figure 51). After the second cross-linking reaction and passivation, there is a small decrease (~5 %) in pre-edge intensity along with a slight increase in peak width. Similar to 2C-Ti, a slight decrease in pre-edge intensity may be caused by higher coordination of the titanium centers. However, the pre-edge positions of sample 4 and 5 remain aligned at 4969.4 eV, consistent with 4-coordinated Ti centers. Therefore, it is reasonable to believe that 4-coordinated titanium sites are dominant in the 3C-Ti catalyst, while a very small number of sites may coordinate to methoxy or hydroxyl groups and have higher coordination.

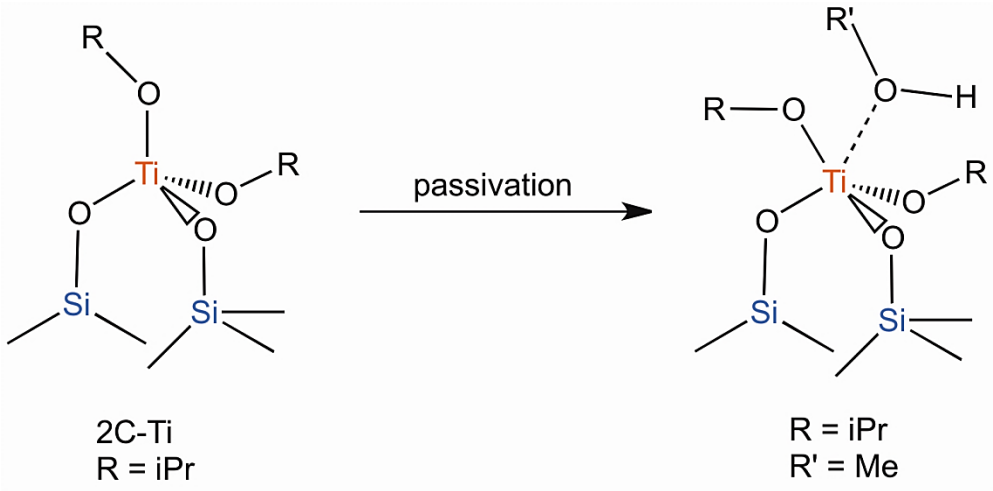


Figure 50. Illustration of the titanium centers in 2C-Ti change from 4- to 5-coordinated

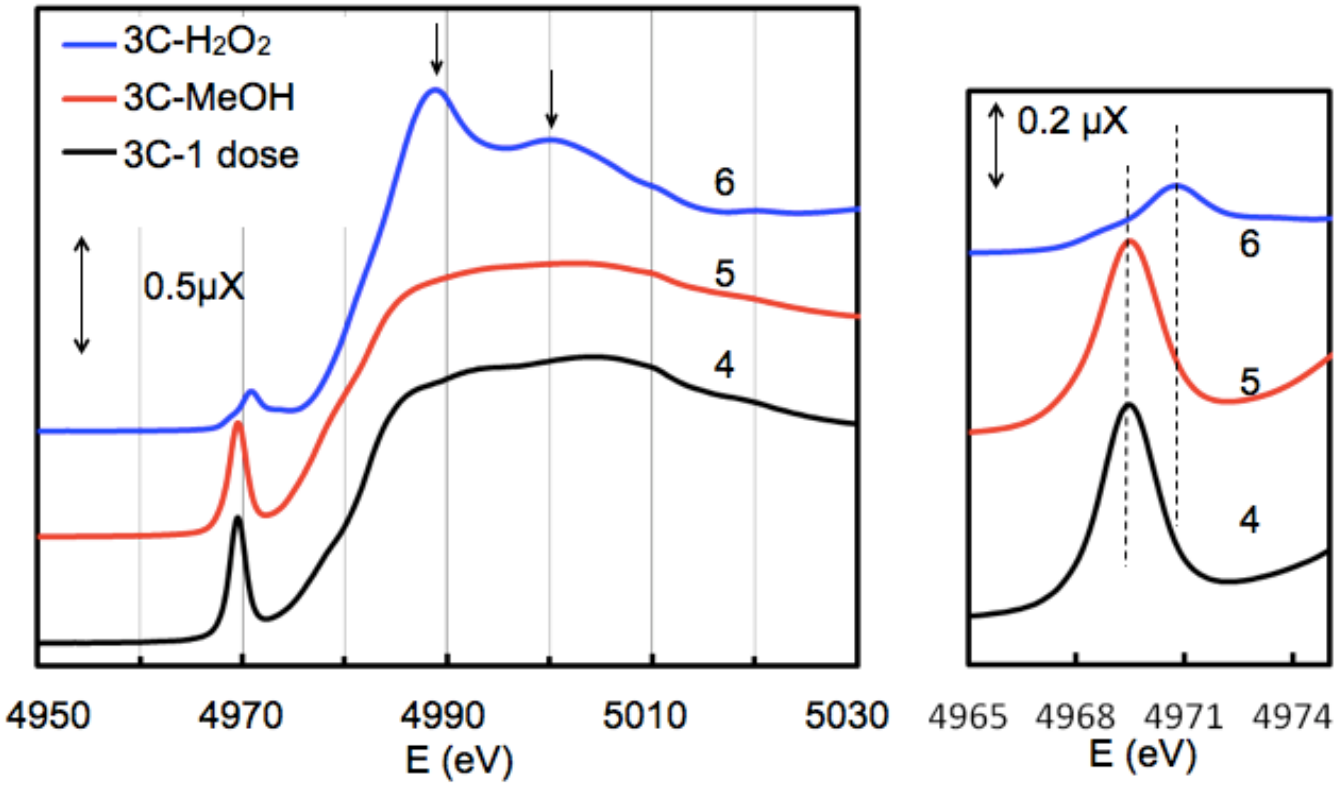


Figure 51. (left) Stacked XANES region of sample 4-6 of 3C-1 dose, 3C-MeOH and 3C-H_2O_2); (right) zoomed in pre-edge peaks

3. 4C-1 dose, 4C-MeOH (sample 7, 8)

Figure 52 shows an overlaid XANES region of 4C samples with the major parameters summarized in Table 9. The single pre-edge peak is consistent with 4-coordinated Ti sites in 4C-1 dose (sample 7). After further cross linking and passivation, the slight peak broadening due to structural disorder is observed again in 4C-MeOH (sample 8), same as in 2C-MeOH and 3C-MeOH. It is worth noticing that 2C, 3C and 4C-Ti at each stage of synthesis share great similarity in XANES region. Pre-edge peak broadening and decreased peak height have been observed in all catalysts in this study, and are ascribed to structural disorder while remaining 4-coordination in amorphous materials. The results of XANES spectra are consistent with the existence of pseudo tetrahedral titanium sites in all samples except for the peroxide samples (samples 3, 6, 9).

3.4.3 EXAFS results of 2C-, 3C-, and 4C-1 dose

Gravimetric measurements and XANES spectra indicate that the chloride ligands on Ti precursors have been removed from around Ti and replaced with oxygen from the corners of the different bb cubes. The first shell around 2C- or 3C-Ti centers is more complex than 4-connected by having two types of oxygen atoms. Two models for 2C- or 3C-Ti are constructed, i.e. “2 Ti-O” and “1 Ti-O” models (Figure 53). “2 Ti-O” model comprises two shells of oxygen at slightly different distances from Ti, i.e. Ti-O-iPr (~1.78 Å) and Ti-O-Si (~1.84 Å). The bond lengths and angles reported in literature for titanium complexes with analogous structures are also taken into consideration. The major difference in these models is the connectivity, i.e. the number of silicones in the second shell around titanium. Structural models of the general form $[Ti(OSi)_x(OiPr)_{4-x}]$ (x = 2, 3 or 4) were built with literature data and/or optimized with ChemDraw.

In summary, the first shell around the Ti site is predicted to be composed of singly bound oxygen atoms from a mix of alkoxide (Ti-O-iPr) and silicate (Ti-O-Si) groups depending on the connectivity achieved for Ti at the time of synthesis. A combination of characterization including gravimetric measurement, NMR, IR, DRUV and XANES agree with 4-coordinated Ti sites $[TiO_4]$ in these samples.

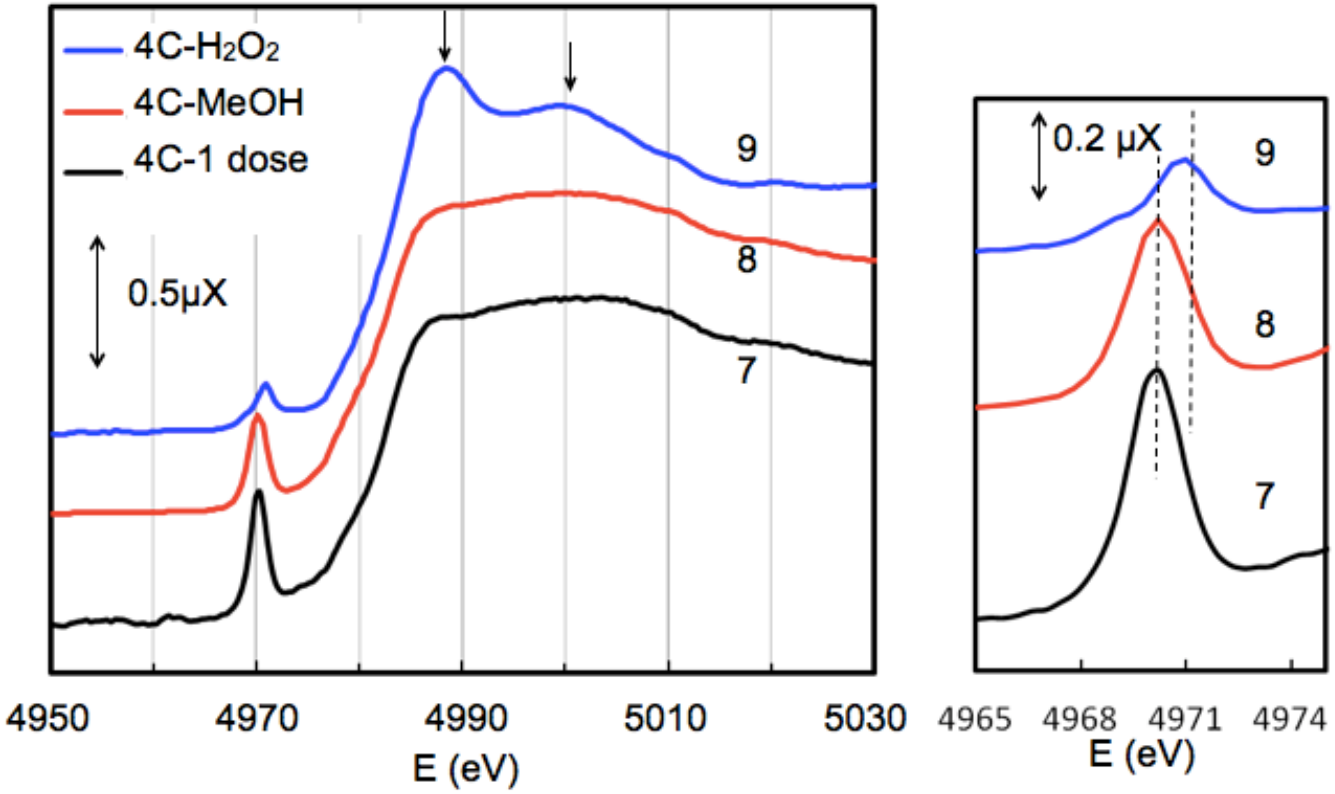


Figure 52. (left) Stacked XANES region of sample 7-9 of 4C-1 dose, 4C-MeOH and 4C-H_2O_2); (right) zoomed in pre-edge peaks

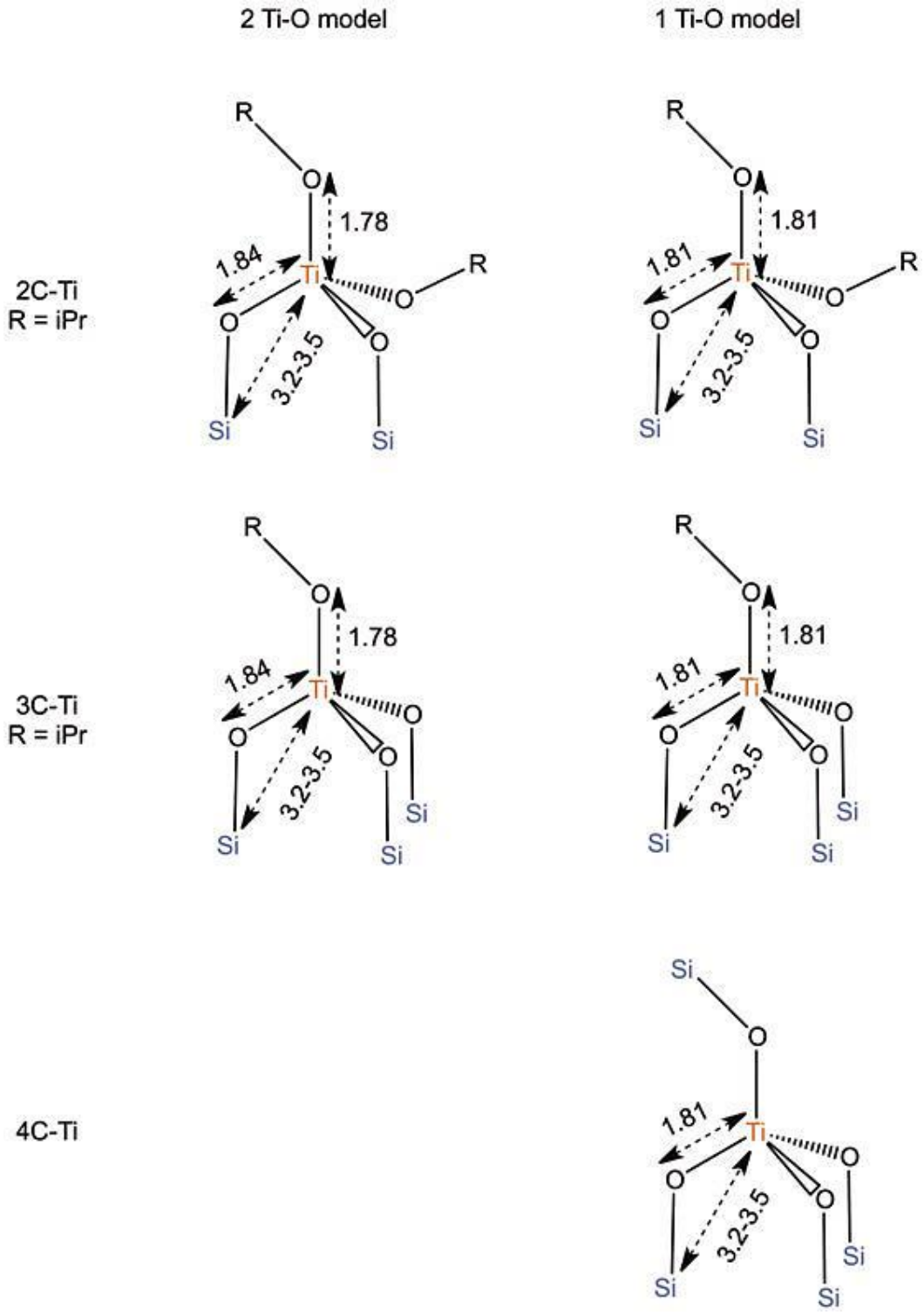


Figure 53. EXAFS molecular models for 2C-Ti (2 models), 3C-Ti (2 models), 4C-Ti (1 model)

k^3-weighted phase-uncorrected R-space plots of 2C- and 3C-Ti after first cross linking reaction are displayed in Figure 54 and 55. The feature below 1 Å (low-R) is an artifact generated from errors in background subtraction in the low k region, which is observed in R-space plots of most samples in this study. Just beyond this low-R component, the R space plots show only single feature with the maximum at ~1.4 Å, consistent with the first shell of oxygen (after correcting the R-space for phase shifting). Therefore, a simplified structural model ("1 Ti-O", Figure 53) composed of a single first shell of oxygen [TiO_4Si_x] (x = 2 or 3) was also constructed and fit with the EXAFS data. The absence of the chloride feature predicted to be at ~1.9 Å in phase-uncorrected plot (Figure 54) confirms that all chloride groups are removed after the first reaction between the titanium precursor and Si_8 building block.

If titanium centers were to aggregate and form cluster sites or titania domains, features for Ti-O-Ti groups are expected to appear at the distance of ~2.7 Å from titanium center in R-space plots. A signal corresponding to Ti-O-Ti is not observed in the spectra of any atomically dispersed titanium samples. The absence of this feature confirms the atomic dispersion of titanium centers

The selected k range for Fourier transform and R range for FEFF fitting are marked with red frames in Figure 54-56. FEFF multiple scattering theory was used to derive theoretical phase and amplitude functions for single scattering paths used to model EXAFS data for each sample. Figure 54 displays $\chi(k)$ and R space plots overlaid with fits of 2C-1 dose sample. The EXAFS data was fit to two models, respectively, i.e. 2 Ti-O and 1 Ti-O models. Both models give reasonable fits to the data and the structural parameters are summarized in Table 10 including the goodness-of-fit (reduced chi square, χ^2). Debye-Waller factor (σ^2) that reflects the dynamic disorders around absorber atom decreases clearly in 2 Ti-O models compared to 1 Ti-O. Changes in χ^2 are commonly used to compare two EXAFS models statistically. The result from comparing 1-shell and 2-shell oxygen models suggests that there is no significant difference between the two in modeling the EXAFS spectrum of 2C-1 dose.[86] In other words, EXAFS data is not able to resolve two distinct shells of oxygen atoms around the Ti centers for 2C-1 dose sample.

The 3C-1 dose sample that also contains two types of oxygen in first shell displays the same behavior in EXAFS modeling. EXAFS modeling of 3C-1 dose is displayed in Figure 55 and the main parameters summarized in Table 11. Two molecular models are fitted to the data, and essentially identical fitting parameters are obtained. EXAFS is again incapable of resolving signals from bond distances within 0.1 Å from one another. Nevertheless, the fitting parameters

agree with the existence of 4-coordinated Ti center in both 2C- and 3C-Ti after the first reaction in synthesis. The bond distance obtained from 1-shell model (1.80 Å) in either case is consistent with the values for T_d-geometry Ti-O reported in literature.

4C-1 dose, as expected, shows a well-defined single first-shell feature in R space (Figure 56). The correspondence between the theoretical functions and experimental EXAFS data strongly support the 4-connected [$Ti(OSi)_4$] model. Table 12 summarizes the final structural parameters obtained from the fit.

A second shell of silicon atoms should be located at a distance of ~3.2 - 3.6 Å from Ti.[85] The number of silicon atoms is equivalent to the connectivity around titanium center. This shell of silicon atoms can successfully be modeled to the second shell feature with the data for the data of 4C-1 dose. The R-space plot (Figure 56) shows a second shell feature at reasonable bond distance, and therefore is modeled as silicon atoms. However, modeling a second shell of silicon atoms for 2C- and 3C-Ti samples is challenging. 2C-1 dose data shows a feature at ~3 Å in R space possibly corresponding to the second shell of silicon, but the feature only appears with large k-weight (≥ 3). In the case of 3C-1 dose, no feature above the noise level in the data is observed beyond 2.5 Å in R space (Figure 55).

Thermal and structural disorders in amorphous samples can broaden the signal and lower its intensity. 2C- and 3C-Ti centers, compared to fully embedded 4C-Ti, are more labile and consequently exhibit more disorders. The second shell features in R-space plots of 2C- and 3C-Ti are possibly weakened for this reason. Moreover, the low signal to noise level may be related to the low Ti content (1.0-1.5 wt%), because these are “1 dose” samples that contain reasonable amount of tin.

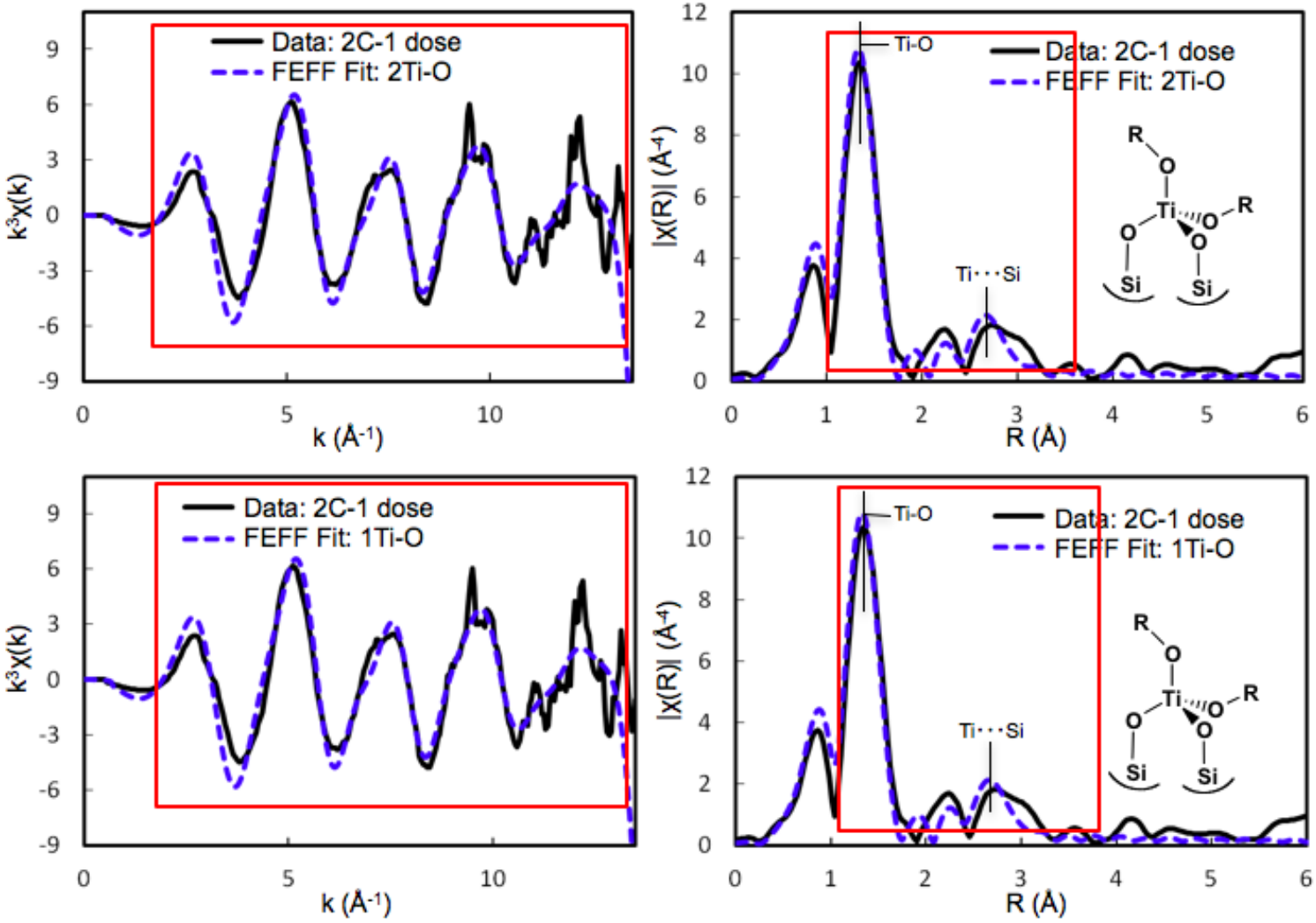


Figure 54. 2C-1 dose in χ(k) and k3-weighted R space functions with two structural models

Table 10. Structural parameters obtained from fits to 2C-1 dose

	2C-1 dose: 2Ti-O Model			2C-1 dose: 1Ti-O Model	
	Ti-O (TiOSi)	Ti-O (TiOiPr)	Ti---Si	Ti-O	Ti---Si
CN (set)	2	2	2	4	2
R (Å)	1.78 ± 0.01	1.83 ± 0.01	3.19 ± 0.04	1.80 ± 0.01	3.19 ± 0.04
σ^2 (Å^2)	0.0054		0.0066	0.0059	0.0068
S_0^2 (set)	0.96			0.96	
E_0 (eV)	-6.8 ± 2.8			-6.2 ± 2.6	
Reduced X^2	162			141	
R factor	0.102			0.099	

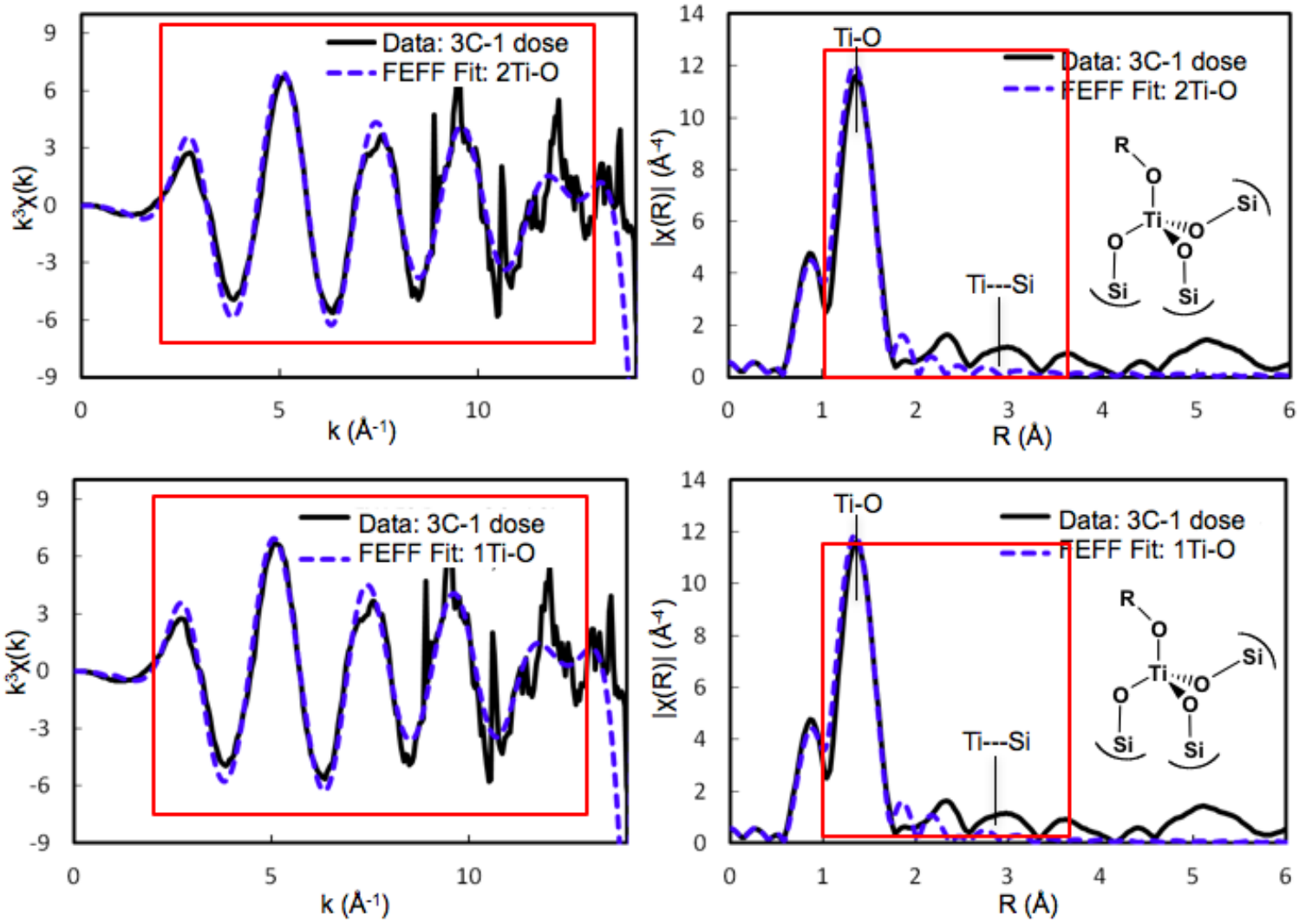


Figure 55. 3C-1 dose in χ(k) and k3-weighted R space functions with two structural models

Table 11. Structural parameters obtained from fits to 3C-1 dose

	3C-1 dose: 2Ti-O Model			3C-1 dose: 1Ti-O Model	
	Ti-O (TiOSi)	Ti-O (TiOiPr)	Ti---Si	Ti-O	Ti---Si
CN (set)	3	1	3	4	3
R (Å)	1.79 ± 0.01	1.86 ± 0.01	3.44 ± 0.34	1.80 ± 0.01	3.40 ± 0.22
σ^2 (Å^2)	0.0035		0.0472	0.0044	0.0376
S_0^2 (set)	0.96			0.96	
E_0 (eV)	-3.3 ± 2.2			-4.3 ± 2.3	
Reduced X^2	24			27	
R factor	0.062			0.069	

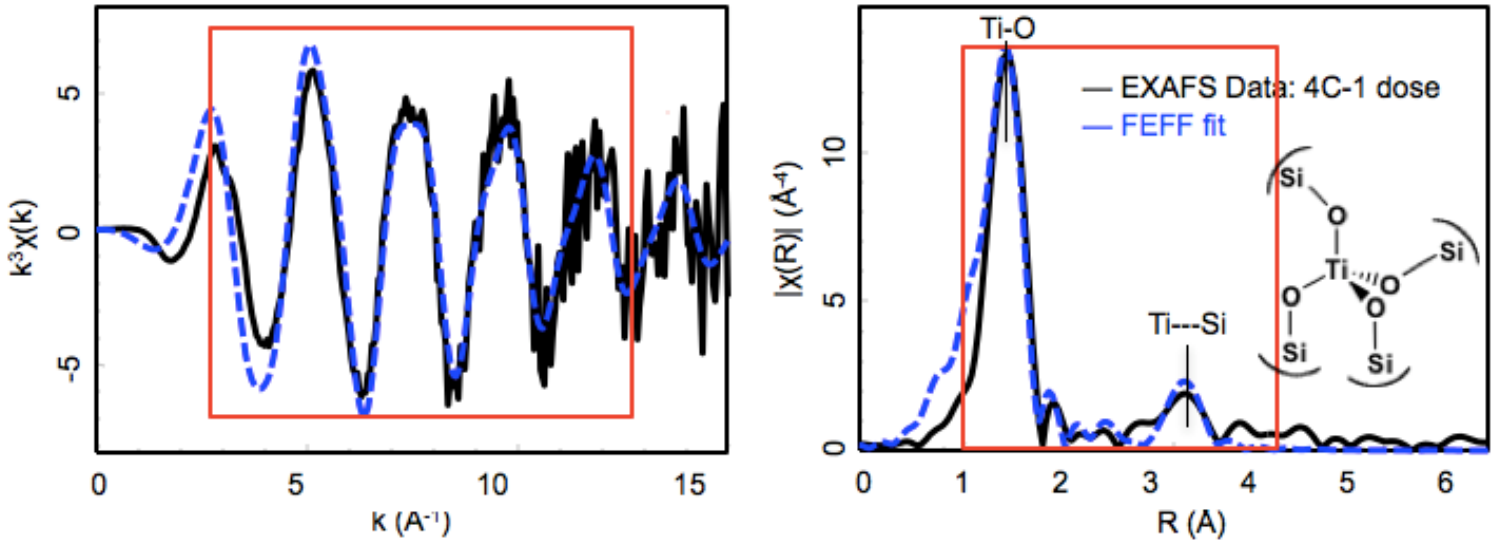


Figure 56. EXAFS fitting of 4C-1 dose in k3 space and k3-weighted R space functions

Table 12. Structural parameters obtained from fits to 4C-1 dose

4C-1 dose		
	Ti-O	Ti---Si
CN (set)	4	4
R (Å)	1.80 ± 0.00	3.49 ± 0.02
σ^2 (Å^2)	0.0041	0.0065
S_0^2 (set)	0.96	
E_0 (eV)	-6.8 ± 0.9	
Reduced X^2	7.8	
R factor	0.081	

3.4.4 EXAFS results of 2C-, 3C-, and 4C-MeOH

Ti oligomers after first crosslinking reaction were further crosslinked with $SiCl_4$ to form rigid matrices with long-range structure. The materials were then passivated with methanol in toluene before EXAFS data collection or being used as catalysts. Approximately double the amount of titanium content is expected for the passivated samples. Indeed, increased signals for the second shell Ti---Si relative to the first shell Ti-O are observed. Reasonable fittings in $\chi(k)$ and R spaces are obtained for each of these samples. k^3-weighted R space plots of samples before and after passivation are presented in Figure 57-59 and the fitting parameters summarized in Table 13-15.

Coordination with methanol on part of 2C- and 3C-Ti centers (Figure 50) is suggested by decreased height of pre-edge peaks in XANES spectra, and is again observed as a feature at ~1.9 Å in phase-uncorrected R-space plots. The coordination number obtained from EXAFS fitting reflects an average number of all titanium atoms in the matrix. Coordination number for 2C-MeOH equals 4, indicating that majority of titanium centers remain 4-coordination but possibly a small fraction coordinates with neutral methanol molecules. The spectra and fitting parameters are presented in Figure 57 and Table 13. The 3C-MeOH (Figure 58 and Table 14) shows modified first shell feature with maxima at ~1.4 Å and ~1.9 Å in phase-uncorrected R space. EXAFS modeling suggests the total number of four oxygen atoms around each Ti atom. But two types of oxygen atoms must be modeled, i.e. 3 oxygen (Ti-O, ~1.82 Å) and 1 oxygen (Ti---O(H)CH_3, ~2.10 Å). Figure 59 presents the overlay R space plots of 4C-1 dose and 4C-MeOH. The same atom separations for Ti-O bonds are obtained and summarized in Table 15.

In the cases of 3C- and 4C-Ti, the first shell feature in samples after passivation appears broader and less intense (Figure 58 and 59). The decrease in amplitude usually comes with an increase in Debye-Waller factor. At the end of synthesis both 2C and 3C catalysts have the second shell features improved in intensity. The increase in structural rigidity, as a result of the further cross linking reaction, is likely to decrease the effect of thermal disorder and to cause less peak broadening.

It is worth mentioning that there is a significant difference in titanium content between stage 1 and 2. At stage 2, majority of the trimethyltin groups are removed through passivation, and therefore Ti wt% increases by a factor of 2-5 compared to stage 1. The increase in titanium content at stage 2 explains the enhanced signal to noise level and also better defined second shell features in the R space plots.

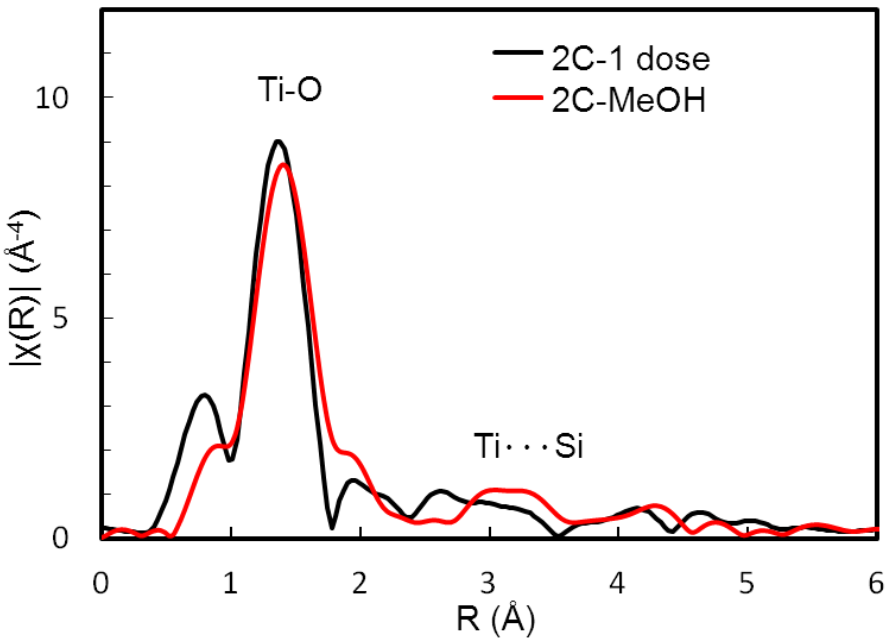


Figure 57. R space of 2C-MeOH overlaid with 2C-1 dose

Table 13. EXAFS modeling parameters of 2C-MeOH

2C-MeOH		
1Ti-O Model	Ti-O	Ti···Si
CN (set)	4	2
R (Å)	1.83 ± 0.01	3.50 ± 0.04
σ^2 (Å^2)	0.0048	0.0047
S_0^2 (set)	0.96	
E_0 (eV)	-1.0 ± 2.7	
Reduced X^2	165	
R factor	0.103	

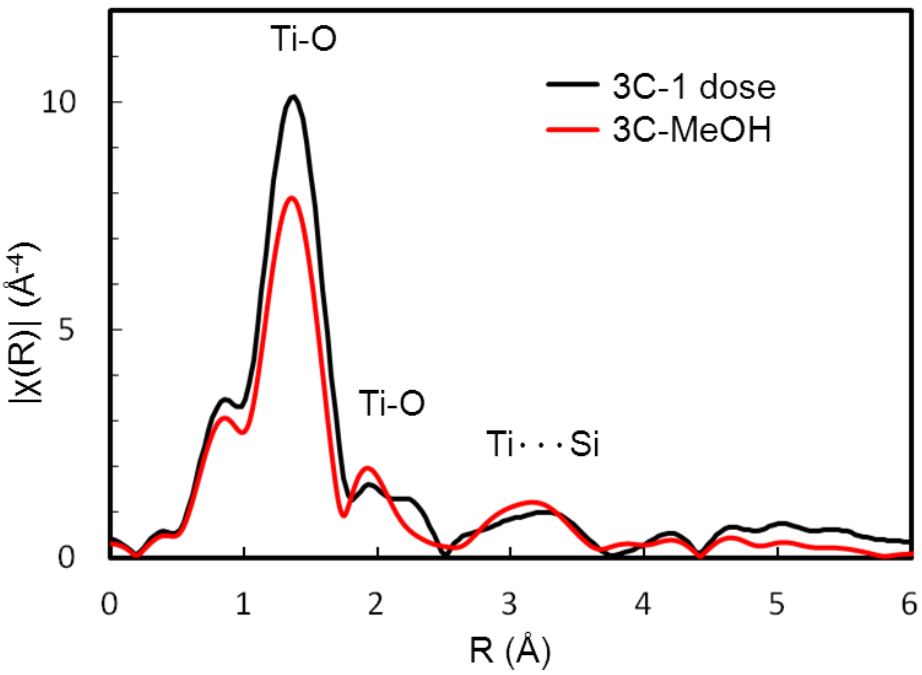


Figure 58. R space of 3C-MeOH overlaid with 3C-1 dose

Table 14. EXAFS modeling parameters of 3C-MeOH

3C-MeOH			
2Ti-O Model	Ti-O (TiOSi)	Ti-O (TiOiPr)	Ti···Si
CN (set)	3	1	3
R (Å)	1.82 ± 0.01	2.10 ± 0.01	3.55 ± 0.07
σ^2 (Å^2)	0.0042		0.0227
S_0^2 (set)	0.96		
E_0 (eV)	1.5 ± 1.9		
Reduced X^2	396		
R factor	0.056		

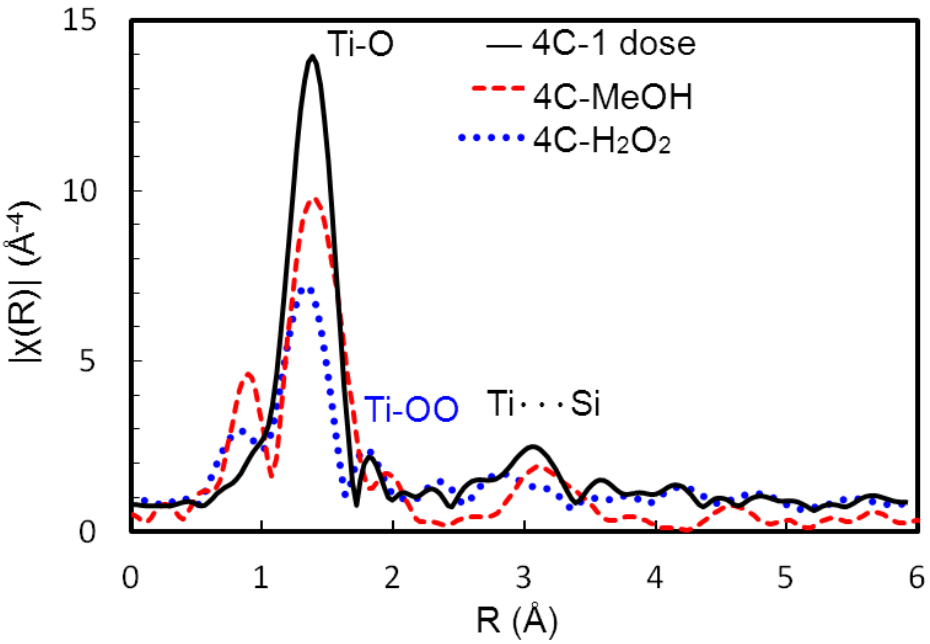


Figure 59. R space of 4C-MeOH, 4C-H_2O_2 overlaid with 4C-1 dose

Table 15. EXAFS modeling parameters of 4C-MeOH

	4C-MeOH	
	Ti-O	Ti···Si
CN	4	4
R (Å)	1.81 ± 0.01	3.49 ± 0.05
σ^2 ($Å^2$)	0.0061	0.0155
S_0^2 (set)	0.96	
E_0 (eV)	5.8 ± 2.3	
Reduced X^2	132	
R factor	0.097	

3.5 Characterization of Ti-peroxide System

3.5.1 TS-1/peroxide system

It is crucial to understand the interaction between the Ti sites and aqueous H_2O_2 in the context of the catalytic activity that these materials exhibit. One of the major advantages of TS-1 over other titanosilicates is its prominent catalytic activity and stability with aqueous H_2O_2 as oxidant agent. Compared to alkyl peroxides, the oxidation reactions using H_2O_2 are more environmental friendly and generate only water as a by-product. DRUV and XAS studies have been conducted to investigate the structure of TS-1/H_2O_2, and suggest that the 4-coordinated Ti centers in TS-1 bind H_2O_2 in a side-on η^2-fashion.[62] The Ti-η^2-peroxo complex exhibits a distinctive yellow color. It was also found that without excess of water present, the yellow Ti-η^2-peroxo transforms to colorless η^1-hydroperoxide species (Figure 60). An unsaturated coordination sphere is considered to be critical for catalytic activity. Similar to TS-1, the color change (yellow) was also observed with the titanium samples in these researches upon contact with aqueous H_2O_2. This indicates that similar structural changes may occur in these tetrahedral sites. Therefore, it is crucial to characterize these titanium-peroxide species, the formation of which is directly related to the catalytic activity of these sites.

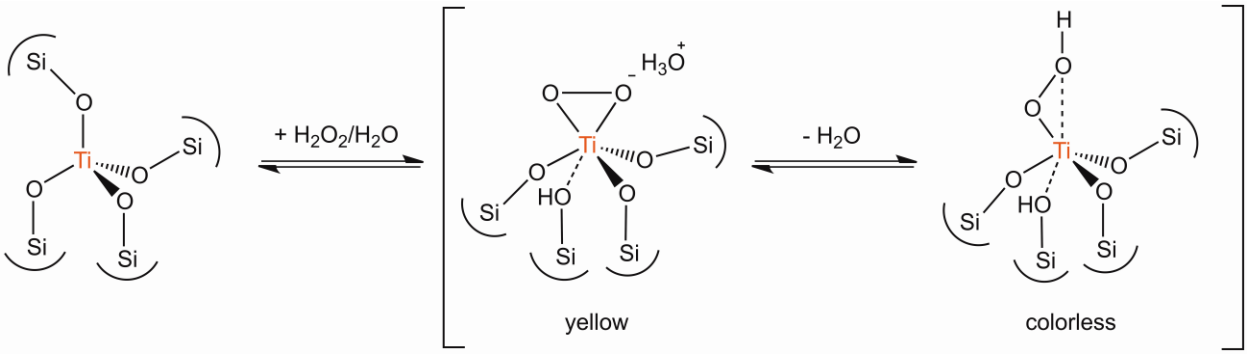


Figure 60. Titanium center in TS-1 after exposed to aqueous hydrogen peroxide

3.5.2 DRUV spectra of peroxide samples

Ti catalysts/H_2O_2 systems (sample 3, 6 and 9) have been investigated. Figure 61 presents the spectra of 2C-H_2O_2, 3C-H_2O_2 and 4C-H_2O_2. After contact with aqueous H_2O_2, significant changes are observed in the spectra (section 3.3). Instead of the Gaussian curves with single maximum as seen previously (Figure 48), peroxide exposed samples show two prominent absorption features, one at 260-290 nm and the other at 370-390 nm. A similar pattern has been observed in TS-1/H_2O_2 system which has been described as 6-coordinated Ti centers.[62] Significant red shift of LMCT ($Ti^{4+}O^{2-} \rightarrow Ti^{3+}O^{-}$) occurs. The maximum of the band is located at ~285 nm which is ascribable to higher coordination around Ti centers. A new feature at ~385 nm has been previously assigned to η^2-peroxo moiety to Ti center with possible contribution from O^{2-} species.[62] According to the DRUV spectra Ti-η^2-peroxo species form in 2C-, 3C-, and 4C-H_2O_2 samples.

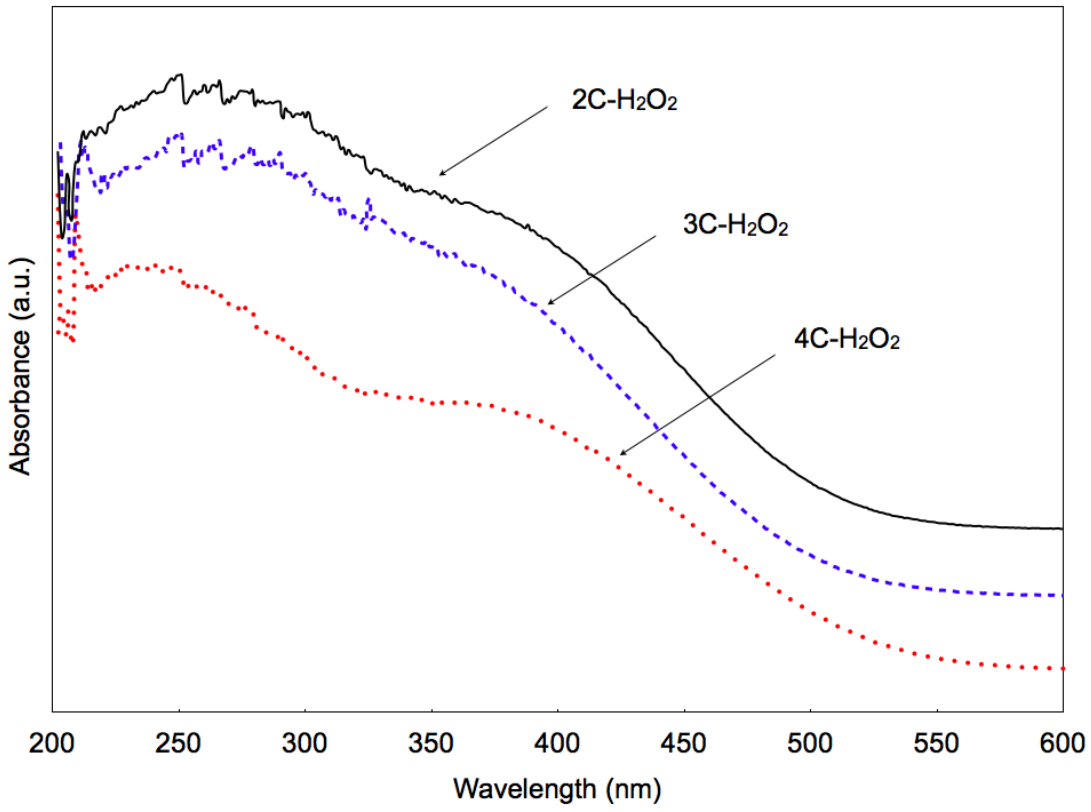


Figure 61. 2C- 3C- and 4C-Ti after contact with aqueous H_2O_2 (sample 3,6,9)

3.5.3 XAS results of peroxide samples

XANES and EXAFS spectra were collected on 2C-H_2O_2, 3C-H_2O_2 and 4C-H_2O_2. Exposure of the passivated samples described above to aqueous H_2O_2 causes an immediate color change in the powder from off-white to deep yellow. A similar color change has been observed in the study of TS-1/H_2O_2 due to the formation of Ti-η^2-peroxo structure. Ti-peroxo species decomposes in air and decolorize in air within ~5 hours. Ti-free silicate platform did not show any color change after contact with aqueous H_2O_2, strongly suggesting that the color change involves the structural change on titanium centers.

XANES spectra of peroxide samples, 2C-H_2O_2 (sample 3), 3C-H_2O_2 (6), and 4C-H_2O_2 (9) share common features with one another but are distinctly different from those of the as-synthesized catalysts. (Figure 49, 51, 52 and parameters in Table 9) After contact with aqueous H_2O_2, pre-edge peak in the XANES region changes significantly in pre-edge position and intensity. The weak pre-edge peaks (< 20 % height of the main edge) and small shoulders on each side of the main pre-edge peak form a fingerprint for 6-coordinated octahedral sites. The pattern of multiple low intensity pre-edge peaks has been observed in titania and TS-1 after contact with aqueous H_2O_2.[59, 88] Furthermore, the pre-edge position, compared to the 4-coordinated titanium centers is blue shifted by ~1 - 2 eV. According to calculations of the Fermi energy in previous studies, the new pre-edge position is consistent with the electronic transition between orbitals in O_h-symmetry Ti.[88, 102] Another important feature is the double-peak on top of the main absorption edge, in contrast to what is observed for the parent titanium centers (4-coordinated) which shows a single, broad white line. The double-peak feature has been assigned to Ti-peroxo structure and has been observed in TS-1 and other titanium silicate materials exposed to aqueous H_2O_2.[62]

The changes observed in the pre-edge and edge features of the data are consistent with the formation of pseudo octahedral Ti sites containing a η^2-peroxo ligand. It is clear that Ti sites have changed from 4- to 6-coordinated after contact with aqueous H_2O_2. The formation of Ti-peroxo structure is proposed based on the observations in color change upon contact of H_2O_2 and the unique double-peak feature on the main edge of XAS spectra. Based on the combination of these data, the structural model [$Ti(OSi)_4(\eta^2\text{-}OOH_2)$] is applied in EXAFS modeling. The fitting spectra and parameters are displayed in Figure 62 and Table 16. Interestingly, during the collection of EXAFS spectra, spectra of 2C-H_2O_2 (sample 3) and 3C-H_2O_2 (6) change significantly from scan to scan, indicating the structural change (implying chemical changes also) on titanium centers. At the end of the collection, the color of sample

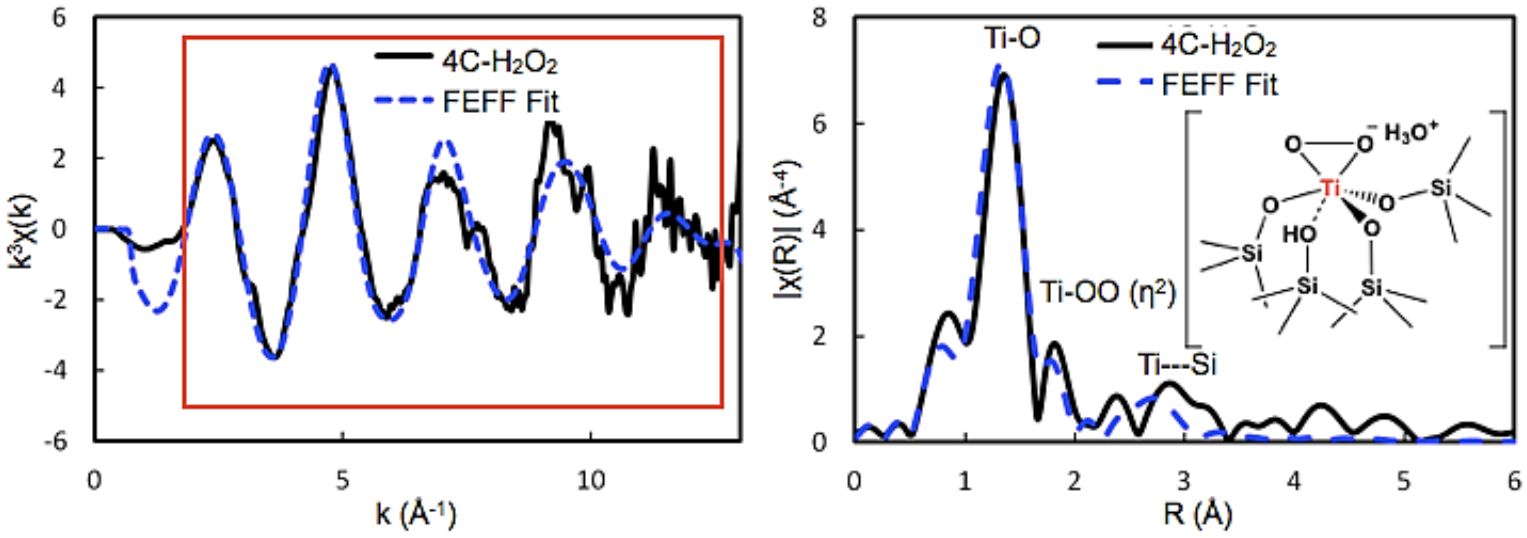


Figure 62. EXASF fitting of 4C-H_2O_2 data in k and R spaces

Table 16. EXAFS fitting parameter of 4C-H_2O_2 data

	4C-H_2O_2		
	Ti-OO(η^2)	Ti-O(TiOSi)	Ti---Si
CN	1.95 ± 0.40	4.05 ± 0.40	4.05 ± 0.40
R (Å)	2.02 ± 0.01	1.84 ± 0.01	3.44 ± 0.06
σ^2 ($Å^2$)	0.0067		0.0237
S_0^2 (set)	0.96		
E_0 (eV)	-8.9 ± 2.9		
Reduced X^2	40		
R factor	0.082		

powders changed from yellow to dark brown. It appears that both materials are sensitive to exposure to X-rays and change rapidly for this reason. XAS data is not provided for 2C- and 3C-Ti-peroxo samples in this dissertation. The sensitivity to X-ray is possibly assoiciated with the lower connectivity between titanium and matrix in 2C- and 3C-Ti.

3.6 Conclusion of Atomically Dispersed Titanium Centers

Isolated atomic titanium catalysts are prepared using a building block based methodology. Titanium centers at three stages of synthesis are investigated, i.e. after first crosslinking reaction (stage 1), after passivation (stage 2) and after exposure to aqueous hydrogen peroxide (stage 3). A variety of characterization, including gravimetric analysis, vibrational spectroscopies, DRUV and XAS, are utilized to investigate the structure of titanium centers. The spectral data and modeling studies strongly agree with isolated 4-coordinated titanium centers. No evidence for cluster or crystalline (Ti-O-Ti) domains is observed in any of the titanosilicate samples. The synthetic methodology characterizes the connectivity around titanium center by gravimetric analysis, which agrees with the expected 2, 3 or 4-connected titanium centers.

DRUV and EXAFS modeling on the 4C-H_2O_2 (sample 9) suggest the structure of 6-coordinated Ti centers with η^2-peroxo. During the catalytic reaction, 4-coordinated titanium centers must coordinate with small molecules (substrate and oxidant) and form 6-coordinated intermediates, essential for fulfilling the catalytic process. Rigid saturated coordination such as 6-coordinated titanium in titania anatase has been demonstrated to be catalytically inactive in epoxidation of olefin or hydroxylation of phenol. The structural flexibility of transforming between tetrahedral to octahedral geometry is believed to be critical for the catalytic activity of titanium centers. 2C- H_2O_2 and 3C-H_2O_2 appear to be X-ray sensitive, which can be understood with the labile structures and lower connectivity compared to 4C-Ti. But DRUV and XANES spectra are consistent with 6-coordinated titanium centers in 2C- H_2O_2 and 3C- H_2O_2. The as-synthesized 2C-MeOH, 3C-MeOH, 4C-OH (samples 2, 5, 8) are used as the catalysts in alkylphenol oxidation with aqueous H_2O_2 (Chapter 5).

Chapter IV. Synthesis and Primary Characterization of Isolated Tetranuclear Titanosilicate Catalyst

4.1 Synthesis and Gravimetric Analysis

4.1.1 Tetranuclear titanium precursor

The tetranuclear titanium cluster, $[Ti_4(\mu_3\text{-}O)_2Cl_6(\mu_2\text{-}O_2CPh)_6]$, is prepared following the literature.[73] The reaction equation is shown below.

$$4TiCl_4 + 8PhCO_2H \longrightarrow [Ti_4(\mu_3\text{-}O)_2Cl_6(\mu_2\text{-}O_2CPh)_6] + 8HCl + 2PhCOCl$$

Equation 4-1

Benzoic acid (C_6H_5COOH, crystalline, ACS certified) is used as purchased without further purification. n-Octane (99+%, Fischer Scientific) is distilled and stored in a glass vessel under nitrogen prior to use. $TiCl_4$ is mixed with C_6H_5COOH at a molar ratio of 1 : 2, and heated in refluxing octane (b.p. 125 ºC) for ~5 hours. The desired product precipitates from the solution as a yellow solid within a short period of time. HCl and C_6H_5COCl are generated as byproducts. Once the reaction is complete and cooled to room temperature, the solution is then decanted under nitrogen flow. The yellow solid is washed with pure n-octane and subsequently dried at 100 ºC under vacuum for 12 hours. The product, $[Ti_4Cl_6(\mu_2\text{-}O_2CPh)_6(\mu_3\text{-}O)_2]$, is obtained in 90% yield. Figure 63 (a) displays the X-ray crystal structure of the cluster from the literature.[73] The structure is comprised of two groups of octahedrally coordinated titanium atoms and two triply bridging oxygen dianion ligands. The six chloride ligands are all terminally coordinated and the benzoate ligands bridge between different titanium atoms in the complex. The coordination environments of the two types of titanium(IV) cations are cis-$TiCl_2O_4$ and $TiClO_5$. The two coordination geometries around titanium in the Ti_4O_2 core of the complex are shown in Figure 63 (b).

The IR spectrum of this product shows the major characteristic bands (1590s, 1490s, 1170s, 1020s, 650s, section 4.2.1) similar to what is reported in the literature.[73] ICP analysis indicates 15.5 wt% Ti, consistent with estimated 16.5 wt% Ti based on the molecular formula. The titanium cluster exhibits good stability under nitrogen atmosphere but appears to be moisture sensitive, consistent with the reactivity of Ti-Cl groups on the cluster.

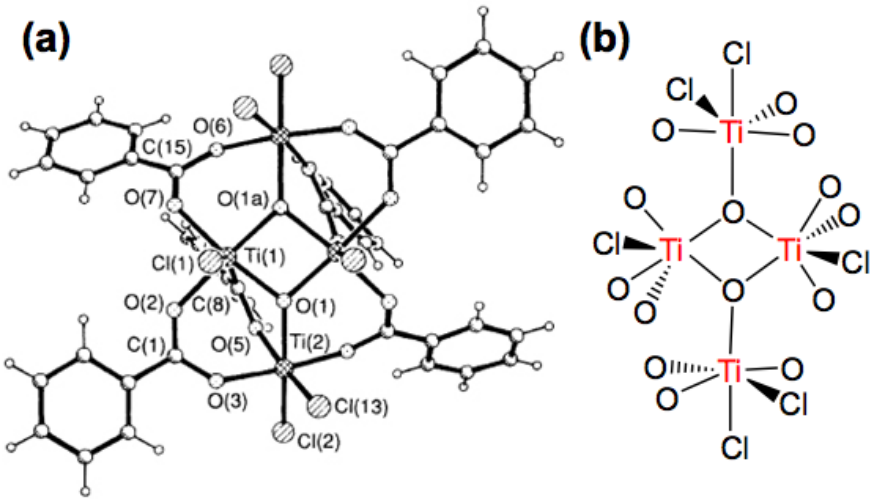


Figure 63. (a) X-ray crystal structure of $[Ti_4(\mu_3\text{-}O)_2Cl_6(\mu_2\text{-}O_2CPh)_6]$ (Reprinted from reference [73]); (b) Simplified cluster structure with carbon and hydrogen atoms omitted

According to the literature[73], the structure $[M_4O_2]$ seems also favorable in $[\{Ph_2Sn(O_2CCCl_3)]\}_2O]_2$ cluster, emphasizing the stability of the $[M_4O_2]$ unit.

4.1.2 Synthesis of tetranuclear titanium catalyst

$[Ti_4(\mu_3\text{-}O)_2Cl_6(\mu_2\text{-}O_2CPh)_6]$ cluster (abbreviated as Ti_4O_2) is used as a tetranuclear titanium precursor to react with silica building block (bb) at a molar ratio of [1 Ti_4O_2 : 4 bb]. The reaction takes place in toluene at 80 ºC while stirring at 400 rpm. Initially, a mixture of bb (white) and Ti_4O_2 (yellow) solids is suspended in a clear solution of toluene. The yellow color gradually disappears over a period time of ~24 hours. Volatiles are subsequently removed under vacuum at 80 ºC, and then the residue is dried under the same conditions for ~12 hours. The only volatile byproduct is $ClSnMe_3$ identified by NMR. Approximately 4 equivalents of $ClSnMe_3$ per Ti_4O_2 are formed according to gravimetric analysis.

After the first crosslinking reaction between Ti_4O_2 and bb, colorless crystals (diameter = ~0.5 mm) are observed on the surface of the Schlenk vessel and white amorphous solid at the bottom. The crystals were separated by sublimation onto a cold finger (vacuum, 100 ºC), and found to be trimethyltin benzoate ($PhCO_2Sn(CH_3)_3$) by NMR and X-ray crystallography. The weight change by gravimetric analysis indicates ~6.0 equivalents of $PhCO_2Sn(CH_3)_3$ per Ti_4O_2

are formed. Based on the gravimetric data, all but two of the chloride ligands and all of the benzoyl ligands in the original complex are lost in the reaction with the tin bb. The titanium-containing material is named as "Ti_4O_2-bb", and later characterized with IR, DRUV and XAS (section 4.2).

To be used as a catalyst, Ti_4O_2-bb undergoes a second step of crosslinking with inert linker $SiCl_4$ at a molar ratio of [2 $SiCl_4$: 1 bb]. The reaction is carried out in toluene at 80 ºC, and stirring at 400rpm. After ~48 hours, volatiles are removed under vacuum at 80 ºC and a dry white powder is obtained. In order to remove any remaining trimethyltin groups, chlorotrimethylsilane (TMSCl) is then added to the solid, and let react at 80 ºC for 12 hours. Volatiles are again removed once reaction is complete. Before used as a catalyst, the solid is passivated with methanol in toluene, following the same procedure described in Chapter 2 section 2.1.4.

4.1.3 Synthesis of tetranuclear titanium-POSS analogue

In order to understand the complex reaction between Ti_4O_2 and bb, a molecular analogue (Ti_4O_2-POSS) to the embedded Ti_4O_2 (Ti_4O_2-bb) was prepared using polyhedral oligomeric silsesquioxane (Ph_7-POSS). Both POSS and bb are derivatives of the cubic silsesquioxane. Only one corner (out of eight) on POSS is functionalized with -$OSn(CH_3)_3$, and the rest are capped with inactive phenyl groups (Figure 64). In other words, only one corner on POSS is available to crosslink with Ti_4O_2 cluster.

The synthesis of Ti_4O_2-POSS involves a one-step crosslinking reaction. Ti_4O_2 is mixed with POSS at a molar ratio of [1 Ti_4O_2 : 8 POSS]. Toluene is used as the solvent. The reaction takes place at 80 ºC with stirring at 400rpm for ~24 hours. After removing the volatiles, a white solid is obtained as the product. The byproduct $ClSn(CH_3)_3$ is observed as expected. There is no indication of trimethyltin benzoate or any other byproducts. Gravimetric analysis shows that ~4.4 equivalents of $ClSn(CH_3)_3$ are formed per Ti_4O_2 cluster.

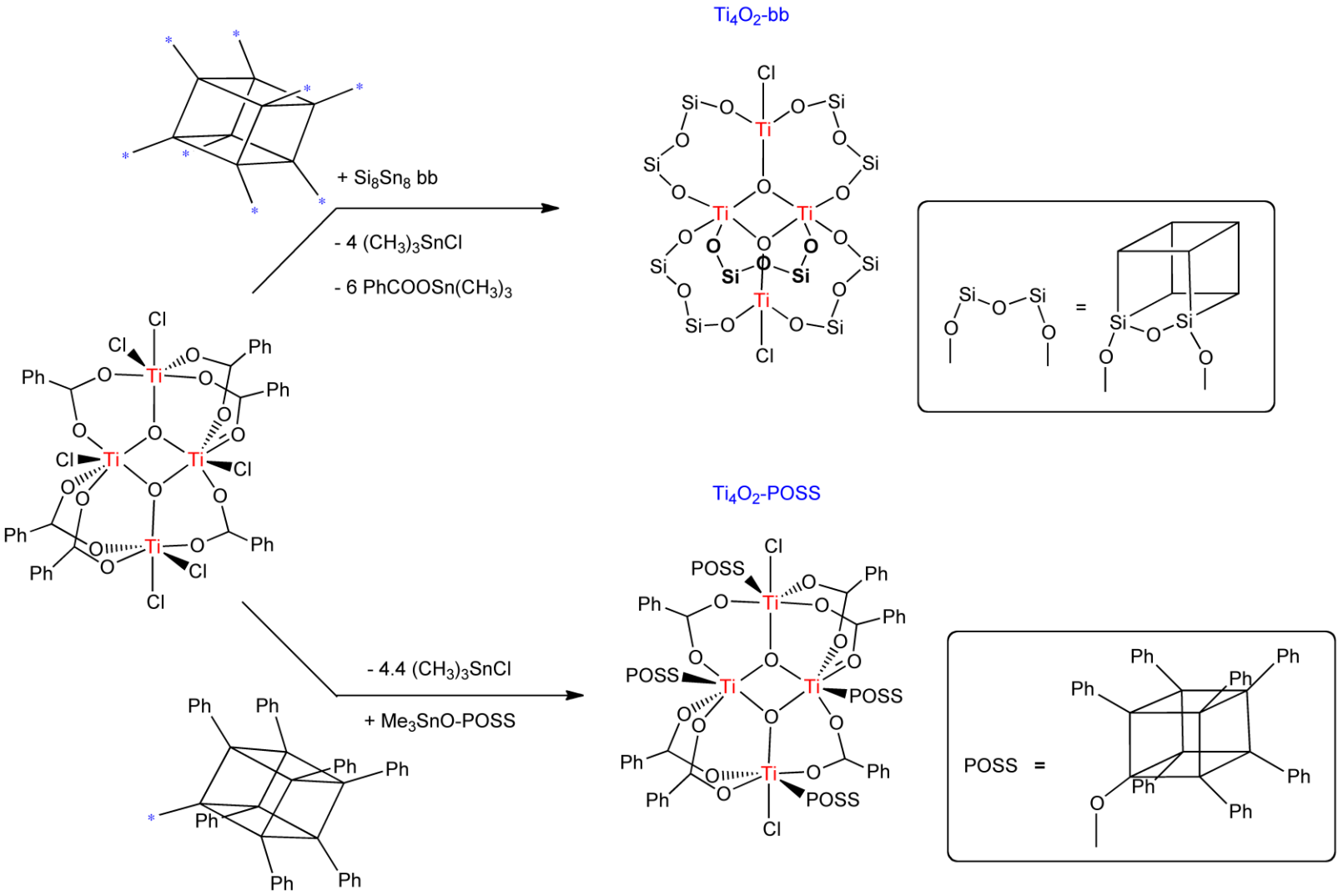


Figure 64. Gravimetric results and hypothesized titanium centers in Ti_4O_2-bb and Ti_4O_2-POSS (blue stars symbolize -O-SnMe3 active corners on bb or POSS)

4.1.4 Summary of synthesis

Benzoyl titanium cluster and trimethyltin functionalized bb are employed to prepare well-defined polunuclear titanium centers within silica matrices. The reaction equation must be established in order to define the structure of titanium centers in the catalyst before studying its catalytic activity.

In the reaction between Ti_4O_2 and Si_8 building block (bb), formation of Ti-O-Si is confirmed by IR signature band at 960 cm^{-1}. The amount of byproduct is quantified and converted into the stoichiometric ratio of byproduct to bb, indicating that 4 out of 6 chloride groups on each Ti_4O_2 cluster are reacted. All benzoyl groups on the titanium cluster are removed in the form of trimethyltin benzoate ($PhCO_2SnMe_3$). $PhCO_2SnMe_3$ is only formed when using octatin-bb rather than POSS, which suggests that the reaction requires neighboring reactive corners (-$SnMe_3$) on the cubic silsesquioxane. Based on these data, it is reasonable to hypothesize that reaction between the Ti_4O_2 complex and bb takes place simultaneously on the neighboring corners of bb. The final structure in Ti_4O_2-bb must be a neutral species after generating the proper amount of each byproduct based on gravimetric analysis. Taking these observations into consideration (and DRUV and X-ray data discussed in sections 4.2.2 and 4.2.3), the titanium centers in Ti_4O_2-bb are likely to coordinate with fewer ligands than those in the Ti_4O_2 cluster (6-coordinated). The reactions and the titanium centers in Ti_4O_2-bb (one of the possibilities that contain bridging Si-O-Si) and Ti_4O_2-POSS are shown in Figure 64. Other possible structures that cannot be ruled out based on the data in hand are summarized in Figure 65. The hypotheses will be discussed in more detail in the context of XAS, DRUV, and vibrational spectroscopic data presented in the following sections.

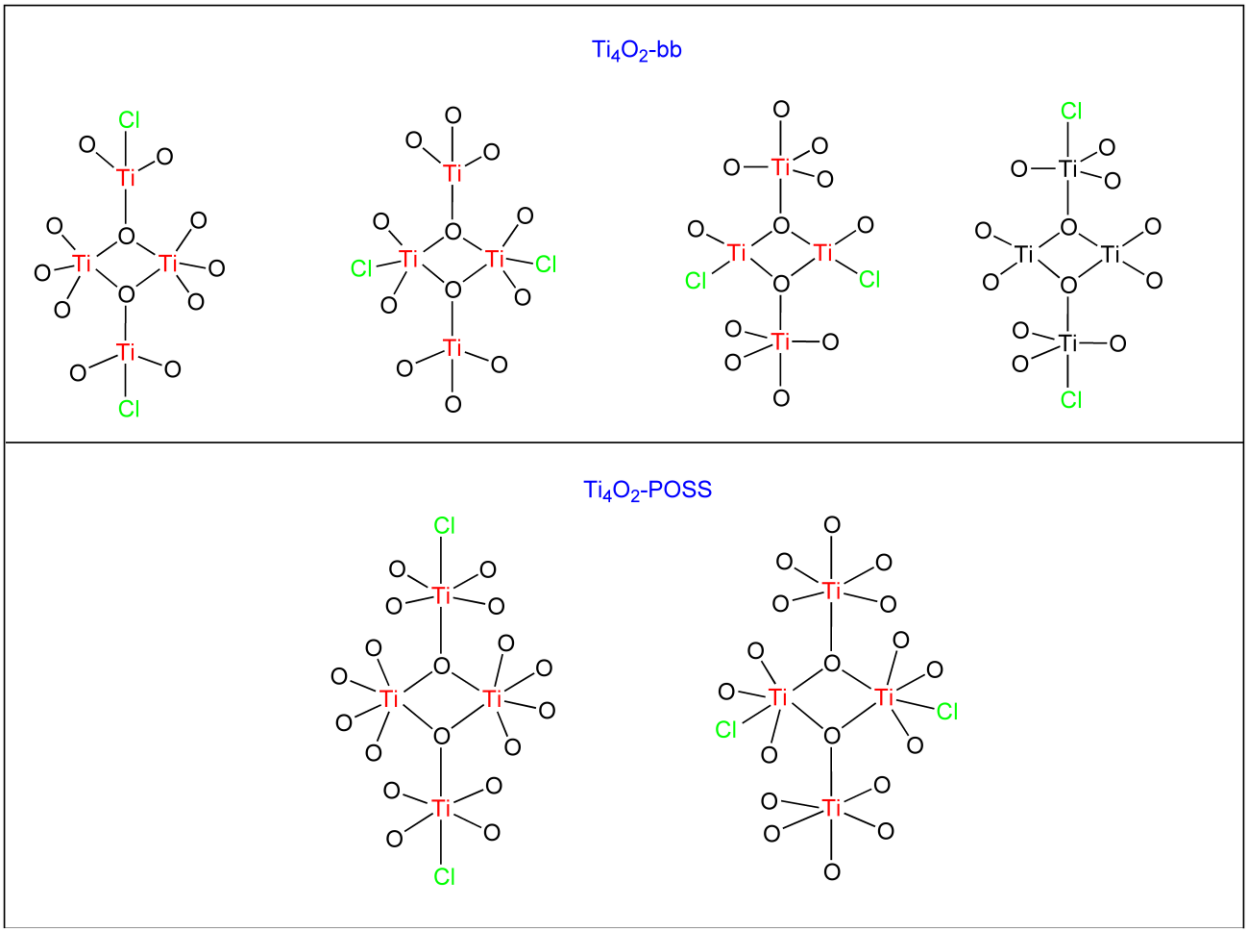


Figure 65. (Top) Possible tetranuclear titanium centers in Ti_4O_2-bb catalyst (all μ_2-oxygen atoms are connected to silicon atoms); (bottom) possible tetranuclear titanium centers in Ti_4O_2-POSS analogue (μ_2-oxygen atoms are connected to either carbon or silicon atoms)

4.2 Characterization of Embedded Tetranuclear Titanium Center

4.2.1 Vibrational spectra

1.Infrared spectra

Figure 66 compares the IR spectra of Ti_4O_2 cluster and Ti_4O_2-bb. It is clear that Ti_4O_2-bb exhibits strong vibration bands from silica (Si-O-Si). Most importantly, Ti-O-Si vibration at 960 cm^{-1} band is clearly observed in the infrared spectrum of Ti_4O_2-bb and not in the Ti_4O_2 cluster, indicating the successful linkage between Ti_4O_2 cluster and bb. The spectrum of Ti_4O_2 cluster shows a band right above 3000 cm^{-1} arising from C-H aromatic stretching, which decreases significantly in the spectrum of Ti_4O_2-bb. This change is consistent with the loss of benzoyl groups after the Ti_4O_2 cluster is embedded in the bb matrix.

2.Raman spectra

The sample powder is pressed into a self-supported pellet and then sealed in an air-tight container under nitrogen. Transparent windows are on both side of the container that allows the laser to pass through. Raman spectra are collected using a Horbia Jobin Yvon T64000 spectrometer (600 or 1800 grooves/mm) equipped with a Synapse CCD detector, and excited at 487.9 nm with a Coherent Innova 200 argon ion laser.

Raman spectrometry is a powerful tool used to qualitatively identify chemical compositions. The spectra (Figure 67) of Ti_4O_2 cluster and Ti_4O_2-bb contains the information about the vibrations of specific functionalities. As expected, the spectrum of Ti_4O_2 cluster exhibits clearly the features of Ti-Cl (~409 cm^{-1})[103, 104] and Ti-O-Ti (~843, ~1002 cm^{-1}).[96] In typical IR spectra, these vibrations severely overlap with asymmetric vibration bands of silica (900-1300 cm^{-1}), and therefore are hard to identify. The Raman spectrum of Ti_4O_2-bb shows a very weak Ti-Cl peak compared to the one in Ti_4O_2 cluster. The decrease in intensity agrees with the gravimetric result which indicated that 4 out of 6 chloride groups per Ti_4O_2 are removed after reacting with bb. Ti-O-Ti features are observed in both Ti_4O_2 and Ti_4O_2-bb. As expected, vibrational bands of Si-O-Si (silica) and Si-C (TMS) are also observed in the spectrum of Ti_4O_2-bb. It is also important to note that the absence of signature bands for titania anatase (140 cm^{-1}, 513 cm^{-1}, 637 cm^{-1}) rules out the possibility of forming any titania domains.[48]

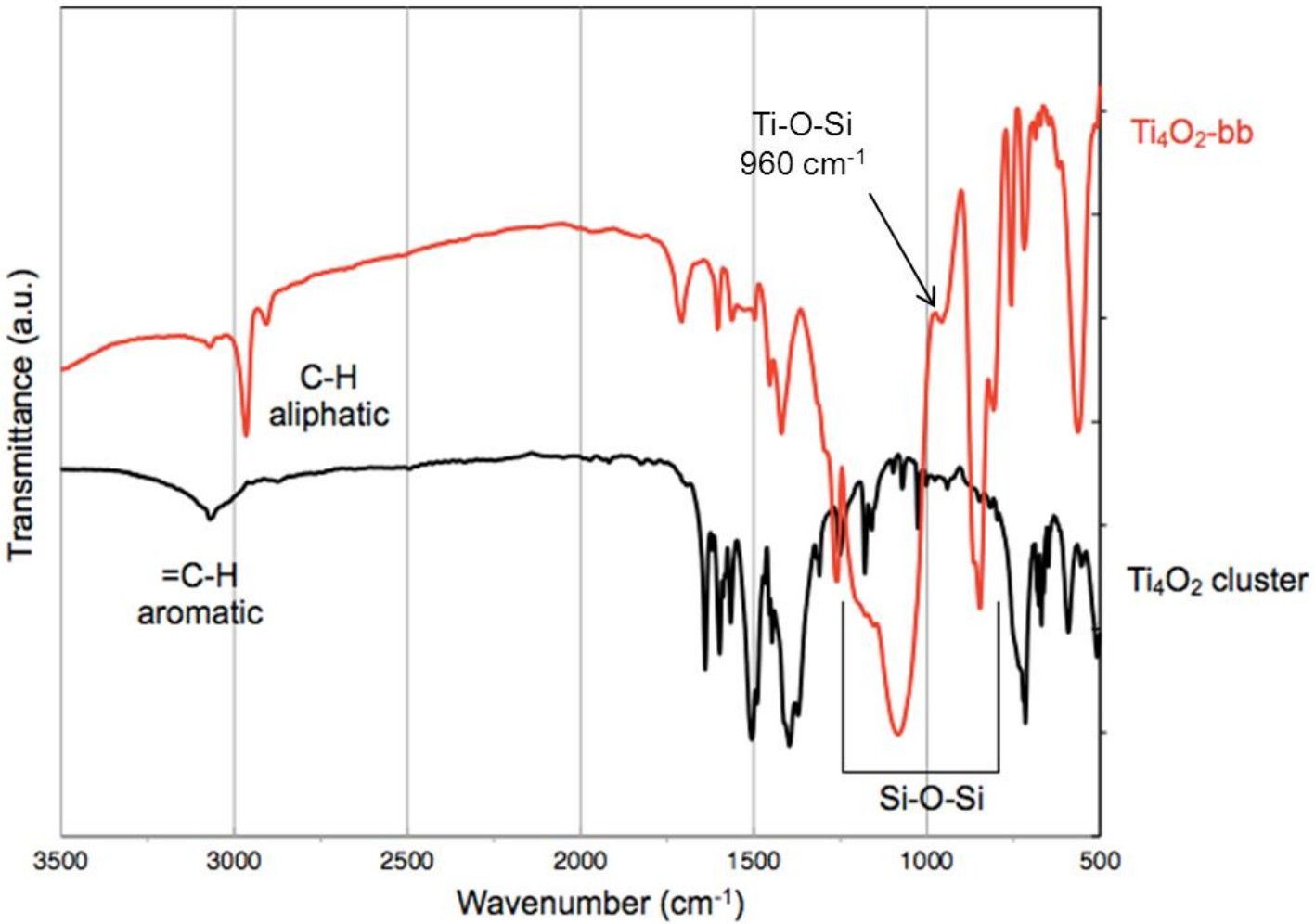


Figure 66. IR spectra of embedded tetranuclear titanium center (absorption band of Ti-O-Si vibration)

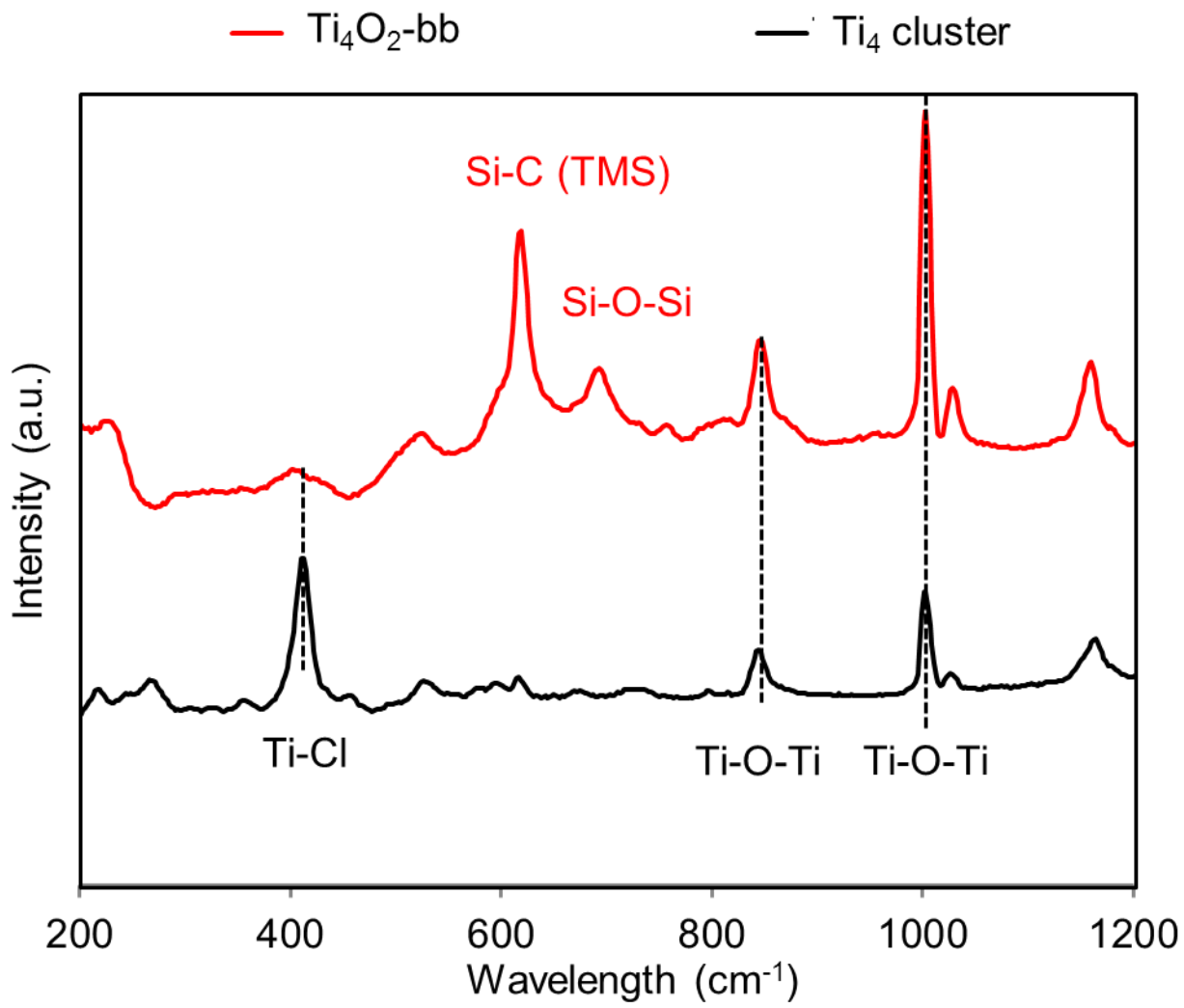


Figure 67. Raman spectra of tetranuclear titanium center before and after the reaction with bb

4.2.2 DRUV

Figure 68 shows the DRUV spectra of Ti_4O_2 cluster and Ti_4O_2-bb with distinctly different absorption features. The spectrum of Ti_4O_2 cluster exhibits a broad band that begins at ~450 nm. The absorption band in Ti_4O_2-bb blue shifts significantly which begins at ~370 nm. The blue shift is thought to be associated with the removal of benzoyl groups (μ_2-O_2CPh) in Ti_4O_2-bb. As discussed in section 3.3.2 (Chapter 2), absorption above 300 nm is observed when Ti-O-Ti bridges are present. The band of Ti_4O_2-bb is much broader than that of isolated 4-coordinated titanium in silicate. The maximum in the absorption band of isolated tetrahedral titanium centers in TS-1 is observed at ~210 nm and those of atomically dispersed titanium centers (pseudo-tetrahedral) at 225 nm (Figure 48). In either case, the edge of the absorption band is below ~300 nm, consistent with the absence of Ti-O-Ti.

The maximum in the absorption band observed for Ti_4O_2-bb is estimated to occur at ~275 nm. Absorption between 250-290 nm may also be due to titanium centers with higher coordination numbers (5 or 6).

The DRUV spectra indicate a change in the structure of active centers, related primarily to the loss of benzoyl groups. The edge and maximum of UV absorption bands are influenced by many factors including coordination number, nuclearity of titanium clusters (presence of Ti-O-Ti groups) and particle size (titania). It is therefore difficult to derive coordination number from DRUV spectra with confidence. The position of the maximum of the absorption band (~275 nm) for Ti_4O_2-bb suggests that Ti-O-Ti groups are still present in the titanium sites.

4.2.3 XANES

XANES is a powerful technique to investigate the coordination sphere around titanium centers. XANES spectra of Ti_4O_2 cluster, Ti_4O_2-bb and Ti_4O_2-POSS were collected following the procedures described in Chapter 2, and presented in Figure 69. The corresponding parameters are summarized in Table 17.

1. Ti_4O_2 cluster

The spectral features in the XANES region are closely associated with the local structures of titanium centers. Ti_4O_2 cluster is comprised of 6-coordinated (pseudo-octahedral) titanium centers before reacting with bb. As expected, its XANES spectrum (black line) shows multiple pre-edge peaks with very low intensity (14%) relative to the edge jump, indicating Laporte forbidden electronic transitions (1s to 3d) in the presence of centrosymmetry (O_h).

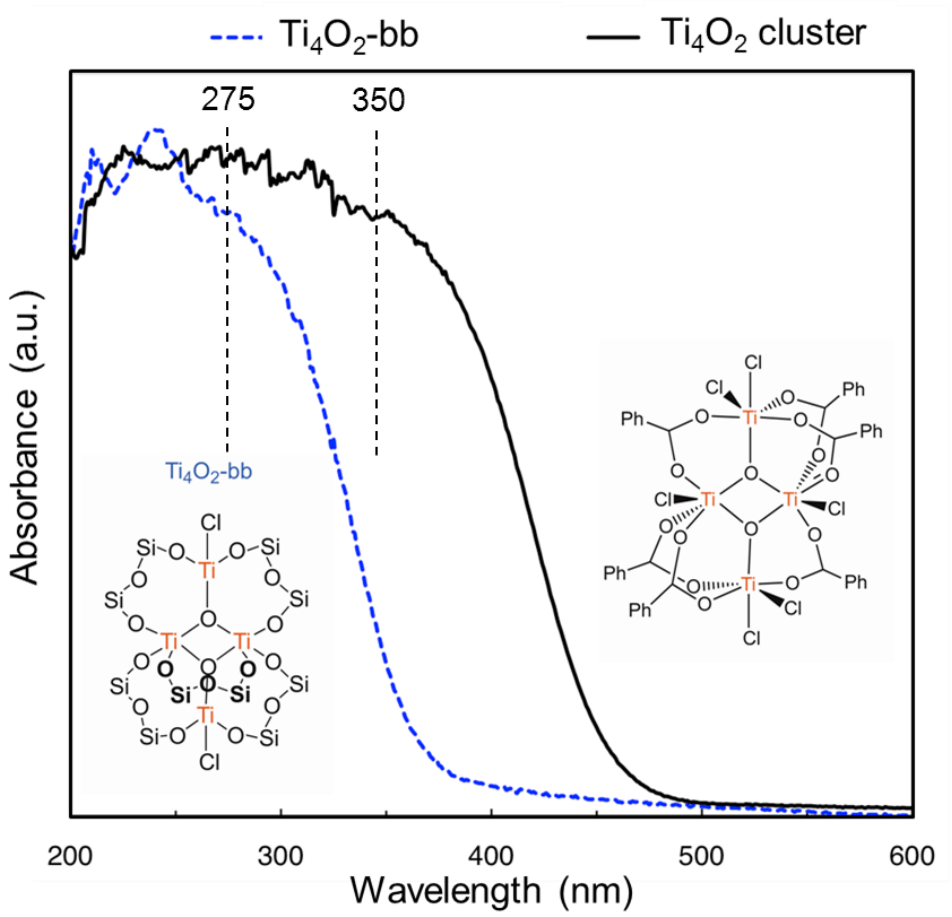


Figure 68. DRUV spectra of tetranuclear titanium center before and after the reaction with bb

Table 17. Ti K-edge parameters for tetranuclear titanium samples

Entry	Samples	Description	Pre-edge Peak Energy/eV	Peak Width ΔFWHM/ eV	Peak Intensity/%	Main Edge /eV
1	Ti_4O_2	$[Ti_4(\mu_3\text{-}O)_2Cl_6(\mu_2\text{-}O_2CPh)_6]$	4971.0 (4968.5; 4973.5) [a]	-	14	4979.5
2	Ti_4O_2-bb	Ti_4O_2 + Si_8Sn_8 bb	4970.0	1.8	70	4980.5
3	Ti_4O_2-POSS	Ti_4O_2 + POSS-$OSnMe_3$	4971.0	-	13	4980.5

[a] Multiple pre-edge features are observed.

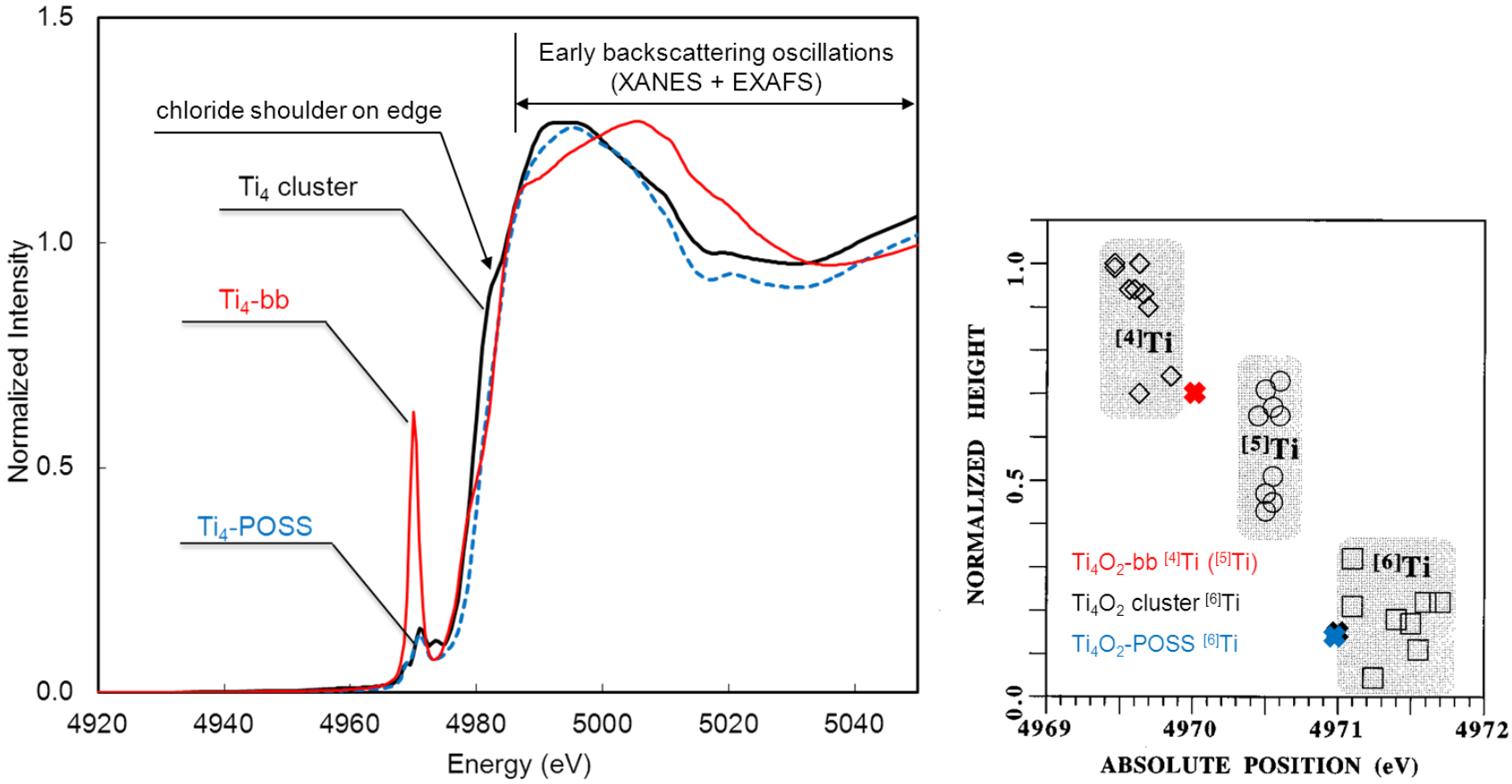


Figure 69. (Left) XANES and early EXAFS regions of Ti_4O_2, Ti_4O_2-bb and Ti_4O_2-POSS; (right) (gray pre-edge data from reference 88) coordination numbers of titanium in each material according to the position and height of pre-edge peaks

The absorption shoulder on the main edge (~4985 eV) arises from the shakedown transition (1s to 4p) when chloride ligand is present in the first shell.[87] According to the relationship between pre-edge feature and coordination number, the position of pre-edge peak (4971.0 eV) for the Ti_4O_2 cluster complex falls on the lower edge of 6-coordinated titanium center. (Figure 69)

2. Ti_4O_2-bb

Vibrational and DRUV spectroscopies suggest that significant changes occured to the coordination of titanium centers during the formation of Ti_4O_2-bb. The similar effects are observed in the XANES spectra. The difference in ligand environment is supported by the drastically different oscillatory regions above the main edge. These oscillations vary sensitively with the neighboring atoms and their distances from the absorber atom.

Ti_4O_2-bb (red line in Figure 69) exhibits a sharp and intense (70%) pre-edge peak, suggesting the absence of a center of symmetry. This pre-edge feature is not consistent with 6-coordianted titanium. The position of pre-edge peak in Ti_4O_2-bb (4970.0 eV) is consistent with a coordination number between 4 and 5 coordination. (Figure 69) As discussed in section 4.1.4, a mixture of 4- and 5-coordinated titanium centers may be present in Ti_4O_2-bb. (Figure 64-65) The hypothesized structure is based on the gravimetric analysis and charge balance. In that case, an average of pre-edge peaks (height and position) from 4- and 5-coordinated titanium would be consistent with the peak deviated from either coordination.

Lastly, most of the chloride ligands are reacted and removed from the shell around titanium. A small absorption at 4980 eV (overlaid on black line) is due to the unreacted chloride on titanium. But compared with Ti_4O_2 cluster, the intensity of the chloride shoulder is much lower.

3. Ti_4O_2-POSS

The XANES spectrum of Ti_4O_2-POSS (Figure 69) strongly suggests that titanium centers remain 6-coordinated by showing multiple, weak pre-edge peaks. The position of the major pre-edge peak (middle) is located at 4971.0 eV. The oscillatory parts of Ti_4O_2-POSS and Ti_4O_2 cluster share a similar shape, except for the loss of chloride shoulder in Ti_4O_2-POSS.

4.3 Conclusion of Tetranuclear Titanium Sites

In order to investigate the properties of Ti-O-Ti structures within silicate matrices, the tetranuclear titanium cluster, $[Ti_4(\mu_3\text{-}O)_2Cl_6(\mu_2\text{-}O_2CPh)_6]$, is utilized as the precursor to be embedded within a silicate bb-based matrix. The stable $[Ti_4(\mu_3\text{-}O)_2]$ core contains Ti-O-Ti structure that, according to the literature, exhibits unique catalytic properties.

This is one of the first studies that focus on the reaction between a chlorotitanate cluster with cubic, tin-functionalized silsesquioxane, $Si_8O_{20}(SnMe_3)_8$. Comparison experiments are designed to understand the reactions and, most importantly, to define the structure of the titanium sites in Ti_4O_2-bb catalyst. Ti_4O_2-bb and analogous Ti_4O_2-POSS are synthesized following the method of sequential additions.

Gravimetric analysis provides the stoichiometric ratios of products formed during each reaction. The structures of titanium centers are proposed as illustrated in Figure 64-65 (section 4.1.4) and subsequently characterized by IR, Raman, DRUV and XAS. Many previous studies on titanosilicates have summarized the important signature features in these different spectroscopies. The existence of Ti-O-Ti and Ti-O-Si in Ti_4O_2-bb is confirmed by IR, Raman and DRUV. The comparison between XANES spectra of Ti_4O_2-POSS and Ti_4O_2-bb demonstrates the different mechanism of each reaction, and consequently, the different ligand environments around titanium. Benzoyl bridges between titanium centers appear to be replaced by the neighboring trimethyltin corners on bb or by Ti-O-Si links from separate cubic building blocks. Without excluding the possibilities of other structures, the various lines of data are most consistent with the formation of tetrahedral, 4-coordinate titanium atoms occurring in Ti_4O_2 units in the matrix, and the presence of some 5-coordinate titanium centers cannot be ruled out.

Ti_4O_2-bb is passivated to remove remaining tin and chloride before used in catalysis. In the following chapter, the property of Ti_4 catalyst is investigated in the oxidation reaction of alkylphenol, and compared with atomically dispersed titanium centers.

Chapter V. Secondary Characterization: Catalytic Properties in Alkylphenol Oxidation with Aqueous Hydrogen Peroxide

5.1 Background and Experimental

5.1.1 Heterogeneous activation of aqueous hydrogen peroxide

Catalytic oxidation contains a large variety of important chemical reactions as well as the corresponding catalysts for converting petroleum-based feedstocks to high-value chemicals. In these reactions aqueous hydrogen peroxide (H_2O_2/H_2O) is an important oxidant usually more preferred than organic peroxides. Generally when H_2O_2 is used as the oxidant, it is possible to practice green chemistry, and meanwhile lower the cost by easier purification of the product. The byproduct from using H_2O_2 is completely non-toxic (water). H_2O_2 has a high content of active oxygen, making the oxidation atom-efficient. Catalysts are required, in most reactions, to activate the H_2O_2 molecule. Over the years, a variety of sophisticated catalysts have been developed, including homogeneous molecular catalysts, biomimetic catalysts and single-site heterogeneous catalysts (SSHCs).

Simple methods to separate catalyst from products have been the initial driving force for preparing heterogeneous systems. Later, many studies showed that the presence of support has beneficial effects more than merely an inert backbone. The bonding between metal center and support can lead to preferred orientations of the substrate at the catalytic sites and therefore higher selectivity. Besides the activity and selectivity, catalysts must be stabilized to survive aqueous H_2O_2. Metal centers are susceptible to aggregation thereby becoming inactive, which is why homogeneous catalysts are less ideal in these reactions. SSHCs that contain immobilized and isolated active centers may prevent these centers from aggregation.

However, one major issue with heterogeneous catalysts is that the reaction may only occur at catalytically accessible sites, in other words, some inaccessible or inactive sites remain unused during the reaction. The catalytic properties of each metal center on a support depend not only on the method of preparation but also the precursor of titanium and Si sources. Thus, in many ways SSHCs are preferred due to the homogeneous distribution of active centers and consequently high specific reactivity and selectivity they exhibit. Among these catalysts TS-1 may be the most well-known example that exhibits remarkable activities and selectivity in, for example, the epoxidation of olefin. The interaction between TS-1 and H_2O_2 has been proposed by Khouw *et. al*. (Figure 70), and later supported by several others.[59, 105, 106]

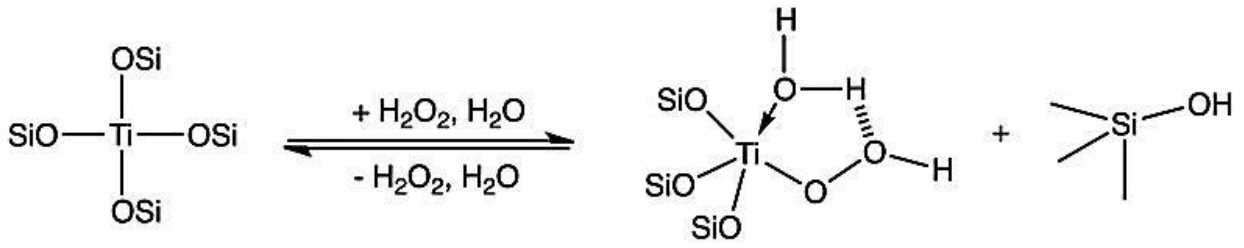
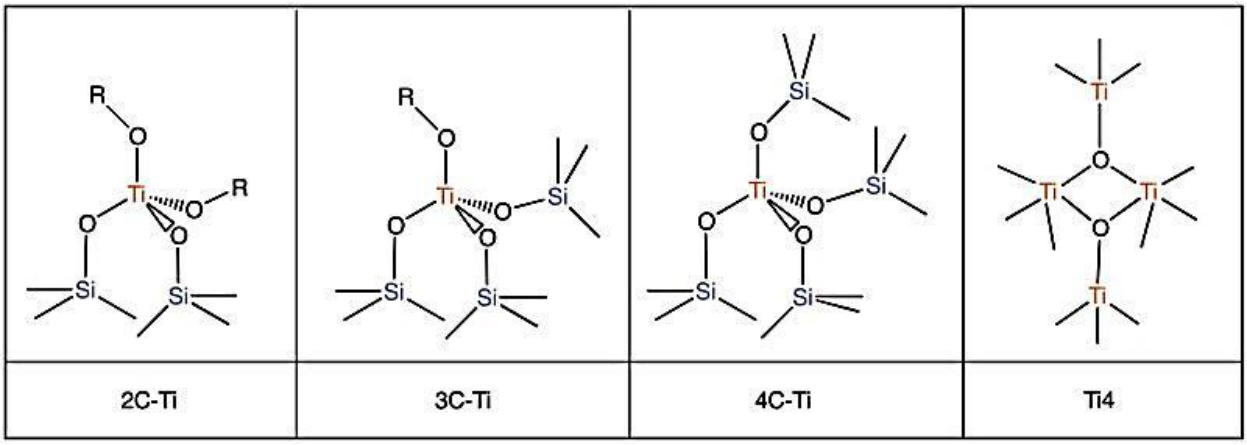


Figure 70. Titanium center in TS-1 interacts with H_2O_2 during catalytic oxidation

5.1.2 Titanosilicates in alkylphenol oxidation reactions

2C-, 3C-, 4C-Ti and Ti_4 building block materials synthesized in this research (Figure 71) have been investigated as catalysts in the oxidation of 2, 3, 5-trimethylphenol (TMP) with aqueous H_2O_2. The unique synthetic methodology may have potentially overcome the issues with heterogeneous materials arising from the distribution of sites. According to the characterization data in Chapter 3 and 4, these materials possess the following properties desired for titanosilicates used in oxidation reactions with H_2O_2: (1) ~100% of the titanium from each of the precursors is incorporated with the matrices, and potentially turns into an active center; (2) high site homogeneity of titanium centers with targeted connectivity and nuclearity; (3) site isolation that prohibits titanium dimerization and leaching; and (4) meso-sized pore structures that accommodate large substrates such as alkyl-substituted phenol.

Besides making efficient catalysts, the major goal of this research is to investigate the influence of varying connectivity and nuclearity of titanium center and to establish a clear structure-function relationship. Titanium-catalyzed oxidation reaction of alkylphenol to the corresponding benzoquinone was studied by Kholdeeva *et al.*[50, 52] The titanosilicate catalysts used in the previous studies were prepared by grafting titanium precursors onto mesoporous silica followed by calcination. In the work by Kholdeeva and coworkers, a catalyst prepared with polynuclear titanium precursor exhibited higher activity and selectivity than those with mononuclear titanium, assuming mononuclear titanium species remain isolated at low enough content. The connectivity around titanium center is believed to have major impact on catalytic properties, but currently has only been addressed in terms of surface and embedded titanium centers. This research hopes to take advantage of the well-defined sites in the materials prepared here in order to study the influence of the specific connectivity (2C-, 3C- and 4C-Ti) and nuclearity (mono- vs. tetranuclear)



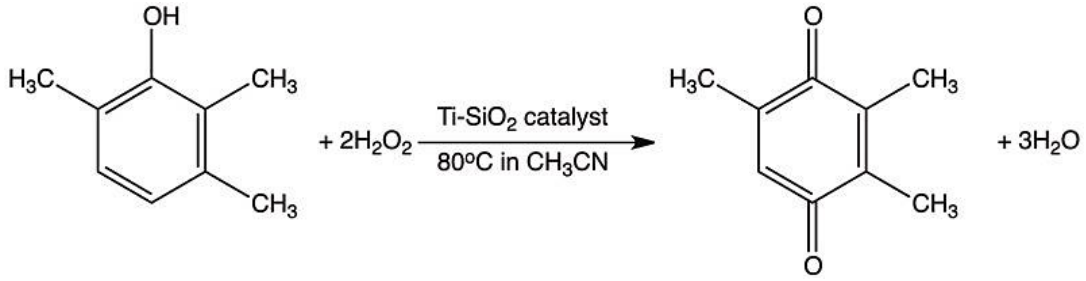


Figure 71. Four types of titanium centers synthesized and used for TMP oxidation

5.1.3 Experimental

4 mL glass vials with septum caps are used to contain the reaction components and a small magnetic stir bar. 8.0-29.0 mg (0.012 mmol of titanium) of passivated catalyst, i.e. 2C-Ti or 3C-Ti, 4C-Ti or Ti_4) is ground into fine powder before being added to the reaction vial. 2, 3, 6-trimethylphenol (TMP, 97+%, Sigma-Aldrich) was used as received. 27 mg (0.20 mmol) of TMP is added into the vial as the substrate, and 10 mg (0.065 mmol) biphenyl (BP) as the internal standard for quantification purposes. Anhydrous acetonitrile (3.0 mL) is used as the solvent. TMP and BP are soluble in CH_3CN, and the catalyst powder is suspended in the solution during the reaction. The vial is then brought to 80^{o}C and allowed to equilibrate for 5 min. The initial concentrations of TMP and BP are quantified at this point by taking a small aliquot (0.50 µL) from the suspension (while stirring), subsequently injected into gas chromatography-flame ionization detector (GC-FID).

To initiate the oxidation reaction, 163 mg (2.4 mmol) of aqueous H_2O_2 (50% w/w) was added through the septum of the vial. The reaction is kept at 80 ^{o}C while stirring at 400 rpm for ~3 - 6 hours. 0.5 µL aliquots for GC-FID are taken through the septum periodically to monitor the reaction process.

Comparison experiments are done with fumed silica, silicate bb-based platform and Ti-MCM-48, respectively, under the same reaction conditions as above. The silicate platform is described in section 2.1.4, Chapter 2, and contains 0.0 wt% Ti and 1.6 wt% Sn. Ti-MCM-48 is prepared following the literature, and contains 3.5 wt% Ti and has a surface area of 1200 m^2/g.[95] In these comparison experiments, approximately 16.4 mg (0.012 mmol) Ti-MCM-48, 20 mg fumed silica or 20 mg silicate platform is added instead of the titanium-containing catalysts.

5.1.4 Characterization of products

1. ^{1}H NMR and GC-MS

Proton NMR identified the desired product 2, 3, 5-trimethyl-p-benzoquinone (TMBQ) after first separated by silica gel chromatography. Gas chromatograph-mass spectroscopy (GC-MS) was used to identify all the products. Small amounts of byproducts from epoxidation and dimerization reactions were observed (epoxy-benzoquinone < 10 %, bisphenol < 5% yield) but not investigated in detail.

The characterization data from GC-MS ^{1}H NMR are summarized below:

2,3,5-Trimethyl-phenol (TMP). GC-MS (EI) m/z (relative intensity): 136 (91, $[M]^+$), 135 (22, $[M-H]^+$), 121 (100, $[M-CH_3]^+$), 91 (23, $[M-3CH_3]^+$)

Biphenyl (BP). GC-MS (EI) m/z (relative intensity): 154 (100, $[M]^+$), 153 (30, $[M-H]^+$), 76 (10, $[M-C_6H_6]^+$)

2,3,5-Trimethyl-1,4-benzoquinone (TMBQ). GC-MS (EI) m/z (relative intensity): 150 (100, $[M]^+$), 122 (47 $[M-CO]^+$), 107 (64, $[M-CO, -CH_3]^+$), 79 (48, $[M-2CO, -CH_3]^+$). ^1H NMR ($CDCl_3$, ppm): 6.59 (s, 1H, H quinone), 2.05-2.10 (m, 9H, $3CH_3$)

2,3,6-Trimethyl-2,3-epoxy-1,4-benzoquinone or 2,5,6-trimethyl-2,3-epoxy-1,4-benzo-quinone. GC-MS (EI) m/z (relative intensity): 166 (7, $[M]^+$), 151 (100, $[M-CH_3]^+$), 138 (17, $[M-CO]^+$), 124 (33, $[M-CCH_3, -CH_3]^+$), 109 (13, $[M-CCH_3, -2CH_3]^+$).

2,2',3,3',5,5'-Hexamethyl-4,4'-bisphenol. GC-MS (EI) m/z (relative intensity): 270 (100, $[M]^+$), 255 (57, $[M-CH_3]^+$), 240 (61, $[M-2CH_3]^+$), 225 (15, $[M-3CH_3]^+$), 210 (3, $[M-4CH_3]^+$), 195 (7, $[M-5CH_3]^+$)

2. GC-FID

GC-flame ionization detector (GC-FID) is used to quantify the amount of each product using internal standard biphenyl (BP). A response factor (RF) is commonly used to quantify the amount of compound A, conc(A) (mmol/g), according to the integration of peak area, area(A) (counts).

$$RF(A) = \frac{area(A)}{conc(A)} \qquad \text{Equation 5-2}$$

Response factor is measured with a series of solutions with known concentrations, followed by plotting the area as a function of concentration, as shown in Figure 72. In this way, the response factors for TMP, BQ and TMBQ are measured to be 15.7, 24.3 and 22.1 [counts/(mmol·g^{-1})], respectively.

In this research, an internal standard biphenyl is employed to calibrate the amount of each compound. The amount of biphenyl used was approximately one half the number of mmoles of TMP initially present in the reaction. The ratio of RF(TMP) or RF(TMBQ) to RF(BP) is practically used instead of the absolute RF values. The advantage from using relative response factor (RRF) is to avoid the mechanical errors associated with measuring sample aliquots, and instrumental errors.

$$RRF(TMP) = \frac{RF(TMP)}{RF(BP)} = \frac{15.7}{24.3} = 0.65$$ Equation 5-3

$$RRF(TMBQ) = \frac{RF(TMBQ)}{RF(BP)} = \frac{22.1}{24.3} = 0.91$$ Equation 5-4

Based on equations above, it is easy to obtain the amounts of TMP and TMBQ according to the peak areas and the constant amount of BP in the solution, n[BP] (mmol).

$$n[TMP](mmol) = \frac{area(TMP)}{area(BP)} \times \frac{n[BP](mmol)}{RRF(TMP)}$$ Equation 5-5

$$n[TMBQ](mmol) = \frac{area(TMBQ)}{area(BP)} \times \frac{n[BP](mmol)}{RRF(TMBQ)}$$ Equation 5-6

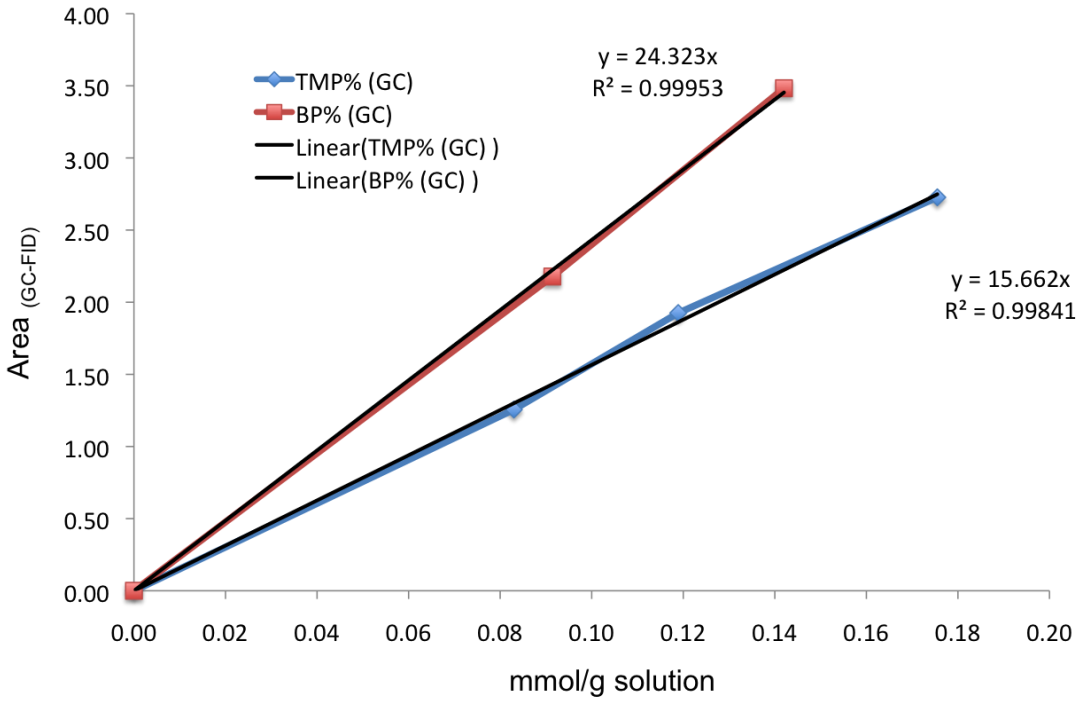


Figure 72. Linear relation of FID signal as a function of the concentration, biphenyl (red) and TMP (blue)

During the reaction, the amount of TMP is recorded and plotted as a function of time. (Figure 73) Turn over frequency (TOF) for each catalyst is obtained according the first data point of the curve, typically about five minutes after the addition of peroxide. The amount of titanium in the catalyst used is expressed as the number of sites, [Ti] (mmol) leading to the following expression for turnover frequency:

$$TOF = \frac{n[TMP]_{initial} - n[TMP]_t}{[Ti](mmol) \times t(\min)}$$ Equation 5-7

Alternatively, some researchers use the derivative of the initial part of the curve to determine TOF's. Both methods of calculating TOF's are effective and have been reported.[112-114] Generally, lower TOF values are seen from the method used in this research

Conversion of TMP and selectivity of the desired product TMBQ are calculated based on the final, overall conversion after the reaction has been stopped ($n[TMP]_{final}$ and $n[TMBQ]_{final}$) using the equations below.

$$conversion\ (\%) = \left(1 - \frac{n[TMP]_{final}}{n[TMP]_{initial}}\right) \times 100\ \%$$ Equation 5-8

$$selectivity\ (\%) = \frac{n[TMBQ]_{final}}{n[TMP]_{final} - n[TMP]_{initial}} \times 100\ \%$$ Equation 5-9

5.2 Evaluation of Catalytic Activity

5.2.1 Results and discussion

1. Conversion and TOF

When a titanium-containing material is used in phenol oxidation, the color of the catalyst (insoluble particles) changes from white to bright yellow immediately after the addition of H_2O_2. Within five minutes the solution turns yellow due to the formation of 2, 3, 5-trimethyl-p-benzoquinone (TMBQ).

In the comparison reactions where fumed silica or titanium-free platform is added instead, the solid (white) and solution (colorless) never change color quantitatively indicating low activity. The results of quantitative measurements agree with this observation. TMP conversions and yields of the desired product TMBQ are summarized in Table 18. Little to no conversion was observed when titanium-free materials are used, i.e. no catalyst (blank), fumed silica and silicate platform.

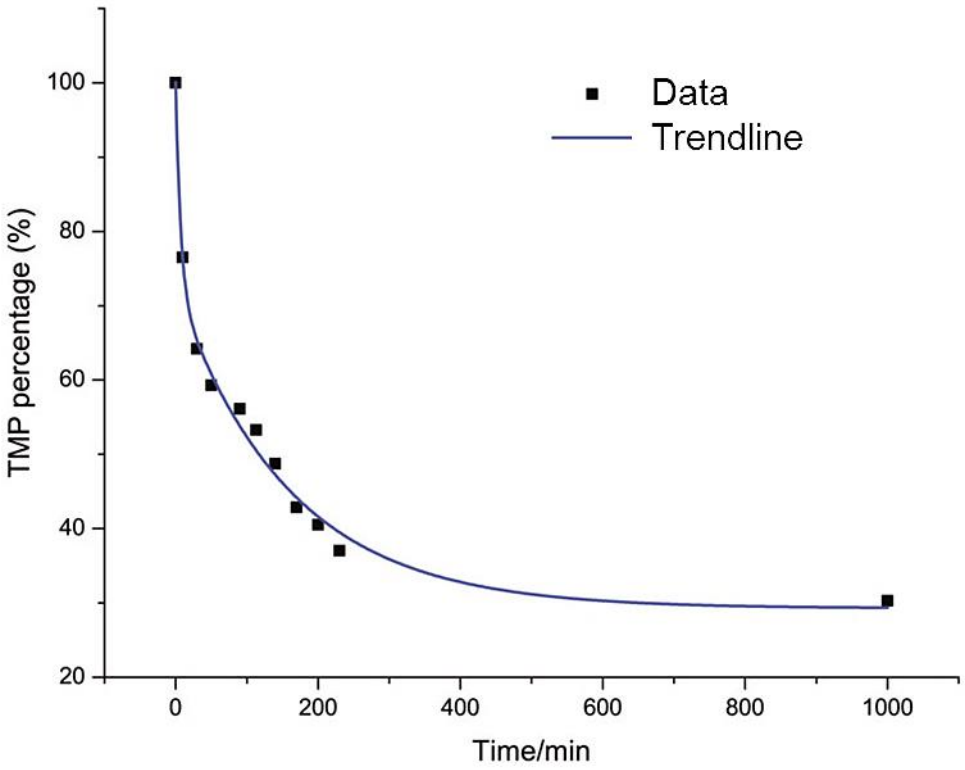


Figure 73. A plot of percentage of unreacted TMP vs. time

Table 18. Results of catalytic properties in oxidation of TMP to TMBQ

Blank controls & Ti catalysts	TMP Conversion% (± 3 %)	TMBQ Selectivity% (± 3 %)	TMBQ Yield%	Initial TOF (min^{-1})
TS-1	18	37	7	0.25
Ti-MCM-48	56	73	41	0.75
4C-Ti	26	43	11	0.35
3C-Ti	23	36	8	0.51
2C-Ti	90	80	73	1.58
Ti_4	96	93	89	1.72
No catalyst	0		-	
Silica, fumed	1		-	
$SiCl_4$ platform	3		-	

The results from comparison experiments demonstrate that the under the current conditions, the oxidation of alkylphenol does not occur without a titanium-containing catalyst. Neither the alkyltin functional groups from the bb nor porous silicate matrices catalyze the oxidation of phenol. No conversion is observed from titanium-free silicate platform that shares similar mesostructures with the titanium catalysts (2C-, 3C-, 4C-Ti and Ti_4) and contains approximately double the amount of tin (1.6 wt% Sn) as the latter. In contrast, all titanium-containing catalysts exhibit considerable activity with high selectivity for the desired benzoquinone product. Therefore, the lack of catalytic activity in the comparison reactions demonstrates that titanium atoms in the matrices are the only active centers in this reaction.

Different catalytic activities and selectivities have been observed for the atomically dispersed titanium catalysts (2C-, 3C- and 4C-Ti). Under the same reaction conditions, 2C-Ti shows significantly higher conversion as well as selectivity toward TMBQ than 3C- and 4C-Ti. Normalized to a per site basis, the TOF of 2C-Ti is also higher than 3C and 4C-Ti by a factor of 3-5. Among all catalysts, tetranuclear titanium centers (Ti_4) exhibit the highest conversion and selectivity toward TMBQ.

Diffusion does not have a major influence in phenol oxidation involving titanium silicates with pore sizes > 2.6 nm, based on previous studies. [72, 106] A free radical mechanism was proposed for the oxidation of phenol, involving the coordination with substrate and H_2O_2 to the titanium center. Varying stirring rate (200 – 1000 rpm) does not affect the reaction rate, confirmed in this research by comparing the TOFs at 200 rpm and 400 rpm. But, for the purpose of consistency, the stirring rate of 400 rpm was used in all experiments in this research.

Turnover frequencies directly characterize the catalytic nature of the material. The structural differences between these titanium sites may explain the evidently different TOF's observed. Given that all catalysts in this research share similar structure of building block matrices, different accessibility of titanium sites is believed to play a key role in catalytic activity. Compared to 3C- and 4C-Ti, fewer silicon atoms are present around the titanium centers in 2C-Ti and Ti_4. Based on gravimetric analysis, approximately 2.5 silicon atoms surround each titanium center in Ti_4. Higher connectivity in 3C- or 4C-Ti may result in steric hindrance, and as a result less accessible titanium centers. In Figure 74, a 4C titanium site is shown. In most mechanisms proposed to explain oxidation reactions catalyzed by titanium, an initial step involves coordination of either water or peroxide with the simultaneous breaking of a Si-O-Ti link to silicate support.[106] This is potentially a high energy step from both steric and electronic perspectives. Access to a 4C-Ti center will be more restricted than to 3C- or 2C-Ti center.

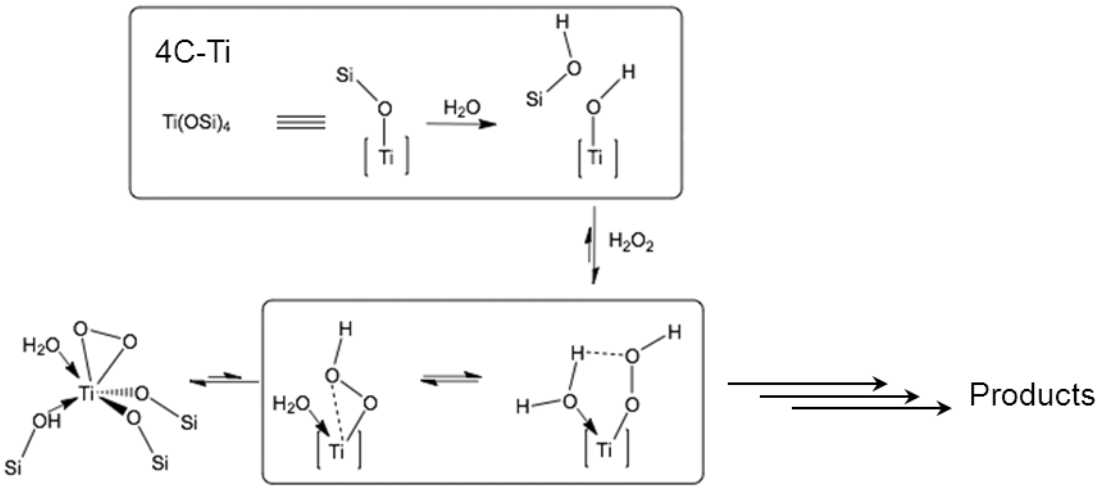


Figure 74. Activation of 4-connected titanium center with aqueous hydrogen peroxide

Furthermore, to coordinate peroxide or substrate will also require significant movement of the titanium atom with respect to the cage of Ti-O-Si bonds that surrounds it. The energy barriers associated with such movement for 2C- and 3C-Ti centers are expected to be significantly lower due to there being fewer Ti-O-Si linkages to deform.

The observation of higher activity and selectivity from polynuclear centers than mononuclear agrees with the previous results, where a free radical mechanism involving two neighboring titanium centers was proposed for the oxidation of phenol.[52] When only isolated mononuclear titanium centers are available, radicals (HO· and C_6H_5O·) must travel longer distances in order to complete the catalytic cycle.

Ti-MCM-48 (6.9 wt% Ti) and TS-1 (2.0 wt% Ti) were also investigated in the oxidation reaction and the catalytic properties compared with those reported above. The conversion and selectivity of TMP by TS-1 are both very low. Poor catalytic performance of TS-1 is expected because of the small pore sizes that prohibit the diffusion of bulky substrates such as TMP to the titanium sites. Ti-MCM-48 exhibits mediocre conversion and selectivity, lower than 2C-Ti or Ti_4. The mesoporous framework must not block TMP from entering the pores. The catalytic behavior is likely to result from the local environment around titanium, possibly a mixture of multiple types of titanium centers with different connectivities to the silicate surface.

2. Decomposition of hydrogen peroxide

Besides the factor of accessibility, the difference in connectivity of titanium centers seems to play a role in the efficiency of utilizing hydrogen peroxide, and as a result in the conversion of TMP. It has been reported that the surface-grafted and framework titanium centers decompose H_2O_2 at distinctly different rates.[72] Experiments were therefore designed to examine the influence of the connectivity (2C-, 3C-, and 4C-Ti) on the rate of H_2O_2 decomposition. NMR spectroscopy has been proven a powerful technique in quantifying small amounts of H_2O_2,[72, 111] and was used to monitor the decomposition of hydrogen peroxide by atomically dispersed titanium centers and TS-1 (2.0 wt% Ti). Figure 75 displays a typical NMR spectrum of a solution containing H_2O_2 and chloroform.

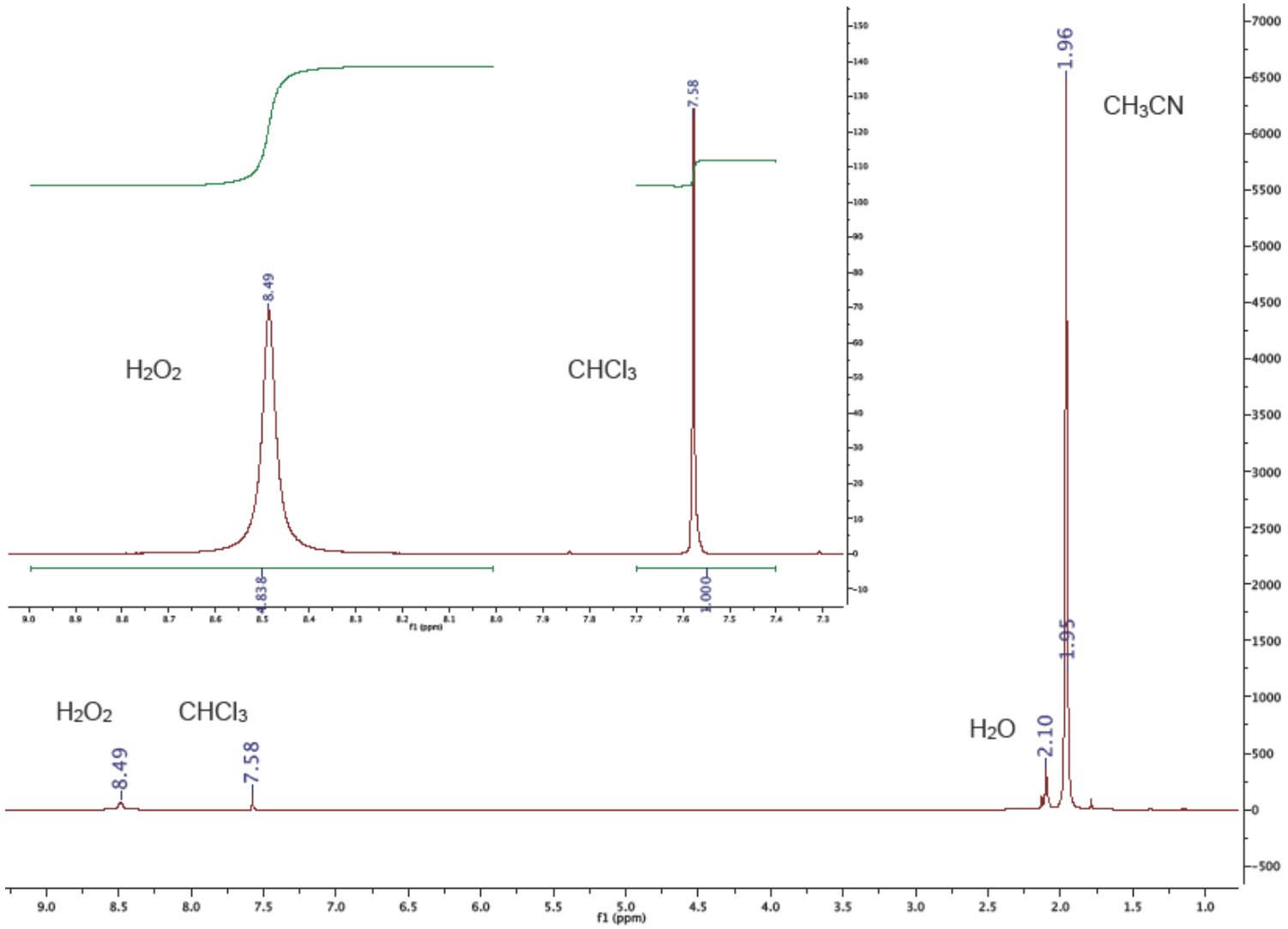


Figure 75. ^{1}H NMR spectrum of hydrogen peroxide with chloroform as internal standard

A NMR tube is charged with 0.5 mL deuterated acetonitrile (CD_3CN), 1.3 - 4.0 mg of the catalyst (0.0020 mmol Ti), 27 mg H_2O_2/H_2O (50 % w/w) (0.40 mmol H_2O_2), and 20 mg $CHCl_3$ (0.17 mmol, internal standard). Bruker Avance 400 MHz variable temperature high-resolution NMR is set at 80 ºC ~20 minutes before the NMR tube is loaded. NMR spectra of the solution are automatically collected at 5-30 minutes intervals for 8 hours. Figure 76 shows the stacked spectra of H_2O_2 and chloroform region at 0, 1 and 2 hour(s). The peak area of H_2O_2 decreases due to decomposition. Meanwhile, the peak broadening observed may be associated with the affinity of the surface for H_2O_2 and as a result rapid proton exchange between surface hydroxyl groups and H_2O_2.[72] The amount of residual H_2O_2 is determined via relative peak integration versus internal standard (chloroform, $CHCl_3$). Assuming similar mixing characteristics for all solutions in these NMR experiments, TOFs for each catalyst in decomposing H_2O_2 are obtained according to the relation of H_2O_2 concentration and time (min). The results of TOF (min^{-1}, ±10 %) are as below:

4C-Ti (3.06) > 3C-Ti (2.11) > 2C-Ti (0.42) > TS-1 (0.23).

Under the conditions described above, 4C-Ti appears to be the most active catalyst in decomposing H_2O_2, and microporous TS-1 the least active. Interestingly, except for TS-1, the catalytic activity in decomposing H_2O_2 follows the opposite order than that observed for the oxidation of TMP, as summarized below:

TS-1 (0.25) < 4C-Ti (0.35) < 3C-Ti (0.51) < 2C-Ti (1.58).

In titanosilicate/H_2O_2/TMP reactions, both reactions are believed to occur simultaneously, i.e. decomposition of H_2O_2 (side reaction) and oxidation of TMP (desired reaction). The efficiency of utilizing peroxide to oxidize TMP depends on activity of the catalysts in both reactions. The low efficiency of utilizing H_2O_2 by 3C- and 4C-Ti can be reasonably explained by the fast peroxide decomposition side reaction. Therefore, with the same substrate to peroxide ratio, 2C-Ti exhibits higher TMP conversion and higher peroxide efficiency. TS-1 exhibits the lowest TOF in either reaction, possibly related to the small pore sizes and the hydrophobic surfaces that repel H_2O_2.

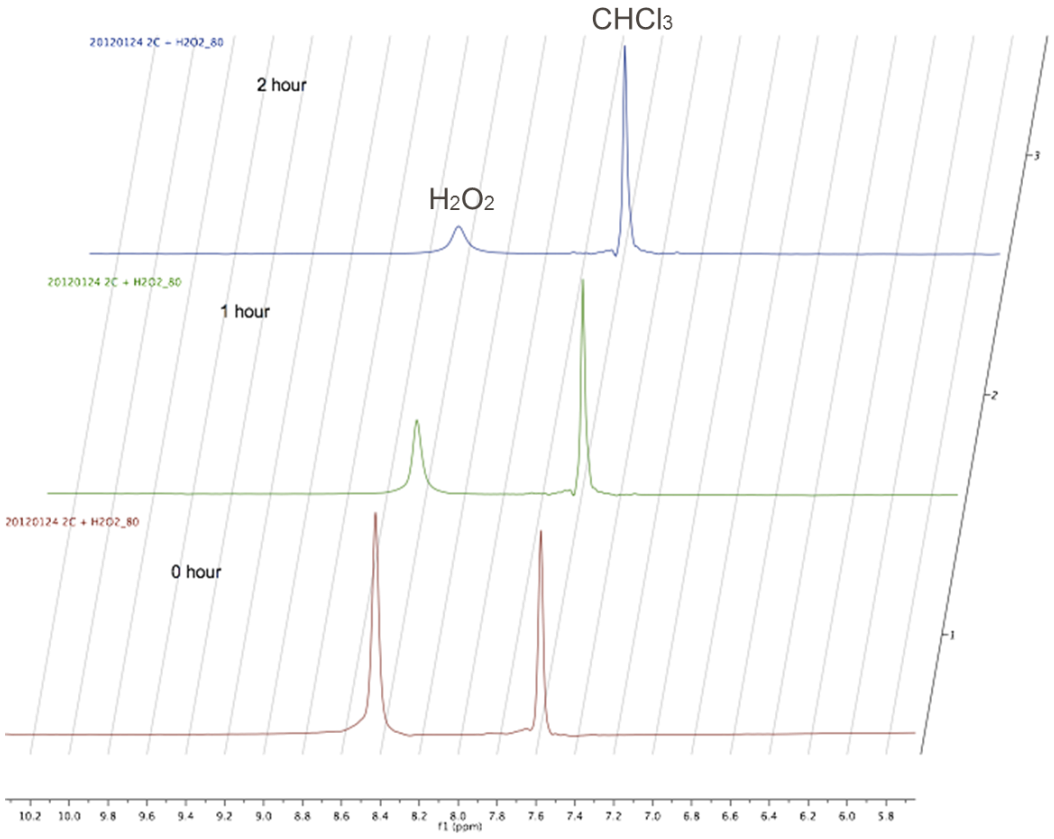


Figure 76. ^{1}H NMR peak area of H_2O_2 decreases due to decomposition t = 0, 1, 2 hour (bottom to top)

The difference in TOFs observed in H_2O_2 decomposition may also result from different mechanisms by each type of titanium center. Reaction orders that reflect and depend on the reaction mechanisms were therefore investigated for 2C-, 3C-, 4C-Ti catalyst and TS-1. According to the reaction law, reaction order is related to initial reaction rate (ln[Rate]) and the concentration of the compound (ln[A]).

$$Rate = k[A]^x$$

$$\ln(Rate) = x\ln[A] + constant \qquad \text{Equation 5-10}$$

In principle, the reaction order (x) should be intrinsic to the reaction mechanism, and not vary with the concentration [A]. Therefore, the value of x can be obtained from the plot of ln(Rate) and ln[A]. The same NMR experiment procedure described above was followed to investigate reaction mechanisms. The reactions are maintained at 80 °C. The initial reaction rate (mmol H_2O_2/min) is measured with decrease in the amount of H_2O_2 during the first minute of reaction. For each catalyst, 3-6 data points (identical replicates) of rate and [H_2O_2] concentration are plotted together on logarithm scales (Figure 77). Linear relations are seen in all cases, and the slope of each line equals the reaction order (Table 19). An uncertainty of approximately 10-20 %, arising mainly from measuring the mass of catalysts (± 0.5 mg), is estimated.

The two plots of TS-1 (top in Figure 77) involve different amounts of TS-1, and apparent reaction order (x) remains consistent in both cases, supporting the validity of the experimental approach. 4C-Ti shows the reaction order of 3.3, 1.3 for 3C-Ti, and 1.0 for 2C-Ti. Within the uncertainty, reaction orders can be grouped into two categories, (1) 4C-Ti and TS-1, and (2) 2C-Ti and 3C-Ti.

These results may be understood with the nature of the titanium centers and consequently different catalytic mechanisms. Heterogeneous activation of H_2O_2 by titanosilicate has been extensively studied. Many believe that in order for 4-connected titanium to coordinate with H_2O_2, at least one of the Ti-O-Si linkage must be broken usually through hydrolysis.[72] Figure 78 illustrate the catalytic process that starts with hydrolysis of Ti-O-Si around 4-connected center, followed by the coordination with H_2O_2. In the case of 3C- and 2C-Ti, lower connectivity leaves an “open”, more easily exchanged site (Ti-OR) ready for peroxide coordination, and therefore breakage of Ti-O-Si becomes unnecessary. The higher reaction order of H_2O_2 with 4C-Ti and TS-1 may be caused by the extra step of hydrolysis prior to the catalytic cycle.

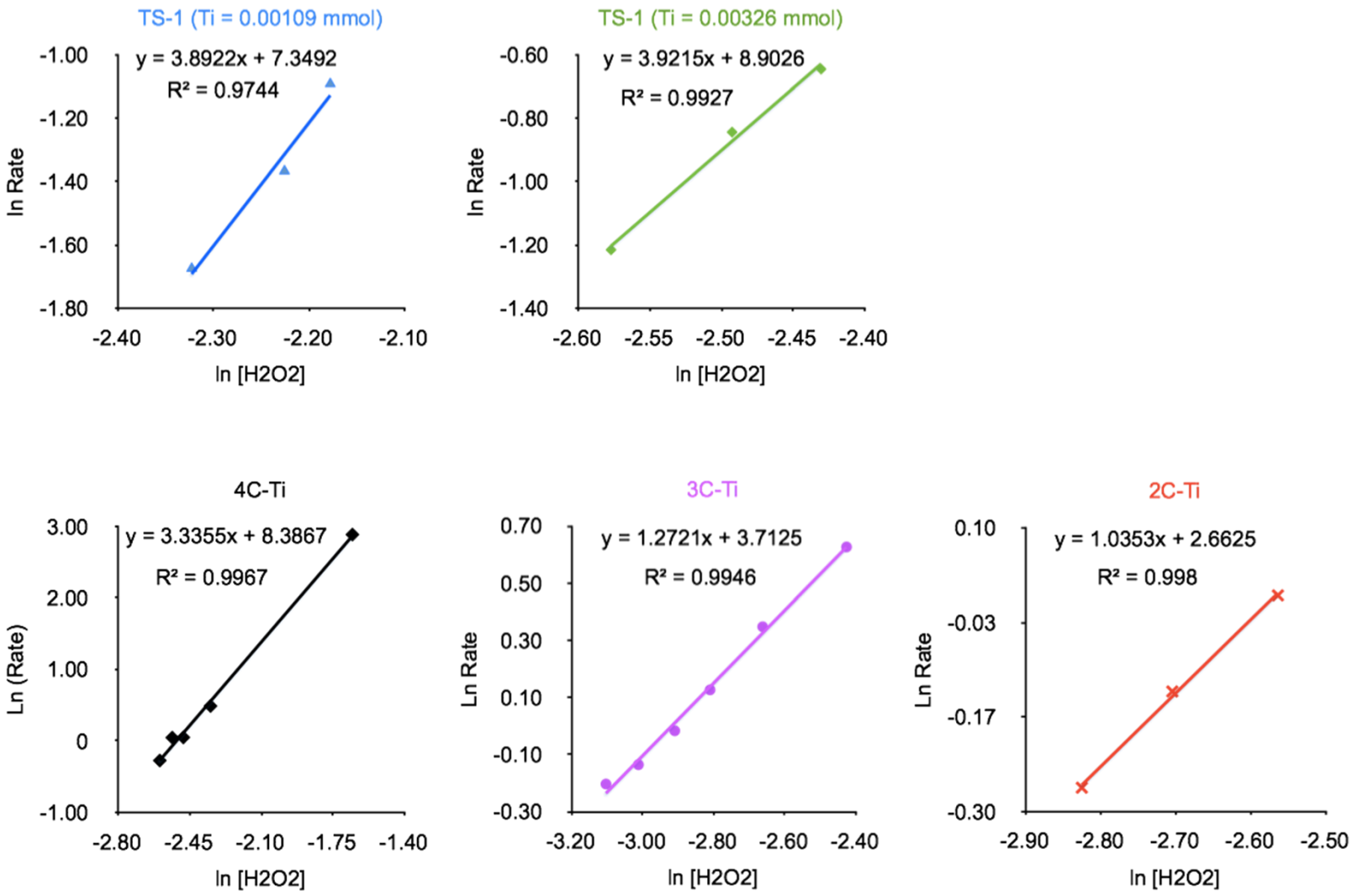


Figure 77. ln(Rate) vs. ln[H_2O_2] in peroxide decomposition catalyzed by 2C-, 3C-, 4C-Ti (bottom) and TS-1(top)

Table.19 Reaction orders obtained from ln(Rate)-ln[H_2O_2] relationship

$\ln(Rate) = x\ln[A] + constant$ Slope (x)	
TS-1	3.9 ± 0.8
4C-Ti	3.3 ± 0.7
3C-Ti	1.3 ± 0.3
2C-Ti	1.0 ± 0.2

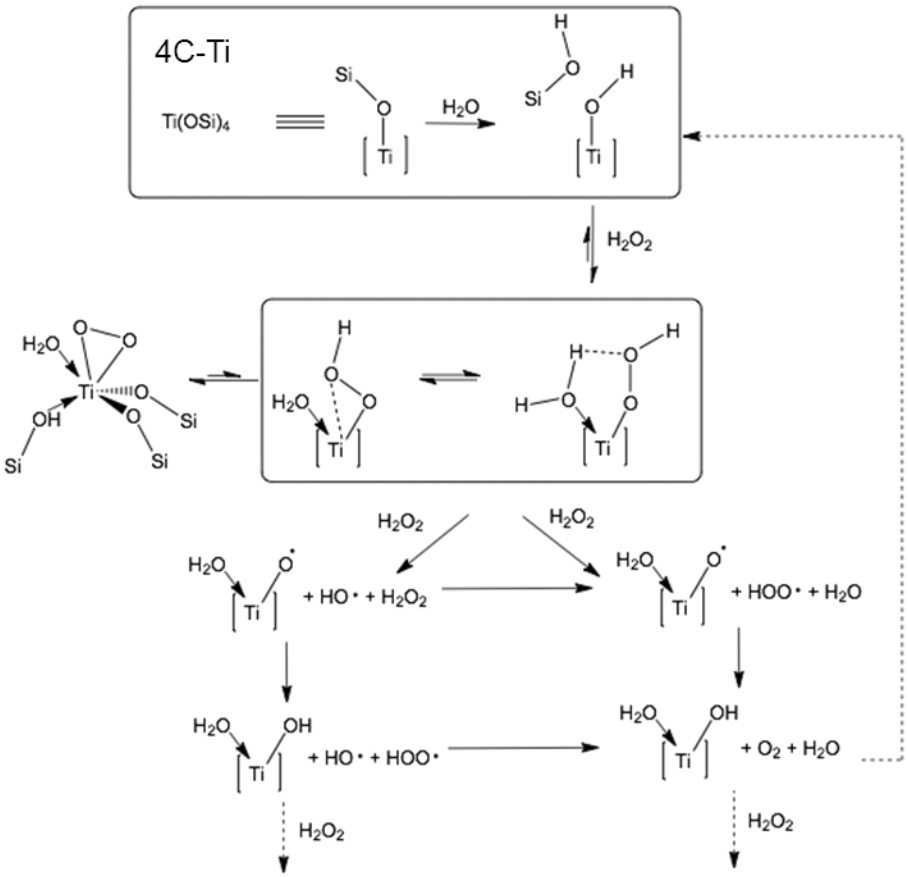


Figure 78. Free radical mechanism on titanium center with hydrogen peroxide (Reproduced from reference 72)

5.2.2 Stability and recyclability

The stability of catalytic sites is crucial to heterogeneous catalysts. Leaching of metal is one of the major reasons that prevent heterogeneous catalysts from many practical applications.[61] Leaching of titanium from many titanosilicate catalysts is also a commonly observed problem. TS-1 is one of the few Ti-silicate materials that are stable to aqueous hydrogen peroxide media and function well as a recyclable catalyst under such conditions.[54, 59, 62] Previously, stability of titanium-silsesquioxane complexes that represent 1-connected (1C) and 3-connected (3C) titanium centers were studied, trying to establish the relationship between connectivity and stability of titnaium.[107] The study supported the hydrothermal stability of 3C titanium complex, whereas significant titanium leaching occurs to 1C complex.[107] Taking advantage of the well-defined titanium centers in the catalysts prepared here, an investigation of their stability under actual catalyst conditions was performed. The recyclability of 2C-Ti, that exhibits superior catalytic activity in TMP oxidation, was carefully examined.

Catalysts are used in TMP oxidation under normal reaction conditions for 4 - 6 cycles. After each cycle, the catalysts are recycled by hot filtration, then washed with acetonitrile, and dried under vacuum. After 4-6 cycles, the catalyst and combined mother liquor (both catalysis and washes) are digested with an HF/HNO_3 solution and then analyzed with ICP-AES. The results of Ti content are summarized in Table 20. Little to no titanium is observed in the mother liquor. The Ti content in the recycled materials is close to the original values for each type of catalyst. The small decreases in titanium content may possibly be due to mechanical losses during the recycling. In summary, ICP analysis suggests all titanium centers synthesized in this research are stable against leaching and most, if not all, titanium remains incorporated in the bb matrices.

Good recyclability with respect to catalytic activity is also observed with all catalysts in this research. Some believe that 2-connected titanium in silicate is vulnerable to leaching because of the low connectivity.[107] Activity results for recycled 2C-Ti are shown in Figure 79. Four consecutive catalytic cycles are run with 2C-Ti in a vial. After each cycle of the reaction, the catalyst is recycled following the procedure above. Similar amount of time (~1 hour) is taken for each cycle, at the end of which consistent selectivity of TMBQ is observed, as well as a small decrease in TMP conversion, possibly due to the loss of catalyst during recycling.

Table 20. Stability of titanosilicate catalysts

Sample	Ti wt%		
	Initial Cat.	Recycled Cat.[a]	Mother Liquor[a,b]
2C-Ti	2.7	2.5	0.01
	7.6	6.8	0.10
3C-Ti	5.5	5.1	0.05
	4.2	3.9	0.03
4C-Ti	2.1	1.9	0.02
	3.2	2.6	0.02
Ti_4	5.1	4.5	0.04
	9.0	8.1	0.11

[a] Recycled catalyst and mother liquor collected after 4 - 6 cycles of reaction

[b] Titanium (mg) / recycled catalyst (mg) × 100%

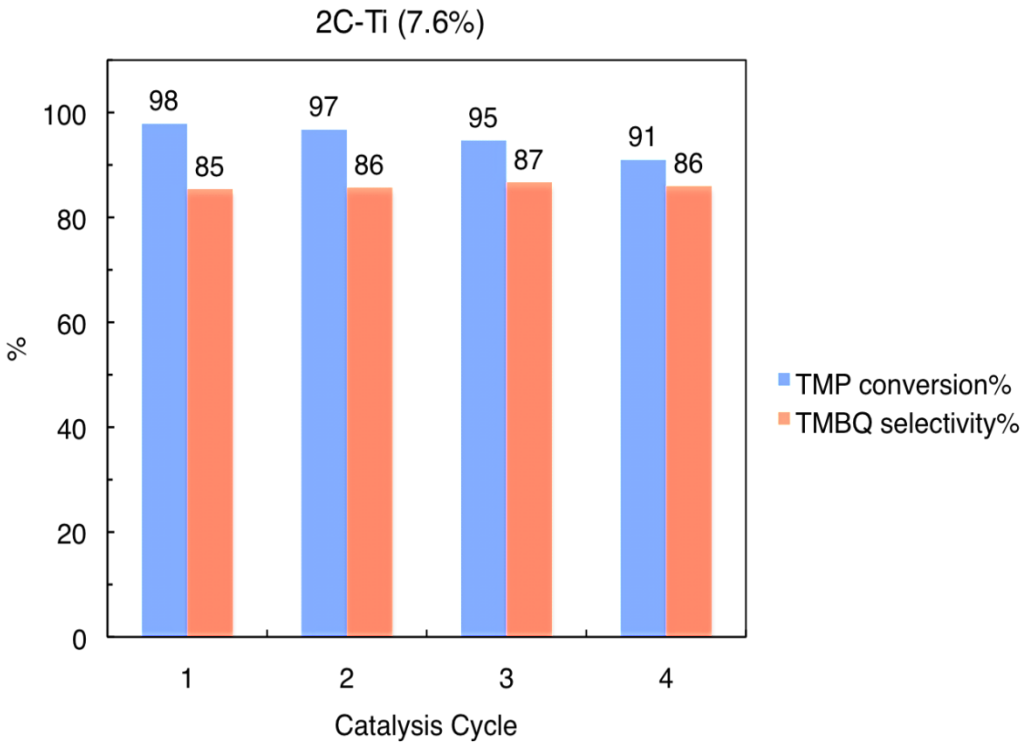


Figure 79. Recyclability of 2C-Ti catalyst in terms of conversion and selectivity

5.3 Summary

Isolated mononuclear (2C-, 3C-, and 4C-Ti) and tetranuclear (Ti_4) titanium centers in silicate matrices are applied to the oxidation of alkylphenol (TMP) to the corresponding 1, 4-benzoquinone with aqueous hydrogen peroxide (H_2O_2). High to fair TMP conversion and selectivity are observed with different connectivity and nuclearity of titanium centers. Under the reaction conditions investigated, 2C-Ti and T_4 exhibit distinctly higher activity (turnover frequency) than 3C- and 4C-Ti by a factor 3 - 5. According to the literature, a multi-titanium free radical mechanism may be involved in the phenol oxidation, which may explain the excellent yield of alkylbenzoquinone (TMBQ) from the polynuclear center, Ti_4.

The major side reaction in this catalysis system is decomposition of H_2O_2, and as a result only a fraction of H_2O_2 is used in oxidizing TMP and lowering the conversion. Titanium in silicate matrices is responsible for catalyzing both phenol oxidation and H_2O_2 decomposition. Turnover frequencies (TOFs) for different connectivity are in the sequence of 4C-Ti > 3C-Ti > 2C-Ti. It is clear that the catalytic activity in H_2O_2 decomposition is affected by the connectivity around titanium. Furthermore, the reaction order of H_2O_2 decomposition with each catalyst is obtained according to the rate law (ln(Rate) versus ln[H_2O_2]). Two categories of reaction order are observed: 4C-Ti, TS-1 (>3.0); 2C-Ti, 3C-Ti (~1.0). This observation can be understood in terms of the similarity in structures: 4C-Ti and TS-1 both contain 4-connected titanium centers, whereas 2C- and 3C-Ti have more open site(s) in the coordination sphere around titanium. The higher reaction order may be due to the hydrolysis of Ti-O-Si in 4C-Ti and TS-1 before the catalytic cycle begins. Among atomically dispersed titanium catalysts, 2C-Ti with lower connectivity is both the most active and most efficient catalyst in utilizing H_2O_2 as the oxidant and thus achieves higher conversion of TMP. Based on the data in hand, it appears that different mechanisms are involved in activating H_2O_2 with 2C-, 3C- and 4C-Ti, leading to the different activity observed for each type of titanium center.

Stability and recyclability are examined with each catalyst. Elemental analysis is conducted with recycled solids and mother liquors. All catalysts synthesized in this research, including 2C-Ti and Ti_4 exhibit excellent stability against leaching, and high recyclability. To our knowledge, this is the first study that clearly characterizes the stability of 2-connected titanium in silicate. The desired stability and recyclability promises potential practical applications of these materials.

Chapter VI. Conclusion and Future Research

6.1 Conclusion

6.1.1 Single-site catalysts with targeted titanium centers

The local environment including coordination, connectivity and nuclearity, and etc. around catalytically active titanium centers in a silicate matrix has a major influence on the activity and mechanism, and consequently the conversion and selectivity they exhibit. However, because of the challenges in both synthesis and characterization of any specific type of site, very few studies have focused on the influence from, for example, varying connectivity around titanium centers.

One of the major contributions of this research is the preparation of targeted titanium active centers in the silicate matrices using the method of sequential additions in which octatin silsesquioxane building block and selected mono- or poly-nuclear titanium precursors were employed. With the purpose of investigating the effects of connectivity and nuclearity around titanium, this research focuses on a total of four types of titanium(IV) centers, including three types of atomically dispersed (pseudo) tetrahedral centers, namely, 2C-, 3C- and 4C-Ti, and a tetranuclear titanium center, Ti_4.

A variety of spectroscopies and techniques are utilized to characterize the structures of these catalysts, including gravimetric analysis, ICP-AES, IR, Raman, DRUV spectroscopies and XAS. In all cases, ICP results confirm the incorporation of all titanium from the precursor compounds into the final titanosilicate matrix. The formation of Ti-O-Si linkages is supported by the signature Ti-O-Si vibration observed in the IR. The number of Ti-O-Si bond, i.e. connectivity achieved by a titanium center is quantified by gravimetric analysis. DRUV and XAS spectra strongly support the formation of isolated pseudo-tetrahedral titanium centers in 2C-, 3C- and 4C-Ti.

The formation of tetranuclear titanium centers in silicate appears more complicated than the mononuclear species in the reaction of the tin building block with the Ti_4 precursor. To understand the reaction process and predict the final structure of catalyst, a phenyl POSS analogue was prepared, characterized and compared with the actual tetranuclear titanium catalyst. DRUV and Raman spectra suggest the presence of Ti-O-Ti groups in the final material, and gravimetric analysis indicates the formation of averagely 2 - 3 Ti-O-Si linkages on

average per titanium. According to XANES spectra, the coordination number of titanium center clearly changed from 6 to possibly a mixture of 4 and 5 after the incorporation. Proposed structures of all catalysts are illustrated in Figure 80.

To our knowledge, this is the first study that successfully prepares and controls the local environment around titanium centers in silicate on a microscopic level. Moreover, a wide range of titanium contents and meso-sized pore structures are also available in these materials, promising huge potential in both fundamental and industrial applications, some of which were confirmed in the catalysis study here.

6.1.2 Catalytic properties and mechanistic study

The catalytic properties of these catalysts in the oxidation of alkylphenol to corresponding benzoquinone were studied. As expected, distinctly different conversions and selectivities were observed from each type of catalyst under the same reaction conditions. The turnover frequencies (TOFs) follow the order of Ti_4 > 2C-Ti > 3C-Ti and 4C-Ti.

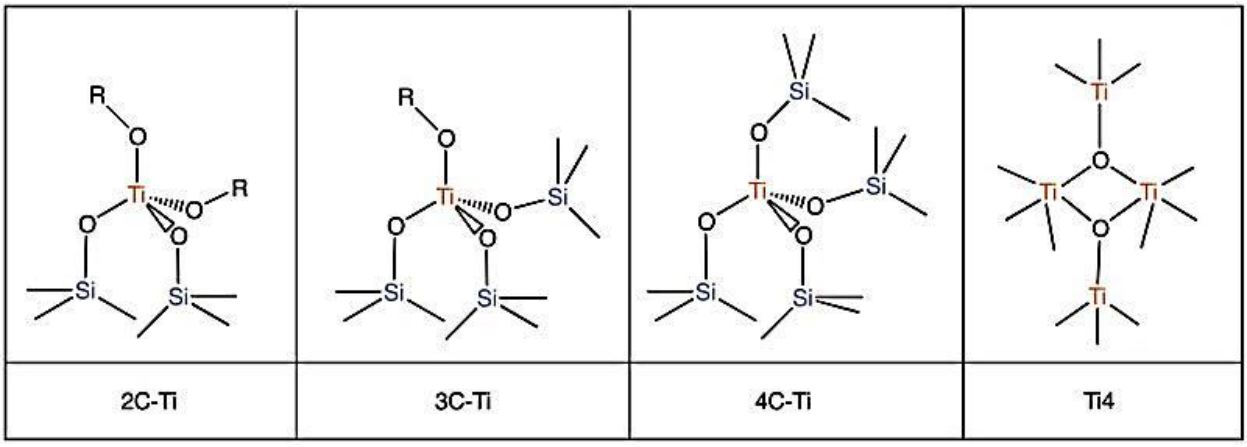


Figure 80. Four types of titanium centers in building block matrices: 2C-Ti, 3C-Ti, 4C-Ti and Ti_4 (surrounding -OSi bonds are omitted)

To our knowledge, this is the first report of superior catalytic activity of 2C-Ti to analogous atomically dispersed titanium catalysts with higher connectivities. In most studies of TS-1 catalyzed reactions, the breakage of a Ti-O-Si bond is thought necessary for initiating a catalytic cycle with isolated 4-connected titanium centers $Ti(OSi)_4$. The necessity of open coordination sites around titanium may explain the observation in this research of higher activity from 2C-Ti. The catalytic pathway involving 2C-Ti has a possibly lower activation barrier for coordination with small molecules without having to break existing Ti-O-Si linkages. 3C-Ti exhibits similar catalytic activity to 4C-Ti in the titled reaction, which deserves further studies in terms of the reaction mechanism.

The higher catalytic activity of polynuclear titanium groups than atomically dispersed titanosilicate is consistent with previous studies reported by Kholdeeva *et al.* that also proposed a free radical mechanism that requires multiple active centers.[50, 52, 106]

All catalysts prepared here were carefully studied for evidence of titanium leaching in aqueous environments. None of the catalysts showed obvious leaching after multiple (4 - 6) cycles of catalytic reaction. Excellent recyclability is observed for all catalysts, including the least connected 2C-Ti. These observations are the first clear evidence for the stability of 2-connected titanium species in silicate against leaching, as well as being an active catalyst in the oxidation of alkylphenol with aqueous hydrogen peroxide. The better accessibility of titanium centers in 2C-Ti may contribute to the higher TOF observed in comparison to 3C- and 4C-Ti analogues.

The major side reaction, i.e. hydrogen peroxide decomposition, during the catalytic oxidation, was also investigated with NMR spectroscopy, in order to understand the different efficiencies of peroxide utilization by different titanium centers. Embedded titanium centers, 4C-Ti, which are the least active in oxidizing alkylphenol, show the highest TOF in decomposing hydrogen peroxide, followed by 3C-Ti and then 2C-Ti. The results demonstrate that in a catalyst/H_2O_2/trimethylphenol (TMP) system, 4C-Ti preferably catalyzes H_2O_2 decomposition to oxidation of TMP, while 2C-Ti the opposite. Differences in the local coordination environments around titanium centers as well as their accessibility to peroxide and substrate are believed to play major roles in accounting for these reactivity trends.

Finally, the reaction orders of H_2O_2 decomposition associated with catalytic mechanisms were obtained by plotting ln(Rate) versus ln[H_2O_2]. Similar reaction orders were exhibited by 4C-Ti and by TS-1 both of which contain isolated 4-coonected titanium centers $Ti(OSi)_4$. In

contrast, lower connectivity sites, 2C- and 3C-Ti, show similar and lower reaction orders for peroxide decomposition.

6.1.3 Structure-function relationship

The most important goal of this research is to establish a relationship between structure of titanium centers in silicate and their catalytic properties. Based on the numerous previous studies on titanosilicates, it is believed that new synthetic approaches such as the building block methodology used here are necessary in order to be able to target synthetically specific active sites in these materials on an atomic level. The synthetic approach developed in the research described here allows, for the first time, the unique catalytic behaviors of each type of catalyst titanium sites to be studied and compared. The different catalytic properties observed on 2C-, 3C-, and 4C-Ti clearly demonstrate the importance of local environments around active centers, in the context of well-known meso- and macro-scale properties including porous framework structure, surface hydrophobicity/hydrophilicity, existences of impurities, and etc.. A more open coordination sphere around titanium contributes to higher efficiency hydrogen peroxide utilization in alkylphenol oxidation reactions by suppressing the decomposition of hydrogen peroxide. Polynuclear titanium centers are favored in the presumed free radical catalytic mechanism in the title reaction.

6.2 Direction of Future Research

6.2.1 Incorporation of various titanium clusters

The building block methodology has been proven an effective approach of isolation and stabilization of metal-oxo clusters that have chloride groups. The nuclearity of metal centers in silicate matrices has been observed to affect the catalytic activity in many ways. Taking advantage of this synthetic approach, a relationship between the size of incorporated cluster and catalytic properties may be established following the method used in this research. The candidates for titanium precursor include titanium dimer, trimer or larger complexes, for example, hexatitnaium complex $[(Cp^*TiCl)(\mu\text{-}O)_2(Cp^*Ti)_2(\mu\text{-}O)(\mu\text{-}O)_2]_2Ti$, in which Cp* is $\eta^5\text{-}C_5Me_5$.[105]

6.2.2 Epoxidation catalyzed by mesoporous single-site titanosilicates

Epoxidation of olefin includes a number of important reactions catalyzed by titanosilicates of which the titanosilicate TS-1 is a good example. Many studies have been done to investigate the mechanisms of titanium-catalyzed epoxidation. The series of catalysts prepared in this research have exhibited excellent stability and are good candidates for the use

in epoxidation reactions. The well-characterized single-site structure may provide critical knowledge concerning the effects of connectivity and nuclearity of titanium centers on their epoxidation activity. These single-site mono- or poly-nuclear titanium centers may also contribute to better understanding of the mechanisms in the titanium-catalyzed reactions such as olefin epoxidation. The types of titanium centers favored in atom transfer process of epoxidation will possibly differ from those involving the free radical process in phenol oxidation, i.e. Ti_4 and 2C-Ti. Based on the literature, 4-connected titanium centers such as TS-1 are expected to be the most active and selective active sites. By utilizing the materials prepared in this research, an important piece of evidence may be obtained to prove (or disprove) this hypothesis.

List of References

1. Modak, J., Haber process for ammonia synthesis. *Resonance* **2002,** *7*, 69-77.
2. Bhaduri, S.; Mukesh, D., *Homogeneous Catalysis*. John Wiley & Sons, Inc., **2002**, i-xiv.
3. Wróblewska, A., Liquid phase epoxidation of allylic compounds with hydrogen peroxide over titanium silicalite catalysts. *Journal of Molecular Catalysis A: Chemical* **2005,** *229*, 207-210.
4. Wróblewska, A.; Fajdek, A., Epoxidation of allyl alcohol to glycidol over the microporous TS-1 catalyst. *Journal of Hazardous Materials* **2010,** *179*, 258-265.
5. Katsuki, T. In *Titanium-catalyzed epoxidation*, Wiley-VCH Verlag GmbH, **1998**, 261-271.
6. Bourikas, K.; Kordulis, C.; Lycourghiotis, A., The role of the liquid- solid interface in the preparation of Supported Catalysts. *Catalysis Reviews* **2006,** *48*, 363-444.
7. Valden, M.; Lai, X.; Goodman, D. W., Onset of catalytic activity of gold clusters on titania with the appearance of nonmetallic properties. *Science* **1998,** *281*, 1647-1650.
8. Koo, K. Y.; Roh, H.-S.; Seo, Y. T.; Seo, D. J.; Yoon, W. L.; Bin Park, S., A highly effective and stable nano-sized Ni/MgO–Al_2O_3 catalyst for gas to liquids (GTL) process. *International Journal of Hydrogen Energy* **2008,** *33*, 2036-2043.
9. Bell, A. T., The Impact of nanoscience on heterogeneous catalysis. *Science* **2003,** *299*, 1688-1691.
10. Gamba, A.; Tabacchi, G.; Fois, E., TS-1 from First Principles. *Journal of Physical Chemistry A* **2009,** *113*, 15006-15015.
11. Deschner, T.; Lonstad, B.-T.; Widenmeyer, M.; Anwander, R., Functionalization of MCM-41 and SBA-1 with titanium(iv) (silyl)amides. *Journal of Materials Chemistry* **2011,** *21*, 5620-5628.
12. Dinse, A.; Khennache, S.; Frank, B.; Hess, C., Oxidative dehydrogenation of propane on silica (SBA-15) supported vanadia catalysts. *Journal of Molecular Catalysis. A* **2009,** *307*, 43-50.
13. Schreier, M.; Teren, S.; Belcher, L.; Regalbuto, J. R.; Miller, J. T., The nature of 'overexchanged' copper and platinum on zeolites. *Nanotechnology* **2005,** *16*.
14. Jiao, L.; Regalbuto, J. R., The synthesis of highly dispersed noble and base metals on silica via strong electrostatic adsorption: I. Amorphous silica. *Journal of Catalysis* **2008,** *260*, 329-341.
15. Woolery, G. L.; Alemany, L. B.; Dessau, R. M.; Chester, A. W., Spectroscopic evidence for the presence of internal silanols in highly siliceous ZSM-5. *Zeolites* **1986,** *6*, 14-16.
16. Van der Lee, M. K.; van Dillen, J.; Bitter, J. H.; de Jong, K. P., Deposition precipitation for the preparation of carbon nanofiber supported nickel catalysts. *Journal of the American Chemical Society* **2005,** *127*, 13573-13582.

17. Lekhal, A.; Glasser, B. J.; Khinast, J. G., Impact of drying on the catalyst profile in supported impregnation catalysts. *Chemical Engineering Science* **2001,** *56*, 4473-4487.
18. Sanchez, C.; Livage, J.; Henry, M.; Babonneau, F., Chemical modification of alkoxide precursors. *Journal of Non-Crystalline Solids* **1988,** *100*, 65-76.
19. Hay, J. N.; Raval, H. M., Synthesis of organic−inorganic hybrids via the non-hydrolytic sol−gel Process. *Chemistry of Materials* **2001,** *13*, 3396-3403.
20. Andrianainarivelo, M.; J. P. Corriu, R.; Leclercq, D.; Hubert Mutin, P.; Vioux, A., Non-hydrolytic sol-gel process: zirconium titanate gels. *Journal of Materials Chemistry* **1997,** *7*, 279-284.
21. Andrianainarivelo, M.; Corriu, R.; Leclercq, D.; Mutin, P. H.; Vioux, A., Mixed oxides SiO_2-ZrO_2 and SiO_2-TiO_2 by a non-hydrolytic sol-gel route. *Journal of Materials Chemistry* **1996,** *6*, 1665-1671.
22. Thomas, J. M., The Bakerian Lecture, 1990: New microcrystalline catalysts. *Philosophical Transactions of the Royal Society of London. Series A: Physical and Engineering Sciences* **1990,** *333*, 173-207.
23. Mintova, S.; Olson, N. H.; Valtchev, V.; Bein, T., Mechanism of zeolite a nanocrystal growth from colloids at room temperature. *Science* **1999,** *283*, 958-960.
24. Corma, A.; Serra, J. M.; Serna, P.; Valero, S.; Argente, E.; Botti, V., Optimisation of olefin epoxidation catalysts with the application of high-throughput and genetic algorithms assisted by artificial neural networks (softcomputing techniques). *Journal of Catalysis* **2005,** *229*, 513-524.
25. Rashkeev, S. N.; Lupini, A. R.; Overbury, S. H.; Pennycook, S. J.; Pantelides, S. T., Role of the nanoscale in catalytic CO oxidation by supported Au and Pt nanostructures. *Physical Review B* **2007,** *76*, 035438.
26. Synthesis and characterization of TiO2-incorporated silica foams. *Journal of Materials Science* **2009**.
27. Thomas, J.; Raja, R.; Lewis, D. W., Single-site heterogeneous catalysts. *Angewandte Chemie-International Edition* **2005,** *44*, 6456-6482.
28. McKittrick, M. W.; Jones, C. W., Toward single-site, immobilized molecular catalysts: site-isolated Ti ethylene polymerization catalysts supported on porous silica. *Journal of the American Chemical Society* **2004,** *126*, 3052-3053.
29. Maschmeyer, T.; Rey, F.; Sankar, G.; Thomas, J., Heterogenous catalysts obtained by grafting metallocene complexes onto mesoporous silica. *Nature* **1995,** *378*, 159-162.

30. Jarupatrakorn, J.; Tilley, T. D., Silica-supported, single-site titanium catalysts for olefin epoxidation. *Journal of the American Chemical Society* **2002,** *124*, 8380-8388.
31. Thomas, J. M.; Raja, R., Significance of mesoporous crystals for catalytic application. In *Studies in Surface Science and Catalysis*, Osamu, T., Ed. Elsevier: 2004; Vol. Volume 148, pp 163-211.
32. Sakthivel, A.; Zhao, J.; Kühn, F. E., Cyclopentadienyl molybdenum complexes grafted on zeolites – synthesis and catalytic application. *Catalysis Letters* **2005,** *102*, 115-119.
33. Shannon, I. J.; Maschmeyer, T.; Oldroyd, R. D.; Sankar, G.; Thomas, J. M.; Pernot, H.; Balikdjian, J.-P.; Che, M., Metallocene-derived, isolated Mo(VI) active centres on mesoporous silica for the catalytic dehydrogenation of methanol. *Journal of the Chemical Society, Faraday Transactions* **1998,** *94*, 1495-1499.
34. Fujdala, K. L.; Tilley, T. D., An Efficient, Single-source molecular precursor to silicoaluminophosphates. *Journal of the American Chemical Society* **2001,** *123*, 10133-10134.
35. Drake, I. J.; Fujdala, K. L.; Bell, A. T.; Tilley, T. D., Dimethyl carbonate production via the oxidative carbonylation of methanol over Cu/SiO2 catalysts prepared via molecular precursor grafting and chemical vapor deposition approaches. *Journal of Catalysis* **2005,** *230*, 14-27.
36. Fujdala, K. L.; Tilley, T. D., New vanadium tris(tert-butoxy)siloxy complexes and their thermolytic conversions to vanadia−silica materials. *Chemistry of Materials* **2002,** *14*, 1376-1384.
37. Pietrzyk, P.; Podolska, K.; Mazur, T.; Sojka, Z., Heterogeneous binding of dioxygen: EPR and DFT evidence for side-on nickel(II)–superoxo adduct with unprecedented magnetic structure hosted in MFI zeolite. *Journal of the American Chemical Society* **2011,** *133*, 19931-19943.
38. Abbet, S.; Sanchez, A.; Heiz, U.; Schneider, W. D.; Ferrari, A. M.; Pacchioni, G.; Rösch, N., Acetylene cyclotrimerization on supported size-selected Pdn clusters (1 ≤ n ≤ 30): One atom is enough! *Journal of the American Chemical Society* **2000,** *122*, 3453-3457.
39. Nicholas, C. P.; Ahn, H.; Marks, T. J., Synthesis, apectroscopy, and xatalytic properties of cationic organozirconium adsorbates on “super acidic” sulfated alumina. “single-site” heterogeneous catalysts with virtually 100 active sites. *Journal of the American Chemical Society* **2003,** *125*, 4325-4331.

40. Raja, R.; Thomas, J. M.; Jones, M. D.; Johnson, B. F. G.; Vaughan, D. E. W., Constraining asymmetric organometallic catalysts within mesoporous supports boosts their enantioselectivity. *Journal of the American Chemical Society* **2003,** *125*, 14982-14983.
41. Jones, M. D.; Raja, R.; Thomas, J. M.; Johnson, B. F. G.; Lewis, D. W.; Rouzaud, J.; Harris, K. D. M., Enhancing the enantioselectivity of novel homogeneous organometallic hydrogenation catalysts. *Angewandte Chemie* **2003,** *115*, 4462-4467.
42. Bianchini, C.; Burnaby, D. G.; Evans, J.; Frediani, P.; Meli, A.; Oberhauser, W.; Psaro, R.; Sordelli, L.; Vizza, F., Preparation, characterization, and performance of tripodal polyphosphine rhodium catalysts immobilized on silica via hydrogen bonding. *Journal of the American Chemical Society* **1999,** *121*, 5961-5971.
43. Corma, A.; Garcia, H., Supramolecular host-guest systems in zeolites prepared by ship-in-a-bottle synthesis. *European Journal of Inorganic Chemistry* **2004,** *2004*, 1143-1164.
44. Knops-Gerrits, P.-P.; De Vos, D.; Thibault-Starzyk, F.; Jacobs, P. A., Zeolite-encapsulated Mn(2) complexes as catalysts for selective alkene oxidation. *Nature* **1994,** *369*, 543-546.
45. Trevisan, V.; Signoretto, M.; Colonna, S.; Pironti, V.; Strukul, G., Microencapsulated chloroperoxidase as a recyclable catalyst for the enantioselective oxidation of Sulfides with hydrogen peroxide. *Angewandte Chemie* **2004,** *116*, 4189-4191.
46. Baur, W., On the cation and water positions in faujasite. *The American Mineralogist* **1964,** *49*.
47. Jacob, C. R.; Varkey, S. P.; Ratnasamy, P., Selective oxidation over copper and manganese salens encapsulated in zeolites. *Microporous and Mesoporous Materials* **1998,** *22*, 465-474.
48. Notari, B., Titanium silicalites. *Catalysis Today* **1993,** *18*.
49. Dutoit, D. C. M.; Schneider, M.; Hutter, R.; Baiker, A., Titania–silica mixed oxides: IV. Influence of Ti content and aging on structural and catalytic properties of aerogels. *Journal of Catalysis* **1996,** *161*, 651-658.
50. Kholdeeva, O. A.; Trukhan, N. N., Mesoporous titanium silicates as catalysts for the liquid-phase selective oxidation of organic compounds. *Russian Chemical Reviews* **2006,** *75*, 411-432.
51. Bouh, A.; Rice, G.; Scott, S., Mono- and dinuclear silica-supported titanium(IV) complexes and the effect of TiOTi connectivity on reactivity. *Journal of the American Chemical Society* **1999,** *121*, 7201-7210.
52. Kholdeeva, O. A.; Ivanchikova, I. D.; Guidotti, M.; Pirovano, C.; Ravasio, N.; Barmatova, M. V.; Chesalov, Y. A., Highly selective oxidation of alkylphenols to benzoquinones with

Hydrogen peroxide over silica-supported titanium catalysts: Titanium cluster site versus titanium single Site. *Advanced Synthesis & Catalysis* **2009,** *351*, 1877-1889.

53. Taramasso, M.; Perego, G.; Notari, B., Preparation of porous crystalline synthetic material comprised of silicon and titanium oxides. U.S. Pat. 4, 410, 501, **1983**.
54. Bordiga, S.; Damin, A.; Bonino, F.; Lamberti, C., Single site catalyst for partial oxidation reaction: TS-1 case study. *Topics in Organometallic Chemistry* **2005,** *16*, 37-68.
55. Notari, B., Microporous crystalline titanium silicalites, In *Advances in Catalysis,* Academic Press, **1996,** *Vol 41*, 253
56. Gleeson, D.; Sankar, G.; Catlow, C. R. A.; Thomas, J. M., The architecture of catalytically active centers in titanosilicate (TS-1) and related selective-oxidation catalysts. *Physical Chemistry Chemical Physics* **2000,** *2*, 4812-4817.
57. Shannon, R., Revised effective ionic radii and systematic studies of interatomic distances in halides and chalcogenides. *Acta Crystallographica Section A* **1976,** *32*, 751-767.
58. Henry, P. F.; Weller, M. T.; Wilson, C. C., Structural investigation of TS-1: Determination of the true nonrandom titanium framework substitution and silicon vacancy distribution from powder neutron diffraction studies using isotopes. *The Journal of Physical Chemistry B* **2001,** *105*, 7452-7458.
59. Bordiga, S.; Bonino, F.; Damin, A.; Lamberti, C., Reactivity of Ti(IV) species hosted in TS-1 towards H_2O_2–H_2O solutions investigated by ab initio cluster and periodic approaches combined with experimental XANES and EXAFS data: a review and new highlights. *Physical Chemistry Chemical Physics* **2007,** *9*, 4854-4878.
60. Deka, R. C.; Nasluzov, V. A.; Shor, E. A. I.; Shor, A. M.; Vayssilov, G. N.; Rosch, N., Comparison of all sites for Ti substitution in zeolite TS-1 by an accurate embedded-cluster method. *Journal of Physical Chemistry B* **2005,** *109*, 24304-24310.
61. Sheldon, R. A.; Wallau, M.; Arends, I.; Schuchardt, U., Heterogeneous catalysts for liquid-phase oxidations: Philosophers' stones or Trojan horses? *Accounts of Chemical Research* **1998,** *31*, 485-493.
62. Bonino, F.; Damin, A.; Ricchiardi, G.; Ricci, M.; Spano, G.; Daloisio, R.; Zecchina, A.; Lamberti, C.; Prestipino, C.; Bordiga, S., Ti-peroxo species in the TS-1:H_2O_2:H_2O system. *Journal of Physical Chemistry B* **2009**, *108,* 3573-3583.
63. De Vos, D. E.; Dams, M.; Sels, B. F.; Jacobs, P. A., Ordered mesoporous and microporous molecular sieves functionalized with transition metal complexes as catalysts for selective organic transformations. *Chem. Rev* **2002,** *102*, 3615-3640.

64. Blasco, T.; Corma, A.; Navarro, M.; Pariente, J., Synthesis, characterization, and catalytic activity of Ti-MCM-41 structures. *Journal of Catalysis* **1995,** *156*, 65-74.
65. Ratnasamy, P.; Srinivas, D.; Knözinger, H., Active sites and reactive intermediates in titanium silicate molecular sieves. *Advances in Catalysis*, Academic Press, **2004,** *48*, 1-169.
66. Barker, C. M.; Gleeson, D.; Kaltsoyannis, N.; Catlow, C. R. A.; Sankar, G.; Thomas, J. M., On the structure and coordination of the oxygen-donating species in Ti[upward arrow]MCM-41/TBHP oxidation catalysts: a density functional theory and EXAFS study. *Physical Chemistry Chemical Physics* **2002,** *4*, 1228-1240.
67. Wan, Y.; Zhao, D., Ordered Mesoporous Materials. In *Synthesis of Solid Catalysts*, Wiley-VCH Verlag GmbH & Co. KGaA, **2009**, 277-300.
68. Jung, W. Y.; Baek, S. H.; Yang, J. S.; Lim, K. T.; Lee, M. S.; Lee, G. D.; Park, S. S.; Hong, S. S., Synthesis of Ti-containing SBA-15 materials and studies on their photocatalytic decomposition of organce II. *Catalysis today* **2008**, *131*, 437-443.
69. Fraile, J. M.; Garcia, J. I.; Mayoral, J. A.; Vispe, E., Catalytic sites in silica-supported titanium catalysts: silsesquioxane complexes as models. *Journal of Catalysis* **2005,** *233*, 90-99.
70. Quadrelli, E. A.; Basset, J.M., On silsesquioxanes' accuracy as molecular models for silica-grafted complexes in heterogeneous catalysis. *Coordination Chemistry Reviews* **2010,** *254*, 707-728.
71. Aish, E. H.; Crocker, M.; Ladipo, F. T., Tripodal titanium silsesquioxane complexes immobilized in polydimethylsiloxane (PDMS) membrane: Selective catalysts for epoxidation of cyclohexene and 1-octene with aqueous hydrogen peroxide. *Journal of Catalysis* **2010,** *273*, 66-72.
72. Yoon, C.; Hirsekorn, K.; Neidig, M.; Yang, X.; Tilley, T., Mechanism of the decomposition of aqueous hydrogen peroxide over heterogeneous Ti-SBA-15 and TS-1 selective oxidation catalysts: Insights from spectroscopic and DFT studies. *ACS Catalysis* **2011**, *1*, 1665-1678.
73. Alcock, N. W.; Brown, D. A.; Roe, S. M., Synthesis of new titanium-oxo cluster compounds: X-ray structure of the tetranuclear oxide[$Ti_4Cl_6(\mu_2\text{-}O_2CPh)_6(\mu_3\text{-}O)_2$]. *Journal of the Chemical Society. Chemical Communication* **1992**, 846-848.
74. Clark, J. C.; Barnes, C. E., Reaction of the $Si_8O_{20}(SnMe_3)_8$ building block with silyl chlorides: A new synthetic methodology for preparing nanostructured building block solids. *Chemistry of Materials* **2007,** *19*, 3212-3218.

75. Lee, M.-Y.; Jiao, J.; Mayes, R.; Hagaman, E.; Barnes, C. E., The targeted synthesis of single site vanadyl species on the surface and in the framework of silicate building block materials. *Catalysis Today* **2011,** *160*, 153-164.
76. Hutter, R.; Mallat, T.; Baiker, A., Titania-silica mxed oxides II. Catalytic behavior in olefin epoxidation. *Journal of Catalysis* **1995,** *153*, 177-189.
77. Feher, F. J.; Weller, K. J., Synthesis and characterization of labile spherosilicates: $[(Me_3SnO)_8Si_8O_{12}]$ and $[(Me_4SbO)_8Si_8O_{12}]$. *Inorganic Chemistry* **1991,** *30*, 880882.
78. Kamigaito, M.; Sawamoto, M.; Higashimura, T., Alkoxy-substituted titanium(IV) chlorides as Lewis acid activators for living cationic polymerization of isobutyl vinyl ether: Control of Lewis acidity in the design of initiating systems. *Macromolecules* **1995,** *28*, 5671-5675.
79. Zhang, F. Z.; Guo, X. W.; Wang, X. S.; Li, G.; Zhou, J. C., The active sites in different TS-1 zeolites for propylene epoxidation studied by ultraviolet visible absorption spectroscopies. *Catalysis Letters* **2001**.
80. Srinivas, D.; Manikandan, P.; Laha, S. C.; Kumar, R.; Ratnasamy, P., Reactive oxo-titanium species in titanosilicate molecular sieves: EPR investigations and structure-activity correlations. *Journal of Catalysis* **2003,** *217*, 160-171.
81. Jørgensen, C. K., In *Modern aspects of ligand field theory*. North-Holland, Amsterdam, **1971**.
82. Gao, X.; Wachs, I. E., Titania–silica as catalysts: molecular structural characteristics and physico-chemical properties. *Catalysis today* **1999,** *51*, 233-254.
83. Le Noc, L.; Trong On, D.; Solomykina, S.; Echchahed, B.; Béland, F.; Cartier dit Moulin, C.; Bonneviot, L., Characterization of two different framework titanium sites and quantification of extra-framework species in TS-1 silicalites. In *Studies in Surface Science and Catalysis*, Joe W. Hightower, W. N. D. E. I.; Alexis, T. B., Eds. Elsevier: **1996**, *Vol. 101*, 611-620.
84. Halasz, I.; Liang, J.; Fitzgerald, G., Zeolite Confined $Ti(OH)_4$ Nanoparticles in highly active and selective oxidation catalyst. *Catalysis Letters* **2011,** *141*, 948-953.
85. Bordiga, S.; Coluccia, S.; Lamberti, C.; Marchese, L.; Zecchina, A.; Boscherini, F.; Buffa, F.; Genoni, F.; Leofanti, G.; Petrini, G.; Vlaic, G., XAFS study of Ti-silicalite: structure of framework Ti(IV) in the presence and absence of reactive molecules (H_2O, NH_3) and comparison with ultraviolet-visible and IR results. *Journal of Physical Chemistry* **1994,** *98*, 4125-4132.
86. Kelly, S. D.; Hesterberg, D.; Ravel, B., Analysis of soils and minerals using X-ray absorption spectroscopy. *Methods of soil analysis, Part 5 -Mineralogical methods. Ulery, A. L. and Drees, L. R. Madison, WI, USA, Soil Science Society of America* **2008**, 367-463.

87. Fernández-García, M., XANES analysis of catalytic systems under reaction conditions. *Catalysis Reviews* **2002,** *44*, 59-121.
88. Farges, F.; Brown, G. E.; Rehr, J. J., Ti K-edge XANES studies of Ti coordination and disorder in oxide compounds: Comparison between theory and experiment. *Physical Review B* **1997,** *56*, 1809-1819.
89. Bolis, V.; Bordiga, S.; Lamberti, C.; Zecchina, A.; Carati, A.; Rivetti, F.; Spano, G.; Petrini, G., Heterogeneity of framework Ti (IV) in Ti−silicalite as revealed by the adsorption of NH_3. Combined calorimetric and spectroscopic study. *Langmuir* **1999,** *15*, 5753-5764.
90. Bonino, F.; Damin, A.; Bordiga, S.; Lamberti, C.; Zecchina, A., Interaction of CD_3CN and pyridine with the Ti (IV) centers of TS-1 catalysts: A spectroscopic and computational study. *Langmuir* **2003,** *19*, 2155-2161.
91. On, D. T.; Bonneviot, L.; Bittar, A.; Sayari, A.; Kaliaguine, S., Titanium sites in titanium silicates: An XPS, XANES and EXAFS study. *Journal of Molecular Catalysis* **1992**, *74*, 233-246.
92. Fan, W; Duan, R. G.; Yokoi, T.l Wu, P.; Kubota, Y., Synthesis, crystallization mechanism, and catalytic properties of titanium-rich TS-1 free of extraframework titanium species. *Journal of the American Chemical Society* **2008,** *9,* 880-882.
93. Farges, F., A Ti K-edge EXAFS study of the medium range environment around Ti in oxide glasses. *Journal of Non-Crystalline Solids* **1999,** *244*, 25-33.
94. Prestipino, C.; Solari, P. L.; Lamberti, C., EXAFS and XANES investigation of the ETS-10 microporous titanosilicate. *The Journal of Physical Chemistry B* **2005,** *109*, 13132-13137.
95. Zhao, D.; Budhi, S.; Rodriguez, A.; Koodali, R., Rapid and facile synthesis of Ti-MCM-48 mesoporous material and the photocatalytic performance for hydrogen evolution. *International Journal of Hydrogen Energy* **2010**.
96. Ricchiardi, G.; Damin, A.; Bordiga, S.; Lamberti, C.; Spano, G.; Rivetti, F.; Zecchina, A., Vibrational structure of titanium silicate catalysts. A spectroscopic and theoretical study. *Journal of the American Chemical Society* **2001,** *123*, 11409-11419.
97. Lin, W. Y.; Frei, H., Photochemical and FT-IR probing of the active site of hydrogen peroxide in Ti silicalite sieve. *Journal of the American Chemical Society* **2002,** *124*, 9292-9298.
98. Lu, J.; Kosuda, K. M.; Van Duyne, R. P.; Stair, P. C., Surface acidity and properties of TiO_2/SiO_2 catalysts prepared by atomic layer deposition: UV−visible diffuse reflectance, DRIFTS, and visible Raman spectroscopy studies. *The Journal of Physical Chemistry C* **2009,** *113*, 12412-12418.

99. Scarano, D.; Zecchina, A.; Bordiga, S.; Geobaldo, F.; Spoto, G.; Petrini, G.; Leofanti, G.; Padovan, M.; Tozzola, G., Fourier-transform infrared and Raman spectra of pure and Al-, B-, Ti- and Fe-substituted silicalites: Stretching-mode region. *Journal of the Chemical Society, Faraday Transactions* **1993,** *89*, 4123-4130.

100. Zimny, K.; Carteret, C.; Stebe, M. J.; Blin, J. L., Multitechnique investigation of mesoporous titanosilicate materials prepared from both the self-assembly and the liquid crystal mechanisms. *Journal of Physical Chemistry C* **2011,** *115*, 8684-8692.

101. Farges, F., Coordination of Ti in crystalline and glassy fresnoites: A high-resolution XANES spectroscopy study at the Ti K-edge. *Journal of Non-Crystalline Solids* **1996,** *204*, 53-64.

102. Li, G. G.; Bridges, F.; Booth, C. H., X-ray-absorption fine-structure standards: a comparison of experiment and theory. *Physical Review B* **1995,** *52*, 6332-6348.

103. Barrow, H.; Brown, D. A.; Alcock, N. W.; Clase, H. J.; Wallbridge, M. G. H., Reactions of titanium tetrachloride with carboxylic acids. Crystal and molecular structure of the dinuclear titanium oxo Compound[{$TiC_{12}(O_2CBu)(BuCO_2H)\}_2O$]. *Journal of the Chemical Society-Dalton Transactions* **1994**, 195-199.

104. Miyaoka, H.; Kuze, T.; Sano, H.; Mori, H., Raman spectra of titanium di-, tri-, and tetra-chlorides. *International Journal of Modern Physics B* **2001**, *15*, 3865-3868.

105. Khouw, C. B.; Dartt, C. B.; Labinger, J. A.; Davis, M. E., Studies on the catalytic oxidation of alkanes and alkenes by ttanium silicates. *Journal of Catalysis* **1994,** *149*, 195-205.

106. Zalomaeva, O. V.; Trukhan, N. N.; Ivanchikova, I. D.; Panchenko, A. A.; Roduner, E.; Talsi, E. P.; Sorokin, A. B.; Rogov, V. A.; Kholdeeva, O. A., EPR study on the mechanism of H_2O_2-based oxidation of alkylphenols over titanium single-site catalysts. *Journal of Molecular Catalysis A-Chemical* **2007,** *277*, 185-192.

107. Abbenhuis, H. C. L.; Krijnen, S.; vanSanten, R. A., Modelling the active sites of heterogeneous titanium epoxidation catalysts using titanium silasequioxanes: Insight into specific factors that determine leaching in liquid-phase processes. *Chemical Communications* **1997**, 331-332.

108. Ahn, W. S.; Kang, K. K.; Kim, K. Y., Synthesis of TS-1 by microwave heating of template-impregnated SiO_2–TiO_2 xerogels. *Catalysis Letters* **2001,** *72*, 229-232.

109. Guo, X.; Li, G.; Zhang, X.; Wang, X., Synthesis of titanium silicalite-I from TPABr system. In *Studies in Surface Science and Catalysis*, Can, L.; Qin, X., Eds. Elsevier, **1997**, *Vol. 112*, 499-508.

110. Thangaraj, A.; Eapen, M. J.; Sivasanker, S.; Ratnasamy, P., Studies on the synthesis of titanium silicalite, TS-1. *Zeolites* **1992,** *12*, 943-950.

111. Stephenson, N. A.; Bell, A. T., Quantitative analysis of hydrogen peroxide by H-1 NMR spectroscopy. *Analytical And Bioanalytical Chemistry* **2005**, *381*, 1289-1293.

112. Cunningham, J.; Hodnett, B. K.; Ilyas, M.; Tobin, J., Dehydrogenation versus dehydration of aliphatic alcohols on metal oxides. *Faraday Discussions of the Chemical Society* **1981**, 283-302.

113. Bariås, O. A.; Holmen, A.; Blekkan, E. A., Propane dehydrogenation over supported Pt and Pt–Sn catalysts: Catalyst preparation, characterization, and activity measurements. *Journal of Catalysis* **1996**, *158*, 1-12.

114. Boudart, M., Turnover rates in heterogeneous catalysis. *Chemical Reviews* **1995**, *95*, 661-666.

115. Chen, J.; Hu, N.; Zhan, J.; Li, Y., The new polynuclear titanium(IV) complex [(Cp*TiCl)(mu-O)$_2$(Cp*Ti)$_2$(mu-O)(mu-O)$_2$]$_2$Ti (Cp* is eta5-C_5Me_5). *Acta Crystallographica Section C* **2005** *C61*, m337-m338

Vita

Nan Chen grew up in Tianjin, China, and graduated from Tianjin Shiyan High School in July 2003. She then entered Peking University and received her B.S. in chemistry from Peking University (China) in July 2007. She started her research in inorganic chemistry as an undergraduate student. The results of her research were published in “Highly Symmetrical CdS Tetrahedral Nanocrystals Prepared by Low Temperature Cehmical Vapor Depostiion Using Polysulfide as the Sulfur Source” by Crystal Growth & Design in 2008.

In August 2007, she joined the Chemistry Department at the University of Tennessee, Knoxville, where she pursued the PhD degree in chemistry under the guidance of Professor Craig E. Barnes. Her research was focused on the single-site titanium silicate catalysts. The project was part of an ongoing research program to develop new synthetic methodologies for the targeted preparation of heterogeneous catalysts. She completed the requirements for the Doctor of Philosophy in chemistry in August 2012.